

EDUARDO NUNES

INTER-RELATIONSHIP OF SKIN PASS, 2D AND 3D ROUGHNESS
PARAMETERS, STAMPABILITY AND PAINTABILITY ON COLD ROLLED STEEL
SHEETS FOR THE AUTOMOTIVE INDUSTRY

São Paulo

2014

EDUARDO NUNES

INTER-RELATIONSHIP OF SKIN PASS, 2D AND 3D ROUGHNESS
PARAMETERS, STAMPABILITY AND PAINTABILITY ON COLD ROLLED STEEL
SHEETS FOR THE AUTOMOTIVE INDUSTRY

A Thesis submitted to the Escola
Politécnica da Universidade de São
Paulo, in conformity with the requirements
for the degree of Doctor of Science.

Area of concentration:

Metallurgical and Materials Engineering

Supervisor: Prof. Dr. Ronald Lesley Plaut

São Paulo

2014

Este exemplar foi revisado e alterado em relação à versão original, sob responsabilidade única do autor e com anuência de seu orientador.

São Paulo, 26 de fevereiro de 2014.

Assinatura do autor _____

Assinatura do orientador _____

FICHA CATALOGRÁFICA

Nunes, Eduardo

Inter-relationship of skin pass, 2D and 3D roughness parameters, stampability and paintability on cold rolled steel sheets for the automotive industry / E.Nunes. -- ed. rev.— São Paulo, 2014.

247 p.

Tese (Doutorado) – Escola Politécnica da universidade de São Paulo. Departamento de Engenharia Metalúrgica e de Materiais

1. Estampagem 2. Pintura 3. Rugosidade I. Universidade de São Paulo. Escola Politécnica. Departamento de Engenharia Metalúrgica e de Materiais II.t.

DEDICATION

*I dedicate this work to my
lovely wife, children, parents
and grandparents.*

ACKNOWLEDGMENTS

To God.

To my wife Ivy.

To my father Levi, mother Vera and my brother Alexandre.

To Prof. Dr. Ronald and his wife Hirma.

Other Prof. Drs. that in a certain way have contributed very much to my metallurgical engineering knowledge, namely: Ivan Falleiros, Cyro Takano, Marcello Mourão, Fernando Landgraf, Claudio Schon, Nelson Lima, André Tchipstchin, Antonio Ramirez, Angelo Padilha and Zhebour Panossian.

To my GM colleagues Msc. Jose Carlos Santos and Dr. Marco Colosio, for their technical guidance.

To Dr. Christian Wichern (NanoFocus) and Dr. Thomaz Stoughton (GMNA), for being part of the external examiners and to Dr. Carlos Sakuramoto (GMB) and Prof. Dr. Gilmar Batalha (EPUSP) for being part of the internal examiners. All, for their technical support.

To Prof. Drs. Angelo Padilha, Amilton Sinatora, Claudio Schon (EPUSP) and Marco Colosio (GMB) and Dr. Antenor Filho (Armco), for being part of the alternates examiners.

To Dr. Susan Hartfield-Wunsch (GMNA), Dr. Duane Moryc (GMNA), Dr. Ivênio Teixeira (Usiminas) and Dr. Stefan Tschersche (WaldrichSiegen GmbH & Co), Dipl.Ing. Roland Meier (Walzen Service-Center), Eng. Sergio Marigonda (Byk Gardner), Eng. Marcello Montagnani (Taylor Hobson), Susuma Matsumura (GKN Sintermetals) for their technical guidance.

To Antonio Fabiano (Usiminas), Ciro Pinheiro, Byll Raynek and Mark Dilling (Zygo), Herbert Mello (HBM), Giovanni Bussolo (Choice), Silvio Abreu (Amepla), Karl-Heinz Strass (Cyber Technologies), Lisias Serra (Metromec), Radu Unanian and Minoru Umeda (GKN Sintermetals) for their technical support.

To my GMB colleagues Thiago Sekeres, Hernani Alves, Rinaldo Garcia, Janaina Rodrigues, Adriano Reis, Cleber Fernandes, Luiz Fantini, Samuel Souza, Fernando Souza, Roberto Piovatto, Cesar Martorelli, Ailton Garcia, Isaac Mendes, Djalma Mello, Sandra Garzusi, Edmilson Garciola, Rita Binda, Renato Freitas, Elisio Sanches, Luciano Santos, Rubens Ribeiro, João Delafiori, Marcelo Tirelli, Ivan Umesaki, Jose Castillo and Luiz Vanzo.

Least but no last, to GMB for the time spent in preparing this Thesis. To GKN Sintermetals, Bodycote (Brasimet), Bardella, EPUSP, FEI and ETFSP for the engineering knowledge.

EPIGRAPH

*“If I have seen further it is by
standing on the shoulders of
Giants” Isaac Newton.*

Thanks Prof. Dr. Ronald!

ABSTRACT

The aim of this research work is to study the inter-relationship, under controlled industrial conditions, among skin pass reductions, surface topography characterized by 2D and 3D roughness parameters, stampability and painted surface finish quality for automotive steel sheet stampings.

Different surface textures obtained from cold rolling finishing have been evaluated in terms of paint appearance (rating and spectral curve) and tentatively related to roughness parameters (2D and 3D) obtained from the cold finished sheets. Some relevant tendencies have been established amongst these parameters.

The results presented here are in accordance with other recently published research showing that there is a clear relationship between these parameters, and that further detailed studies are needed.

Key words: 3D roughness. Sheet metal. Stampability. Paint appearance. Automotive. Skin pass reduction. Surface topography.

RESUMO

O foco do presente trabalho é o estudo, em condições industriais, da inter-relação entre grau de redução do passe de acabamento, topografia superficial caracterizada pelos parâmetros de rugosidade 2D e 3D, estampabilidade e aparência de pintura de chapas de aço para painéis automotivos.

Diferentes texturas superficiais de chapas de aço foram analisadas em termos de aparência de pintura (rating e curvas espectrais) e tentativamente relacionadas com os parâmetros de rugosidades (2D e 3D) obtidos na chapa antes de estampar. Algumas tendências relevantes foram estabelecidas entre estes parâmetros.

Os resultados presentes aqui estão de acordo com publicações recentes mostrando uma clara relação entre estes parâmetros e que trabalhos futuros ainda são necessários.

Palavras chave: Rugosidade 3D. Chapas de aço. Estampabilidade. Aparência de pintura. Automóveis. Grau de redução do passe de acabamento. Topografia superficial.

LIST OF FIGURES

Figure 1.1: Paint quality and importance of perceptual quality in vehicles (GERHART, 2001).	26
Figure 1.2: Quality of the reflected image on the car hood. “Good” has a higher level image details while the “poor” presents a hazy image (TRUNG, 2011).....	27
Figure 1.3: FLD of a typical car stamping.....	28
Figure 2.1: Macro vision of the present research work.....	30
Figure 3.0.1: From the ore to the end product (car body), each process has its contribution to the paint quality. (BIW = body-in-white)	31
Figure 3.1.1: Roll texturing methods: From stochastic ones (as SBT, EDT and Pretex) to the deterministic ones (as LT and EBT) (STAEVES,1998).....	33
Figure 3.1.2: Top: typical EDT Programs. Bottom: EDT main process variables in order to set up typical EDT Programs. Pc =peak count measured in 2D; Ra=surface roughness measured in 2D (WARRENDER et al., 2005; TERPÁK et al, 2010).....	34
Figure 3.1.3: The illustrations indicate the development of the sheet-surface structure for temper rolling (skin-pass) with different elongations, using the work-roll structured by the SBT, EDT, EBT and LT methods (PAWELSKI et al., 1994).....	35
Figure 3.1.4: Transfer characteristics for dry temper rolling (skin-pass) of a hot-dip galvanized (HDG) IF type steel - FeP05 (PAWELSKI et al., 1994).	36
Figure 3.1.5: Transfer characteristics for dry and wet temper rolling (skin-pass) of a hot-dip galvanized steel FeP05 using EBT- textured work rolls. (PAWELSKI et al.,1994 and BFINTEN et al.,1996).	37
Figure 3.1.6: Left: Wear of the work roll during skin-pass rolling and its effect on the surface topography. Right: Roughness deviation along the coil width. (PFESTORF et al., 1998; GEIGER et al.,1997).....	38
Figure 3.1.7: Comparative performance of chromium plated and plain temper mill rolls (SIMÃO and ASPINWALL, 1999)	39
Figure 3.1.8: Relationship between the average surface roughness Ra and average surface waviness Wca for the different plain EDT and Cr-plated EDT roll specimens (♦ : plain EDT; ◇: Cr-plated EDT) (SIMÃO and ASPINWALL, 1999)	40

Figure 3.1.9: Variation of steel sheet roughness (within the usual practical roughness range of 1.6 to $1\mu\text{m}$) as a function of the number of processed coils with Cr-plated EDT rolls (right scale) and the initial roll surface roughness (left scale) (MAYER, 2013).	41
Figure 3.1.10: Example for a section of a barrel surface of a texturized roll. (TSCHERSCHKE, NITSCHKE, 2012)	42
Figure 3.2.1: Schematic outline of micro-plasto-hydrodynamic lubrication and local pressure distribution (BAY et al., 2010)	43
Figure 3.2.2: Top: Typical Stribeck curve relating the different contact mechanisms. $Z = \eta v / p$ (VERMULEN and SCHEERS, 2001). Bottom: An alternative Stribeck curve which considers the sheet metal roughness. $L = \eta v / p Ra$, where Ra is the roughness (LUBBING, HAAR, SCHIPPER, 1996).	44
Figure 3.2.3: Schematic illustration of the mechanism of hydrostatic lubrication pockets (PAWELSKI et al, 1996).	45
Figure 3.2.4: (a) Mechanical–rheological model; (b) surface fractions as a function of vertical penetration (WEIDEL, ENGEL, 2009).	46
Figure 3.2.5: Coefficient of friction versus the angle between the straight grooves and the drawing direction (groove orientation) (BFINTEN et al, 1996).	47
Figure 3.2.6: Proportion of static friction coefficient μ_H to the sliding friction coefficient μ_G , in comparison to the maximum closed void area ratio- α_{clm} (PFESTORF et al., 1998)	47
Figure 3.2.7: Lubricant reservoir (closed void) of EDT (Pretex) structure (GRETHE, 2013).	49
Figure 3.2.8: Volume analysis: a) SBT-texturized b) EDT-texturized (<i>Pretex</i>) (VALENTIN et al., 2008)	49
Figure 3.2.9: Left: Punch force versus stroke for different oil film amounts (g/m^2) applied on the sheet surface (HU, NIEHOFF, VOLLERTSEN, 2003). Right: Coefficient of friction versus emulsion concentration for different types of lubricant (BAY et al., 2010)	50
Figure 3.2.10: A macro view summarizing the stamping process.	51
Figure 3.2.11: Visualization screen of the oil film measurement system. (BLOCK, BERGOLD, ENDERLE, 2011).	52

Figure 3.2.11: Visualization screen of the oil film measurement system. (BLOCK, BERGOLD, ENDERLE, 2011).....	52
Figure 3.2.13: Typical signatures: Force x travel. Alterations caused by increasing tool temperature (BAY, OLSSON, ANDREASEN, 2008).....	52
Figure 3.2.14: Typical influence of sliding velocity, lubricant type, tool surface and contact normal force on the friction coefficient (MERKLEIN, GEIGER, KAUPPER 2008)	53
Figure 3.2.15: Left:Plane strip drawing test: Contact pressure is perpendicular to the sheet displacement direction. Right: Effect of pressure and surface topography on the roughness evolution (PAYEN et al., 2012)	55
Figure 3.2.16: Left: Strip drawing test scheme. Right: Typical Abbot-Firestone curve before and after the strip drawing test (JONASSEN et al., 1997).....	56
Figure 3.2.17: Left: Bending under tension test scheme. Right: Typical Abbot-Firestone curve for the bearing area curve, before and after tension test (JONASSEN et al., 1997)	57
Figure 3.2.18: Effect of lubrication condition and length of sheet displacement on the roughness evolution during plane strip drawing test (RAHARIJAONA, ROIZARD, STEBUT, 1999)	57
Figure 3.2.19: Top: Evolution of area of contact ratio during loading procedure Bottom: Correlation between surface roughness (Ra) change and external pressure (MA et al., 2002).....	58
Figure 3.2.20: Evolution of the Abbott curve (right) in relation to the roughness flattening after a strip drawing pass. There is a decrease in the Rz, 2D-roughness parameter (RAHARIJAONA, ROIZARD, STEBUT, 1999)	59
Figure 3.21:Left: Typical FLD (major/ minor strains- measured in the plane of the sheet). Right: Strain path used for the tested samples with different width (BANABIC et al., 2000)	60
Figure 3.2.22: Left: typical automotive outer panel. Right: FLD strain diagram/ path (Simulations by <i>Autoform</i> , GM of Brazil, 2013).....	61
Figure 3.2.23: Major and minor strain simulation (left) and its corresponding FLD for a typical car outer panel stamping (right). Simulations by <i>Pamstamp</i> (SEKERES et al., 2010).	63
Figure 3.2.24: Left: thinning evolution simulation. Right: major stresses simulation. Simulations by <i>Pamstamp</i> (SEKERES et al., 2010)	63

Figure 3.2.25: Strain path of areas 1 and 2 are close to the fracture (fig.3.2.26)	63
Figure 3.2.26: Relationship between sheet metal thinning and 3D-roughness evolution, Sz (SEKERES et al., 2010).....	64
Figure 3.2.27: Evolution of 2D-roughness peak - valley Rt (top) and waviness peak – valley Wt (bottom) as a function of equivalent strain for specimens of a IF steel (for the 0°, 45° and 90° RD) (UNFER and BRESSAN, 2012)	64
Figure 3.2.28: Ten-point peak-valley 3D-roughness, Sz (Left) and core roughness depth, Sk (Rigth), as a function of ϵ_{vme} for a strain imposed by a Marciniack punch test (WICHERN et al., 2004)	65
Figure 3.2.29: Forming Limit Diagram for the HDG sheet steel with iso- ϵ_{vme} lines and roughness values for different strains (WICHERN et al., 2005).....	66
Figure 3.2.31: Surface roughness evolution as a function of strain for different strain paths imposed by the Marciniak punch deformation (WICHERN et al. 2005)	66
Figure 3.2.32: Major engineering strain vs. minor engineering strain for five different strain paths ranging from drawing to biaxial stretching and its correlation with fig. 3.2.31 (WICHERN et al. 2005 apud TAYLOR et al., 1985)	67
Figure 3.2.33: Blank Holding Force range (deep drawing test) versus r-values (KAWABE et al. 2002).....	68
Figure 3.2.34: FLD -Selected case of a pre-strain of 0.07 (7%) in equibiaxial strain followed by a plane strain path in comparison to the FLD for the as-received material without any pre-strain, for the plane strain condition (STOUGHTON, ZHU, 2004)....	69
Figure 3.2.35: a-Strain based failure criterion FLD; b-stress based failure criterion FLSD (UTHAISANGSUK, PRAHL, BLECK, 2007).....	70
Figure 3.3.1: The layers: from substrate to clear coat (LEX, 2010)	72
Figure 3.3.2: The four major painting requirements (DE MARK, 2013).	72
Figure 3.3.3: Sheet metal roughness transferred to the paint layer (CHOI et al., 2003)	75
Figure 3.3.4 : Result of the design of experiment(DOE). The most interesting result (for the present work), is the influence of approximately 6% of the steel quality on the paint appearance (KLENT, MINKO, 2008)	76
Figure 3.4.1: Left: The visibility of the structures is dependent on the observing distance. The curves in blue and in red show the wavelengths visible to the human eye at a distance of 40 cm and 3 m, respectively. Right: Wave scan evaluation	

method which is based on the wavelength range (SW - 0.3 to 1.2mm and LW – 1.0 to 12 mm), similar to the ones visible to the human eye at the distances of 40cm and 3 m, respectively (LEX, 2010)	78
Figure 3.4.2: <i>Rating(R)</i> is based on a range of wavelengths visible to the human eye at a distance of 40 cm (Short Wave - SW) and 3 m (Long Wave – LW).....	78
Figure 3.4.3: Top: The wave scan with five wavelength scales, W_a , W_b , W_c , W_d and W_e , instead of two, SW and LW from the “common” wave scan. Bottom: Two typical spectral curves. In <i>curve 1</i> , short waves are predominant and the associated reflected image with the haze effect and, in <i>curve 2</i> with predominant long waves and the corresponding reflected image, which is associated with the orange peel effect (LEX, 2010)	79
Figure 3.4.4: Individual <i>rating</i> of Reference Panels, ordered in the horizontal axis from worst to favorite (KLEMT, MINKO, 2008)	80
Figure 3.4.5: Ratio of different structure ranges SW and LW) (intensity x wave length in mm.) (LEX, 2010)	81
Figure 3.4.6: Influence of clear coat film thickness on paint appearance (LEX, 2010)	82
Figure 3.4.7: Influence of the steel quality on the final appearance. Clear coat (topcoat) appearance observed at a distance of 40cm (LEX, 2010).....	83
Figure 3.4.8: Effect of the reduction in scatter in the roughness parameter R_z after E coating and Clear coat (top coat) for 13 different steel sheets (BURGIN, 1996)	84
Figure 3.4.9: Toyota standard image clarity <i>ratings</i> and its correlation with the surface roughness profile (BURGIN, 1996).....	85
Figure 3.4.10: Appearance index A.I. versus peak count (Left) and R_a (Righth) (SCHEERS et al 1998).....	86
Figure 3.4.11: Left: Difference in surface topography of different types of texturized aluminium sheet. Right: Paint appearance for vertically coated panels with different substrate texturizing (tension=0 showing the orange peel, tension=24 showing the mirror-like appearance) (MILLER et al.,2000)	87
Figure 4.1: First run.	88
Figure 4.2: Equipment used in the first run. Technical details (for each equipment), are given in attachment 2.	93
Figure 4.3: Second run.	94

Figure 4.4: Equipment used in the second run, first step. Technical details (for each equipment), are given in the attachment 2.	94
Figure 4.5: Stamping sketches: Tooling and stamped part.	95
Figure 4.6: Region that has passed the draw bead.	95
Figure 4.7: Third run – first step	96
Figure 4.8: Samples submitted to painting after tensile testing. The position 1 is associated to a strain tending to zero (in the tensile testing). Positions 2 to 4 are zones with a continuously increasing strain (in the direction of the rupture zone).....	97
Figure 4.9: (a) Sketch of the “near“-plain strain condition testing. (b) Positions of 2D roughness and thickness evaluations.....	97
Figure 5.1.1: Comparison between sheet metal surface topography. Initial and end of the coil (SBT condition) for different skin pass reduction.....	100
Figure 5.1.2: 3D Roughness parameter evolution. Closed void (Vcl) and max. closed void ratio (α_{clm}) as a function of skin pass reduction % for the initial and end along the coil length (SBT condition).....	100
Figure 5.1.3: Comparison between sheet metal surface topography parameters for the initial and end positions, along the coil length (EDT condition), for different skin pass reductions.	102
Figure 5.1.4: 3D Roughness parameter evolution: closed void (Vcl) and maximum closed void ratio (α_{clm}) as a function of skin pass reduction %, for the initial and end along the coil length – EDT condition	102
Figure 5.1.5: Sheet metal surface topography for test 17 to 22.....	103
Figure 5.1.6: Comparison between sheet metal surface topography parameters (Average Rz and Pc) for the SBT and EDT roll conditions, for different skin pass reductions (Test conditions 1 to 16)	104
Figure 5.1.7: Ra standard deviation for the SBT and EDT roll conditions, for different skin pass reductions (Test conditions 1 to 16).....	105
Figure 5.1.8: Sheet metal surface topography evolution as a function of skin pass reduction. - EDT condition.....	106
Figure 5.1.9: Sheet metal surface topography evolution as a function of skin pass reduction. -SBT condition	106
Figure 5.1.10: Effect of sample size on the results of α_{clm} and Vcl parameters. Measurements were done in the same region (of the sample test n. 11)	107

Figure 5.1.11: Comparison between the bearing area ratio curves for SBT and EDT conditions	107
Figure 5.1.12: Best condition of Vcl and α_{lm} . Sample Nr 18.	108
Figure 5.2.1: First run - First step (same as fig. 4.1, left side).	109
Figure 5.2.2: Effect of sheet metal surface topography (Pc and Rz) on the paint appearance (rating), at the E coat stage	110
Figure 5.2.3: Effect of skin pass reduction on the rating (For tests 1 to 16)	110
Figure 5.2.4: Effect of initial and end of coil for both texturing methods on the rating (For tests 1 to 16)	111
Figure 5.2.5: Left: Tendency line for the 2D roughness parameters listed in table 6. Right: Rz versus rating and Pc versus rating for the 22 test conditions, at the E coat stage	112
Figure 5.2.6: Sheet metal surface topography for the best and the worst rating index/condition (at the E coat stage) and the corresponding 2D roughness parameters - Rz and Pc	113
Figure 5.2.7: First run - Second step (same as fig 4.1, right side).....	114
Figure 5.2.8: The layers: from substrate to clear coat of the best and worst paint appearance (rating) condition of fig. 5.2.5	115
Figure 5.2.9: Roughness profile evolution for the best and worst conditions and their rating index (measured in the first step)	116
Figure 5.2.10: Scanning electron micrographs of (a) pure alumina flakes and (b) alumina flakes coated with TiO ₂ (rutile) as used for pearlescent pigments (MAILE, PFAFF, REYNDERS, 2005)	117
Figure 5.2.11: SEM analysis of the base coat surface topography (top) and its EDS analysis showing the Titanium peaks (bottom). SEM Equipment: Zeiss EVO MA10	118
Figure 5.2.12: Rz roughness evolution along all painted layers.(worst and best samples).....	119
Figure 5.2.13: Spectral curves of the best and worst rating index conditions (mentioned in fig. 5.2.5). Top: E coat, primer and clear coat layers. Bottom: Clear coat layer with higher magnification. Measurements made with the wave scan dual equipment.....	120
Figure 5.2.14: Gloss evolution of the best and worst rating conditions (mentioned in fig. 5.2.5). Measurements made with the glossmeter equipment	121

Figure 5.2.15: DOI evolution of the best and worst rating index conditions (mentioned in fig. 5.2.5). Measurements made with the wave scan dual equipment.	122
Figure 5.2.16: Rating evolution of the best and worst rating conditions (Mentioned on fig. 5.2.5). Measurements made with the wave scan dual equipment	123
Figure 5.2.2.1: Second run (same as fig. 4.3)	123
Figure 5.2.2.2: Second run – First step	124
Figure 5.2.2.3: (Top figure) displacement (mm) x time(s) - Sheet metal surface topography of the “best” and “worst” conditions (and the final speed differences - angular coefficient) (Bottom figure)- Detail of the square shown in the top figure and their surface topographies respective to these curves	125
Figure 5.2.2.4: Second run – Second step.	126
Figure 5.2.2.5: Regions A and B	126
Figure 5.2.2.6: Effect of die contact deformation on sheet metal surface topography	127
Figure 5.2.2.7: Surface topography for region A of fig. 5.2.2.6. Ra and Rz were measured at the white dashed line. Measurements made with the Zygo New View 7000 equipment.....	127
Figure 5.2.2.8: Surface topography for region B of fig. 5.2.2.6 (2D and 3D roughness analysis). Ra and Rz were measured at the white dashed line. Measurements made with the Zygo New View 7000 equipment	128
Figure 5.2.2.9: 2D roughness Rz and Ra at the E coat stage in the regions A and B of fig. 5.2.2.5 (with and without surface roughness flattening).....	128
Figure 5.2.2.10: 3D roughness at the E coat stage in the regions A and B of fig. 5.2.2.5	129
Figure 5.2.3.1: Third run – First step (same as fig. 4.7).....	130
Figure 5.2.3.2: Roughness evolution Rz versus thinning evolution at the positions (1) one to (4) four (fig. 6.2.8).....	131
Figure 5.2.3.3: Gap between 2D and 3D roughness measurements (position shown in fig. 5.2.3.2).....	131
Figure 5.2.3.4: Upper triangle refers to analysis presented in fig. 6.2.15 and lower triangle to the analysis presented in fig. 6.2.16.(both triangles are about 2mm apart)	132

Figure 5.2.3.5: 3D surface topography at the position 4, upper triangle (fig. 5.2.3.4).	133
Figure 5.2.3.6: 3D surface topography at the position 4, lower triangle (fig. 5.2.3.4)	133
Figure 5.2.3.7: Sheet metal roughness evolution under tensile strain condition and its evolution through all the painted layers.	134
Figure 5.2.3.8: 2D Roughness evolution R_z versus thinning evolution at the positions (1) one and four (4) for the “near” plain strain condition sample.....	135
Figure 5.2.3.9: Strain path for the “near” plain strain testing condition	136
Figure 6.1.1: (same as figure 5.1.6) Comparison between sheet metal surface topography parameters (average R_z and P_c) for the SBT and EDT roll conditions, for different skin-pass reductions (test conditions 1 to 16).....	137
Figure 6.1.2: Degree of transfer as function of elongation for SBT and EDT (PAWELSKY, 1996)	138
Figure 6.1.3 (same as fig. 5.1.4): 3D Roughness parameter evolution: closed void (V_{cl}) and maximum closed void ratio (α_{clm}) as a function of skin pass reduction %, for the initial and end along the coil length – EDT condition.....	139
Figure 6.1.4 (same as fig. 5.1.2): 3D Roughness parameter evolution. Closed void (V_{cl}) and maximum closed void area ratio (α_{clm}) as a function of skin pass reduction % for the initial and end of the coil length (SBT condition)	140
Figure 6.1.5 (same as fig. 5.1.7): R_a standard deviation for the SBT and EDT roll conditions, for different skin pass reductions (Test conditions 1 to 16)	140
Figure 6.1.6 (same as fig. 3.1.10): An example of a section of a barrel surface of a texturized roll (TSCHERSCHE, NITSCHKE, 2012)	141
Figure 6.1.7 (same as fig. 3.1.6): Wear of the work roll during skin pass rolling and its effect on surface topography characterized by the 3D parameter V_{cl} and 2D parameter R_a (PFESTORF et al., 1998)	142
Figure 6.1.8 (same as figs. 5.1.3 and 5.1.6): Comparison between sheet metal 2D roughness parameters R_a for the initial and end positions along the coil length (EDT and SBT conditions), for different skin pass reductions.....	143
Figure 6.1.9: Comparison between 3D Roughness parameters, namely, closed void (V_{cl}) and maximum closed void ratio (α_{clm}) for EDT and SBT condition with the results in literature (VALENTIN et al., 2005)	144

Figure 6.1.10 (same as fig. 3.2.7): Lubricant reservoir (closed void) of EDT (Pretex) structure (GRETHE, 2013)	145
Figure 6.2.1 (same as fig. 5.2.2.5): Regions A and B.....	147
Figure 6.2.2: FEA - There was “no significant thinning” in the sample	147
Figure 6.2.3 (same as fig. 5.2.2.6): Effect of the die contact leading to the deformation on the sheet metal surface topography (present work). Sample Nr 12 (EDT condition for 1.0 % skin-pass reduction)	148
Figure 6.2.4 (same as fig. 3.2.16): Left: Strip drawing test scheme. Right: Typical Abbot-Firestone curve before and after the strip drawing test (JONASSEN et al., 1997)	149
Figure 6.2.5: Comparison between Abbot-Firestone curves before and after the strip drawing test from present work (fig. 6.2.3) and those from the literature (fig. 6.2.4).	149
Figure 6.2.6 (same as fig. 3.2.20): Evolution of the Abbott curve (right) in relation to the roughness flattening after a strip drawing pass. There is a decrease in the Rz parameter (RAHARIJAONA, ROIZARD, STEBUT, 1999)	150
Figure 6.2.7 (same as figs 5.2.2.7 and 5.2.2.8): Surface topography for regions A and B (fig.6.2.1).....	150
Figure 6.2.8: Approximately sample position for 2D and 3D roughness measurements	151
Figure 6.2.9 (sames as fig. 5.2.3.2): Evolution of the 2D-Roughness parameter - Rz versus thinning evolution, at the positions (1) one to (4) four (fig. 6.2.8)	152
Figure 6.2.10 (same as fig. 3.2.27): Comparison between present work and data from the literature (UNFER, BRESSAN, 2012) on the evolution of roughness (peak - valley Rt) with strain	152
Figure 6.2.11 (same as fig. 3. 3.2.29): Forming Limit Diagram for the HDG sheet steel with iso- ϵ_{vme} lines and the comparison of the roughness values for different strains. Data were taken from the literature (WICHERN et al. 2005) and from the present work.....	153
Figure 6.2.12 (same as fig. 3.2.31): Plott of Sq and iso- ϵ_{vme} for the HDG sheet steel (WICHERN et al. 2005). Results are compared	154

Figure 6.2.13 (same as fig. 3.2.28): Ten-point peak-valley roughness, Sz as a function of ϵ_{vme} for a strain imposed by the Marciniack punch test (WICHERN et al., 2004) and the results of the present work (tensile test condition).....	154
Figure 6.14 (same as fig. 5.2.3.4): Upper triangle refers to analysis presented in fig. 6.2.15 and lower triangle to the analysis presented in fig. 6.2.16.(both triangles are about 2mm apart)	155
Figure 6.2.15 (same as fig. 5.2.3.5): 3D surface topography at the position 4, upper triangle (fig. 6.2.14)	156
Figure 6.2.16 (same as fig. 5.2.3.6): 3D surface topography at the position 4, lower triangle (fig. 6.2.14)	157
Figure 6.2.17 (same as fig. 5.2.3.3): Gap between 2D and 3D roughness measurements (position shown in fig. 6.2.8).....	158
Figure 6.2.18: Effect of the tip radius of the stylus on the reduction of the amplitude of the irregularities of the surface roughness (DAGNALL, 1998).....	158
Figure 6.2.19: 3D surface roughness evolution. Left: Peak density (Spd) Right: Arithmetic mean peak curvature (Spc), as a function of sheet metal thinning	159
Figure 6.2.20: (Commercial) <i>Pamstamp</i> analysis: “Near” to plain strain condition - FEA analysis- left: true strain distribution. Right: strain path on the FLD for the “near” to plain strain sample. The star points are the ones measured on the sample (fig 6.2.21).	160
Figure 6.2.21 (sames as fig. 5.2.3.8): Evolution of the 2D-Roughness parameter-Rz versus thinning evolution at the positions (1) one and four (4)	161
Figure 6.2.22: Evolution of the 2D-Roughness parameter- Rz as a function of sheet thinning (for the tensile and the near-to-plain strain conditions)	162
Figure 6.2.23: Different strain paths for the tensile and the “near”-plain strain testing conditions	162
Figure 6.2.24: Contact pressure at region B (see fig 6.2.25) is about 150MPa, according to the model suggested by (MA et al., 2002)	165
Figure 6.2.25: (Commercial) <i>Pamstamp</i> analysis: Contact pressure in region B is about 150MPa	166
Figure 6.2.26 (same as fig. 3.2.2): Generalized Stribeck curve (LUBBING, HAAR, SCHIPPER, 1996).....	167

Figure 6.2.27 (same as fig. 5.2.2.3): (Top figure) displacement (mm) x time(s) - Sheet metal surface topography of the “best” and “worst” conditions (and the final speed differences - angular coefficient) (Bottom figure)- Detail of the square shown in the top figure and their surface topographies related to these curves	168
Figure 6.3.1: Samples from “best and worst” <i>rating</i> condition that has been obtained at each stage in the painting process.....	170
Figure 6.3.2: Cross section for both conditions at the clear coat stage and the comparison of layers thickness taken from literature (LEX, 2010).....	171
Figure 6.3.3 (same as fig. 5.2.9): 2D Roughness profile evolution for the “best and worst” <i>rating</i> conditions (measured in the first step)	172
Figure 6.3.4: Sheet metal 3D Roughness for the “best and worst” <i>rating</i> conditions (measured in the first step).....	173
Figure 6.3.5: Phosphate layer- 3D roughness for the “best and worst” <i>rating</i> conditions (measured in the first step).....	174
Figure 6.3.6: E coat layer - 3D Roughness for the “best and worst” <i>rating</i> conditions (measured in the first step).....	175
Figure 6.3.7: Base coat layer- 3D Roughness for the “best and worst” ratings (measured in the first step).....	176
Figure 6.3.8 (same as fig. 5.2.12): Evolution of the 2D roughness parameter- Rz along all paint layers (“worst and best” <i>rating</i> samples)	177
Figure 6.3.9 (same as fig. 3.4.8): Rz roughness evolution along all painted layers for 13 different steel sheets (BURGIN, 1996)	178
Figure 6.3.10 (same as fig. 5. 2.2.10): 3D roughness topography at the E coat stage in the regions A (without deformation) and B (with die contact deformation).....	179
Figure 6.3.11 (same as fig. 5.2.2.9): 2D roughness parameters- Rz and Ra, at the E coat stage in the regions A (without deformation) and B (with die contact deformation)	180
Figure 6.3.12 (same as fig. 5.2.3.7): Evolution of sheet metal roughness (under tensile conditions) and its evolution through all paint layers.....	180
Figure 6.4.1: Paint appearance (rating) as a function of the 2D roughness parameter Pc. Left –present work; Right - (SCHEERS et al., 1998).....	182

Figure 6.4.2: Paint appearance (rating) as a function of the 2D roughness parameter Ra. Left –present work; Right - (SCHEERS et al., 1998)	182
Figure 6.4.3 (same as fig. 5.2.3): Effect of skin-pass reduction (of the sheet) on the paint appearance (<i>rating</i>) - Effect of texturing condition	183
Figure 6.4.4 (same as fig. 5.2.4): Effect of skin-pass reduction (of the steel sheet) on the paint appearance (<i>rating</i>) – Comparing effect of sample position on the coil (for both SBT and EDT texturizing).....	184
Figure 6.4.5 (same as fig. 5.2.6): Worst and best <i>rating</i> surface – sheet surface topographies.....	184
Figure 6.4.6: Rating evolution at the different pain layers (“worst” x “best” <i>ratings</i>). 185	
Figure 6.4.7 (same as fig. 3.4.2): “traditional” rating equation, taking into account the LW (mostly) and SW intensities.....	185
Figure 6.4.8 (same as fig. 5.2.13): Spectral curves for the “best” and “worst” <i>rating</i> conditions measured at the different paint layers	186
Figure 6.4.9 (same as fig. 5.1.13): Spectral curves for the “best” and “worst” surface appearances, measured at the clear coat layer.....	187
Figure 6.4.10 (same as fig. 3.4.7): Comparing spectral curves according to sheet surface finish (LEX, 2010)	188
Figure 6.4.11: Spectral curves for different paint layers (LEX, 2010)	189
Figure 6.4.12 (same as fig. 3.3.4): Result of a design of experiment (DOE). The most interesting result (for the present work), is the influence of approximately 6% of the steel quality being related to paint appearance (KLENT, MINKO, 2008).....	190
Figure 6.4.13 (same as fig.5.2.14): Gloss evolution for the “best and worst” <i>rating</i> conditions.	191
Figure 6.4.14 – Sketch of a PALD (similar approach could be used for a FLSD)....	193

LIST OF TABLES

Table 3.2.1: Main aspects of the painting process used in the present work	74
Table 3.4.1: Top: The size of the surface structure / topography and its correlation with the wavelength of the reflected light. Bottom: Typical equipment and standards used to evaluate the paint appearance characteristics.....	77
Table 4.1: Materials and conditions.....	90
Table 5.1: Blank: 2D roughness measurements for all test conditions. Sample size L=1500mm, W=500mm. The values given in this table are the min. and max. values for the six measurements, for each test condition	98
Table 5.2: 3D and 2D roughness parameters and corresponding paint appearance (<i>rating</i>), at the E coat stage, for the twenty two (22) test conditions. Sample size for the 3D roughness measurements was approximately 1.5x1.5 mm	109
Table 5.2.1: 3D roughness parameters (α_{clm} , v_{cl}) for the best and worst paint appearance (<i>rating</i>) condition of fig. 5.2.5	112
Table 7.5.1: The best sheet metal surface topography (for the present research condition) for stampability and paint appearance and some of the main process variables that influences it.	196

SUMMARY

1	INTRODUCTION	26
2	AIM OF THE PRESENT WORK.....	28
2.1	SCOPE	28
2.2	RESEARCH LIMITATIONS.....	30
3	LITERATURE REVIEW	31
3.1	SURFACE TOPOGRAPHY BEFORE STAMPING.....	32
3.1.1	SURFACE TEXTURING OF THE SKIN PASS ROLLS	32
3.1.2	SKIN-PASS REDUCTION.....	35
3.2	SURFACE TOPOGRAPHY AFTER STAMPING.....	42
3.2.1	FRICTION.....	43
3.2.2	SURFACE TOPOGRAPHY.....	45
3.2.3	LUBRICANT	50
3.2.4	TEMPERATURE.....	52
3.2.5	TOOL SURFACE, CONTACT PRESSURE AND SHEET METAL SLIDING VELOCITY	53
3.2.6	SHEET METAL CHEMICAL TREATMENT	54
3.2.7	SLIDING CONDITIONS	54
3.2.8	STRAIN PATH	59
3.3	PAINTING.....	71
3.4	PAINT APPEARANCE	76
3.5	SUMMARY OF THE LITERATURE REVIEW	87
4	MATERIALS AND METHODS	90
4.1	FIRST RUN.....	92
4.1.1	THE FIRST STEP OF THE FIRST RUN	92
4.1.2	THE SECOND STEP OF THE FIRST RUN	92

4.2	SECOND RUN.....	93
4.2.1	THE FIRST STEP OF THE SECOND RUN	94
4.2.2	THE SECOND STEP OF THE SECOND RUN	95
4.3	THIRD RUN	95
4.3.1	THE FIRST STEP OF THE THIRD RUN.....	96
4.3.2	THE SECOND STEP OF THE THIRD RUN.....	97
5	RESULTS	98
5.1	MATERIAL CHARACTERIZATION (AS RECEIVED CONDITION).....	98
5.2	TESTS.....	108
5.2.1	FIRST RUN.....	108
5.2.1.1	THE FIRST STEP OF THE FIRST RUN	108
5.2.1.2	THE SECOND STEP OF THE FIRST RUN	114
5.2.2	SECOND RUN.....	123
5.2.2.1	THE FIRST STEP OF THE SECOND RUN	123
5.2.2.2	THE SECOND STEP OF THE SECOND RUN	126
5.2.3	THIRD RUN	130
5.2.3.1	THE FIRST STEP OF THE THIRD RUN.....	130
5.2.3.2	THE SECOND STEP OF THE THIRD RUN.....	134
6	DISCUSSION	137
6.1	SURFACE TOPOGRAPHY BEFORE STAMPING.....	137
6.2	SURFACE TOPOGRAPHY AFTER STAMPING.....	146
6.2.1	SURFACE TOPOGRAPHY EVOLUTION DUE TO DIE CONTACT (SURFACE FLATTENING) .	146
6.2.2	SURFACE TOPOGRAPHY EVOLUTION DUE TO SHEET METAL STRAIN WITHOUT DIE CONTACT	151
6.2.2.1	TENSILE STRAIN CONDITION	151
6.2.2.2	“NEAR” TO PLAIN STRAIN CONDITION	159
6.2.2.3	INTER-RELATIONSHIP BETWEEN THE TESTING TWO CONDITIONS: WITH AND WITHOUT DIE CONTACT	163

6.3	PAINING.....	169
6.3.1	PAINTED BEFORE STAMPING.....	170
6.3.2	PAINTED AFTER STAMPING	179
6.3.2.1	DEFORMED WITH DIE CONTACT	179
6.3.2.2	DEFORMED WITHOUT DIE CONTACT	180
6.4	PAINT APPEARANCE	181
6.4.1	PAINTED BEFORE STAMPING.....	181
6.4.2.1	PAINT APPEARANCE (RATING) AT THE E COAT STAGE.....	182
6.4.2.2	PAINT APPEARANCE (RATING) UP TO CLEAR COAT STAGE	184
6.4.2	PAINTED AFTER STAMPING	191
6.5	SUGGESTION FOR FUTURE WORK.....	192
7	CONCLUSIONS	194
	REFERENCES	197
	APPENDIX 1 – STAGES OF THE PAINTING PROCESS	205
	APPENDIX 2 – 3D ROUGHNESS RESULTS.....	216
	ATTACHMENT 1 – 2D AND 3D ROUGHNESS PARAMETERS	222
	ATTACHMENT 2 – LIST OF EQUIPMENTS	236

1 INTRODUCTION

The visual appearance of the painted steel sheet surface has always been given close attention because it is often experienced as a first expression/evaluation of the quality of the product towards the end-user, especially in the automotive and consumer appliances industry. It has a strong impact on the perceptual quality of the customer whose definition is the quality impression in the first 10 min from a purchase consideration point of view. Emotions in the potential buyer during this period will strongly influence in the purchase decision (fig. 1.1). As in most relationships the first impression is the key for its continuity. Therefore, perceptual quality / visual appearance has a direct link to financial performance. According to Aeker, 2002 apud Gerhart, 2011 “perceived quality is the single most important contributor to a company’s ROI (Return on Investment), having more impact than Market Share, R&D, or Marketing Expenditures”.

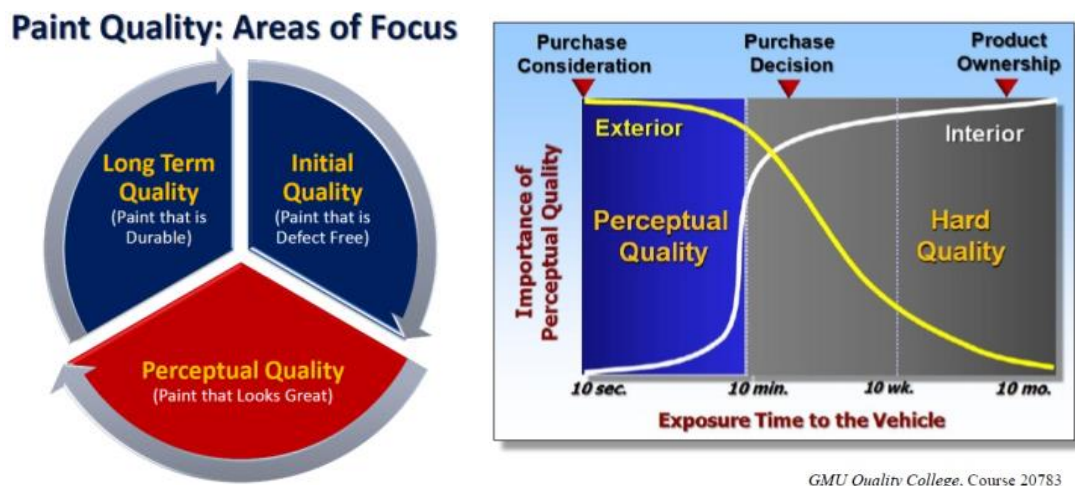


Figure 1.1: Paint quality and importance of perceptual quality in vehicles (GERHART, 2001).

In the left diagram of fig. 1.1 it may be noticed that paint quality is evaluated in three ways: perceptual quality (product appearance), initial quality (paint that is defect free in the first weeks) and long term quality (related to paint durability). On the right side of the same figure it can be seen that the weight of exterior and interior quality (of the vehicle for the customer) varies/changes from the purchase consideration through purchase decision and going towards ending / ownership. As in any relationship, exterior (of the vehicle) has the major influence at the beginning of time (first

impression of the product). Conversely, as time goes by, interior overcomes exterior and becomes of major importance.

More recently however, sheet steel manufacturers (and mainly end users) have also been focusing their attention on the visual appearance of the painted steel sheet as soon as it was clearly established that there was an influence of steel sheet topography on properties such as “orange peel” and image clarity. In fig. 1.2 the loss of contrast, sharpness and distinctness of the reflected image on the car hood can be related to sheet steel surface topography (TRUNG, 2011).

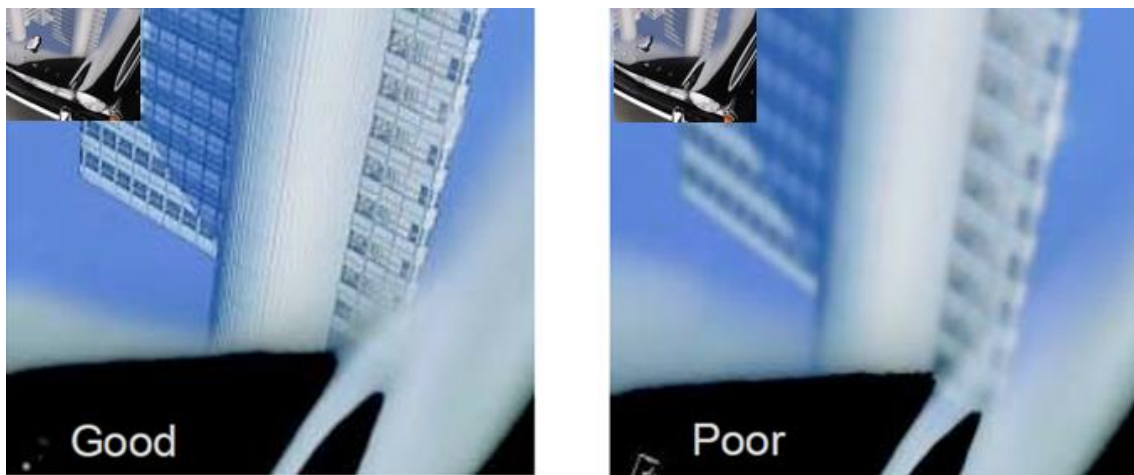


Figure 1.2: Quality of the reflected image on the car hood. “Good” has a higher level of image details while the “poor” presents a hazy image (TRUNG, 2011).

The aspect of the hazy image presented in fig. 1.2 is caused by the interaction (reflection) of light with the surface (with its small structures - lower than 0.1mm height), scattering the light rays. This phenomenon will be explained in greater detail in another chapter, under the topic *paint appearance*.

The main concern related to the paint appearance and stampability of the steel sheet metal may be summarized in fig. 2.1, which shows a typical car stamping in the FLD - Forming Limit Diagram (green area) and in the same stamping the concern related to paint appearance, measured in the dashed squares regions. It must be observed that stampability and paint appearance have to work together to attain the end result of having the appropriate (and simultaneous) performance.

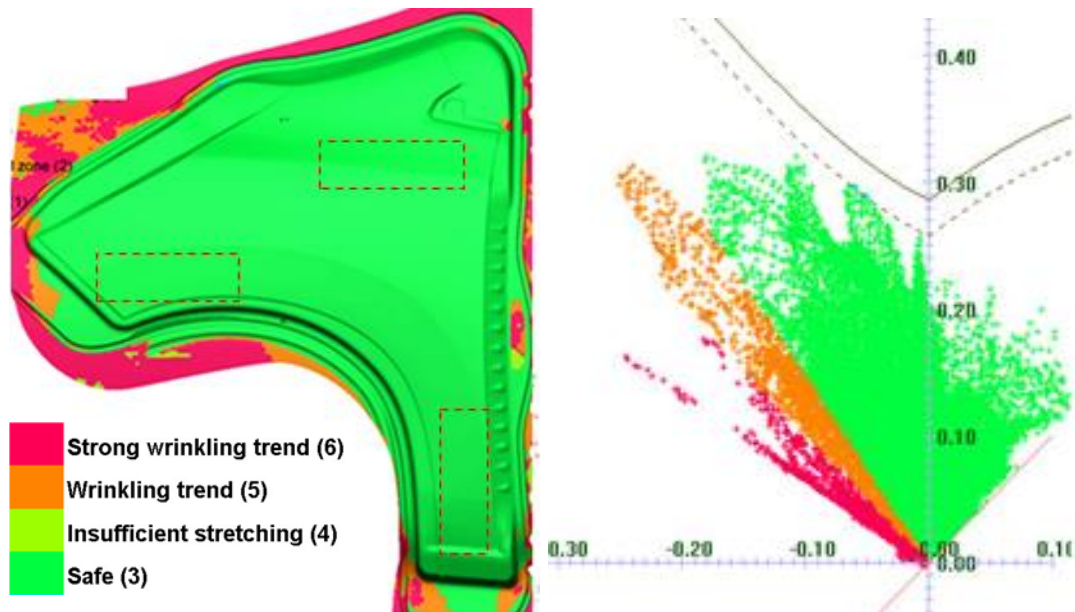


Figure 1.3: FLD of a typical car stamping

Although the Forming Limit Diagram (FLD) “says” that stampability is adequate, it did not “say” anything about paint appearance. Therefore, it might call for a Paint Appearance Limit Diagram (PALD). It seems this type of diagram would be appropriate in order to avoid “surprises” about the paint surface quality just after the car has been painted.

It is the purpose of the present work to establish a link between the material stampability and paint appearance.

2 AIM OF THE PRESENT WORK

The aim of the present research work is to study the inter-relationship, under controlled industrial conditions, among variables such as skin pass reductions, surface topography (characterized by 2D and 3D) roughness parameters, stampability and paint surface finish quality for automotive steel sheet stampings. The main goals are listed below:

- 1 - Compare roll texturing methods SBT and EDT in terms of *stampability* (blank speed) and *paint appearance* (rating);
- 2 - Determine experimentally the best skin pass reduction in terms of degree of transfer (2D x 3D roughness), *stampability* (blank speed) and *paint appearance* (rating);
- 3 - Evaluate the effect of the surface topography before stamping (2D x 3D roughness) on the *paint appearance* (rating, DOI, spectral curves and gloss);
- 4 - Evaluate the effect of the surface topography after stamping (2D x 3D roughness) (strain with and without die contact) on *the paint appearance* (2D x 3D roughness);
- 5 - Determine the optimum range of the 2D and 3D roughness parameters in terms of *paint appearance*.

2.1 Scope

Fig. 2.1 summarizes, in a didactic way, the four main topics of this research work based on the sheet metal roughness evolution. It starts from the skin-pass rolling, where texturing (or texturizing) is impressed on sheet surface, stamping and goes until the last layer of the painted sheet metal called clear coat (also known as top coat) and its correlation with the paint appearance.

The literature review will be divided into four major divisions, namely: surface topography before stamping, surface topography after stamping, painting and paint appearance.

Materials and methods were planned in such a way as to allow the analysis of the effect of surface topography (before stamping and after stamping) on the painted layers and on the paint appearance. The following chapters, namely: results, discussion and conclusions, also obey the same division as the one made in the literature review.

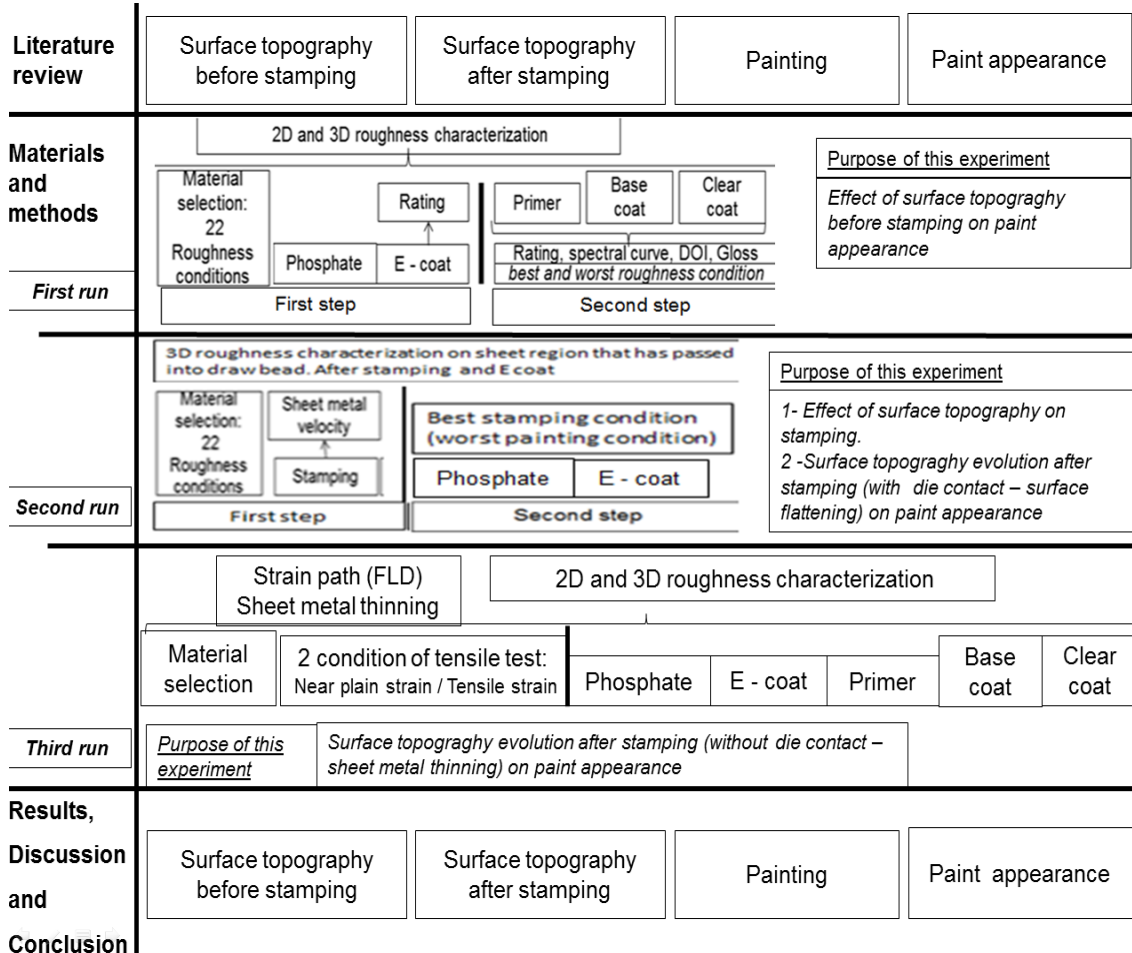


Figure 2.1: Macro vision of the present research work.

Furthermore, appendix one provides information concerning the painting process while appendix two information on 3D roughness results.

Attachment one summarizes technical information taken from the literature related to 2D and 3D roughness parameters and attachment two, also taken from technical literature, supplies technical data on the equipment that have been utilized in this research work.

2.2 Research limitations

The results presented here are specific to the materials (from various mills) and painting process (GMB plant) that have been used in this research. They are qualitative/quantitative preliminary results. The key objective is to assess the main variables that link stampability and paint appearance using low carbon steel sheets. Statistic validation and physical modeling will be performed in future research work.

3 LITERATURE REVIEW

From a birds-eye point of view, Fig. 3.0.1 shows a summary of the production macro processes linked to the production of sheets for a car body. It clearly can be visualized that all of them, some more, other less, will affect paint appearance. Quality of raw materials and the processes involved in their transformation will determine the cleanliness, grain size, crystallographic texture, etc. which, in turn, will affect stampability (formability), paintability and the car body durability / appearance.

The present work will focus attention mainly on operations starting from the skin-pass rolling, going through stamping and finalizing at the painting stage.

Skin-pass rolling prints the surface topography on the sheet metal which, in turn, evolves during stamping and reflects on the painting processes / surface quality / paint appearance.

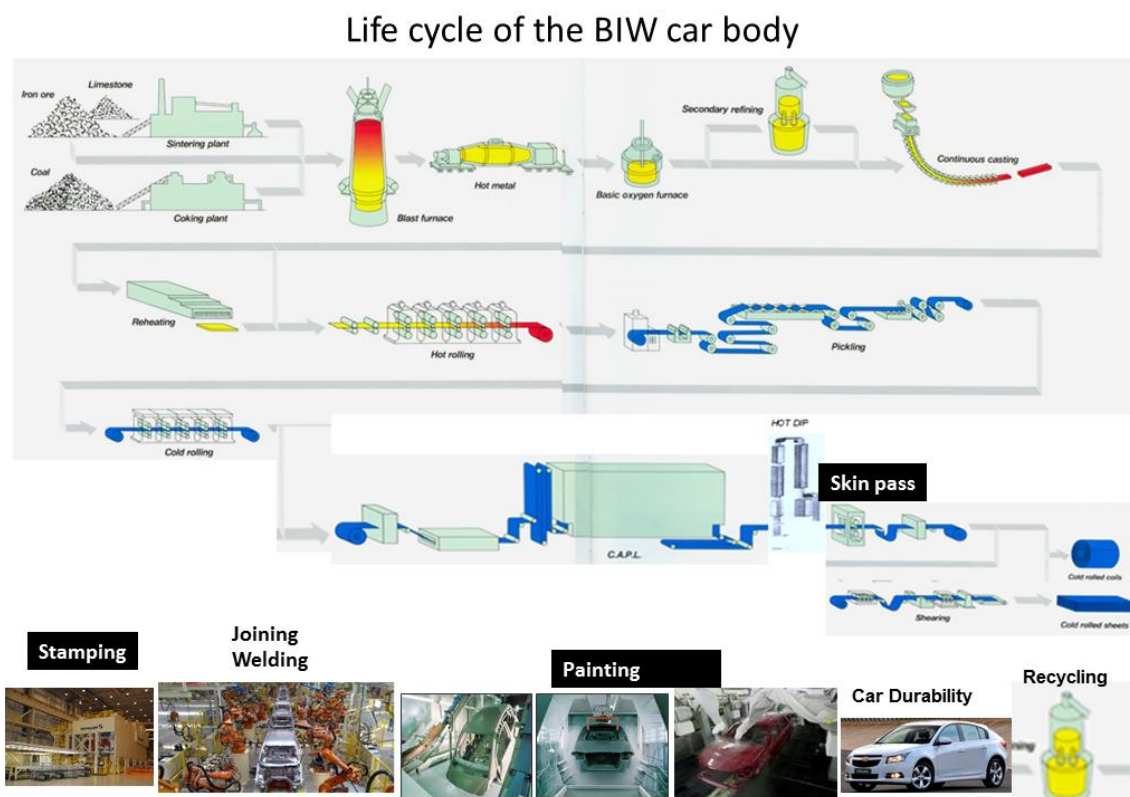
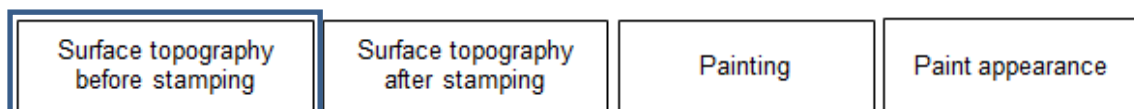


Figure 3.0.1: From the ore to the end product (car body), each process has its contribution to the paint quality. (BIW = body-in-white)

Present work is divided into four chapters, where the major factors/variables influencing roughness evolution and its characterization are presented. From texturing (or texturizing) methods and surface topography impressions onto the sheet metal and all variables that could affect the surface topography evolution until the final painting, are all listed.

In the following it will be presented, in some greater detail, the items concerning the roughness evolution that have been presented in fig.3.0.1.



3.1 Surface topography before stamping

In this chapter it will be presented the main methods applied for surface texturing (also known as surface texturizing), as well as the advantages / disadvantages of each of them. It will also be explained (for the most used texturing method), the main variables affecting its process and some solutions applied to optimize its texturing, using as a criteria the sheet metal stampability and paintability. It also will be shown the effect of the skin-pass reduction (or % of sheet elongation), during skin-pass rolling on the degree of surface topography transference from the skin-pass roll to the sheet metal.

3.1.1 Surface texturing of the skin pass rolls

The **surface texturing** of steel sheets in metal forming is commonly applied by the skin-pass rolls which can be roughened by several alternative methods, as summarized in fig. 3.1.1 (STAEVES,1998).

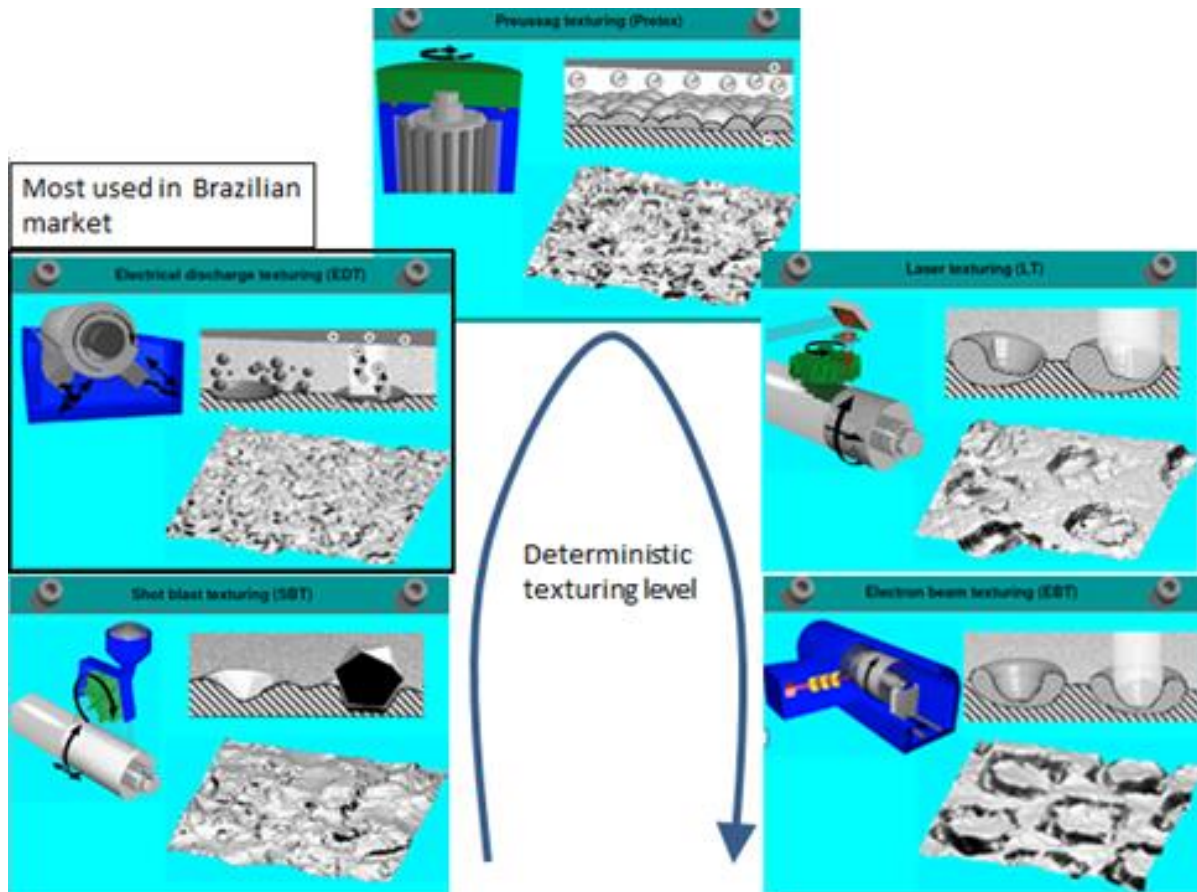


Figure 3.1.1: Roll texturing methods: From stochastic ones (as SBT, EDT and Pretex) to the deterministic ones (as LT and EBT) (STAEVES,1998).

The function of the generated surface by these different methods is to influence the tribological properties in the forming process and to achieve an excellent paint appearance on the finished product. As the common stochastic structures like Shot Blast Texturing (SBT) do not meet all requirements of the production line on the way to the final product, several new structures have been developed such as: EDT (Electro Discharge Texturing), LT (laser texturing), EBT (electron beam texturing), etc. (PFESTORF et al., 1998; ASPINWALL et al, 1992; JONASSON et al., 1997; DEMARE et al., 1997).

In particular, rolling mill rolls finished by Electrical Discharge Texturing (EDT) are the most used in the manufacturing of steel sheet metal for the global automotive market due to its good productivity, repeatability and cost (as compared to the alternative methods mentioned above), associated with a non-directional surface topography resulting in good stampability and paintability. Further explanations will be given in the next topic “skin-pass”. Furthermore, EDT strip topography is able to retain more

lubricant during subsequent forming processes (JONASSON et al., 1997). Consequently, formability is improved with less galling or pick-up / scoring of the strip material.

It should be pointed out that automobile manufacturers have strict requirements for surface topography parameters of cold rolled sheet metal used for the body sheet metal. So, the appropriate selection of operating parameter levels on the mill rolls are essential and allow a limited degree of independence in specifying surface topography (WARRENDER et al., 2005; TERPÁK et al, 2010).

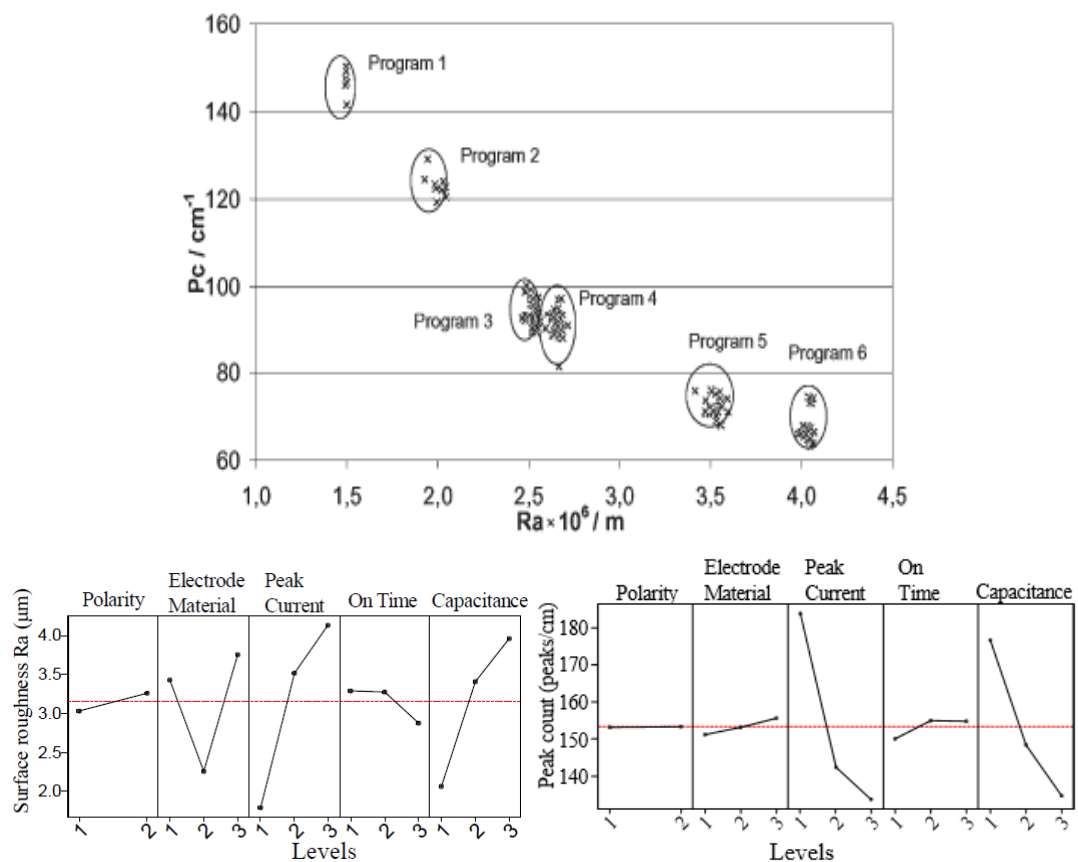


Figure 3.1.2: Top: typical EDT Programs. Bottom: EDT main process variables in order to set up typical EDT Programs. Pc =peak count measured in 2D; Ra=surface roughness measured in 2D (WARRENDER et al., 2005; TERPÁK et al, 2010).

In fig. 3.1.2 it is typically shown the EDT process versatility/flexibility in obtaining different surface topographies (by varying its operating parameters), in order to fulfill the different requirements from the automotive industry.

3.1.2 Skin-pass reduction

After the roll texturing process has been finished, the roll-surface structure has to be transferred to the sheet metal. This process is obtained through the skin-pass rolling. Previous studies (PAWELSKI et al., 1994) performed on the transfer characteristics of the different work roll surfaces onto the sheet metal in terms of skin-pass reductions (temper rolling), are summarized in fig. 3.1.3.

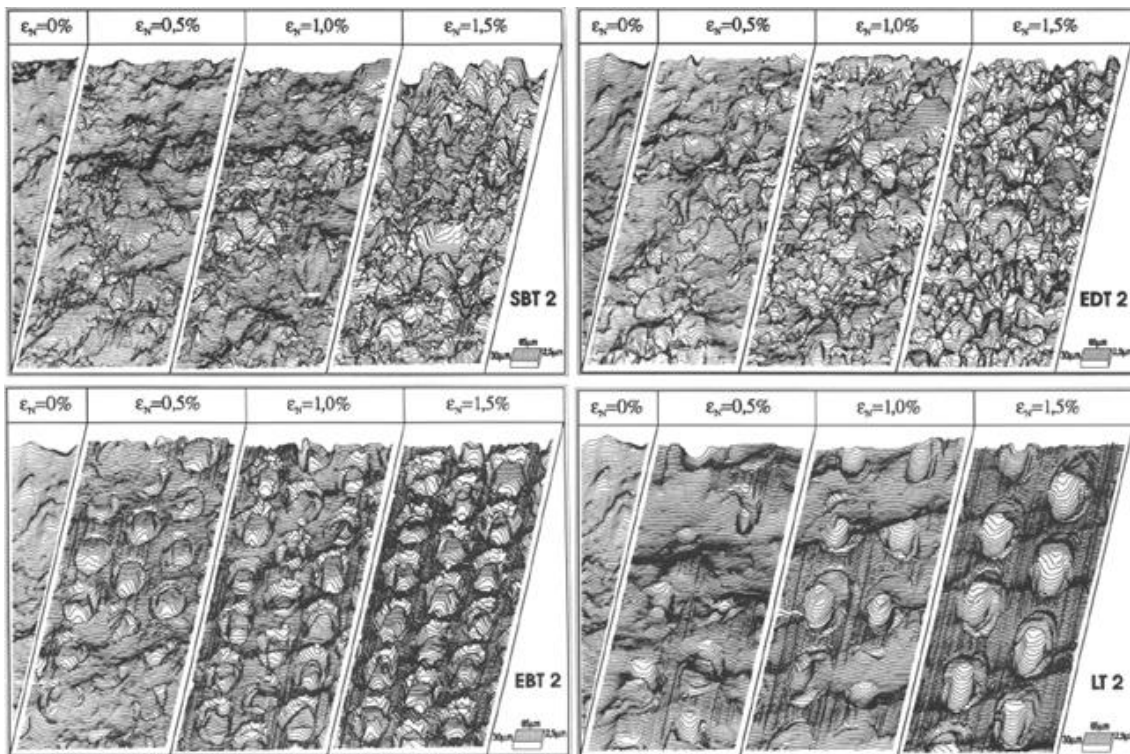


Figure 3.1.3: The illustrations indicate the development of the sheet-surface structure for temper rolling (skin-pass) with different elongations, using the work-roll structured by the SBT, EDT, EBT and LT methods (PAWELSKI et al., 1994).

Following, the concept and correlation between elongation and skin pass reduction is given. In fact, the variation in roll speed, that is observed at the entry and exit of the roll mill stand in the skin-pass rolling operation, enables establishing the strip speed variation (or strip elongation) and the consequent thickness variation, i.e., the thickness reduction in the specific rolling pass.

It has been clearly shown (PAWELSKI et al., 1994), that the degree of transfer is dependent on the elongations (i.e., skin-pass reductions). The skin-pass reduction upper limit should be the saturation (in the degree of transfer, as per fig. 3.1.4).

Ideally, skin-pass reduction would be a compromise between work roll life and sheet metal (SM) yield strength (negative side: higher skin-pass reduction causes higher roll wear rate and increase SM yield strength) and stamping / painting performances (positive side: higher skin-pass reduction increases the surface topography transference degree, which in turn improves the stamping / painting performances), as will be explained in further detail in the following.

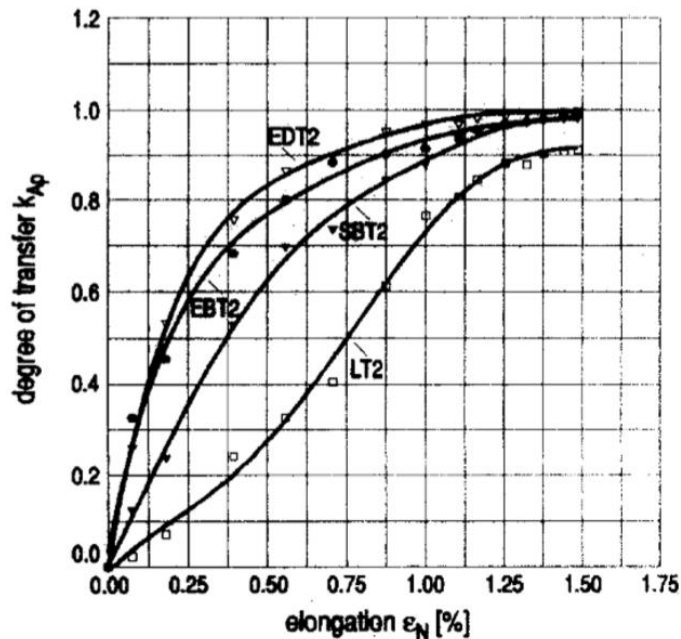


Figure 3.1.4: Transfer characteristics for dry temper rolling (skin-pass) of a hot-dip galvanized (HDG) IF type steel - FeP05 (PAWELSKI et al., 1994).

Another important aspect, as pointed out by Pawelski et al. (1994) (shown in fig. 3.1.4), illustrates the degree of transference for different (surface) textures from the rolling mill rolls onto the steel sheet as a function of the strip elongation. There exists a saturation level, mainly for the EDT texturized sheets. In practical terms this means that finish rolling can be performed with smaller skin-pass reductions (hence decreasing the roll wear and consequently decreasing the roughness mean standard deviation of the steel sheet, as will be seen in the following, in greater detail) and improvements in the degree of transference, if compared to the other texturizing methods. Furthermore, the degree of transference for the deterministic texturizing method becomes impaired due to the simultaneous action of the surface topography and the lubrication, as shown in fig. 3.1.5. The surface topography is designed to produce a beneficial effect for the stamping and the painting subsequent operations

(as for instance, the closed volumes are printed onto the sheet in order to act as mini-reservoirs for the oil which is pressurized during stamping and acting as a continuous thin oil film). Conversely, these mini-reservoirs become detrimental because they retain oil, hence hindering the degree of roughness transference.

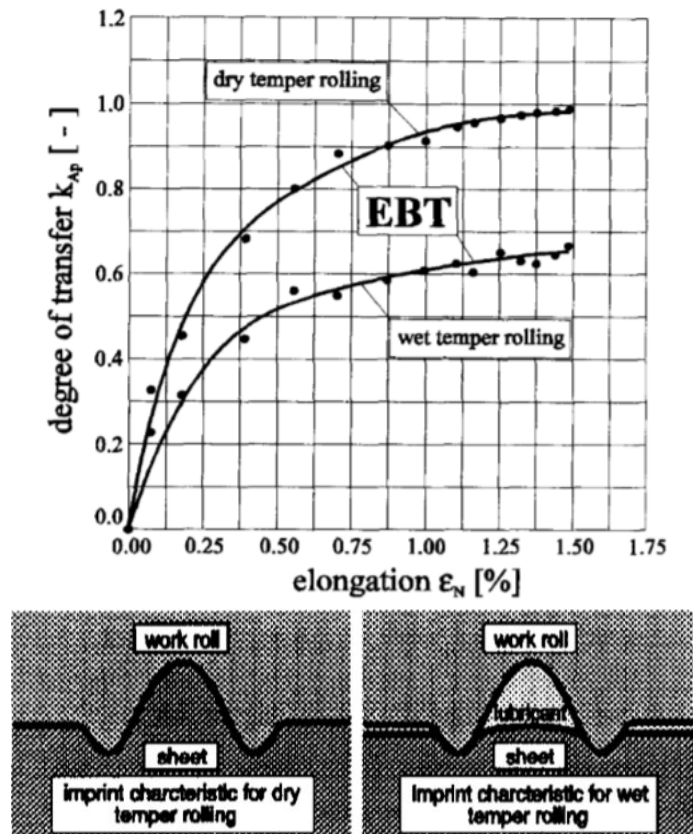


Figure 3.1.5: Transfer characteristics for dry and wet temper rolling (skin-pass) of a hot-dip galvanized steel $FePO_5$ using EBT- textured work rolls. (PAWELSKI et al.,1994 and BFINTEN et al.,1996).

Another disadvantage of the deterministic structures is the fact that when the final steel sheet does not attain its final waviness specification, some steel mills adopt the common praxis (for the stochastic structures), of a re-rolling operation for the necessary corrections. For deterministic structures this approach cannot be employed, because it is practically impossible to maintain the same surface deterministic pattern after two or more skin-pass reductions, hence incurring in major production losses. Due to all these factors it has been observed that the LT, EBT and SBT have ceased to be attractive techniques and the major effort is, nowadays, concentrated solely on the EDT texturing process.

Nevertheless, even due to the heavy investments related to the increase in stampability, paintability and process stability, that have been carried out through the research on deterministic structures that eventually resulted in a non-viability in the industrial scale (as per the reasons pointed out above), they left behind a very positive heritage mainly linked to the simultaneous development of the techniques related to surface characterization(topography) in 3D , as well as the development of new parameters that could be better related to the stamping and painting process parameters. From Attachment 1 (roughness parameters glossary), as some examples, we can point out the α_{clm} (maximum closed void area ratio) and the V_{cl} (volume of closed voids), both parameters having a good relationship with the friction coefficient used in the forming processes. These will be explained in further detail in the topic 3.2.2, associated with the effect of surface topography on friction. In general lines, fig. 3.1.6 illustrates an example related to the variation of these parameters as a function of the work roll life during the skin-pass operation.

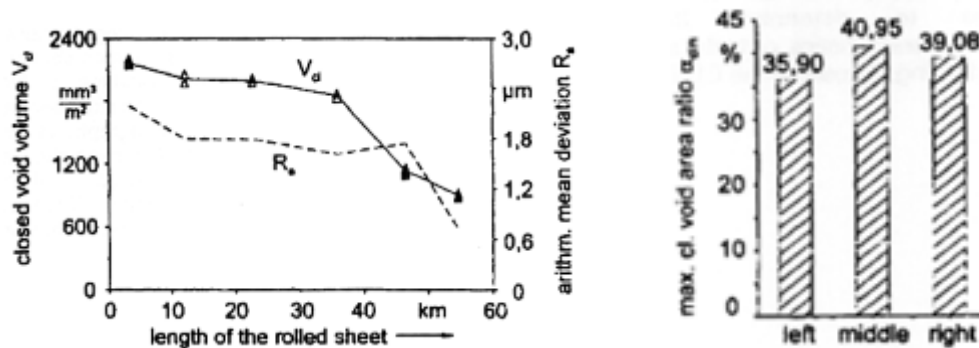


Figure 3.1.6: Left: Wear of the work roll during skin-pass rolling and its effect on the surface topography. Right: Roughness deviation along the coil width. (GEIGER, ENGEL, PFESTORF, 1997 (left); PFESTORF et al., 1998 (right)).

The accentuated decrease in the roughness parameters may be observed, mainly due to roll wear as well as a slight variation along the coil/strip width.

Once the EDT method has been elected globally as being the most viable texturizing method for skin-pass rolling (of the mill rolls, for automotive panels), various research fronts have been established searching for a decrease in the roughness standard

deviation in the sheet, in order to increase process stability during stamping and painting, as well as optimizing the roughness parameters (to increase process performance). One of the ways that has been utilized is linked to the usage of an electrolytic chromium layer deposited onto the texturized roll. The thickness layer may vary from 3 to 30 μm (GRETHE, 2013), with a hardness in the range of 800 to 1200HVN (MAYER, 2013; SIMÃO, ASPINWAAL, 1999). Apart from the hardness increase due to this Cr-layer, the inherent micro-cracks (that are inherent and observed in the layer, due to the process), have been pointed out as being important for the oil-retention and additional lubrication during skin-pass rolling (MAYER, 2013). Practical data obtained from steel mills have shown a threefold increase in roll life of the texturized Cr-plated rolls (OLIVEIRA, 2013). Further, Simão and Aspinwaal (1999) have shown that roll performance is a function of roll roughness, see fig. 3.1.7. It may be observed that as the roll roughness decreases the gain in roll life, associated to the chromium plated versus plain temper, also increases. This difference in roll life related to roll roughness has been associated with the breaking of the roughness peaks (TSCHERSCHKE, NITSCHKE, 2012).

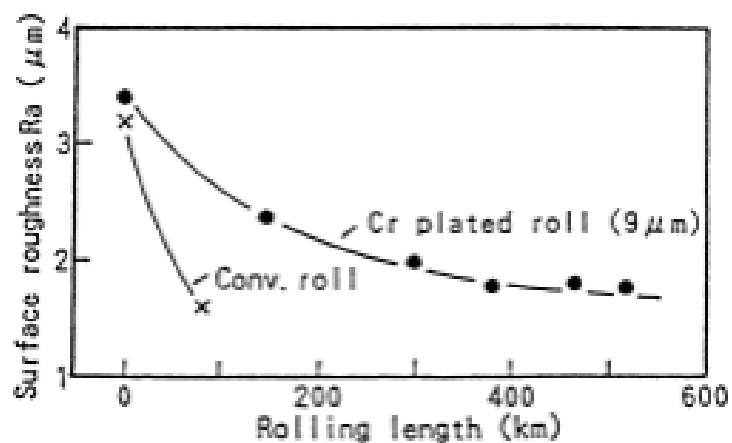


Figure 3.1.7: Comparative performance of chromium plated and plain temper mill rolls (SIMÃO and ASPINWALL, 1999).

Another advantage of working with lower roughness rolls is evidenced in fig. 3.1.8.

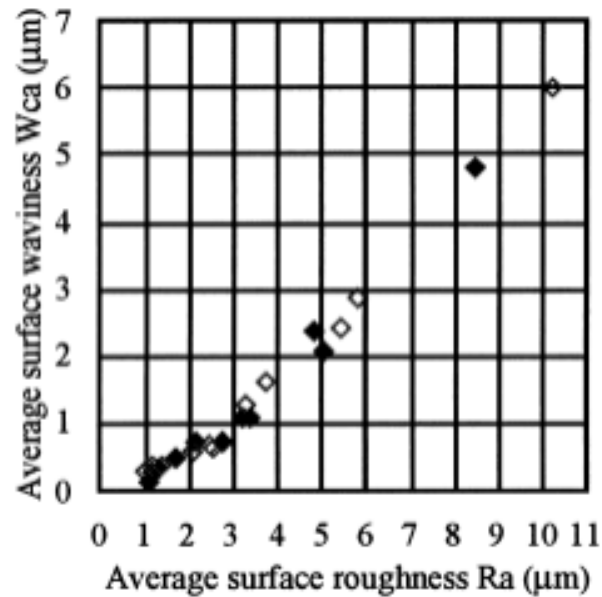


Figure 3.1.8: Relationship between the average surface roughness Ra and average surface waviness Wca for the different plain EDT and Cr-plated EDT roll specimens (◆ plain EDT; ◇: Cr-plated EDT) (SIMÃO and ASPINWALL, 1999).

From this literature it may be observed that as the roll surface roughness Ra increases, the value of Wca (average surface waviness) also increases. This is an important issue because Wca has a deleterious effect on paint appearance (orange peel) which will be described in greater detail in chapter 3.4

These two aspects, namely the rolling mill roll life increase and the improvement in the lubrication of the roll, have conducted to the decrease in the roughness mean standard deviation along the coil, as shown in fig.3.1.9.

Just for an initial general information, in the case of the present work, the range of the sheet metal roughness Ra, varied from 1.66μm (First coil) to 1.41μm (last coil), hence coherent with this figure.

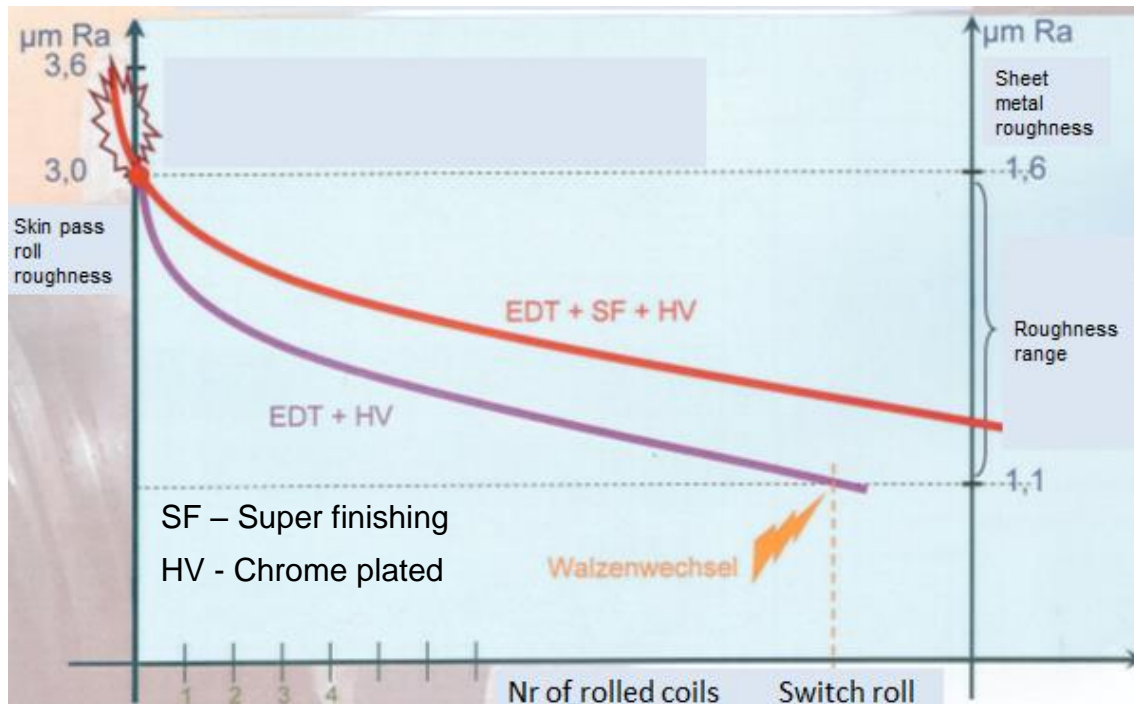


Figure 3.1.9: Variation of steel sheet roughness (within the usual practical roughness range of 1.6 to $1\mu\text{m}$) as a function of the number of processed coils with Cr-plated EDT rolls (right scale) and the initial roll surface roughness (left scale) (MAYER, 2013).

Further, in the fig. 3.1.9 it may also be observed that the skin-pass roll life is determined by the steel sheet surface roughness (its minimum being $Ra=1.1\mu\text{m}$). A further relevant point is related to the ratio roll roughness / sheet roughness provided by the Cr-plated EDT process, as shown in this figure, being roughly 2/1, i.e., for a roll roughness of $Ra=3\mu\text{m}$ a sheet roughness of $1.6\mu\text{m}$ is obtained. As the roll is used in operation, both roughness (of the roll and that of the sheet) decrease due to wear out, decrease to a minimum in the sheet roughness range, in this case of about $1.1\mu\text{m}$. The other curve (EDT+SF+HV), is related to the positive effect on the roll life due to a new process where the Cr-plated EDT roll receives a supplementary belt grinding finish (basically the removal of the high peaks (fig.3.1.10) of the roughness profile), commercially known as “*superfinishing*” (TSCHERSCHKE, NITSCHKE, 2012)

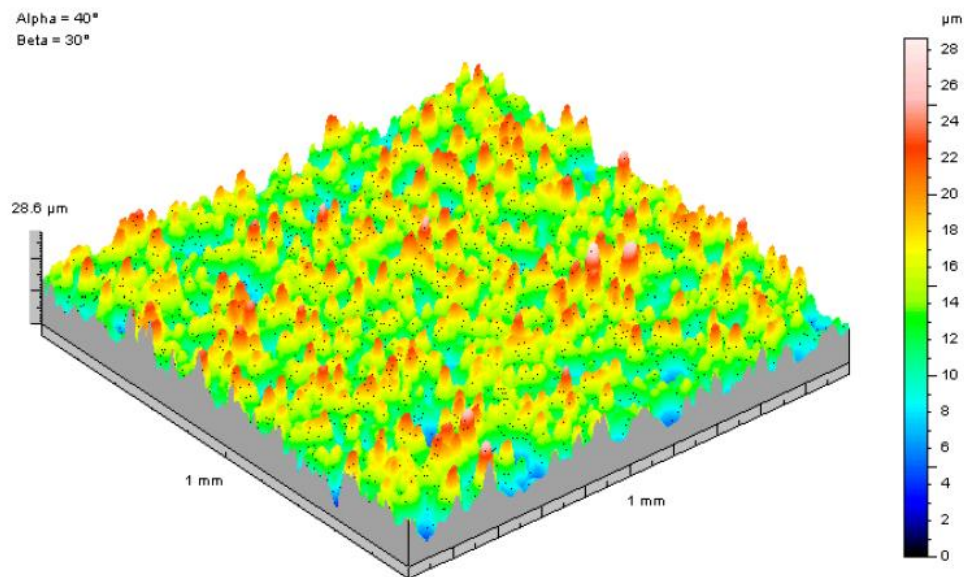


Figure 3.1.10: Example for a section of a barrel surface of a textured roll. (TSCHERSCHE, NITSCHKE, 2012).



3.2 Surface topography after stamping

When paint appearance is in discussion a question always arises: How much does the stamping process affect paint appearance? There is already a consensus that the answer is associated with roughness changes during the stamping process (GRETHE, 2013; SCHEERS et al 1998; MILLER et al.,2000; LEX, 2010). Therefore, didactically, one could say that the two main sources of roughness changes are the ones associated with the contact between tool and the sheet metal and the other one associated with the sheet metal strain path on the FLD. However, the variables related to both roughness change sources are quite similar and have a very close inter-relationship, as it will be summarized in the following, and are mainly concerning the topics on: friction (3.2.1), sheet metal surface topography (3.2.2), lubricant (3.2.3), temperature (3.2.4), tool surface, contact pressure and sheet metal sliding velocity (3.2.5), sheet metal chemical treatment (3.2.6), sliding conditions (3.2.7) and strain path (3.2.8)

3.2.1 Friction

The control of friction is essential in forming processes, mainly because friction determines the properties and the geometry of the obtained piece, even its operation feasibility (PAYEN et al., 2011). During forming operations the steel sheet is forced to slide against the surfaces of the tools. In these tribo-contacts complex phenomena take place and many parameters are interacting, one of them is the surface topography. Surface roughness on the sheet and on the tools causes the contact to take place on a limited number of real contact areas (VERMEULEN and SCHEERS, 2001). According to Klimczak and Jonasson (1994) the ability of steel sheets to develop a large real contact area in the tool/sheet interface may be combined with closed voids that ensure better lubricating conditions, thus preventing galling (lubrication failure occurring at low speed and/or high pressures). Closed voids are described in greater detail in the attachment 1, related to the roughness glossary.

When steel sheets are coated with a soft zinc layer (hot dipping), it is easily smoothed out, creating a larger bearing area as compared to the uncoated materials (JONASSON et al., 1998).

The load at the interface between work piece and die is transmitted by three different kinds of bearing ratios. These are: the real contact area (which is represented by the solid contact), and the **static** and **dynamic** lubricant pockets (which characterize the contact mechanisms in mixed lubrication-ML), as summarized in fig. 3.2.1.

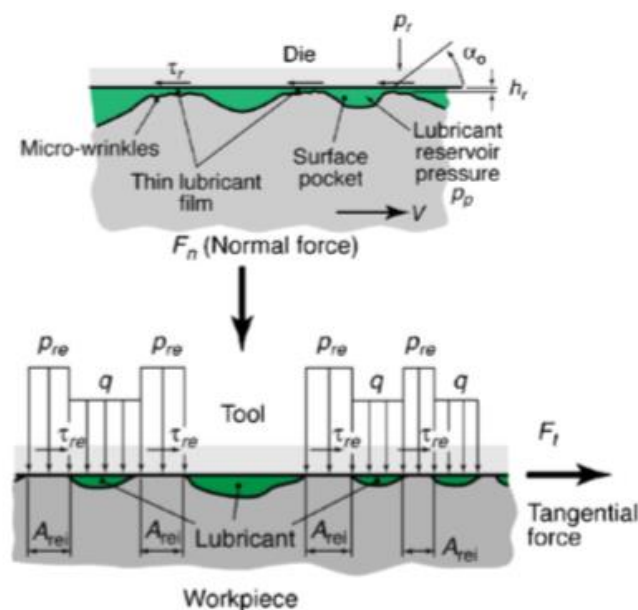


Figure 3.2.1: Schematic outline of micro-plasto-hydrodynamic lubrication and local

pressure distribution (BAY et al., 2010).

About the contact mechanism Vermulen and Scheers (2001) has shown through the Stribeck curve, see fig .3.2.2, top, the other possible regimes which are: boundary lubrication-BL-(accentuated contact between tool and sheet metal) and hydrodynamic lubrication-HL-(no contact between tool and sheet metal).

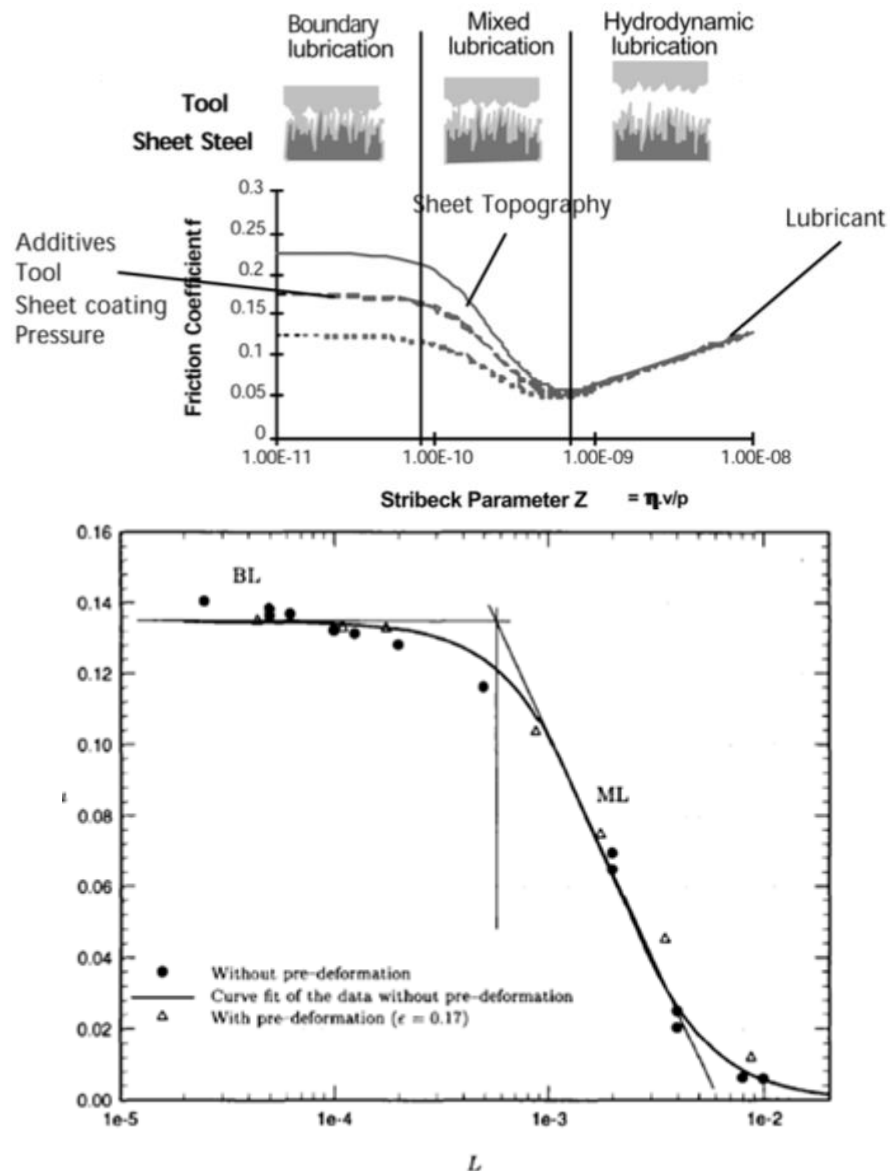


Figure 3.2.2: Top: Typical Stribeck curve relating the different contact mechanisms. $Z = \eta v / p$ (STRIBECK, 1901 apud VERMULEN and SCHEERS, 2001).

Bottom: An alternative Stribeck curve which considers the sheet metal roughness. $L = \eta v / p Ra$, where Ra is the roughness (LUBBING, HAAR, SCHIPPER, 1996).

An initial tentative, in order to position the contact regime for the conditions existing in the present work through the Stribeck curve, an initial estimate of the Stribeck parameter $Z=\eta v/p$ (abscissa of fig. 3.2.2, top), has been performed. The calculated value for Z is of about $3.9E-10$, where η (dynamic viscosity of the oil) = $0.13\text{Pa}\cdot\text{s}$, v (sheet velocity) = 4.5 mm/s and p (contact pressure) = 150 MPa . These values will be reviewed further in the discussion, as per chapter 6.2.2.3.

3.2.2 Surface topography

Many metal forming operations involve liquid lubricants in order to reduce friction at the tool/part interface, to improve the finished part surface quality. In most of these operations the mixed lubrication (ML) regime appears, leading to local asperity contact between the tool and the part surfaces. The in-between pockets function as micro-reservoirs for the lubricant. During processing the reservoirs are deformed and the entrapped lubricant is pressurized and eventually escaping by Micro Plasto Hydrodynamic Lubrication (MPHDL), see fig. 3.2.1, leading to a local non-uniform deformation of the surface layer.

It is of great importance to understand and control the lubrication phenomena in order to reduce friction and improve the resulting surface quality. As pointed out by Bay (2010) and by Dubar (2012) the advantages of using structured sheet surfaces are due to the special lubrication mechanisms appearing when the lubricant is entrapped in the pockets on the surface, pressurized and subsequently extracted from the pockets, as illustrated on fig.3.2.3.

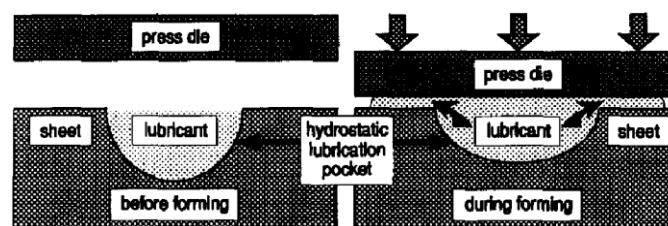


Figure 3.2.3: Schematic illustration of the mechanism of hydrostatic lubrication pockets (PAWELSKI et al, 1996).

Weidel and Engel (2009) apud Sobis et al.(1992) described a model of open and closed lubricant pockets, for which 3D surface parameters have been derived. It concluded that the “forming load” is transmitted from an ideal flat tool, via a lubricant, to the work-piece by three different bearing ratios as shown in fig. 3.2.4 (a). These

bearing ratios are related to: the real contact area (RCA), closed (CLP) and open lubricant pockets (OLP). During the plastic deformation of the asperities (due to the external forming load), the lubricant which is trapped in the roughness valley is pressurized. As the CLPs have no connection to the edge of the contact area, a hydrostatic pressure is built up and a part of the external forming load is transmitted reducing the normal pressure on the RCA, thus decreasing friction. In contrast, as the OLPs have a connection to the edge, the lubricant is squeezed out resulting in a hydrodynamic pressure whose ability for transmitting the forming load is negligible if compared to the hydrostatic pressure in the CLPs. It can be summarized that the CLPs reduce friction in contrast to the OLPs. The ratio of RCA, CLP and OLP is determined numerically by several equidistant penetrations of a plane between the highest and the lowest point of the topography. A typical evolution of the bearing ratios is shown in fig 3.2.4 (b). Two distinctive parameters can be derived from the evolution of the closed void area ratio used for the characterization of the sheet metal: the maximum ratio of the closed void area (α_{clm}) and by integrating the curve, the normalized closed void volume (V_{cl}). These parameters are explained in greater detail in the attachment 1.

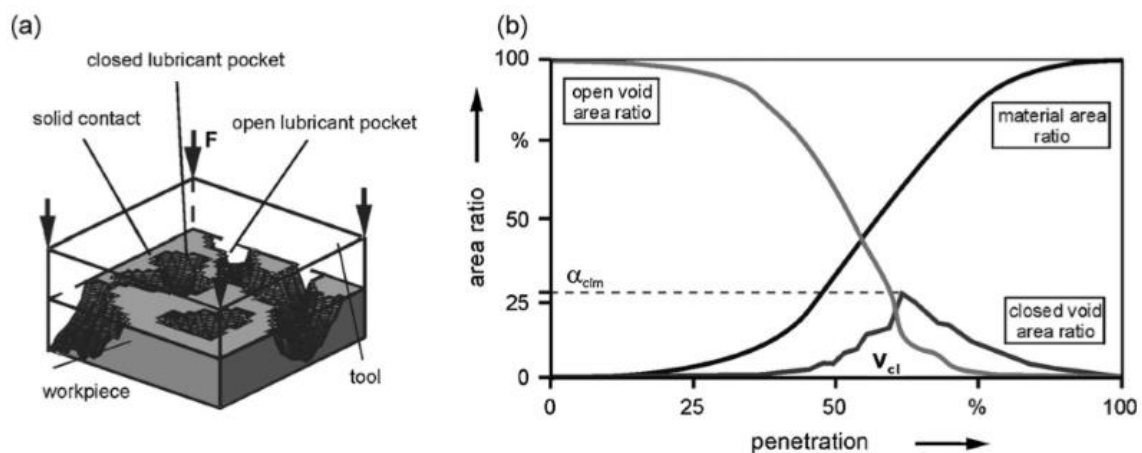


Figure 3.2.4: (a) Mechanical–rheological model; (b) surface fractions as a function of vertical penetration (WEIDEL, ENGEL, 2009).

In other words the concept of open and closed voids were explained by the Bfinten et al, (1996) experiment shown in fig. 3.2.5. When the groove is parallel to the drawing direction, the longitudinal texturizing allows the fluid to leak away from the contacting/sliding interface. Conversely, when it is perpendicular to the drawing direction the transverse topography is probably more important from a dynamic

friction point of view, since it traps the lubricant at the surface, decreasing the coefficient of friction (BFINTEN et al, 1996)

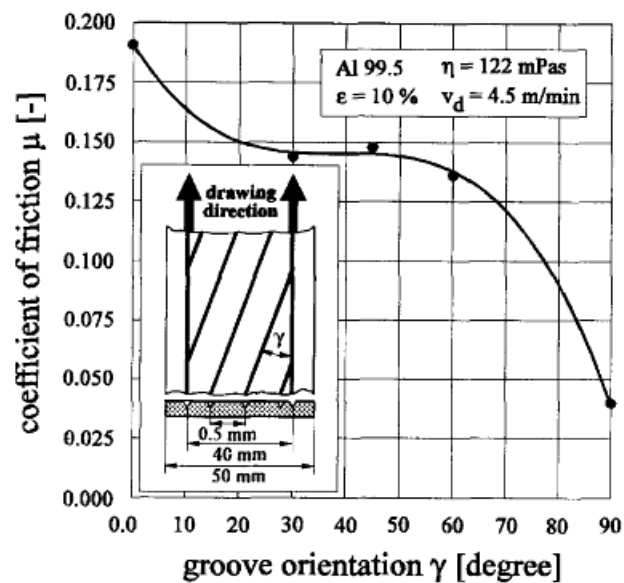


Figure 3.2.5: Coefficient of friction versus the angle between the straight grooves and the drawing direction (groove orientation) (BFINTEN et al, 1996).

Figure 3.2.6 exemplifies this aspect. As the maximum closed void area ratio increases there is a decrease in the proportion: static (sticking) friction coefficient - μ_H / sliding friction coefficient - μ_G (PFESTORF et al., 1998).

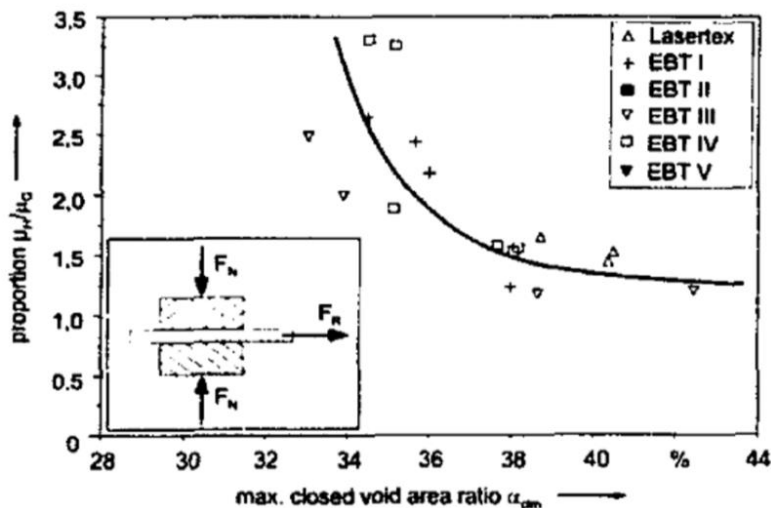


Figure 3.2.6: Proportion of static friction coefficient μ_H to the sliding friction coefficient μ_G , in comparison to the maximum closed void area ratio- α_{csm} (PFESTORF et al., 1998).

Again, the maximum closed void area ratio α_{clm} is explained in greater detail in the attachment 1, related to the glossary on roughness terms.

On the other hand, hydrostatic lubrication pockets are only developed to a slight degree on stochastic surface structures (GEIGER, ENGEL, PFESTORF, 1997). The presence of micro channels connecting lower areas within the structure is a typical feature of such surfaces. The basic function of lubricant storage and the take up of surface-abrasion products is achieved by means of the relatively high roughness with associated high values for the standardized 2D-roughness parameters R_a and R_z . However, the induced long-wave characteristics of stochastic surfaces accompanying such high roughness, reduces the surface quality of the final product after painting (in other words, long-wave structures are relevant to results of the painting process, whereas short-wave textures are decisive for results of the forming process). So far, it becomes clear that the selection of the roughness values always represents a compromise between the forming behavior and the aesthetic appearance of the final product (BFINTEN et al, 1996).

In order to optimize stochastic surface structures, the 3D roughness parameters can also be used, as shown in fig. 3.2.7. This particular figure specifically shows the areas: open (blue) and closed (green) void areas and the material ratio (grey). The term open, in this context, refers to areas where lubricants can be routed to the outside during forming, by contrast to closed cavities where the oil may be retained during forming (GRETHE, 2013).

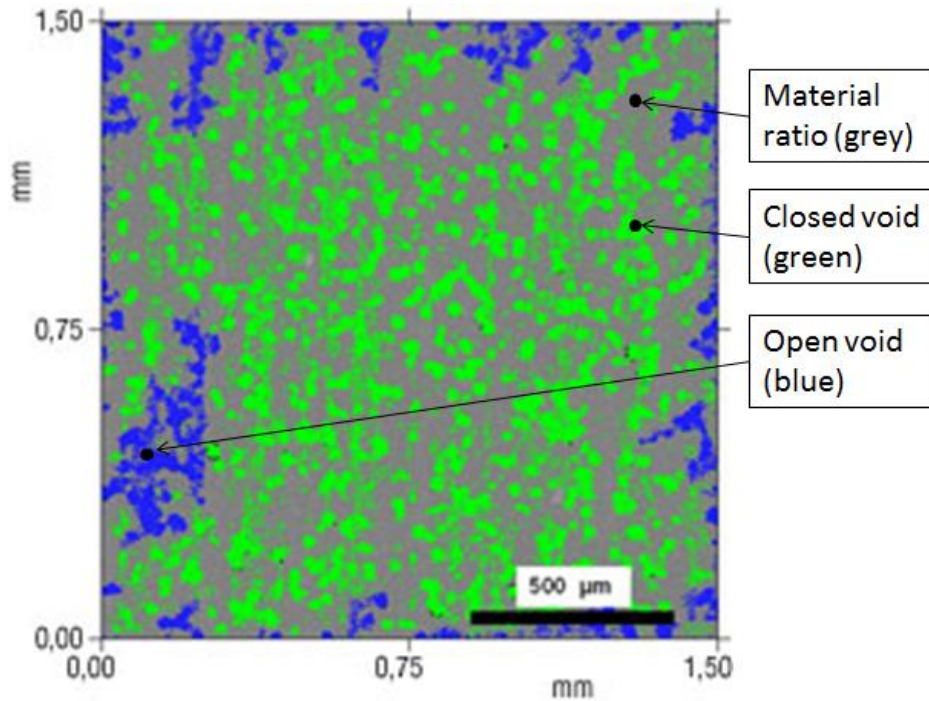


Figure 3.2.7: Lubricant reservoir (closed void) of EDT (Pretex) structure (GRETHE, 2013).

Fig. 3.2.8 shows the same material ratio, closed and open void of the fig. 3.2.7 by using the bearing material area curve.

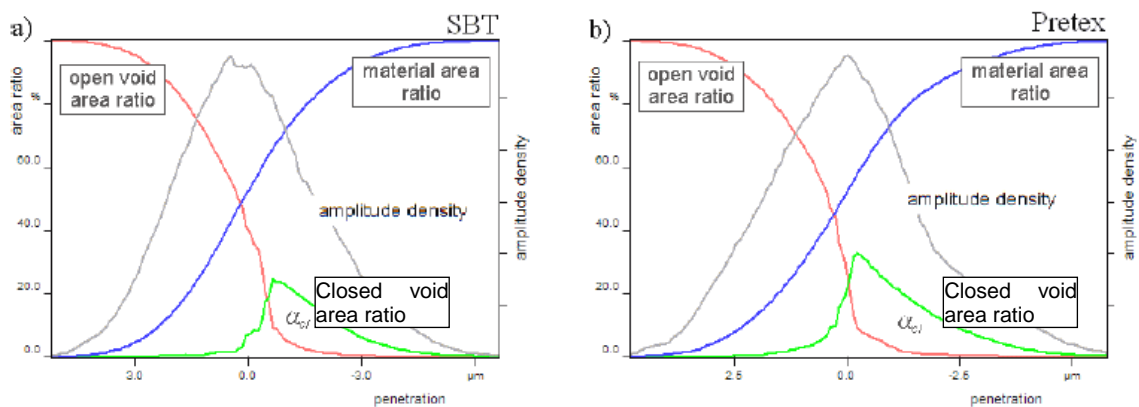


Figure 3.2.8: Volume analysis: a) SBT-texturized b) EDT-texturized (*Pretex*) (VALENTIN et al., 2008).

The figs. 3.2.7 and 3.2.8 will be reviewed further in the discussion, as per chapter 6.1.

3.2.3 Lubricant

The lubricants most frequently used for the stamping of car outer panels are the dry film lubricants applied in an amount of 0.5 to 1.5 g/m² at the rolling mill stage (KIM, 2006; ALTAN, 2005, 2006). Dry film lubricants are solid materials that provide good drawing performance, corrosion protection and they are compatible with almost all commonly used adhesives. They are composed of a suitable resin or binder, lubricating solids, additives and a solvent system (WARD, 2013). The dry film thickness has a direct impact on the friction coefficient, as well as the type of lubricant and its concentration, as evidenced by Hu et al., (2003) and Bay (2010), in fig. 3.2.9.

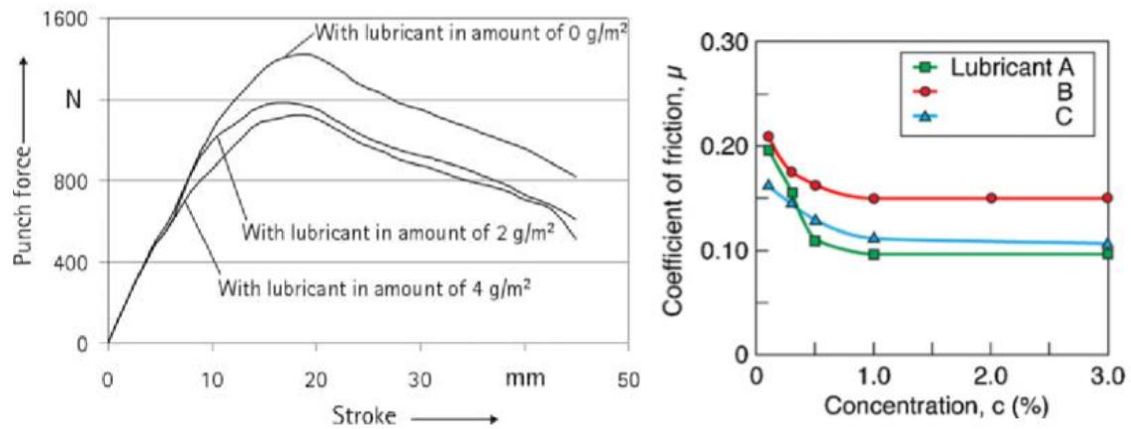


Figure 3.2.9: Left: Punch force versus stroke for different oil film amounts (g/m²) applied on the sheet surface (HU, NIEHOFF, VOLLERTSEN, 2003).

Right: Coefficient of friction versus emulsion concentration for different types of lubricant (BAY et al., 2010).

The lubricant deposition process in itself is well known to be another factor that impacts the sheet metal stampability. There are mainly two strategies: one the lubricant is applied by the mill and the end user control its thickness as exemplified in fig. 3.2.11 and another the lubricant is applied just before to stamping process and there is no need to lubricant thickness control. In particular, the process used in the present work was the second one as illustrated in fig. 3.2.10, where the blank was washed and oiled prior to the forming operation.

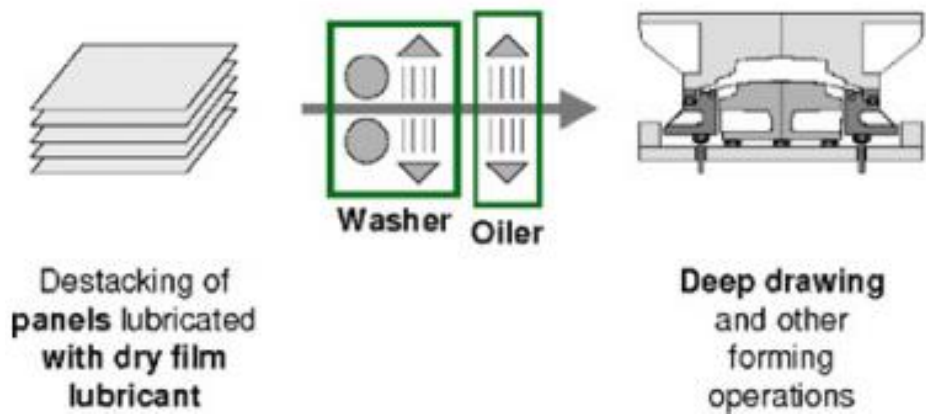


Figure 3.2.10: A macro view summarizing the stamping process.

As just mentioned, some European car makers do not wash / oil in-house, but they control the oil film thickness applied by the steel mill prior to the forming operation, as illustrated in fig. 3.2.11 (BLOCK, BERGOLD, ENDERLE, 2011). This system monitors the oil film thickness along the whole sheet metal on both sides. In case the oil film is not according to specification, the blank is segregated before it goes to the press. Some common types of “lack of lubricant” on oiled mill blanks are illustrated in fig. 3.2.12.

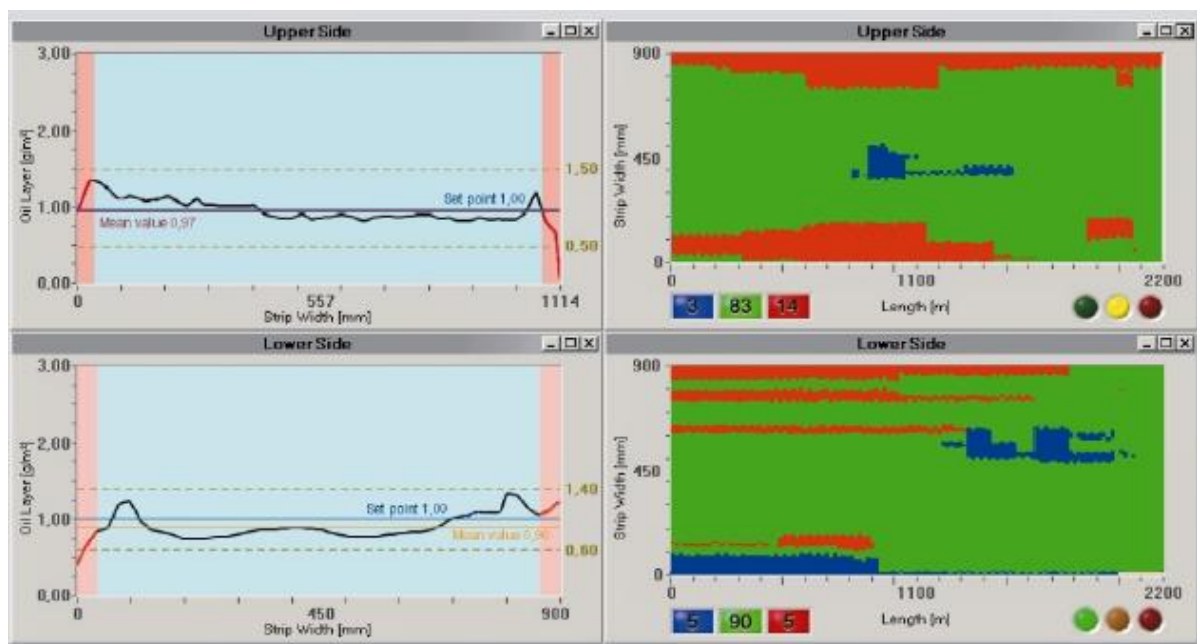


Figure 3.2.11: Visualization screen of the oil film measurement system. (BLOCK, BERGOLD, ENDERLE, 2011).

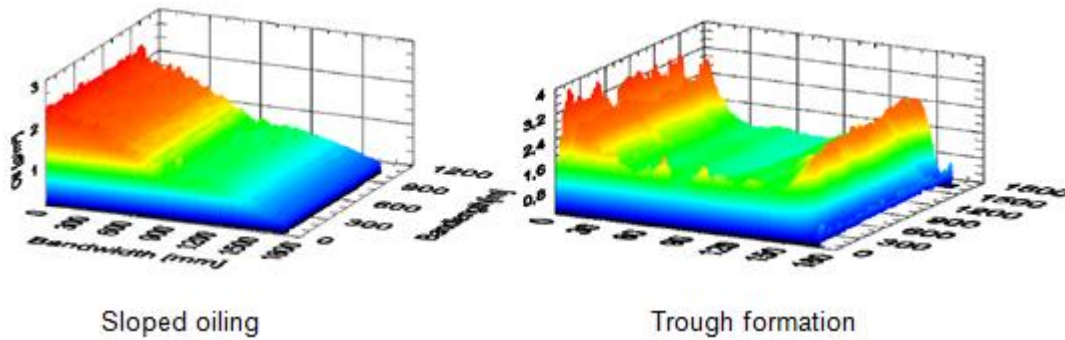


Figure 3.2.12: Some common types of “lack of lubricant” on oiled mill blanks corresponding to fig. 3.23 (BLOCK, BERGOLD, ENDERLE, 2011).

“Lack of lubrication” increases the coefficient of friction and may lead the stamped part to fracture or thinning. In the same way, excess lubricant is also prejudicial: apart from the cost increase it can cause markings on the surface, hence decreasing the final paint appearance.

Here, it should be pointed out that the deleterious effect of thinning on roughness will be explained in the following, in the topic on strain path effect.

3.2.4 Temperature

During stamping operations, after some strokes, the tool temperature starts to increase and if the lubricant loses/changes its lubricity, friction properties will increase, leading to an increase in the punch force as evidenced in fig. 3.2.13.

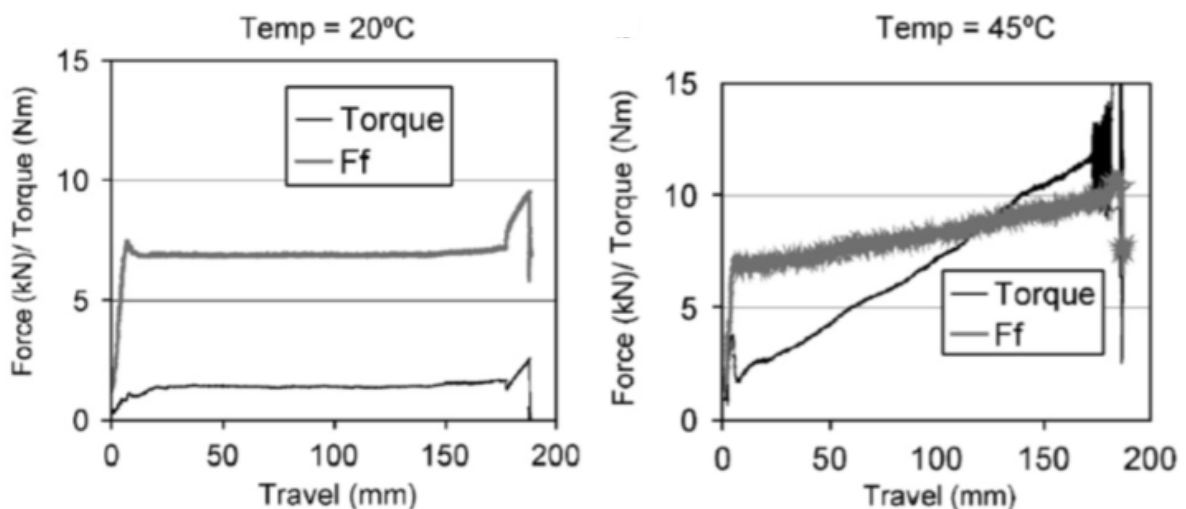


Figure 3.2.13: Typical signatures: Force x travel. Alterations caused by increasing tool temperature (BAY, OLSSON, ANDREASEN, 2008).

If the process is monitored by its signature(load x travel curve) it is possible to interrupt/alter the process, as soon as it has been noticed an increase in the slope of the punch force curve, avoiding galling to occur, hence preventing premature loss in tool life and the corresponding loss in productivity. More details about process signature will be given on the topics 3.2.5 (next one) and in 3.2.8, under “strain path effect”.

3.2.5 Tool surface, contact pressure and sheet metal sliding velocity

Merklein, Geiger, Kaupper (2008) evidenced, as shown in fig. 3.2.14, the dependence of the friction coefficient for different tool surfaces, lubricant types, sliding velocities and contact normal forces. The main reason of this figure is not only to show how friction coefficient is increased or decreased by the effect of the mentioned variables, even as it may be very specific for each situation, but to show that the influence really exists.

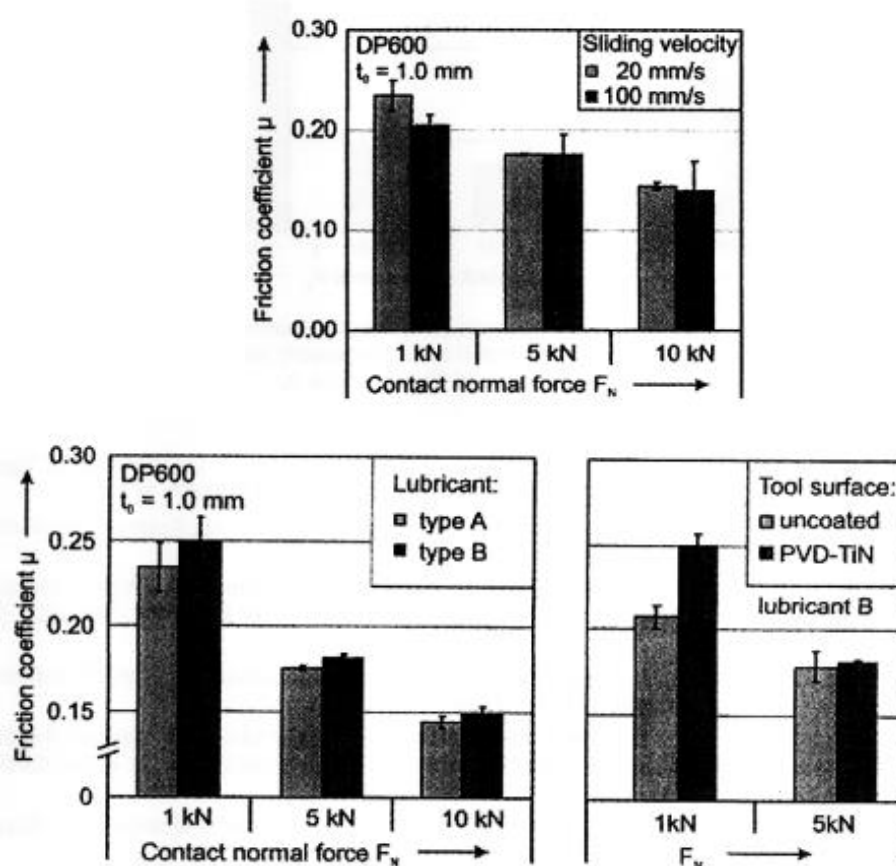


Figure 3.2.14: Typical influence of sliding velocity, lubricant type, tool surface and

contact normal force on the friction coefficient (MERKLEIN, GEIGER, KAUPPER 2008).

One way to understand these influences and how to interact (in a way to increase process robustness), is through the monitoring of these variable is by using “process signature” (HOGENDOORN, 2009; FLETCHER, 2003), as mentioned previously. The most common ways are through the punch force and through the sheet velocity. Any changes in the system, including tooling wear, will lead to a change in the process signatures.

3.2.6 Sheet metal chemical treatment

The most recent technology applied in sheet metal stamping is the surface chemical treatment of the sheet. It consists of an anti-adhesive nano-layer applied after the hot dip galvanizing process. Clearly, each mill has its own commercial name. For example, *Usiminas* calls it the L-Treatment, while *CSN*, *CTP* and *Arcelor NIT* (New Inorganic Treatment) (PAYEN et al., 2012). The main function of this surface treatment is to decrease the friction coefficient and to retard the stick-slip phenomenon which occurs when zinc transfer layer adheres onto the tool and when a given level of contact pressure is reached which, in turn, is dependent on the surface topography. Indeed, Payen et al. (2012) observed that anti-adhesive coatings reduce the local friction shear stress at the boundary contact. As a consequence, the deformation modes of the asperities are changed in such a way that large levels of normal crushing of the asperities can be reached with reduced debris generation (PAYEN et al., 2012).

3.2.7 Sliding conditions

The effect of the sliding conditions, as summarized in figs. 3.2.15, 3.2.16, 3.2.17 and 3.2.18, on the roughness evolution have been studied by several authors (PAYEN et al.; 2012, WICHERN et al., 2000, 2005; JONASSEN et al., 1997; RAHARIJAONA, ROIZARD, STEBUT, 1999). In the figure 3.2.15 the effect of the chemical coating, surface topography and contact pressure were evaluated during a plane strip drawing test (PAYEN et al., 2012).

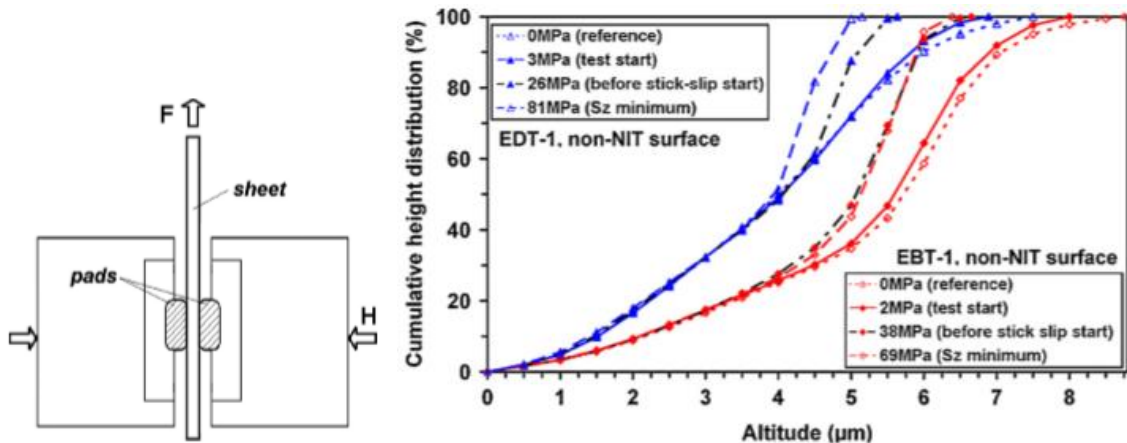


Figure 3.2.15: Left: Plane strip drawing test: Contact pressure is perpendicular to the sheet displacement direction. Right: Effect of pressure and surface topography on the roughness evolution (PAYEN et al., 2012).

This figure presents the bearing area curves (before and after testing) for the sheet metal texturized by the EDT and EBT processes. In both cases the amplitude/altitude (horizontal axis-absissa), represents the distance from the lowest valley (zero) to highest peak and it decreases with increasing pressure (PAYEN et al., 2012).

At this stage it must be pointed out, once again, that the different aspects and concepts related to the Bearing Area Curve and Abbott curve are presented in the attachment 1.

For higher contact normal forces, higher was the reduction in the amplitude roughness parameter (as, for example, in the values of R_a and R_z). These changes in surface topography have been pointed out by several authors as being beneficial to the paint appearance (SCHEERS et al., 1998).

This is an important point because if this friction is benefic what is detrimental?

It may be stated that, higher contact forces can lead to galling and also to an increase in the coefficient of friction, which in turn, can lead to fracture or to the thinning of the sheet of the stamped part.

Further, there are two relevant aspects related to sheet metal thinning:

1. Change in the mechanical property (due to thickness reduction and strain hardening) of the part in that region, so it is necessary to check if it will not compromise the durability and crash performance of the car.
2. It increases the roughness amplitude, so it is necessary to check if it will not compromise the paint appearance.

These aspects will be explained in greater detail in the topic strain path (3.2.8) and paint appearance (3.4), respectively.

Jonassen et al.(1997) compared the roughness evolution (through the bearing area curve before and after stamping) by means of the strip drawing test and the bending under tension test. As shown in figs. 3.2.16 and 3.2.17, the roughness evolution were quite different for these conditions, although both caused a decrease in the roughness amplitude. However, as mentioned before, this effect from the paint appearance point of view (for both sliding conditions), will be benefic.

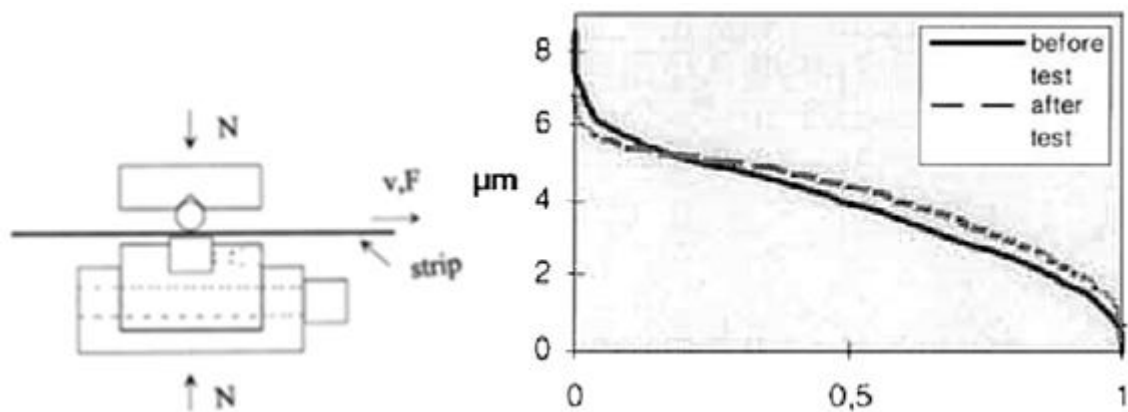


Figure 3.2.16: Left: Strip drawing test scheme. Right: Typical Abbot-Firestone curve before and after the strip drawing test (JONASSEN et al., 1997).

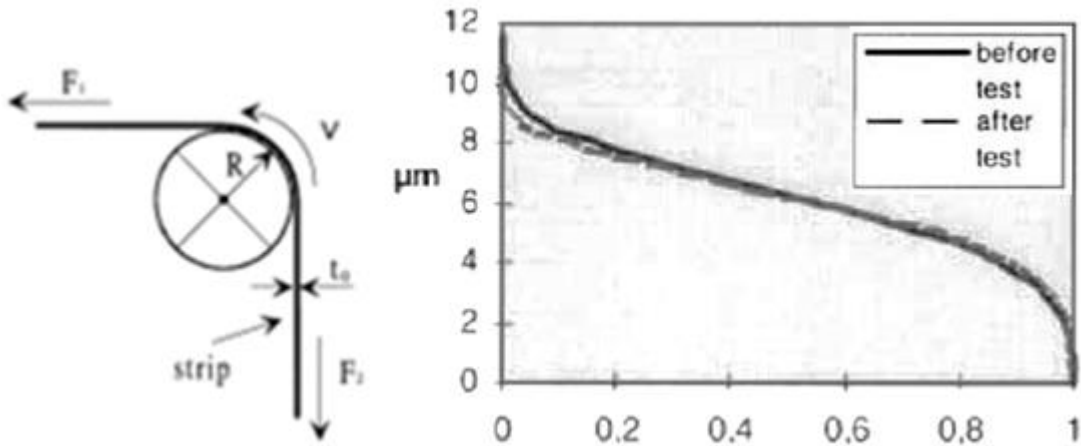


Figure 3.2.17: Left: Bending under tension test scheme. Right: Typical Abbott-Firestone curve for the bearing area curve, before and after tension test (JONASSEN et al., 1997).

Raharijaona, Roizard, Stebut (1999) have evaluated the effect of the lubrication conditions and the length of the sheet displacement on the roughness evolution in a plane strip drawing test (fig. 3.2.18). Once again, although the results were quite different, from the paint appearance point of view, they should be beneficial, mainly due to a decrease in the roughness amplitude.

These bearing area curves (before and after test), will be reviewed further in the discussion, as per chapter 6.2.1.

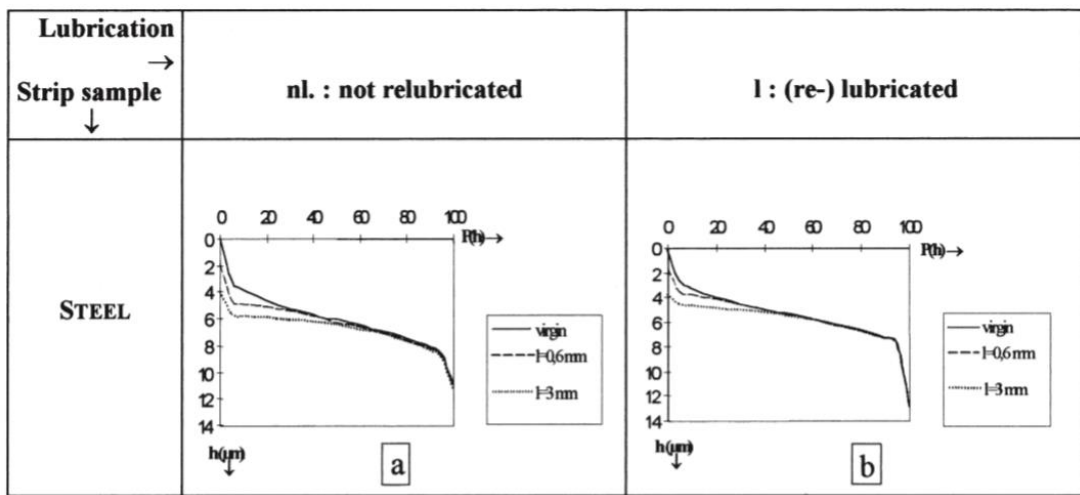


Figure 3.2.18: Effect of lubrication condition and length of sheet displacement on the roughness evolution during plane strip drawing test (RAHARIJAONA, ROIZARD, STEBUT, 1999).

Wichern et al. 2000 have analyzed (3) three modes of surface deformation for hot dip galvanized steels, namely: (1)-"simple pressing", (2)-"pressing with small scale sliding and bending" and (3)-"pressing with gross sliding, stretching and bending". In the case of simple pressing and pressing with small scale sliding and bending the effects on surface topography were similar to these presented in figs. 3.2.16 to 3.2.18, which means surface flattening. In the case of stretching, material tends to broaden its surface height distribution during forming (become roughened). This case will be explained in great detail in the next topic 3.2.8 - strain path.

Ma et al.(2002) developed a model related to asperity flattening in a mixed - film lubrication condition, which consisted in a regression function relating contact ratio as a function of load, friction and sliding velocity.

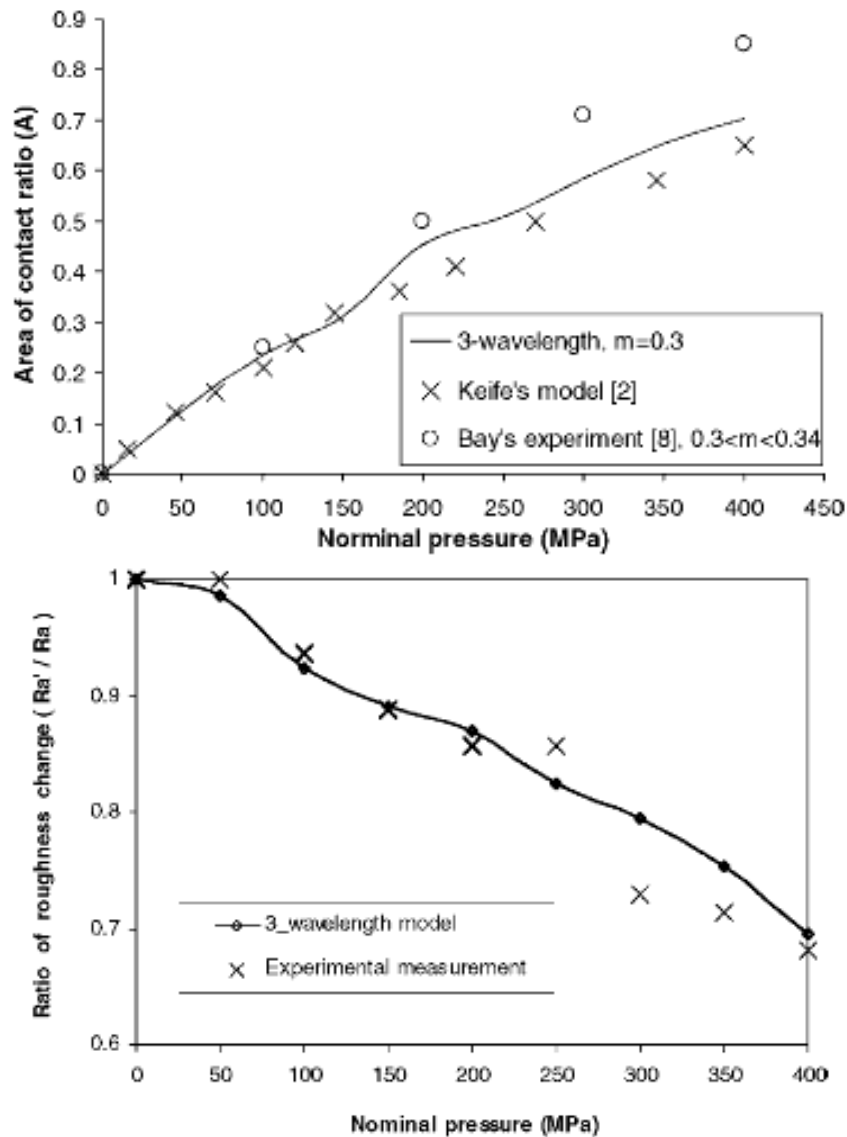


Figure 3.2.19: Top: Evolution of area of contact ratio during loading procedure

Bottom: Correlation between surface roughness (R_a) change and external pressure (MA et al., 2002).

In fig. 3.2.19, top, the area of contact ratio (vertical axis-ordinate) increases as a function of nominal pressure. In the bottom figure, the graph compares the ratio of roughness change (R_a / R'_a) obtained via simulation with experimental measurements as a function of nominal pressure. Here R'_a is the roughness after deformation while R_a is the initial roughness. It can be seen that the roughness decreases with increasing pressure because the tool flattens the sheet asperities.

3.2.8 Strain path

As presented in the previous topic, the contact between tool and the sheet metal, even with higher contact pressure, is benefic for the paint appearance (if galling does not occur), because it causes flattening of the asperities (plastic deformation mainly of the peaks), as shown in fig.3.2.20. Now, what about adding to it the strain path effect?

Again, as mentioned previously, the different aspects and concepts of the Abbott curve are presented in the attachment 1.

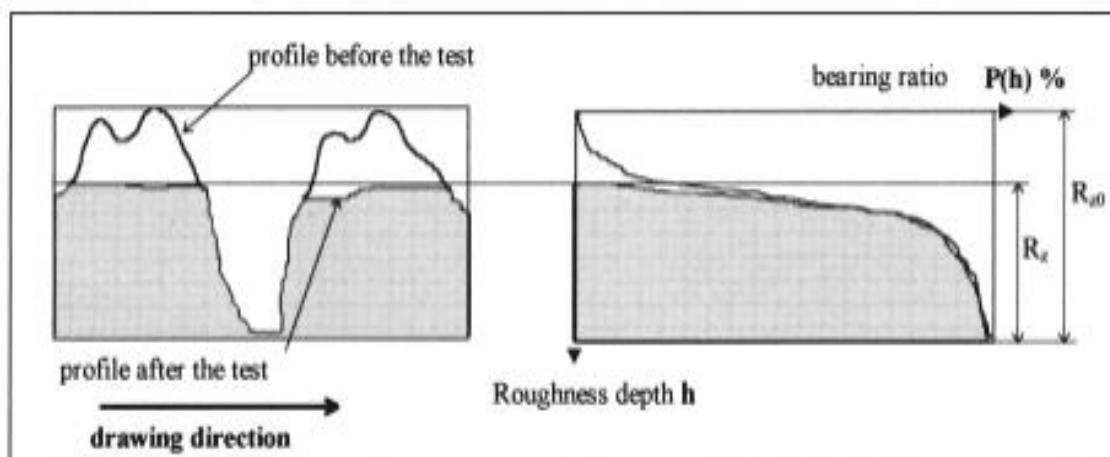


Figure 3.2.20: Evolution of the Abbott curve (right) in relation to the roughness flattening after a strip drawing pass. There is a decrease in the R_z , 2D-roughness parameter (RAHARIJAONA, ROIZARD, STEBUT, 1999).

Several studies were published in which the influence of the steel sheet surface on the final paint appearance has been evaluated. From this literature it could be concluded that the paint appearance decreases with the increasing of all the roughness parameters associated with the amplitude of the 2D-parameters (as for example Ra and Rz - height of profile). Furthermore, paint appearance increases with increasing of the peak and valley density 2D-roughness parameters (as for example Peak Count (Pc) (SCHEERS et al., 1998).

Hence, its should be apparent that strain path does play a major role / influence on the surface topography evolution during stamping, eventually being malefic or not to the paint appearance.

Different types of strain path may be easily visualized through the Forming Limit Diagrams (FLD). Fig. 3.21 shows a FLD with its typical strain path.

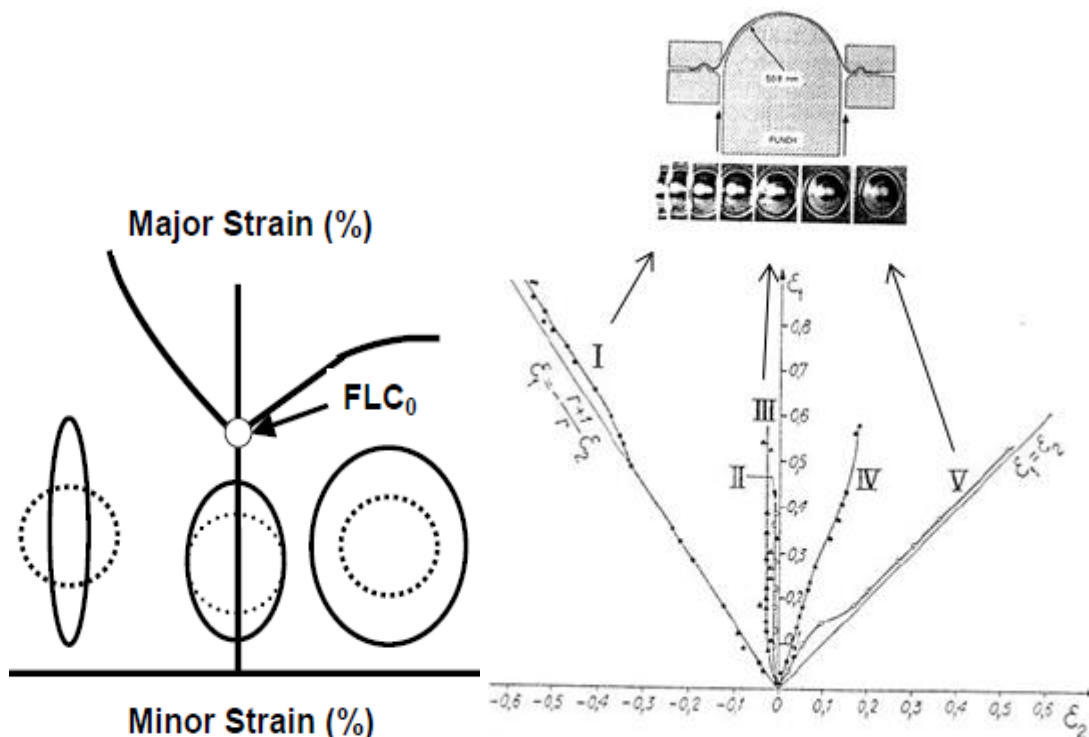


Figure 3.21:Left: Typical FLD (major/ minor strains- measured in the plane of the sheet). Rigth: Strain path used for the tested samples with different width (BANABIC et al., 2000).

The curve which contains FLC_0 (the lowest point of the FLD) is where thinning/fracture occurs under plain strain conditions. The horizontal axis (abscissa), related to the minor strain, contains the strains, negative on the left side (as for the uniaxial tensile test) and positive on the right side (as for the biaxial tensile test). The strain path of each point on the actual stamped part can be measured directly by the impressions of a grid (applied before stamping), and measuring the strains (major and minor), after stamping. It should be pointed out that there are more modern methods that make use of lasers and of stochastic dot-printing applied on the actual sheet surface (MULLER, 2009).

Typically, for the automotive outer panels the main strain paths can be presented as those given in fig.3.2.22.

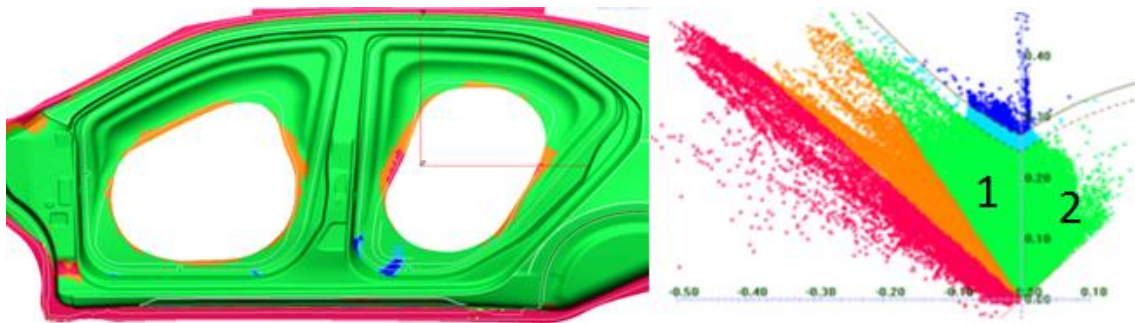


Figure 3.2.22: Left: typical automotive outer panel. Right: FLD strain diagram/ path (Simulations by *Autoform*, GM of Brazil, 2013).

Clearly, in actual practice, strain measurements are performed in order to perform “adjustments” to the simulations due to the variety of factors pointed out previously. From the FEA (Finite Element Analysis), several relevant information are obtained, as for example, strains, strain path, as shown in fig 3.2.23 (right), or major stresses and sheet metal thinning, as shown in Fig. 3.2.24.

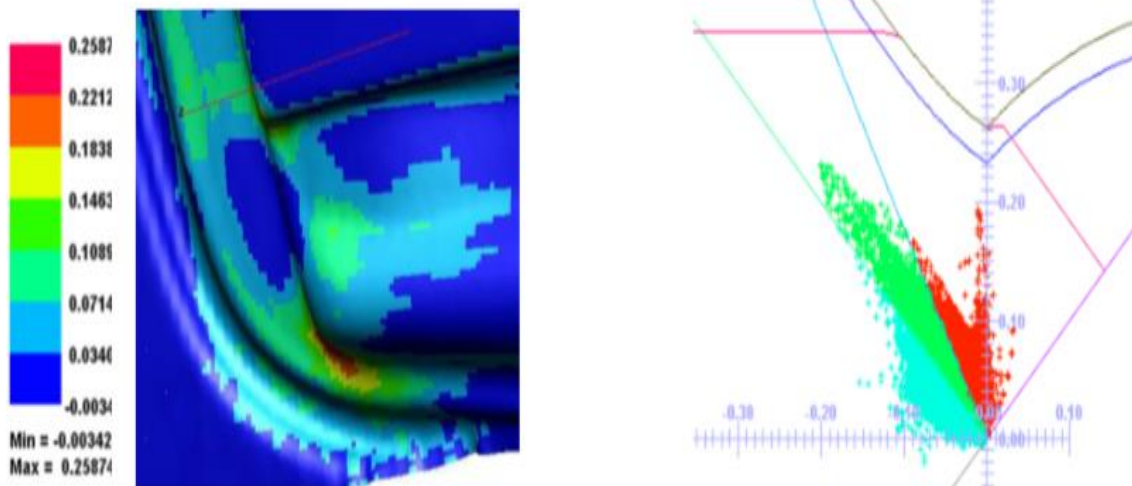


Figure 3.2.23: Major and minor strain simulation (left) and its corresponding FLD for a typical car outer panel stamping (right). Simulations by *Pamstamp* (SEKERES et al., 2010).

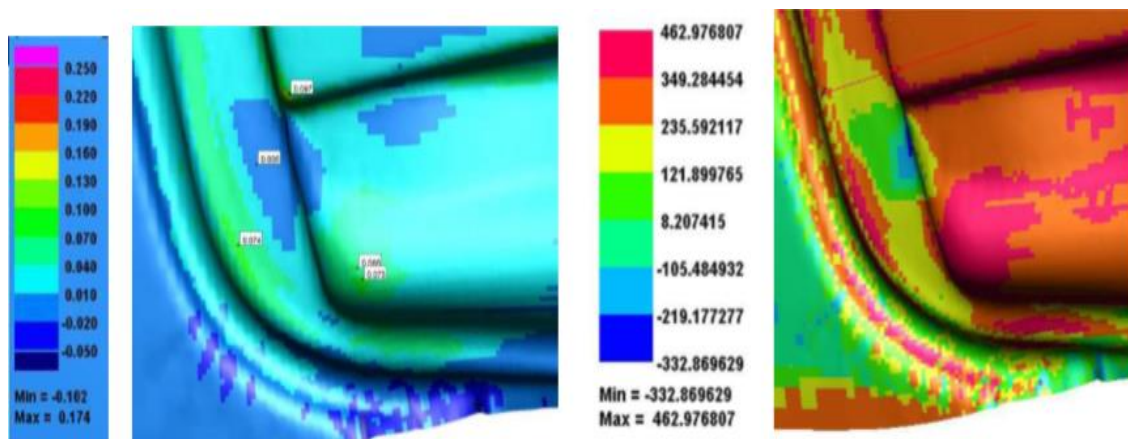


Figure 3.2.24: Left: thinning evolution simulation. Right: major stresses simulation. Simulations by *Pamstamp* (SEKERES et al., 2010).

It must be pointed out that most of the automotive outer panels have a FLD similar to the one shown in fig. 3.2.22 and that several points follow a strain path similar to the one occurring in a tensile test, for which the ratio β is approximately $\beta = -0.5$ (where $\beta = \epsilon_2 / \epsilon_1$).

A previous work to this one (SEKERES et al., 2010), has analyzed the 3D surface topography in three points on the strain path (near to the condition $\beta = \sim -0.5$), for an outer car panel that thinned and fractured during the try-out stage, as shown in figs. 3.2.25 and 3.2.26.

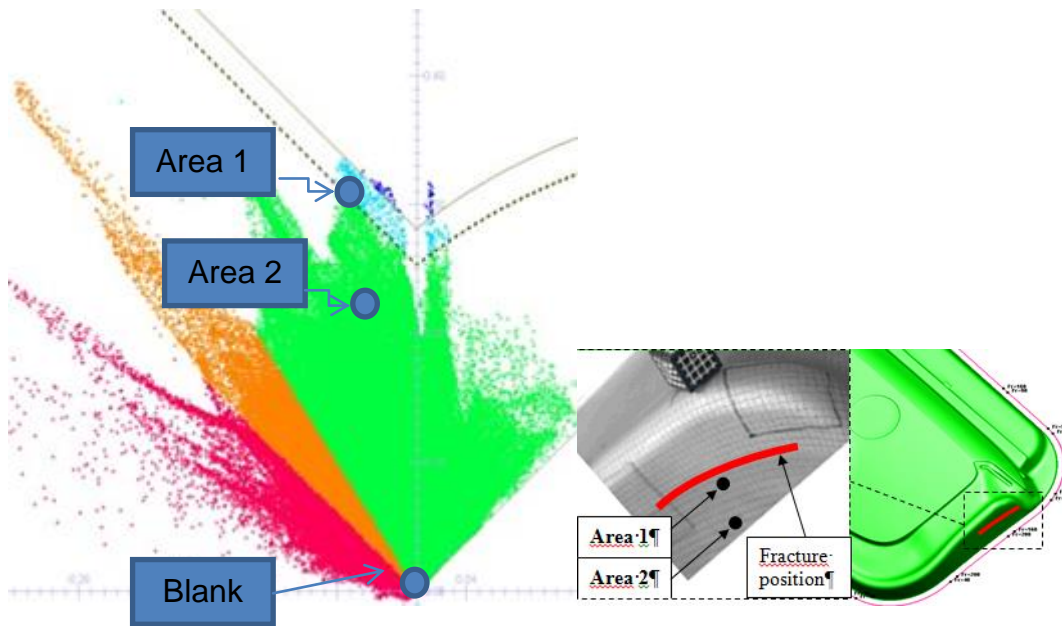


Figure 3.2.25: Strain path of areas 1 and 2 are close to the fracture (fig.3.2.26).

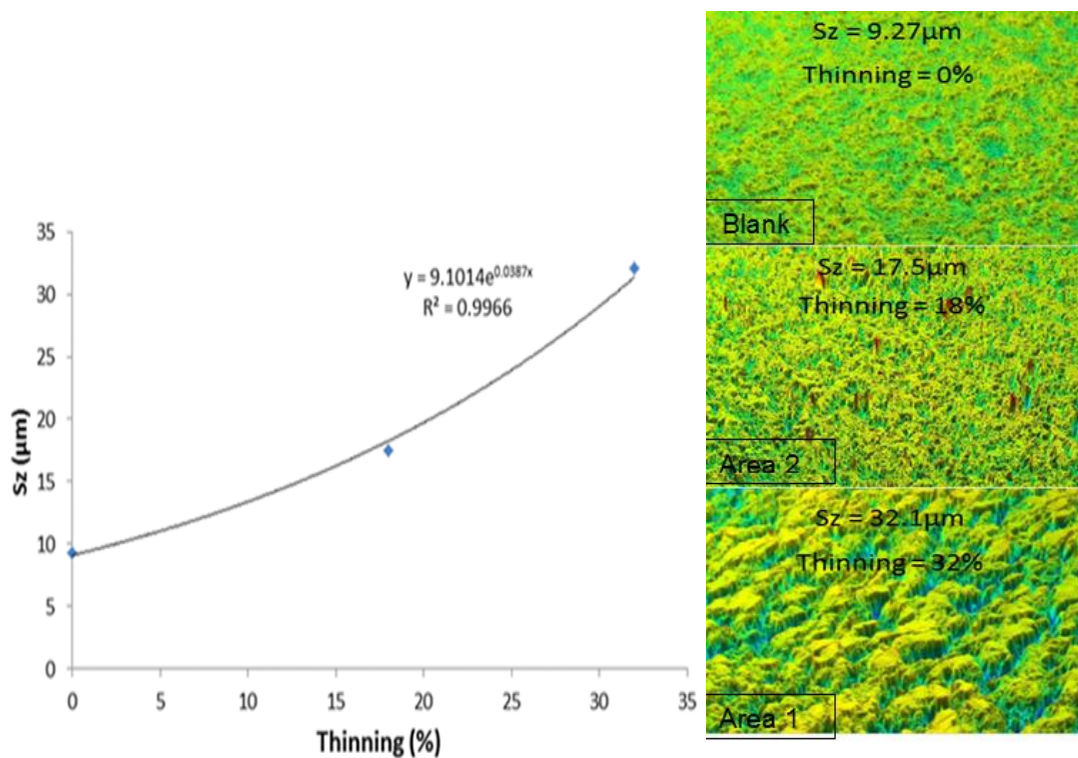


Figure 3.2.26: Relationship between sheet metal thinning and 3D-roughness evolution, S_z (SEKERES et al., 2010).

The same previous research has shown (fig. 3.2.26) that the amplitude 3D-parameter S_z (see attachment 1) increases in an exponential manner with steel sheet thinning. The consequence will be a decrease in paint appearance, as will be further evidenced in the present research.

Unfer and Bressan (2012) evaluated the sheet roughness evolution and waviness behavior during the straining in a uniaxial tensile state. The results are shown in fig. 3.2.27.

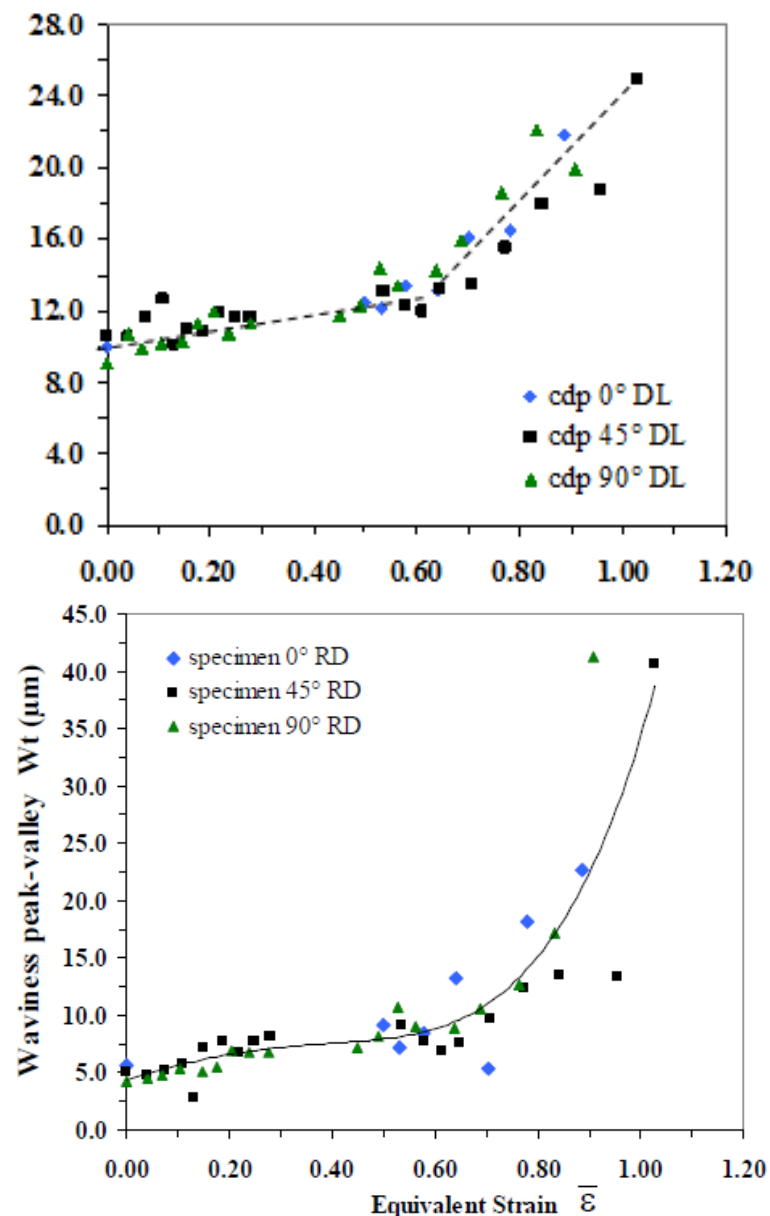


Figure 3.2.27: Evolution of 2D-roughness peak - valley R_t (top) and waviness peak - valley W_t (bottom) as a function of equivalent strain for specimens of the IF steel (for the 0°, 45° and 90° RD) (UNFER and BRESSAN, 2012).

From this work it has been concluded that roughness and waviness evolution presented two stages during the tensile test. A first stage for strain up to $\epsilon = 0.60$ and a second stage, when local necking starts, with a steeper slope until specimen rupture.

Wichern et al.(2004) has analyzed surface roughening as a function of equivalent strain for hot dipped galvanized (HDG) steel sheet using a Marciniack punch test, as shown in fig 3.2.28. It concluded also that the 3D-roughness parameters S_z and S_k increase with strain increasing, although S_k with a lower standard deviation.

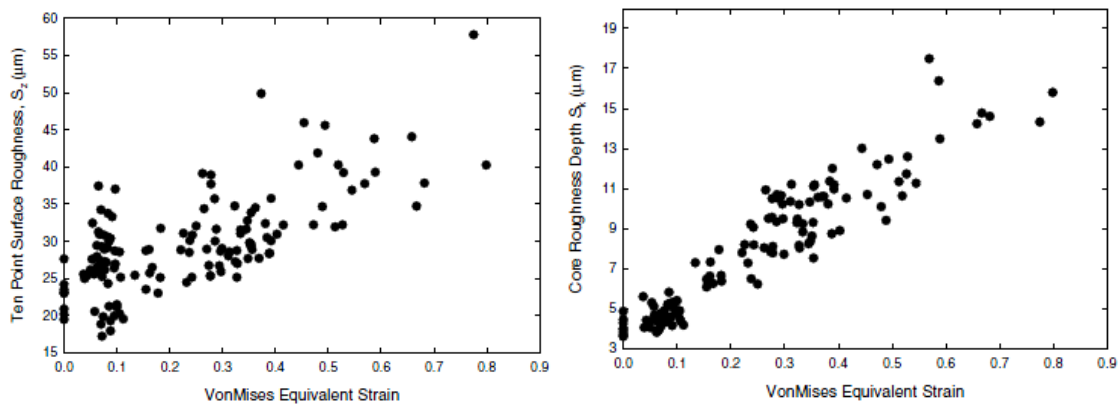


Figure 3.2.28: Ten-point peak-valley 3D-roughness, S_z (Left) and core roughness depth, S_k (Right), as a function of ϵ_{vme} for a strain imposed by a Marciniack punch test (WICHERN et al., 2004).

In fig. 3.2.29 Wichern et al. (2005) analyzed the influence of the strain path on the roughness evolution. The 3D surface roughness, S_q , of the sheet surface was reported for five different strain levels. The mentioned evolution can clearly be seen by the five levels of roughness increase, represented by the different symbols.

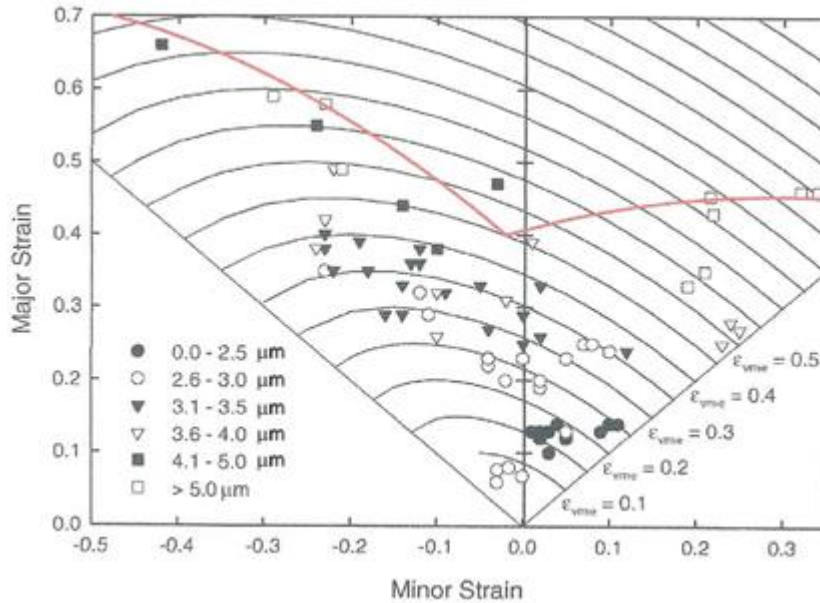


Figure 3.2.29: Forming Limit Diagram for the HDG sheet steel with iso- ϵ_{vme} lines and roughness values for different strains (WICHERN et al., 2005).

Fig. 3.2.30, (from the same research), shows a plot of roughness versus strain, ϵ_{vme} (VonMises equivalent strain), for the eight strain paths linked to the Marciniak punch deformation (given by the different Marciniak sample width). Hence, it becomes clear that strain path also influences the roughness evolution.

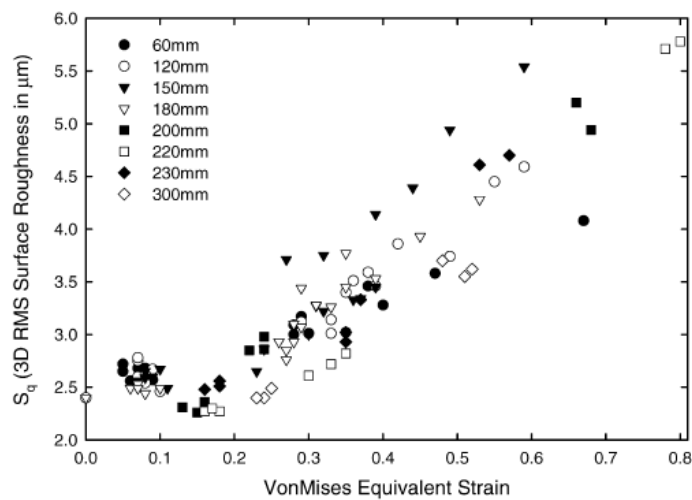


Figure 3.2.31: Surface roughness evolution as a function of strain for different strain paths imposed by the Marciniak punch deformation (WICHERN et al. 2005).

In greater detail, it should be noted that these eight strain paths were realized / obtained through the use of test specimens with different widths, namely: 60, 120,

150, 180, 200, 220, 230, and 300 mm. The 60mm wide specimen corresponds to a drawing strain path, the 180mm wide specimen corresponds to the plane-strain strain path, and the 300mm wide specimen corresponds to a biaxial stretching strain path, as shown in fig. 3.2.32.

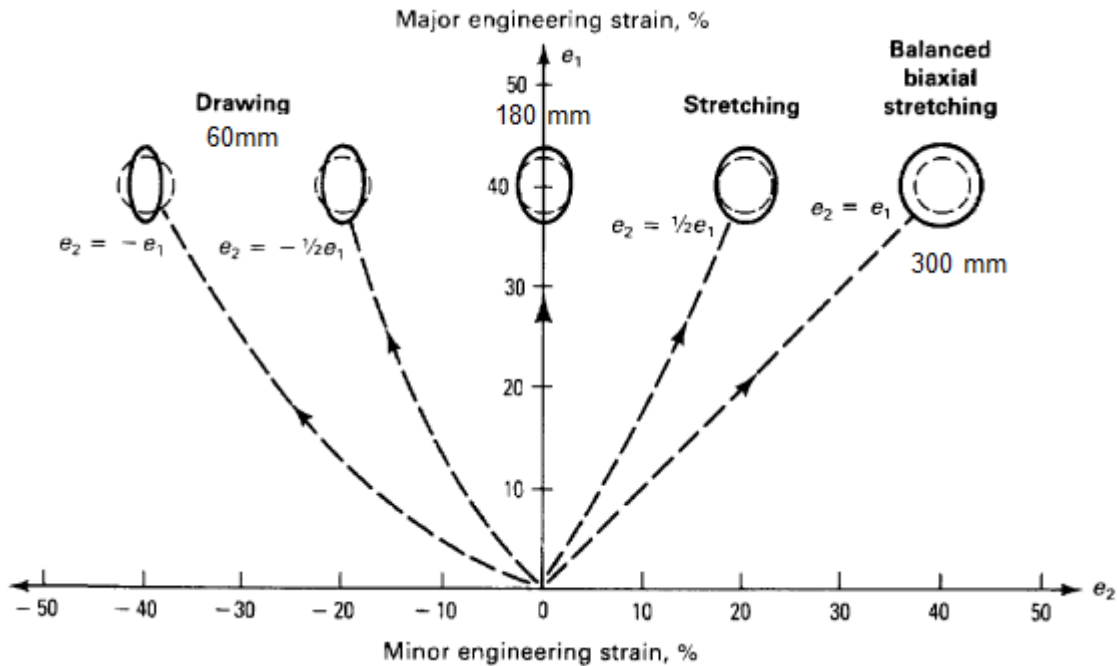


Figure 3.2.32: Major engineering strain vs. minor engineering strain for five different strain paths ranging from drawing to biaxial stretching and its correlation with fig. 3.2.31 (TAYLOR et al., 1985 apud WICHERN et al. 2005).

Further, from this literature (WICHERN et al. 2005) , it could be concluded that roughness increases with strain and that the plane strain path shows the greatest rate in roughening if compared to the strains relative to either drawing or biaxial stretching strain paths. This means that the roughening rate is clearly dependent on the strain path. In others words, the roughening rate is dependent of the thinning degree (SEKERES et al., 2010; WICHERN et al., 2005; UNFER, BRESSAN, 2012). In terms of mechanisms, surface roughening as has been pointed out by Grilhe (1992) as being related to the rate of dislocations arriving at the sheet metal surface. Also, it is well known that one way of minimizing thinning during stamping is by improving the “r” values (the Lankford value). This can be achieved by controlling the reduction in thickness (during rolling) and by the annealing temperature. Normally achieved r values are about 2.2 for IF (interstitial free steels).

Kawabe et al. (2002) apud Nishimura et al (2000) has achieved r values of about 3 by using a high intensity lubrication condition during rolling, by avoiding the shear texture at the sheet surface, leading possibly to a more homogeneous texture between sheet metal surface and core. The results of a better r , in terms of formability, are shown in fig. 3.2.33.

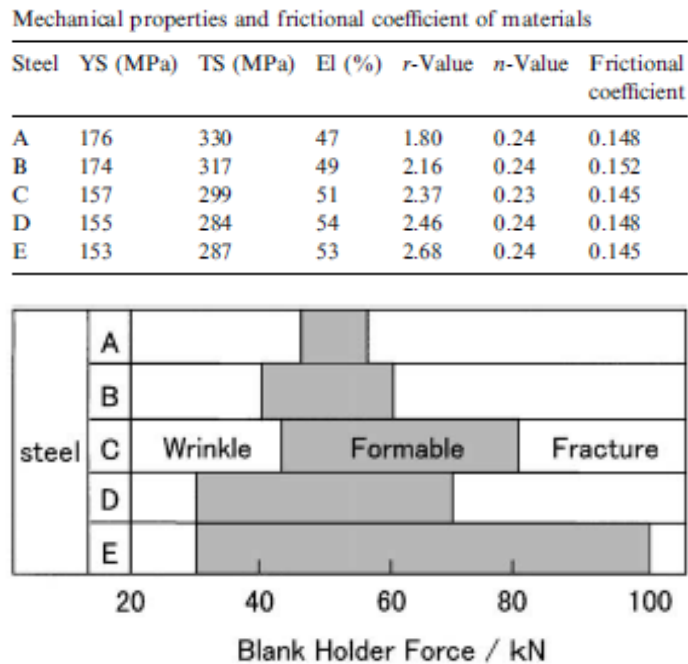


Figure 3.2.33: Blank Holding Force range (deep drawing test) versus r -values (KAWABE et al. 2002).

So, it might be concluded that one way to decrease roughening for a specific part during stamping is by increasing the intensity of the α -fiber, which means having a material more resistant to thinning (DUCHÊNE et al., 2002; HUTCHINSON, RYDE, BATE, 2005; FERREIRA FILHO et al., 2005). As a consequence, it could improve also its paint appearance.

Alternatively, bending and sliding modes of deformation cause a smoothing of the sheet surface. Sliding deformation produced during flat-die friction testing causes a decrease in roughness that is identical to those occurring in the interrupted cupping operation. (WICHERN et al., 2005)

Nowadays several researchers have pointed out that the strain path suffers significant changes when stamping is performed in several stages (KLEEMOLA, PELKKIKANGAS, 1997; ARRIEUX et al. 1982), and also nonlinear strain paths are

involved in the first draw die (STOUGHTON, ZHU, 2004) making the analysis even more complex. Indeed, it has been clearly demonstrated that initial stamping stages should be selected to follow the negative side (uniaxial tensile stress path) of the FLD and followed, for the later stages, to the right side of the FLD (biaxial tensile stress path). The reverse path, normally leads to a significant decrease in stampability, as shown in fig. 3.2.34 (STOUGHTON, ZHU, 2004, STOUGHTON, 2013).

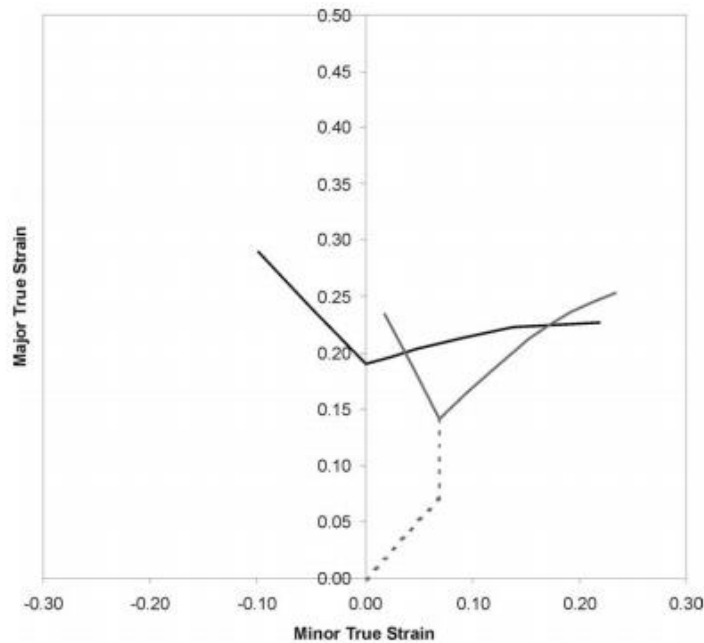


Figure 3.2.34: FLD -Selected case of a pre-strain of 0.07 (7%) in equibiaxial strain followed by a plane strain path in comparison to the FLD for the as-received material without any pre-strain, for the plane strain condition (STOUGHTON, ZHU, 2004; STOUGHTON, 2013).

Notice the shifting of the FLC_0 to the right hand side and its decreased value. The opposite effect occurs when a tensile strain path is followed by a plain strain condition. i.e a shifting to the left hand side and an increase in the FLC_0 . (STOUGHTON, ZHU, 2004).

This is a standing problem that is presently being critically analyzed in the literature, mainly due to the different strain paths that are possible in the stampings performed in several / multi-steps, because the FLD changes its shape and position (STOUGHTON, ZHU, 2004). This typical aspect is not taken into consideration in the software of the (at this time available / existing) commercial programs. These, still

make use of the FLD as being that one valid for the one-step stamping operation (STOUGHTON, ZHU, 2004). In order to overcome this standing problem Stoughton (2002) proposed the use of the stress-based FLSD which has shown to be insensitive to the loading history, as presented in fig. 3.2.35.

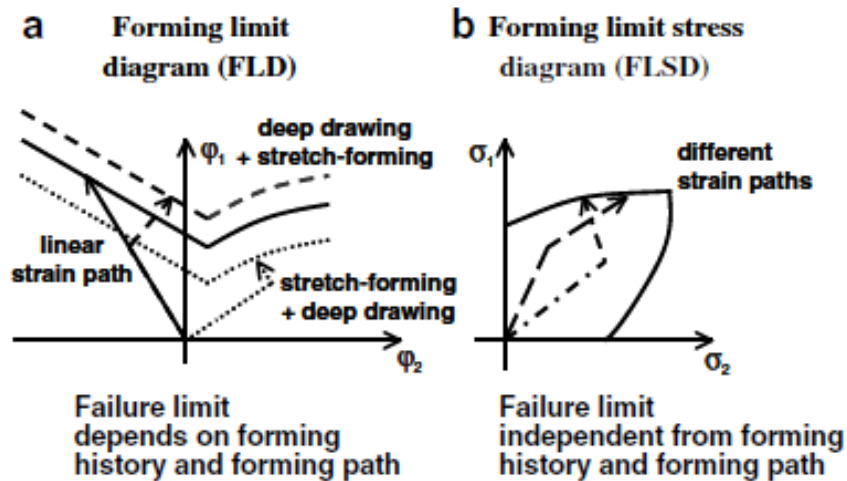


Figure 3.2.35: a-Strain based failure criterion FLD; b-stress based failure criterion FLSD (UTHAISANGSUK, PRAHL, BLECK, 2007).

From the literature (BANABIC et al., 2000) and from the industrial practice it has been clearly shown that there are several ways/options to change/alter the strain path, some of them are listed as follows:

a) Material:

a1 – Improving the crystallographic texture, by increasing the χ -fiber intensity, which means to have a material that is more resistant to thinning (through maximization of the “r” parameter). The intensity of the χ -fiber will be defined mainly by the steel chemical composition, cold rolling strain and the annealing processing conditions (DUCHÊNE et al., 2002; HUTCHINSON, RYDE, BATE, 2005; FERREIRA FILHO et al., 2005).

a2 – Use of a chemical coating: It consist of an anti-adhesive nano-layer applied on the zinc (HDG) layer (by the steel mill), in order to decrease the friction coefficient between the tool and the sheet. This is frequently used due to its efficacy that has already been proven in the automotive press shop (and also due to its very low cost).

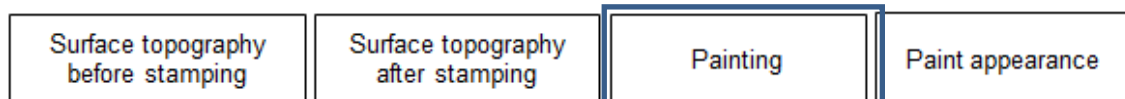
b) Process:

Monitoring the stamping process by means of the process signature made it possible to see changes due to, as for example, tool wear and operating temperature, sheet metal oil film thickness, roughness and material properties, which in turn, could lead to different stress states and strain rates (BANABIC et al, 2000). There are some press resources that can be used to adjust the process signature, as for example, applying a variable Blank Holding Force - BHF (DOEGE, ELEND, 2001) and/or by a variable punch velocity (SEKERES et al., 2009).

c) Project changes: Here, FEM simulations are essential. Project changes (in the stamped part / tooling), may predict quality problems and solve them in several ways. The most common that can be pointed out are:

c1 – Changes in part design: This is the most complicated way, mainly for outer car panels, because there are several restrictions from the design point of view. It may lead to the statement that: any slight change can “kill the car theme”. From the product engineering point of view it can lead to the requirement of further virtual analysis, mainly related to durability tests.

c2 – Changes in the tooling project: This is the most frequently used “way out”, namely: to add or remove draw beads along the tool edge, change its design / profile in order to regulate the sheet velocity during stamping.



3.3 Painting

Nowadays, every vehicle that is produced has typically the layering system as shown in fig.3.3.1.



Figure 3.3.1: The layers: from substrate to clear coat (LEX, 2010).

In general, what could be expected from the painting process would be associated to: processability, environment, appearance and performance, as illustrated on fig. 3.3.2.

Following will be given a short basic explanation of each one of the above mentioned items, apart from paint appearance, which is the focus of the present work, and that will be explained with greater detail in the next chapter.

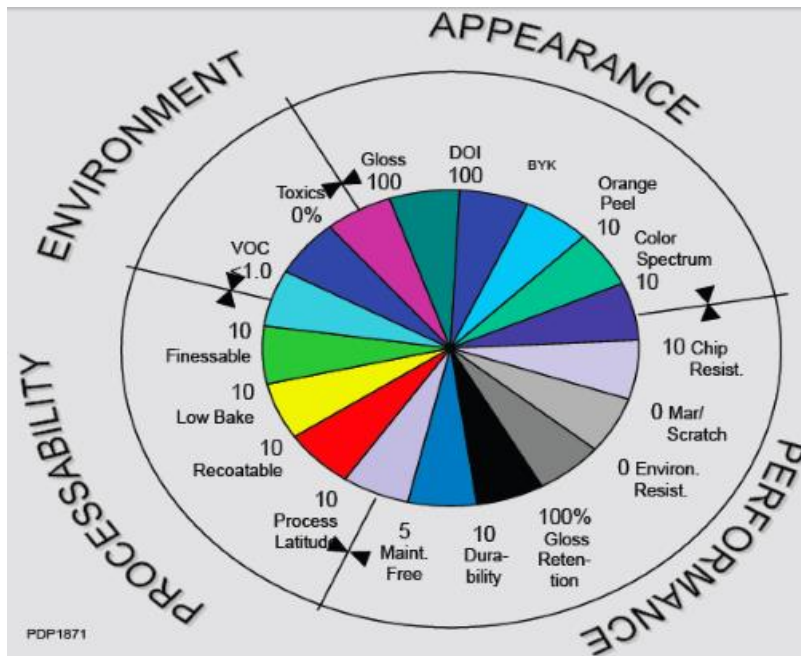


Figure 3.3.2: The four major painting requirements (DE MARK, 2013).

In the fig. above VOC is defined as Volatile Organic Compound - Any compound of carbon that participates in atmospheric photochemical reactions.

Processability

Processability is related to the paint capacity of achieving all the following characteristics, simultaneously with lower cost and higher productivity.

Environment

Globally, governments are enacting or refining regulations that restrict the amount and types of solvents used in the paint. In addition to the environmental regulations, changes in consumer demands and expectations are forcing changes in the coating technologies. Coatings formulations are constantly changing to comply with the emissions guideline for Volatile Organic Compounds (VOC).

Appearance

Appearance is mainly evaluated by four topics: Gloss, DOI (Distinctness of Image), orange peel and color spectrum. These topics, besides color spectrum, will be explained in greater detail in the next chapter, as mentioned previously.

Performance

Performance is related to its resistance to environmental issues such as acids, scratches, stone impact, UV rays, etc. and also to its capacity of long term appearance retention and being maintenance-free.

Table 3.2.1 summarizes, for the painting process used in the present work, the main characteristics and functions of each layer and the related main process variables.

Table 3.2.1: Main aspects of the painting process used in the present work.

Layers	Phosphate	E- Coat	Primer	Base Coat	Top Coat
Material	Fe ₃ (PO ₄) ₂ + ions Zn, Mn, Ni	Epoxy Resin	Polyester	Polyester	Acrylic melamine
Thickness range	2 - 5 µm	15 - 30 µm	20 - 40 µm	15 - 20 µm	25 - 50 µm
Wettability	NA	Medium	High	Medium	High
Function	Sub surface Corrosion, Adherence, Transition layer	Corrosion (barrier)	Physical protection (stone impact), Corrosion (barrier), Wetting, Polish resistant	Physical protection (stone impact), UV protection, Corrosion (barrier),Wetting, Colour	Physical protection (stone impact), Corrosion (barrier),Wetting, UV protection, Scracht resistance, Acid resistance
Deposition method	Quimical	Eletric deposition	Aspersion	Aspersion	Aspersion
Main process variables	Concentration, temperature, time, PH	Concentration, temperature, time, PH, Voltage, Current	Formulation, Air pressure, speed, flow, Temperature, Relative humidity	Formulation, Air pressure, speed, flow, Temperature, Relative humidity	Formulation, Air pressure, speed, flow, Temperature, Relative humidity

Further information about the coating processes for each layer will be described in appendix 1.

Choi et al. (2003) have analyzed the effect of the sheet metal surface topography on the subsequent paint layer. The result are shown in fig 3.3.3.

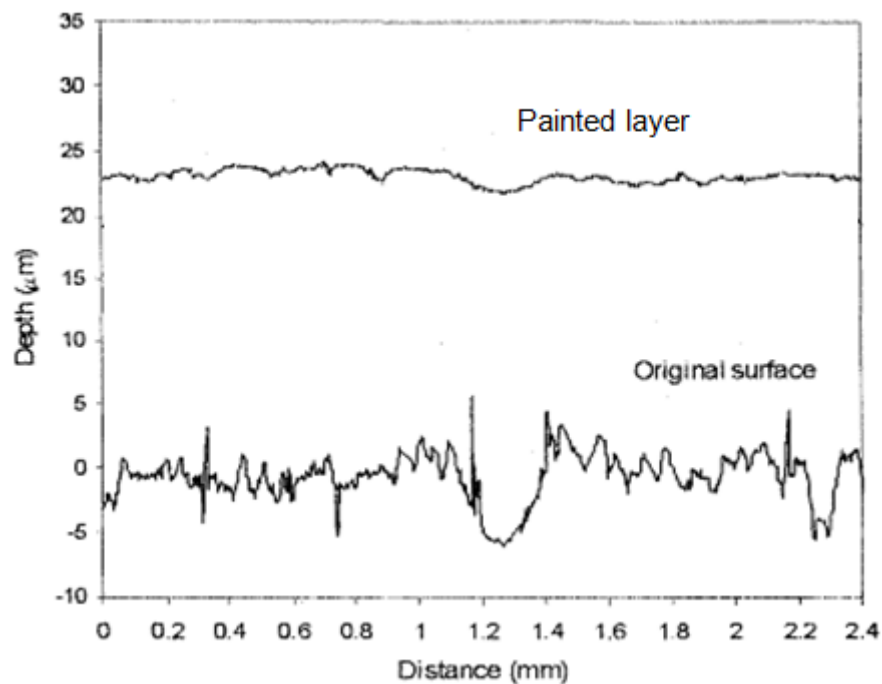


Figure 3.3.3: Sheet metal roughness transferred to the paint layer (CHOI et al., 2003).

From fig. 3.3.3 it may be observed that sheet metal roughness is transferred to the paint layer with a decreasing intensity.

From the literature (LEX, 2010), in a general form, the main process parameters that influence paint appearance are:

- For the E Coat layer: belt speed and voltage, film buildup, additives, solvent makeup, temperature, humidity and ratio of components.
- For the primer, base coat and clear coat layers: Fluid flow, atomization, gun / bell distance, belt speed and voltage, film buildup, flash-off time, additives, solvent makeup, temperature, humidity and ratio of components.

In a more specific research, conducted by Klent and Minko (2008), fig. 3.3.4 shows the results of a DOE (Design of Experiments), pointing out that the main factors affecting paint appearance are associated with: paint material (40%), process control (15%), process (30%) and “basics” (15%). Specifically for the item “basics”, the steel quality represented 40%, or, in a macro view, steel quality was responsible (in that research), for 6% of the total paint appearance.

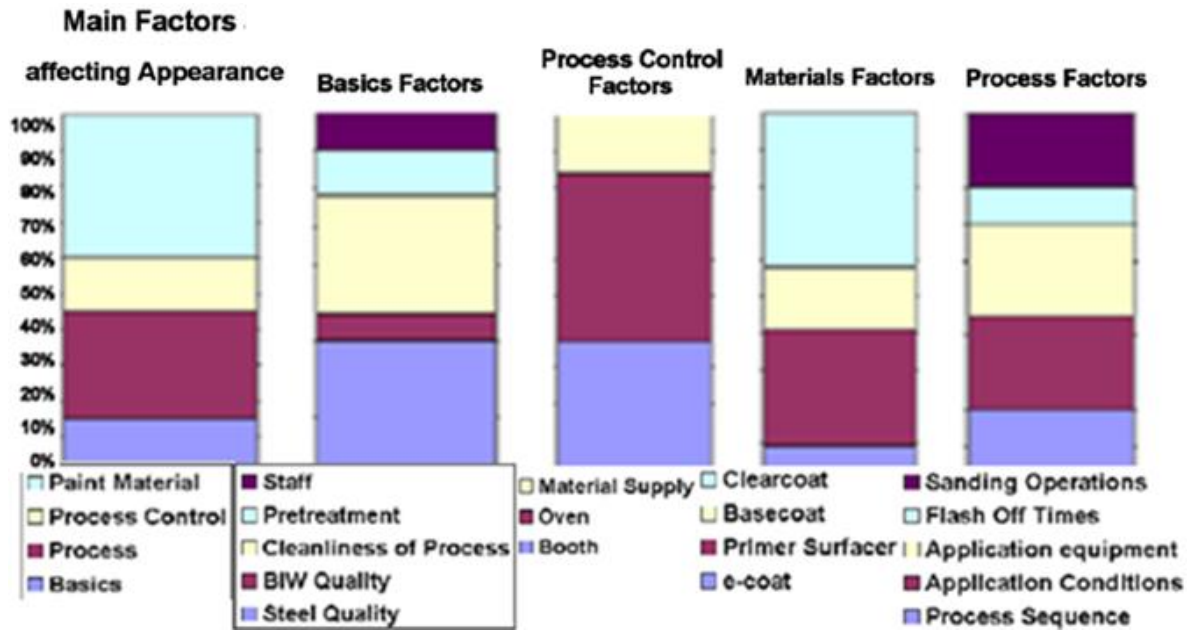
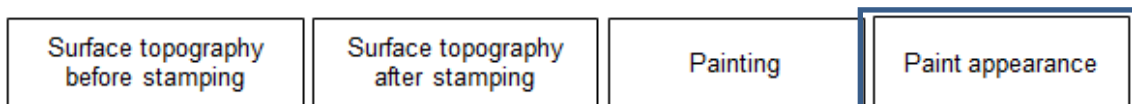


Figure 3.3.4 : Result of the design of experiment(DOE). The most interesting result (for the present work), is the influence of approximately 6% of the steel quality on the paint appearance (KLENT, MINKO, 2008).

Indeed, these results, concerning the main factors affecting paint appearance, will be reviewed further in the discussion, as per chapter 6.4.1.2.



3.4 Paint appearance

One of the main goals of the painting process is to minimize the transference of the sheet metal surface topography amplitude to the clear coat surface. This is evaluated with focus on the quality of the surface and the reflected image. Surface structures with dimensions above 0.1 mm can be seen directly by the unaided eye, smaller structures become manifest by their effect on the directional distribution of the reflected light. Structures at and below 0.1 mm reduce the distinctness of image (DOI); structures in the range of 0.01 mm induce haze and even smaller structures affect the gloss of the surface (STOVER, 2013). Table 3.4.1 summarizes the size of the surface structure / topography related to the wavelength of the reflected light.

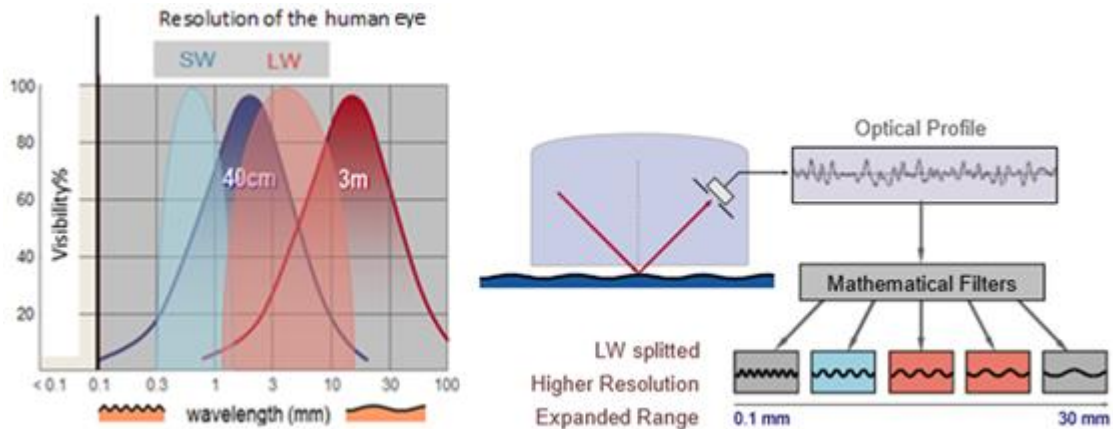


Figure 3.4.1: Left: The visibility of the structures is dependent on the observing distance. The curves in blue (left) and in red (right) show the wavelengths visible to the human eye at a distance of 40 cm and 3 m, respectively. Right: Wave scan evaluation method which is based on the wavelength range (SW - 0.3 to 1.2mm and LW – 1.0 to 12 mm), similar to the ones visible to the human eye at the distances of 40cm and 3 m, respectively (LEX, 2010).

Although several car companies use the same equipment (wave scan), each one of them has their own way to evaluate its paint appearance. GM, for instance, uses a scale called *Rating* (R), that usually varies from 2 (worst) to 10 (best) and its value is calculated from eq. 1 (fig. 3.4.2), which inputs are the intensity (0 to 100%) of the SW and LW created by the interaction of an incident laser beam with the paint surface. In general, for an automotive panel measured at the clear coat layer, the intensity (in percentage) of LW should vary from 5 to 25 and for SW from 10 to 50. As rating values are much more sensitive to LW, some car companies correlated its value to orange peel (LEX, 2010).

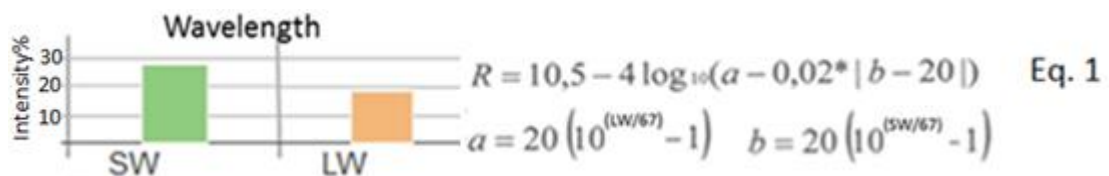


Figure 3.4.2: *Rating*(R) is based on a range of wavelengths visible to the human eye at a distance of 40 cm (Short Wave - SW) and 3 m (Long Wave – LW).

More recently, in order to improve the quality of the paint appearance analysis, Byk Gardner (LEX, 2010) upgraded the wave scan analysis replacing the

classical SW and LW scales by five sub-scales Wa, Wb, Wc, Wd and We which results, in turn, are represented by the spectral curve, as shown in fig. 3.4.3, bottom.

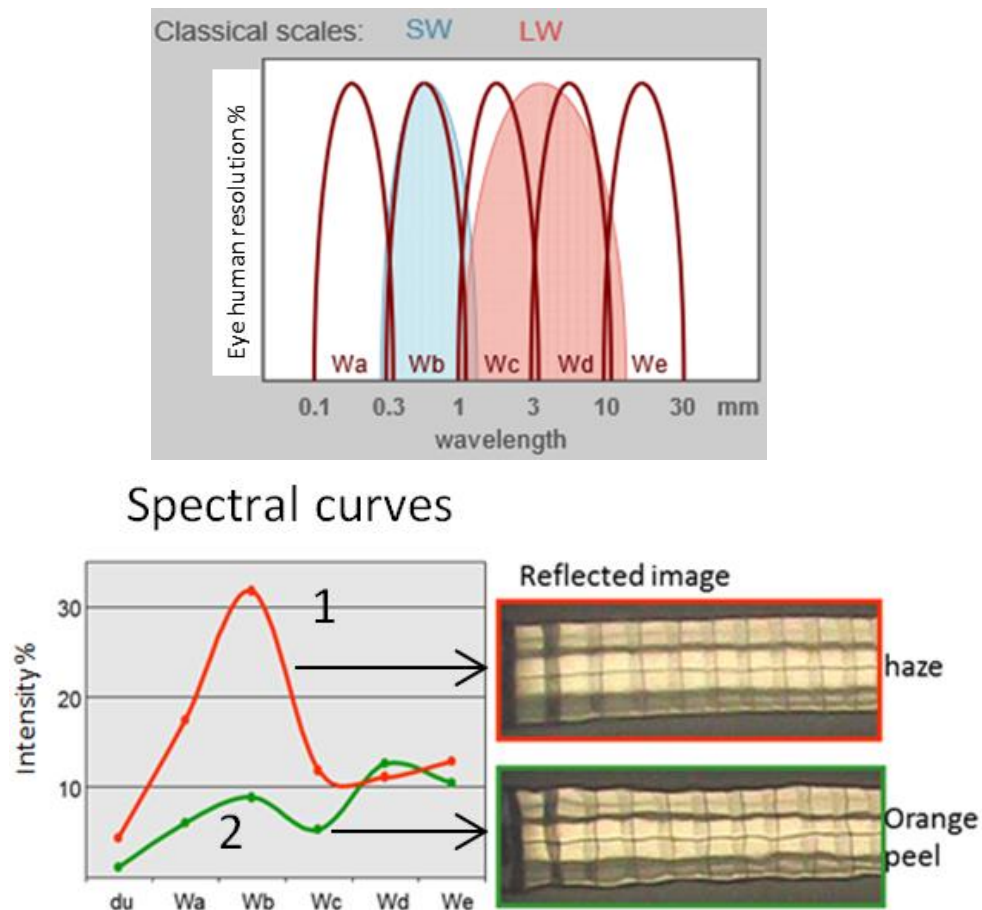


Figure 3.4.3:

Top: The wave scan with five wavelength scales, Wa, Wb, Wc, Wd and We, instead of two, SW and LW from the “common” wave scan.

Bottom: Two typical spectral curves. In *curve 1*, short waves are predominant and the associated reflected image with the haze effect and, in curve 2 with predominant long waves and the corresponding reflected image, which is associated with the orange peel effect (LEX, 2010).

Therefore the question arises: which of the spectral curves is desirable?

To that extent, Klemt and Minko (2008) have studied the public opinion about 10 different painted panels (listed in the horizontal axis - from A to J), for different surface structures (spectral curves), as shown in fig. 3.4.4.

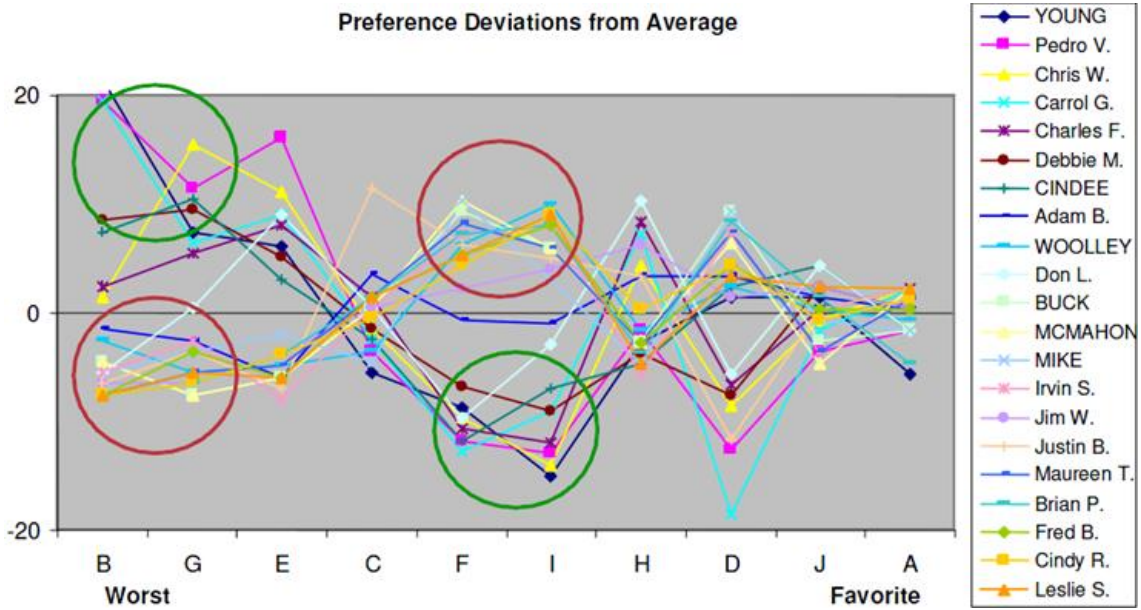


Figure 3.4.4: Individual *rating* of Reference Panels, ordered in the horizontal axis from worst to favorite (KLEMT, MINKO, 2008).

From panels B and G (Worst rating) and panels F and I (intermediate rating) the observers formed two groups of preference: One, insensitive to roughness (SW) and the other one roughness sensing (SW). Both groups “hated” rough surfaces (LW). As an overall average, they prefer a LW-SW balance, as noted on panels J and A. Typically, fig 3.4.5 shows four examples of the ratio of different structure ranges, respectively, accentuated SW and LW, Accentuated SW, predominant LW and finally a balance of LW-SW (the one pointed out as favorite is shown in fig 3.4.4).

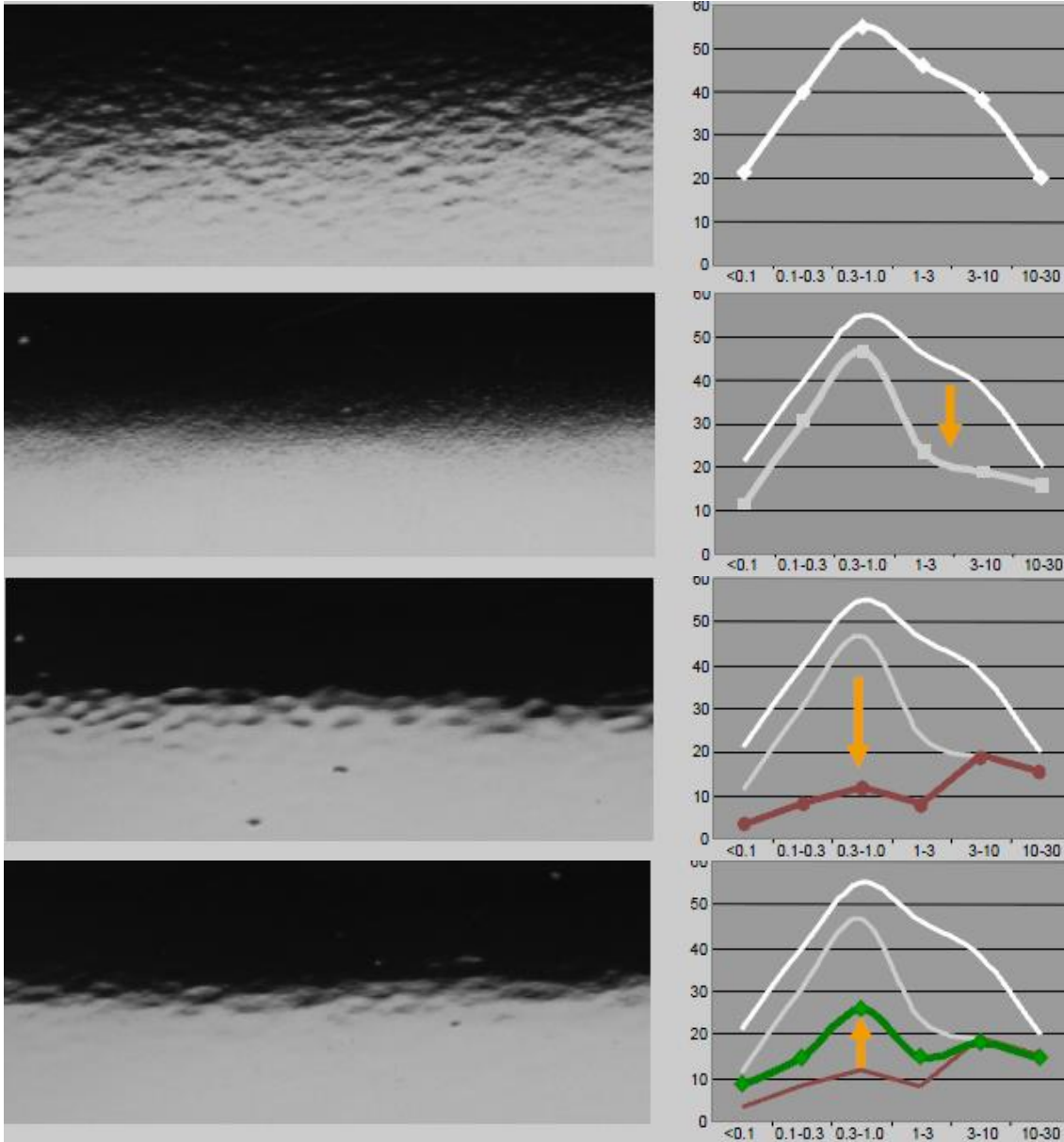


Figure 3.4.5: Ratio of different structure ranges SW and LW) (intensity x wave length in mm.) (LEX, 2010).

In fig. 3.4.5(top), for higher intensities of short and long waves, it shows the combined effect on the surface paint aspect (at 40 cm distance). The appearance is a mixture of haze and orange peel effects. The other two bellows are the same as presented on fig. 3.4.3 with predominant haze and orange peel effects, respectively. The bottom one shows a balance between short and long wave, which is also called the “Sugarloaf Mountain” (in Rio de Janeiro). If this bottom spectral curve is adopted as a reference of good paint appearance by a car maker, it could be used in helping to optimize the appearance, e.g. in determining the optimum clear coat thickness, as shown in fig. 3.4.6.

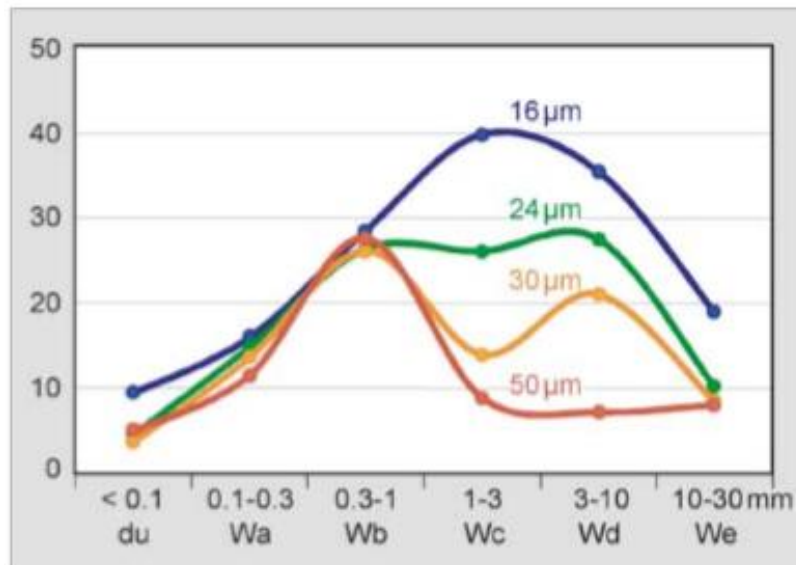


Figure 3.4.6: Influence of clear coat film thickness on paint appearance (LEX, 2010).

In this case, LW was decreased by increasing the clear coat thickness. Using the criteria of the “Sugarloaf Mountain”, in order to achieve better paint appearance, the one with 30 μm would be chosen, (although the 16 and 24 μm would be cheaper) (LEX, 2010).

Lex (2010), see fig. 3.4.7, has also shown that one way of decreasing SW is by decreasing the roughness of the sheet metal. It was also observed that the sheet metal roughness also affected the LW values, but with lower intensity. This aspect has been explained by the research of Simão and Aspinwall, (1999). They have observed a linear correlation between roughness (SW) and waviness (LW) as mentioned in chapter 1.1.2 on skin-pass reduction, (fig. 3.1.8). In fact, as the roll surface roughness R_a increases, the W_{ca} (waviness) also increases. They also suggested that this phenomenon could be a direct consequence of the efforts, during roll texturing, to make the roll with increased roughness.

It is also shown, in fig. 3.4.7 (bottom), the surface paint aspect for both curves (at 40 cm of distance). The one with the “smooth steel” looks like as having a better paint appearance. This point will be discussed in greater detail in chapter.6.4.1.2.

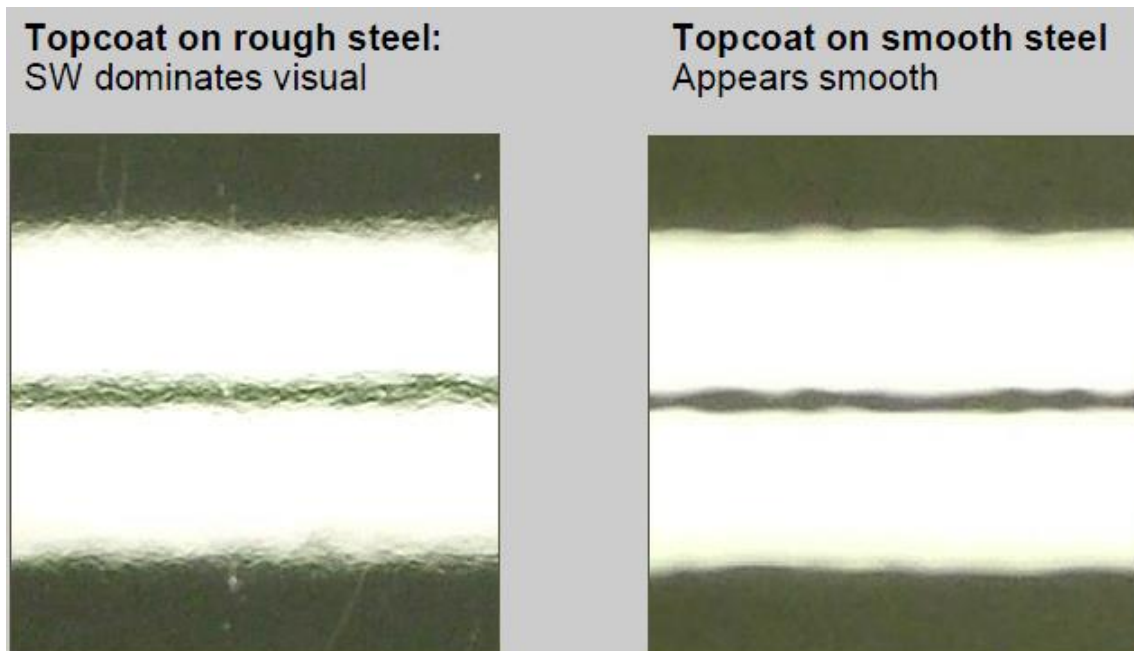
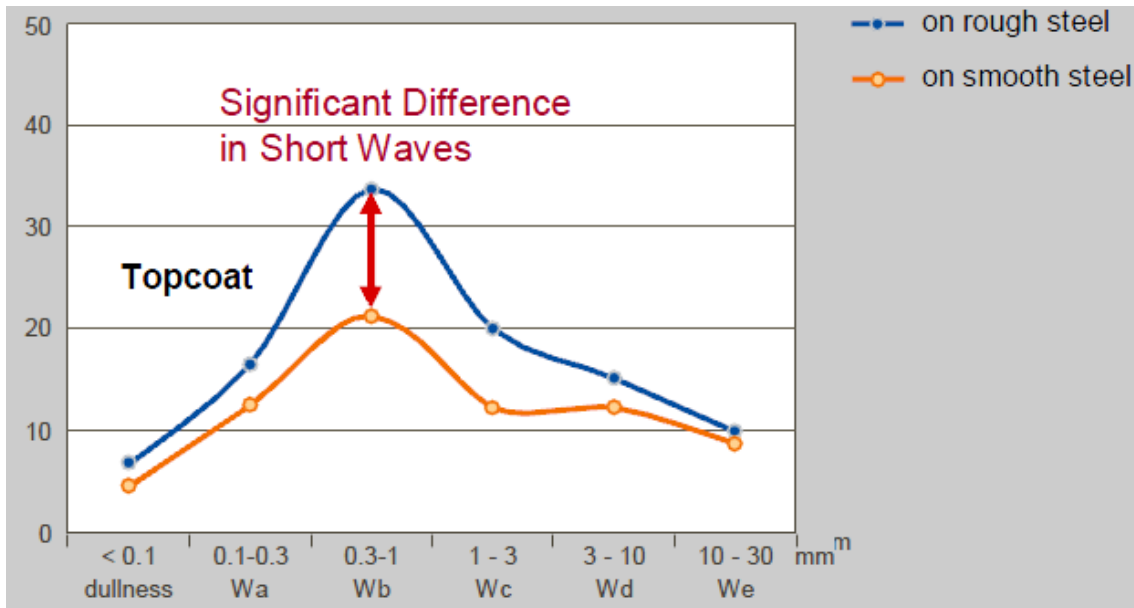
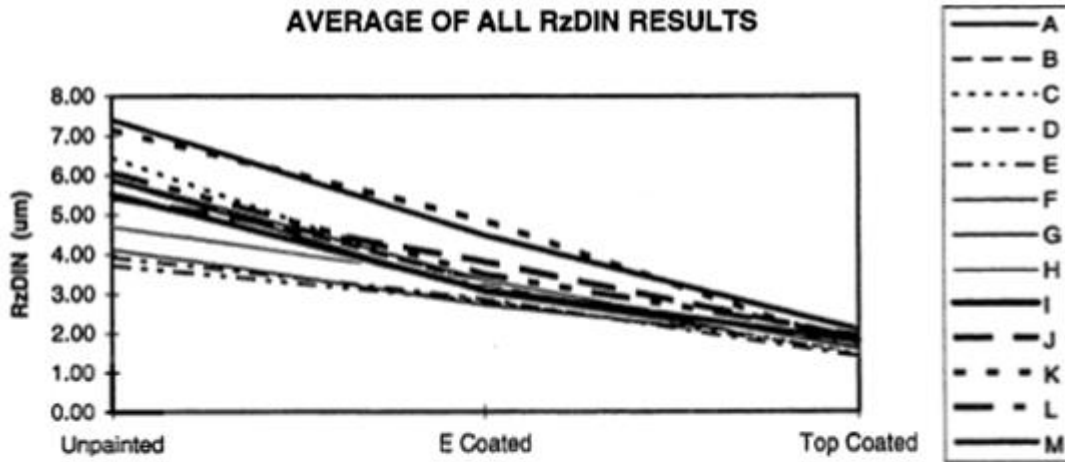


Figure 3.4.7: Influence of the steel quality on the paint appearance at the clear coat stage (topcoat) observed at a distance of 40cm (LEX, 2010).

In the following, the influence of roughness on paint appearance will be described in more detail.

Burgin (1996) has analyzed the roughness evolution of 13 steels (used by the Australian automotive industry). The main purpose was to investigate the effect of various substrates on the image clarity. From fig. 3.4.8 it may be clearly seen the relationship of sheet metal roughness on its clear coat (top coat) roughness, where,

as for a higher roughness at the beginning of the painting process, so will be at the end, although there were significant reductions in the roughness scatter.



PRODUCT CODE	PRODUCT DESCRIPTION	C/MASS (g/m ²) Outer/Inner
A	Zn-Ni E.G. + 1um Organic Overlay	20/20+1
B	Uncoated - CA3SN-E	0
C	Galvanneal + Fe-Zn Flashcoat on Both Sides	60+3/60+3
D	Galvanneal	30/60
E	Galvanneal	60/60
F	Galvanneal	45/45
G	Zn-Ni E.G. + 1um Organic Overlay	0/20+1
H	Galvanneal + Fe-Zn Flashcoat on One Side	30+3/60
I	Galvanneal	45/45
J	Zn-Fe E.G. + Fe-Zn Flashcoat on Both Sides	20+3/20+3
K	Zn-Ni E.G.	20/20
L	Zn E.G.	40/40
M	Zn-Ni E.G. + Fe-P Flashcoat on One Side	30+1/40

Figure 3.4.8: Effect of the reduction in scatter in the roughness parameter Rz after E coating and Clear coat (top coat) for 13 different steel sheets (BURGIN, 1996).

From fig 3.4.9 Burgin (1996) has presented the Toyota (Australia) standard top coated panels which correlate the surface roughness profile with the image clarity ratings varying from 1.0 (poor) to 6.0 (good). This methodology, of correlating surface roughness profile and paint appearance, will be also used in the present work, where a good correlation has been also observed. This will be discussed in greater detail in the chapter 6.3.1.

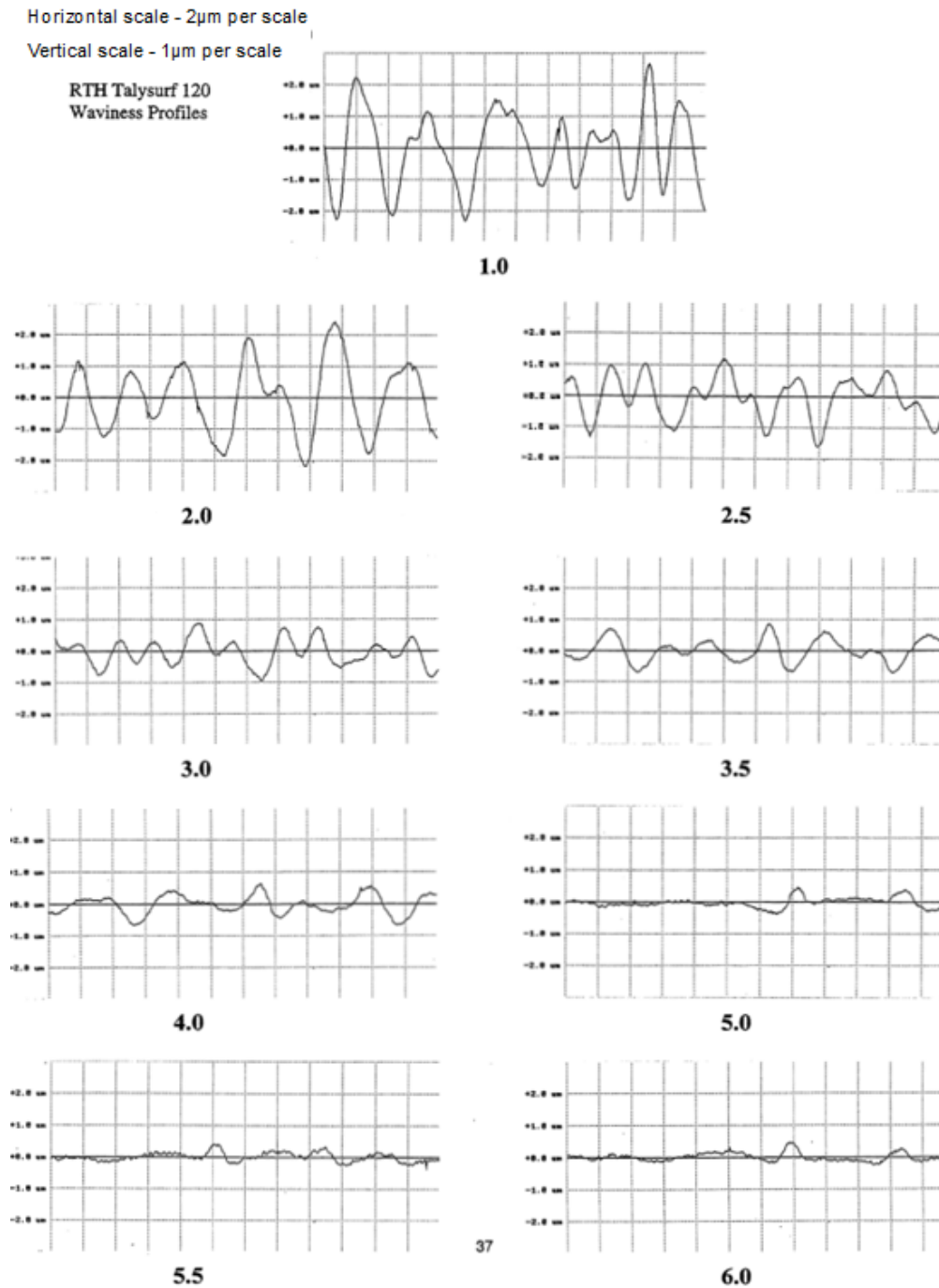


Figure 3.4.9: Toyota standard image clarity *ratings* and its correlation with the surface roughness profile (BURGIN, 1996).

In the literature it is often described that steel sheets having a low R_a and high peak count P_c lead to a better paint appearance. Indeed, Scheers et al (1998) has studied the influence of the sheet metal 2D-roughness parameters R_a and P_c for different surface texturing on the corresponding paint appearance (fig. 3.4.10).

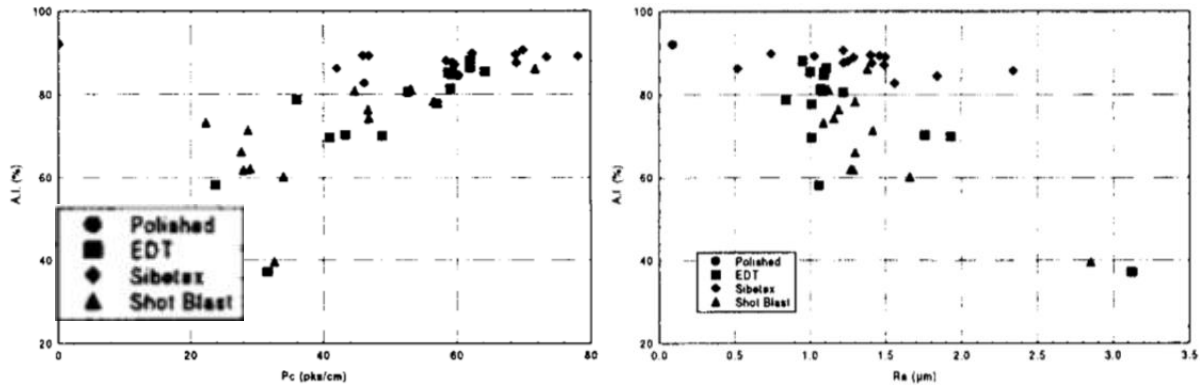


Figure 3.4.10: Appearance index A.I. versus peak count (Left) and Ra(Right) (SCHEERS et al 1998).

They have concluded that for stochastic textured materials, such as SB and EDT, indeed there is a decrease in the paint appearance with increasing Ra. Further, it was observed an increase in the paint appearance with increasing in the peak count Pc. However, on the contrary, with the Sibetex (EBT process), the paint appearance becomes almost independent of Ra. Paint appearance was characterized by means of a weighted average (of gloss, DOI and orange peel), called appearance index A.I. (SCHEERS et al 1998), as given by the equation:

$$A.I = 0.15 \text{ Gloss } (20^\circ) + 0.35 \text{ DOI} + 0.25 \text{ NSIC (orange peel)} + 0.25 \text{ NSIC* (Loss of contrast in the reflected image)}$$

Miller et al.(2000) investigated the effect of surface topography texturing on the paint appearance of automotive (aluminum) panels. They clearly established that increasing the deterministic level of texturing, there was an increase in paint appearance, as shown by fig. 3.4.11. One can state that the inherent variability of the random texturing methods (SB, EDT) are responsible for introducing a wide range of topographic wavelengths on the roll surface and that the substrate waviness features cannot be masked by the paint film and have a detrimental effect on the final paint appearance (GRETHE, 2013).

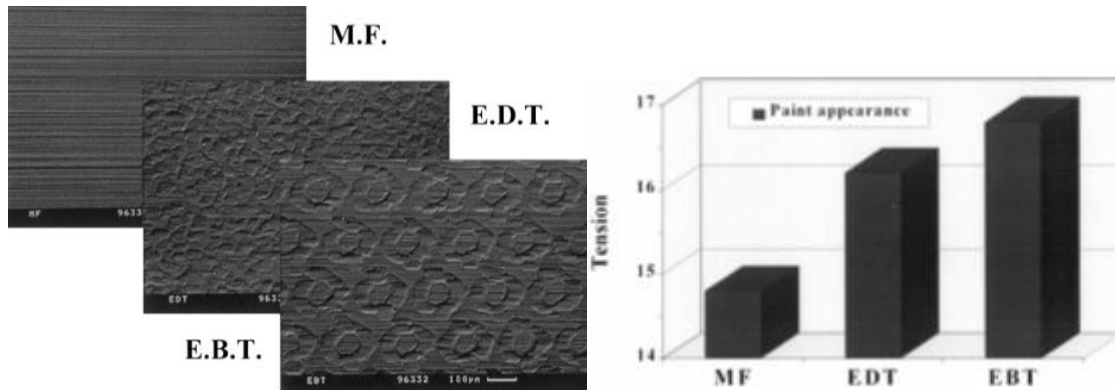
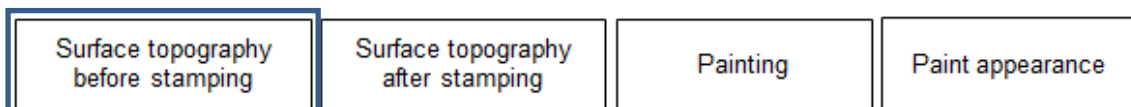


Figure 3.4.11: Left: Difference in surface topography of different types of textured aluminum sheets. Right: Paint appearance for vertically coated panels with different substrate texturing (tension=0 showing the orange peel, tension=24 showing the mirror-like appearance) (MILLER et al.,2000).

3.5 Summary of the literature review

Summarizing, the most relevant aspects of the literature review are given in the following. These are going to be related / discussed along with the results of the present research work.



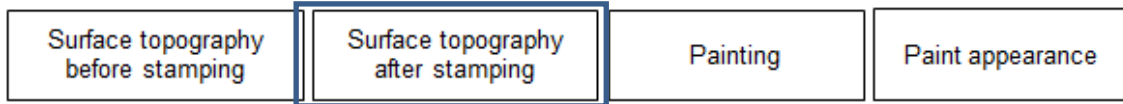
3.5.1.1 - EDT is the most used non-deterministic (stochastic) texturing method due to its better processability (MEYER, 2013), although deterministic texturing methods confer to the sheet metal a better stampability and paintability characteristics (PAWELSKI et al, 1996; MILLER et al.,2000; SCHEERS et al 1998).

3.5.1.2 – Skin-pass reductions as well as the texturing methods, both play an important role on the surface topography transfer degree which, in turn, strongly influence the stamping process and paint appearance (PAWELSKI et al., 1994; 1996; TSHERSCHE, 2012.).

3.5.1.3 - The degree of transfer “saturation” occurs first for the EDT process compared to others processes, like SBT, LT and EBT (PAWELSKI et al, 1994).

3.5.1.4 - The EDT process promotes much less randomness in the surface topography than the SBT process (VALENTIN et al., 2008; PAWELSKI et al, 1996).

3.5.1.5 - Roughness standard deviations, along the coil length (due to roll wear) and along the coil width (due to roll crowning), should be monitored in order to keep the paint appearance quality (PFESTORF et al., 1998; GEIGER et al., 1997).



Roughness evolution during stamping can increase or decrease in amplitude depending on the stamping conditions:

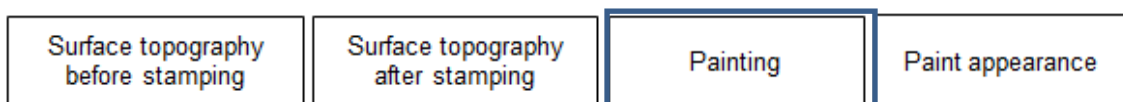
3.5.2.1 - The deformation modes such as sliding, pressing and bending cause a decrease in the surface roughness due to peak flattening (WICHERN et al., 2004; PYEN et al., 2012; JONASSEN et al., 1997; RAHARIJAONA et al., 1999; MA et al., 2002).

3.5.2.2 - Strain without die contact can lead to thinning which causes an increase in the surface roughness, proportional to the degree of thinning (WICHERN et al., 2004; SEKERES et al., 2010; UNFER, BRESSAN, 2012).

3.5.2.3 - Stamping process variables like: type and quantity of lubricant applied on the sheet metal and on the tool, tool temperature, tool surface (hardness, roughness and coatings), sheet metal chemical treatment, process signature, etc., play an important role on material thinning (chapter 3.2).

3.5.2.4 - For the sheet metal there is a FLD (forming limit diagram), however it must also be taken into consideration that there is a further (and more restrictive) limit, in terms of strains, associated with the surface quality (appearance).

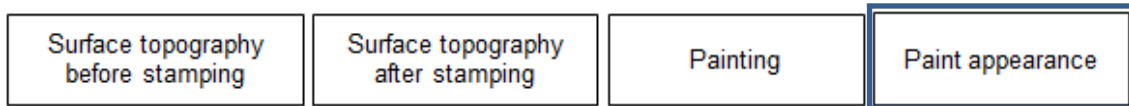
3.5.2.5 – Increasing the values of the 3D sheet metal roughness parameters a_{clm} (maximum ratio of the closed void area) and V_{cl} (closed void) should lead to a decrease in the coefficient of friction during stamping (PFESTORF et al., 1998; WEIDEL, ENGEL, 2009; PAWELSKI et al, 1996; BFINTEN et al, 1996).



3.5.3.1 - Painting process is designed in order to attain the criteria of processability, environment, appearance and performance and it is responsible for the major aspects of paint appearance. However, sheet metal surface topography plays an

important role in improving the paint appearance, and it can possibly lead to cost reductions in the painting process (DE MARK, 2013).

3.5.3.2 - Sheet metal roughness is transferred to all painted layers with a decreasing intensity (CHOI et al., 2003).



3.5.4.1 - Sheet metal surface roughness should have a 2D-roughness parameter $Pc > 60$ peaks/cm (the higher the better) and a 2D-roughness parameter $Ra < 1.5 \mu m$ in order to attain good paint appearance (SCHEERS et al 1998).

3.5.4.2 - The main *rating* scale advantage is due to it is a numerical scale (easy to work with under industrial conditions), however it presents a major disadvantage because it has little information attached to it, mainly relating ranges in wave length (long wave) (LEX, 2010).

3.5.4.3 - For optimizations related to paint appearance the spectral curve is recommended since it represents all wavelengths associated with the surface topography, while the *rating* only presents an average value of the Wc , Wd and We values (LEX, 2010).

3.5.4.4 - The primer and clear coat layers diminished the difference in paint appearance (more accentuated for SW (Wb and Wc) and less for LW (Wd and We) (LEX, 2010).

3.5.4.5 - The E coat and clear coat layers diminished the difference in the 2D-roughness parameter Rz (BURGIN, 1996).

3.5.4.6 For the sheet metal there is a FLD (forming limit diagram), however it must also be taken into consideration that there is a further (and more restrictive) limit in terms of strains, associated with the surface quality (appearance). This approach could be named tentatively as a "PALD- Paint Appearance Limit Diagram", being more restrictive than the FLD.

The next chapter, materials and methods, was planned in order to evaluate all the aspects mentioned above.

4 MATERIALS AND METHODS

This chapter was planned in order to evaluate the inter-relationship, under controlled industrial conditions, among skin-pass reductions, surface texturing methods (SBT and EDT), surface topography (characterized by the 2D and 3D roughness parameters), stampability and paint surface quality, for automotive steel sheet stampings.

To accomplish these objectives, twenty two (22) materials/conditions with different surface topographies were selected, as summarized in table 4.1. They all were supplied by four (4) different steel mills (here named as A, B, C and D). Six (6) material conditions came from three different mills. The other sixteen (16) material conditions (which were assigned also for another D.Sc. research work), were materials coming from mill A.

The twenty two (22) material/conditions were selected for the experiments carried out at the press shop of a Brazilian automotive company (see fig. 4.4). These twenty two (22) material/conditions were analyzed for two texturing methods, namely: SBT=shot blast texturing and EDT= electric discharge texturing. Four (4) skin pass reduction conditions (0.3%, 0.5%, 0.8% and 1%) for each texturing method have been utilized. Further, these materials were analyzed for two conditions: beginning and at the end of the coil, which is approximately 2 km long.

All these conditions will be related to the differences in the steel sheet roughness topography and its evolution (topics 3.1.3 and 3.1.4 of the summary of the literature review).

Table 4.1: Materials and conditions.

TEST	CYLINDER TEXTURE	ROLL CAMPAIGN	SKIN PASS REDUCTION%	MATERIAL SPECIFICATION	MILL
1	SHOT BLAST	INITIAL	0,3	DIN EN10130 DC05	A
2			0,5		
3			0,8		
4			1,0		
5		END	0,3		
6			0,5		
7			0,8		
8			1,0		
9	EDT	INITIAL	0,3		
10			0,5		
11			0,8		
12			1,0		
13		END	0,3		
14			0,5		
15			0,8		
16			1,0		
17	EDT			DIN EN 10346 DX54D+Z	B
18				DIN EN10130 DC03	C
19				DIN EN 10346 DX54D+Z	D
20				DIN EN10130 DC03	B
21				DIN EN 10346 DX54D+Z	C
22				DIN EN 10346 DX54D+Z	D

The blank material used in the tests 1 to 22 has dimensions of approximately 700 x 1500 x 0.7 mm. The 2D roughness measurements (equipment listed in fig. 4.2) were evaluated (according to SEP 1940) in three positions along the width of the blank (left, middle and right) and at two positions along the length (initial and end). Then, blanks were cut from these samples, in the dimensions of 42 mm x 400 mm. The larger dimension was positioned in the longitudinal direction of the blank. At the end, there were approximately 30 samples for each test condition. The 3D roughness measurements (equipment listed in fig. 4.2) were evaluated only in one position from a sample (extracted from approximately the middle of the blank). 2D-roughness parameters are according to ISO 4287, ASME B46 1 and 3D-parameters according to ISO 25178-2 , except C_{lm} and a_{clm}, which were evaluated according to the parameters shown in the research work of Pfestorf (1995). Greater details of these roughness parameters are given in the attachment 1 (pg 225). As mentioned in the introduction / research limitations, the results obtained in this experimental procedure are qualitative / quantitative results. The key objective of this work is to assess the main variables that link stampability and paint appearance using low carbon steel

sheets. Statistic validation and physical modeling will be performed in future research work.

In order to evaluate the topics listed in the summary of the literature review, experiments were subdivided into 3 runs, as following:

4.1 First run

The main aim of the first run was to analyze the influence of the sheet metal surface topography, which comprises skin-pass reduction, texturing methods and sheet metal roughness deviations due to roll life, on the paint surface finish quality (topics 3.5.1.2, 3.5.1.5, 3.5.3.2, 3.5.4.1, 3.5.4.2, 3.5.4.4 and 3.5.4.5 of the summary of the literature review). Due to operational issues related to the processing (all 22 tests were performed until the clear coat stage, under industrial conditions).

The first run (as summarized in fig. 4.1) was sub-divided into 2 steps: First step was the “coarse filter”, aiming at the selection of the “best” and the “worst” conditions and a second step - the “fine filter”, with processing carried out until the clear coat stage.

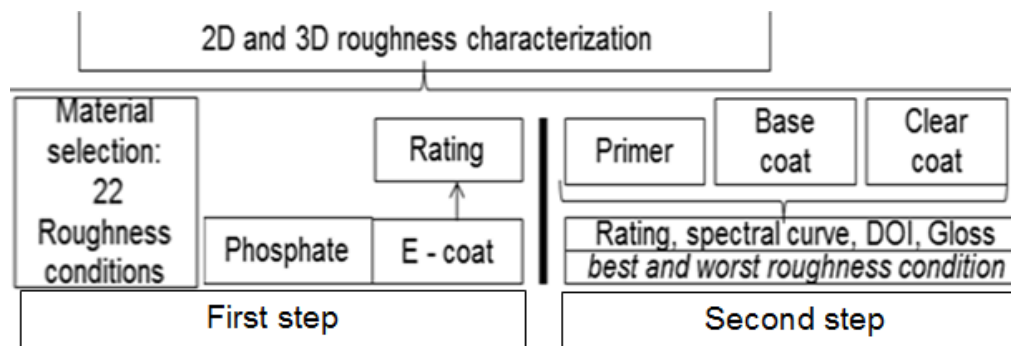


Figure 4.1: First run.

4.1.1 The first step of the first run

In greater detail, the *first step* was as following:

The twenty two (22) conditions of the steel sheets (with 5 samples for each condition), were processed (under industrial conditions), in the paint shop (of GM SCS Brazil), in the process stages named *phosphate* and *E coating*. Following, the 110 samples were evaluated for their *rating* (see *attachment 2 and topic 3.4 for details*). The equipment is listed in fig. 4.2.

4.1.2 The second step of the first run:

The “best and worst” conditions of the *rating* (measured in the first step), were processed (under the same industrial conditions), until the E coat stage and simultaneously in a laboratory (under the same conditions), at BASF São Paulo – Brazil for the sequence of paint processing: primer, base coat and clear coat. These experiments were planned in such a way that, at the end of the painting process, one sample from each process stage (sheet metal, phosphate, E coat, primer, base coat and clear coat) was available. For each sample the roughness profile (2D and 3D), was measured. Also, on the clear coat layer, the following characteristics have been evaluated: *rating*, spectral curve and the DOI= Distinctiveness of image (see *topic 3.4 for details*). The equipment related to the evaluation of DOI, rating and spectral curve, are listed in fig. 4.2.





Equipment					
Model	Surtronic 3+	Form Talysurf Intra	µsurf basic	Wave scan dual	Glossmeter
Application	2D roughness	2D Roughness profile	3D roughness	Rating, DOI and spectral curves	Gloss

Figure 4.2: Equipment used in the first run. Technical details (for each equipment), are given in attachment 2.

As in the experiment (first run), the stamping process influence was not taken into account, a second run was necessary.

4.2 Second run

The second run (summarized in fig. 4.3) was sub-divided into 2 steps in order to evaluate the following main topics:

First step: Analyze the influence of sheet metal surface topography on the stampability of the steel sheets (topics 3.5.1.1, 3.5.1.2 and 3.5.2.5 of the summary of the literature review).

Second step: Analyze the roughness change after stamping, which comprises the deformation modes (strain path) on the steel sheet related to the sliding and bending

during stamping operation, and its effect on the paint appearance (topic 3.5.2.1 of the summary of the literature review).

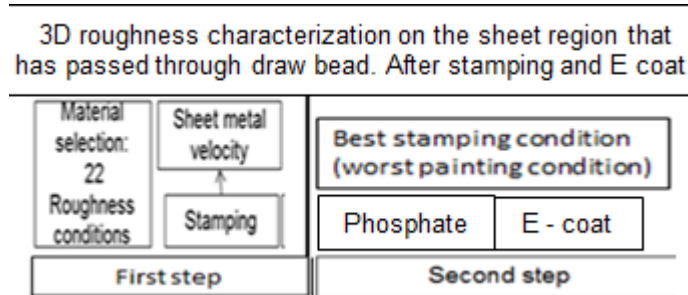


Figure 4.3: Second run.

4.2.1 The first step of the second run:

The *first step* of the second run was as follows:

The twenty two (22) test conditions (again, five samples for each condition) have been stamped under industrial conditions. The equipment’s are listed in fig. 4.4.

Fifteen (15) samples have been used to “stabilize the process”, before starting the actual test counting. A displacement (mm) versus time (s) curve has been collected for each one of the studied samples.



Figure 4.4: Equipment used in the second run, first step. Technical details (for each equipment), are given in the attachment 2.

The sketches of tooling and of the stamped part are shown in fig. 4.5.

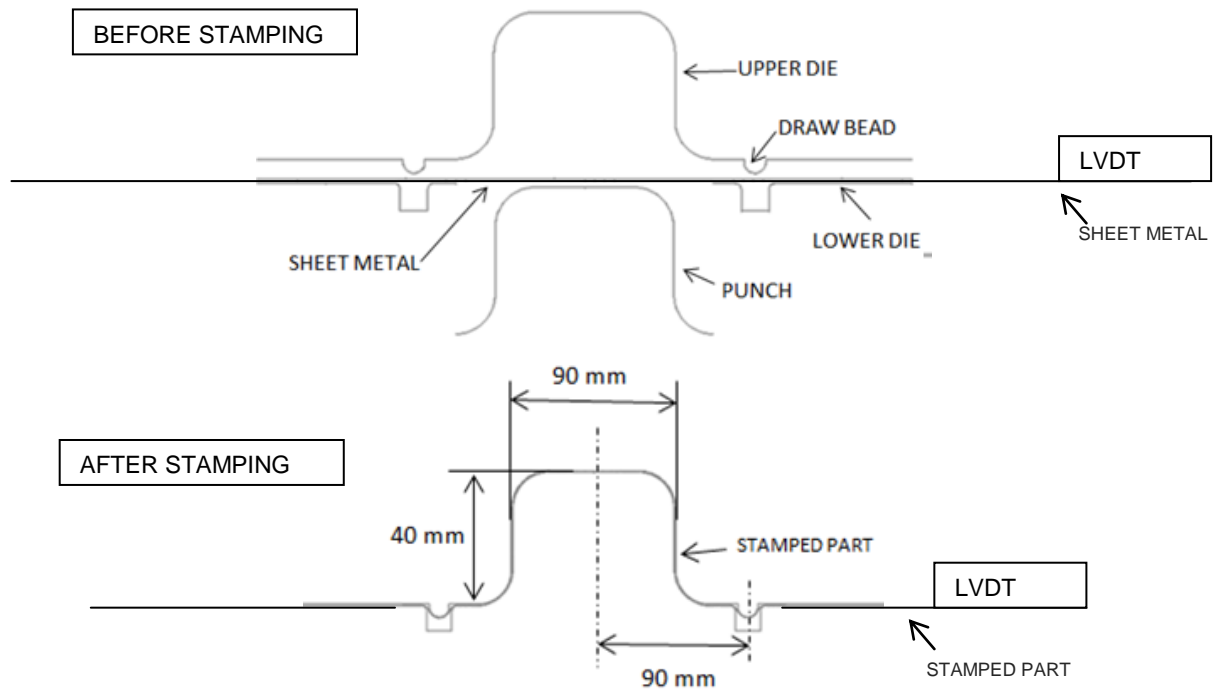


Figure 4.5: Stamping sketches: Tooling and stamped part. Sample width is 42 mm.

4.2.2 The second step of the second run:

The sample that presented a higher velocity (its definition given in fig 5.2.2.3) during stamping has been selected because it was associated with the “worst” paint condition (just remembering the aim of the second step was to analyze the effect of roughness changes after stamping on the paint appearance). The roughness (measured in 2D and 3D), was characterized in the region that has passed through the draw bead, as shown in fig. 4.6. Following, the sample was processed (under the same industrial conditions), until the E coat stage and again the roughness (measured in 2D and 3D), was characterized at the same region that has passed the draw bead.



Figure 4.6: Region that has passed the draw bead.

As in these stamping experiments it has been observed that the sheet samples presented no thinning, it became necessary to conduct a further third run, this in order to evaluate the thinning effect on the roughness evolution.

4.3 Third run

The main aim of the third run was to analyze the influence of the strain applied to the sheet metal (without having any die contact), on the roughness evolution (similar to those areas that occur during the stamping and painting processes) (topic 3.5.2.2, 3.5.3.2 and 3.5.4.6 of the summary of the literature review). This run was sub-divided into 2 steps in order to evaluate the following main topics:

First step: Roughness evolution on a uniaxial tensile test, and then along the all paint layers, as shown in fig.4.7.

Second step: 2D Roughness evolution for a “near” plain strain condition.

4.3.1 The first step of the third run:

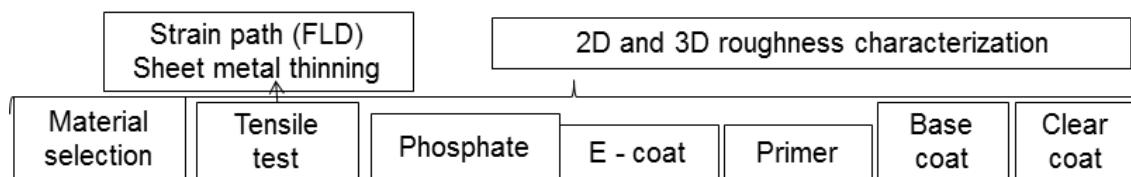


Figure 4.7: Third run – first step.

Another material DIN EN 10346 DX54D+Z, thickness 0.75mm, was submitted to a tensile rupture test (in the LD rolling direction), and the strain path was evaluated in the marked regions as per fig. 4.8 (Positions 1, 2, 3 and 4). These samples were further taken to be painted in a way that, at the end of the painting process, one sample from each process step was available (sheet metal, phosphate, E coat, primer, base coat and clear coat), as shown in fig. 4.8. For each sample, measurements were made to obtain the 2D roughness profile, along the whole sample length, in order to obtain also the associated roughness Rz in the regions close to the positions 1, 2, 3 and 4, as illustrated in fig 4.8.

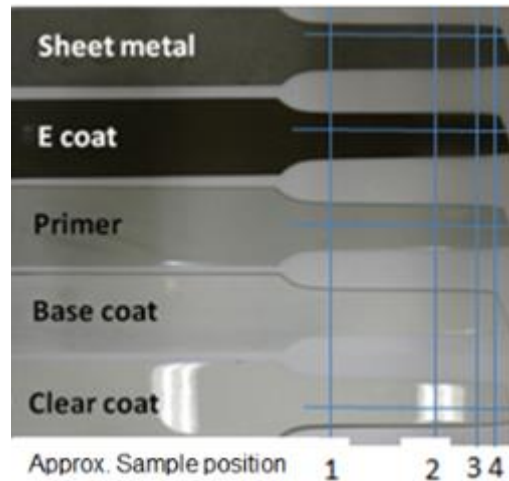


Figure 4.8: Samples submitted to painting after tensile testing. The position 1 is associated to a strain tending to zero (in the tensile testing). Positions 2 to 4 are zones with a continuously increasing strain (in the direction of the rupture zone).

4.3.2 The second step of the third run:

Sample nr. 17 (see table 4.1) was submitted to a tensile rupture test (in the LD rolling direction). Sample geometry was built in such a way to reach a possible plain strain condition during testing. After testing, the thickness, strain and 2D roughness were evaluated in the marked regions as per fig. 4.9 (b) (Positions 1, 2, 3 and 4). The initial geometry of the specimen is shown in the sketch in fig. 4.9 (a).

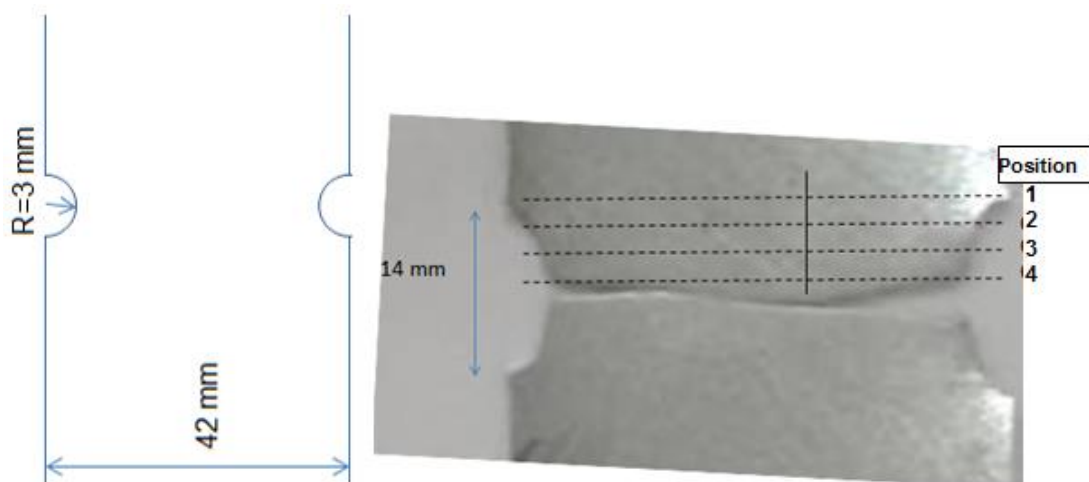


Figure 4.9: (a) Sketch of the “near”-plain strain condition testing. (b) Positions of 2D roughness and thickness evaluations.

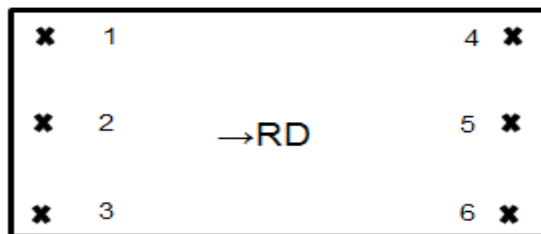
5 RESULTS

In the following the experimental results will be presented, in accordance to the sequence that has been used in chapter 4, related to Materials and Methods.

5.1 Material characterization (as received condition)

The 2D roughness measurements were carried out in 6 points on all the blanks (in the TD to the rolling direction, according to SEP 1940). Results are given in table 5.1.

Table 5.1: Blank: 2D roughness measurements for all test conditions. Sample size L=1500mm, W=500mm. The values given in this table are the average, min. and max. values for the six measurements, for each test condition.



Texturing method	Test condition	Ra				Pc			
		min	max	average	std dev	min	max	average	std dev
SBT	1	1.4	2.06	1.66	0.23	46	62	54	5.7
	2	1.34	1.84	1.45	0.19	50	64	58	5.9
	3	1.04	1.38	1.23	0.1	53	70	63	7.9
	4	1.06	1.42	1.27	0.12	55	82	67	11
	5	1.36	1.86	1.63	0.19	53	62	57	2.9
	6	1.12	1.48	1.32	0.13	51	64	58	5.9
	7	1.14	1.56	1.32	0.13	49	72	60	7.7
	8	1.08	1.26	1.2	0.05	65	81	70	6.3
EDT	9	1.46	1.9	1.62	0.19	49	63	57	5.3
	10	1.48	1.88	1.56	0.13	60	84	70	7.7
	11	1.28	1.56	1.46	0.09	72	86	77	4.9
	12	1.38	1.66	1.50	0.09	74	94	84	8.1
	13	1.35	1.65	1.54	0.13	52	66	60	4.45
	14	1.36	1.62	1.5	0.1	68	81	73	4.4
	15	1.32	1.58	1.45	0.08	73	83	77	3.3
	16	1.4	1.58	1.47	0.06	74	92	79	6.9
EDT	17	1.2	1.32	1.27	0.04	123	144	132	6.9
	18	0.76	0.92	0.82	0.05	108	126	118	6.6
	19	0.52	0.74	0.61	0.07	95	109	100	5.6
	20	0.98	1.26	1.12	0.1	75	90	85	5.5
	21	1.04	1.22	1.12	0.06	91	109	101	6.8
	22	1.08	1.28	1.21	0.06	97	105	101	0.08

The twenty two (22) materials/conditions with different surface topographies were sub-divided into three groups in the left side of the table 5.1. Test conditions one to sixteen come from mill A and they have provided information of skin pass reduction, sample positioning for initial and end of the coil. For these sixteen samples comparison has been made for two texturing methods: SBT (samples one to eight) and EDT (samples nine to sixteen). Test conditions seventeen (17) to twenty two (22) were supplied by three (3) different steel mills (here named as B, C and D). The only information made available by them was that they were all EDT textured rolls.

SBT rolls (Test conditions 1 to 8).

It should be mentioned that, for each coil, there was a specific reduction in thickness in the range of 0.3 to 1.0%. Corresponding samples have been taken at the beginning of the coil (initial) and at the end at the same coil (end), which means approximately at a distance of about 2km - from (initial) to (end) of the same coil. The objective of this procedure is associated with the assessment of the roughness evolution along the coil length.

From the graphs in fig. 5.1.1 (by joining tables 4.1 and 5.1), it may be observed that for the 2D roughness measurements there were no significant differences between the initial and the end of the coil, in terms of roughness. It also can be observed a decrease in the Ra and an increase in the Pc parameters with increasing skin pass reduction.

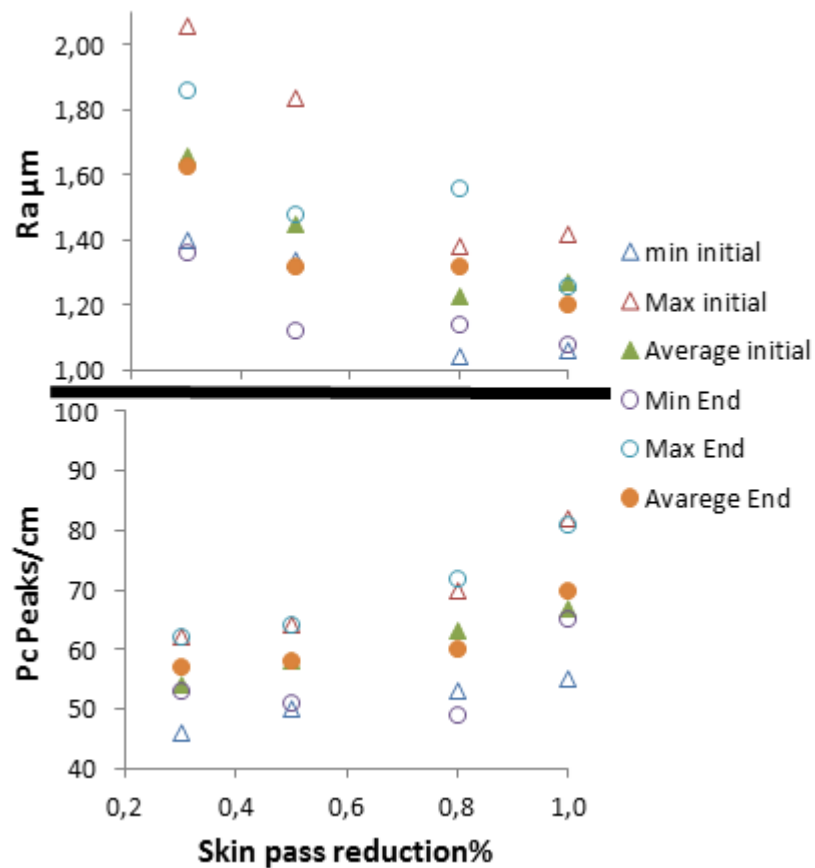


Figure 5.1.1: Comparison between sheet metal surface topography. Initial and end of the coil (SBT condition) for different skin pass reduction.

From the graph in fig. 5.1.2, with roughness measurements performed in 3D, it may be observed that there was no correlation between skin pass reduction and the Vcl and α_{clm} roughness parameters, showing even significant randomness.

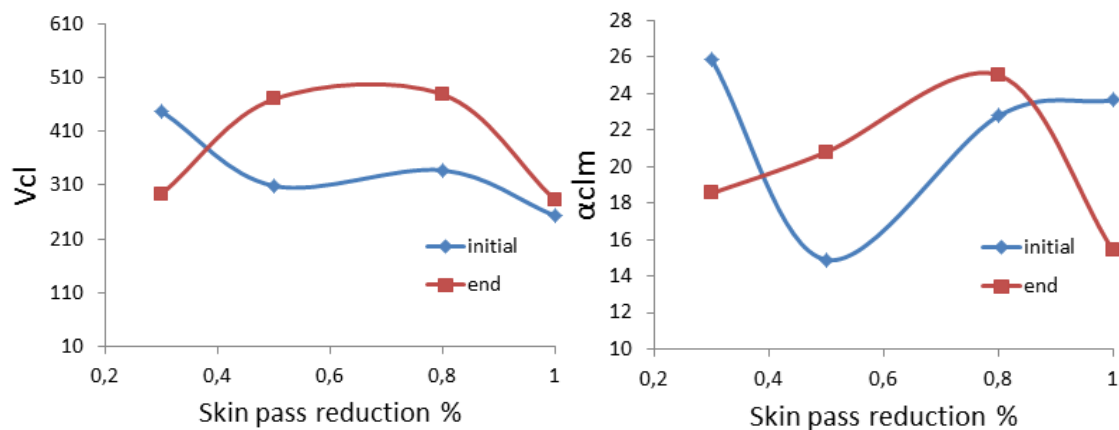


Figure 5.1.2: 3D Roughness parameter evolution. Closed void (Vcl) and max. closed void ratio (α_{clm}) as a function of skin pass reduction % for the initial and end along the coil length (SBT condition).

It must be remembered, again, that the definitions of V_{cl} and α_{clm} are given in the attachment 1.

EDT rolls (Test conditions 9 to 16)

It should be remembered, again, that for each coil there was a specific reduction in thickness in the range of 0.3 up to 1.0%. Corresponding samples have been taken at the beginning of the coil (initial) and at the end at the same coil (end). The objective of this procedure is associated, again, with the roughness evolution along the coil length.

From fig. 5.1.3 (by joining tables 4.1 and 5.1), it may be observed that, for the 2D roughness measurements, there was a significant difference between initial and end of the coil roughness, mostly for R_a versus skin pass reduction up to 0.5%. It also can be observed a decrease in R_a with increasing skin pass reduction up to 0.8% and then a slight increase up to 1.0%. The P_c value has increased with increasing skin pass reduction and it seems it stabilized at about 0.8%.

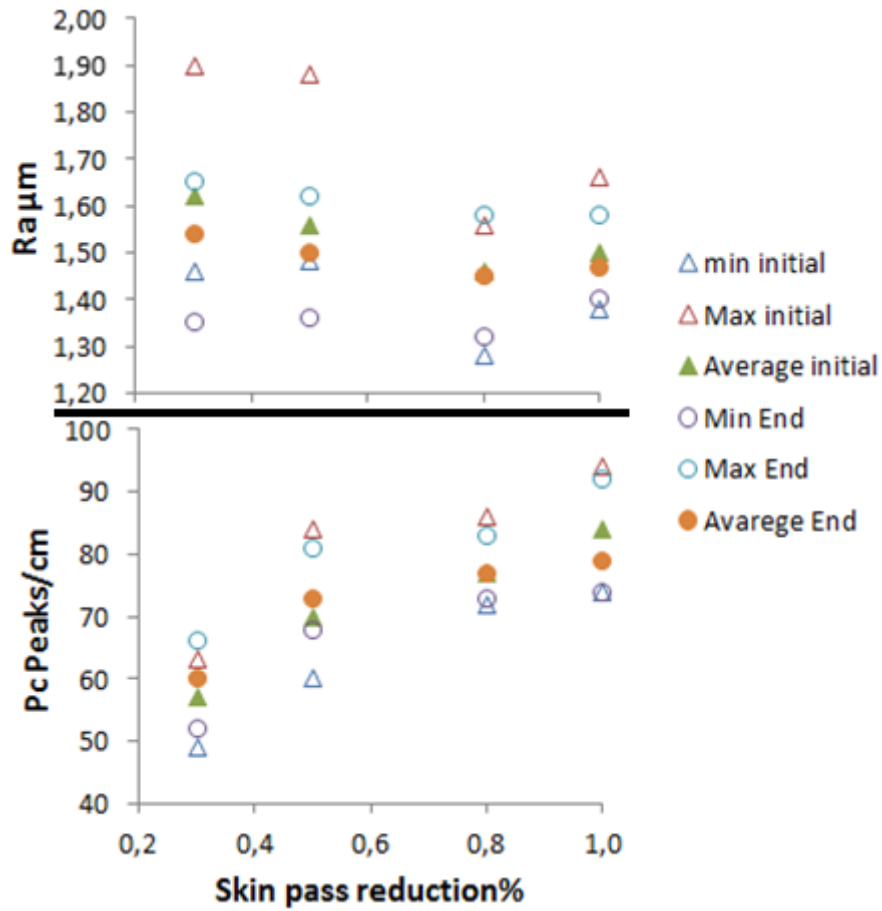


Figure 5.1.3: Comparison between sheet metal surface topography parameters for the initial and end positions, along the coil length (EDT condition), for different skin pass reductions.

Regarding 3D roughness measurements, shown in fig. 5.1.4, there were no significant differences between initial and end along the coil length, for the closed void (Vcl) parameter (left) and for the maximum closed void ratio (α_{clm}) (right).

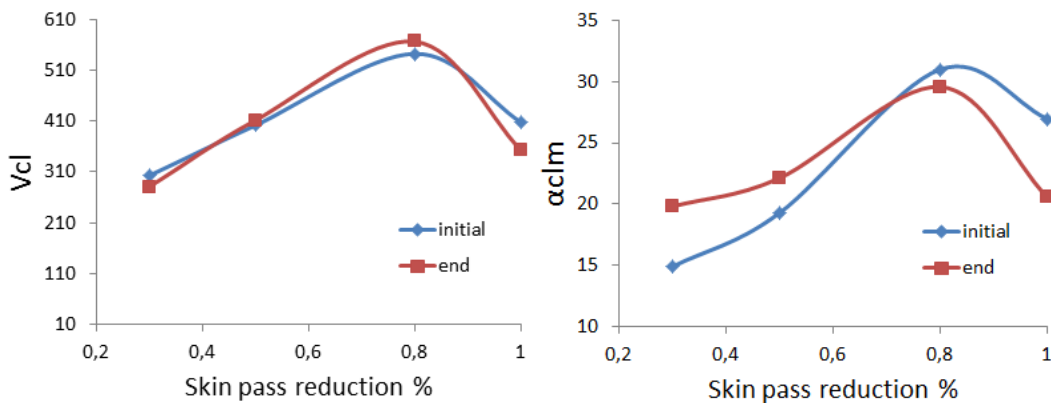


Figure 5.1.4: 3D Roughness parameter evolution: closed void (Vcl) and maximum

closed void ratio (α_{clm}) as a function of skin pass reduction %, for the initial and end along the coil length – EDT condition.

It should be remembered that the definitions of V_{cl} and α_{clm} are given in the attachment 1.

In this fig.5.1.4 it can be observed that the maximum level of V_{cl} and of α_{clm} is achieved for a skin pass reduction of 0.8%.

It should be remembered that these two parameters, as will be pointed out in the discussion, are the most representative ones that may be linked to the stampability and paintability.

EDT rolls (Test conditions 17 to 22)

From fig. 5.1.5 it is shown the 2D roughness characterization (R_a and P_c) for tests seventeen (17) to Twenty two (22).

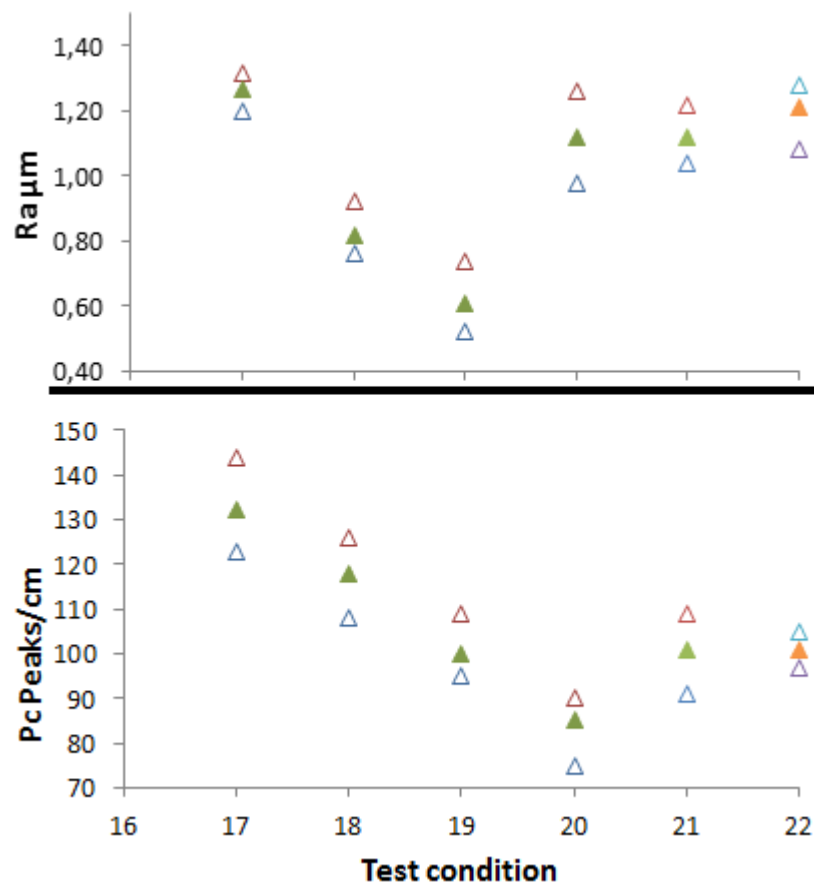


Figure 5.1.5: Sheet metal surface topography for test 17 to 22.

Comparison between EDT and SBT rolls (Test conditions 1 to 16)

From the graph in fig. 5.1.6, the EDT condition has shown a higher Pc value than for the SBT condition. As will be pointed out in the discussion, this may be linked to the improvement in the paint appearance. On the other hand, the SBT condition has shown a lower Rz value, which, as will be also pointed out in the discussion, is better for the paint appearance.

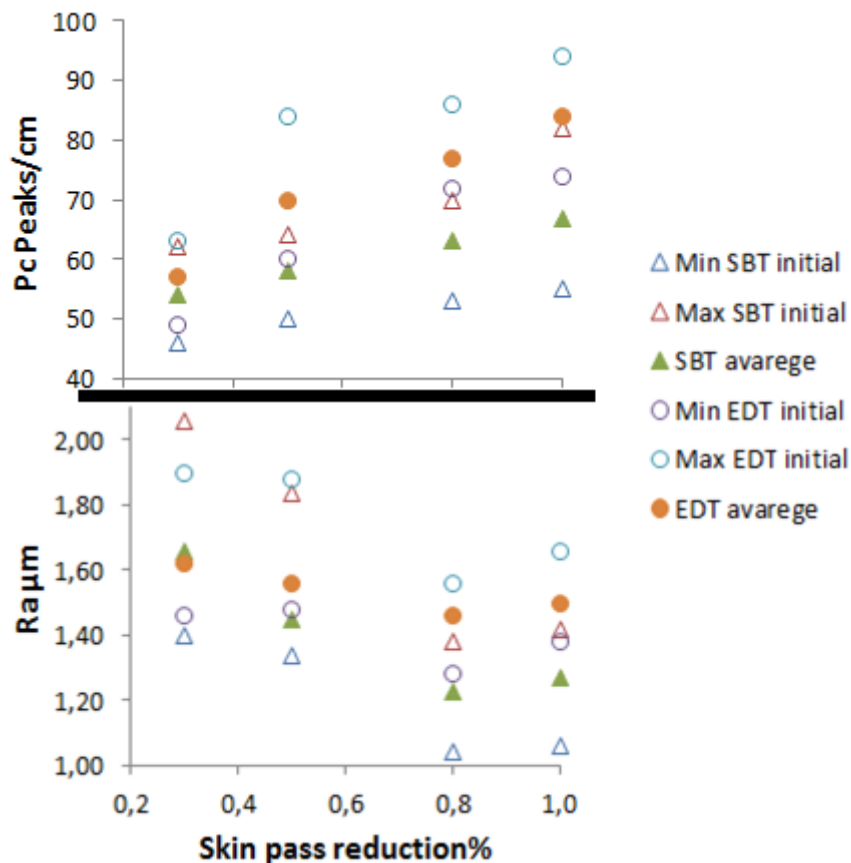


Figure 5.1.6: Comparison between sheet metal surface topography parameters (Average Rz and Pc) for the SBT and EDT roll conditions, for different skin pass reductions (Test conditions 1 to 16).

It can be noted from fig. 5.1.6 the lowest dispersion occurs for EDT with skin pass reduction between 0.8% and 1.0%. Ra standard deviation seems to go in the same direction, as shown in fig. 5.1.7. However the end of the coil for both SBT and EDT at 1.0% of skin pass reduction has shown the lowest value.

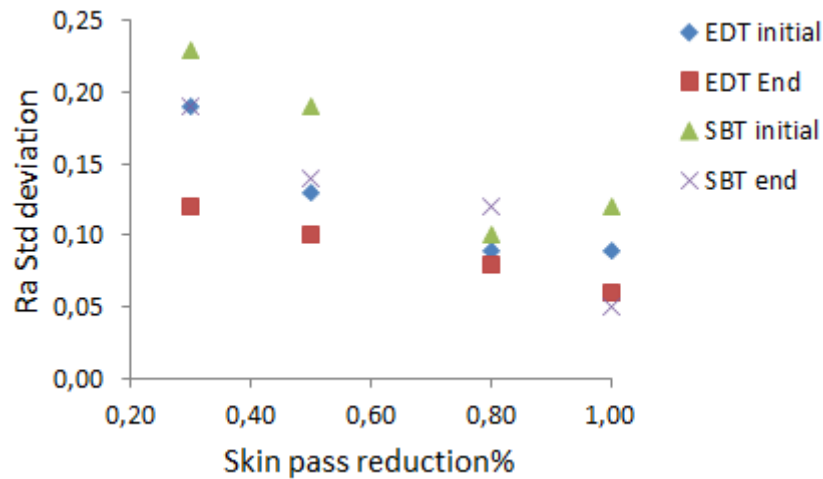


Figure 5.1.7: Ra standard deviation for the SBT and EDT roll conditions, for different skin pass reductions (Test conditions 1 to 16).

From this figure we could ask the reason why we should make a difference between initial and end of the coil? It is well known within the car manufacturing industry the “common approach” that the material having a large standard deviation (initial of the coil) goes for the popular cars whereas the low standard deviation materials (end of coil) goes for the higher grade cars.

Figs. 5.1.8 and 5.1.9 show the evolution of the sheet metal surface topographies for the EDT and SBT roll conditions, respectively. These should be observed along with fig. 5.1.6.

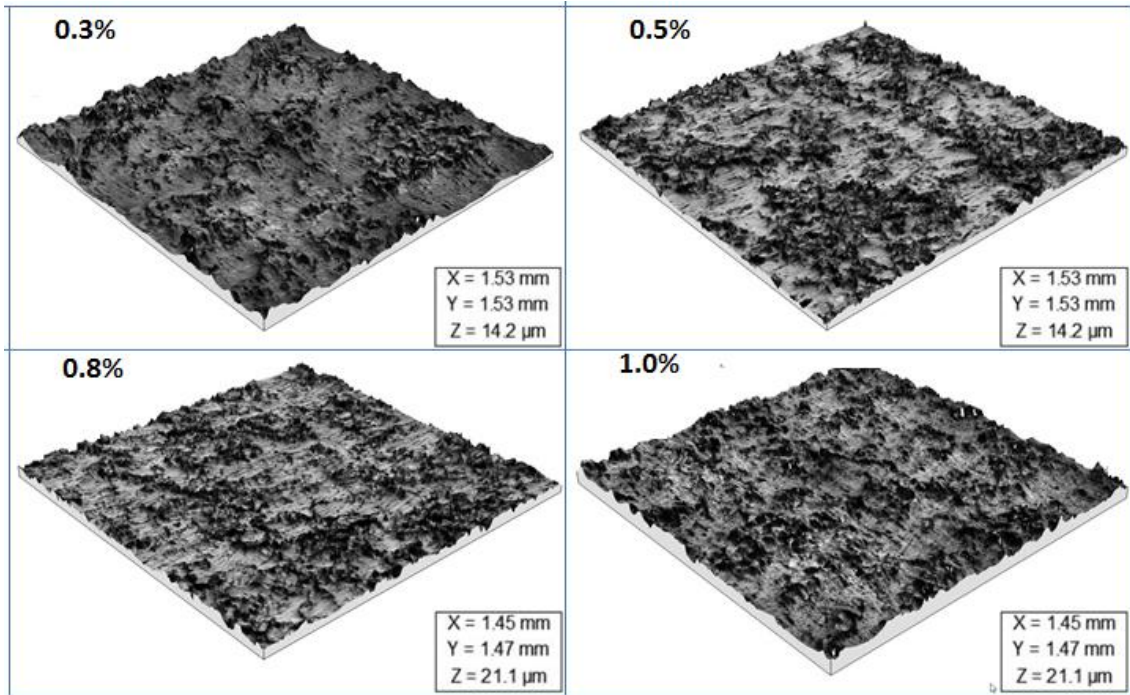


Figure 5.1.8: Sheet metal surface topography evolution as a function of skin pass reduction. - EDT condition (NanoFocus).

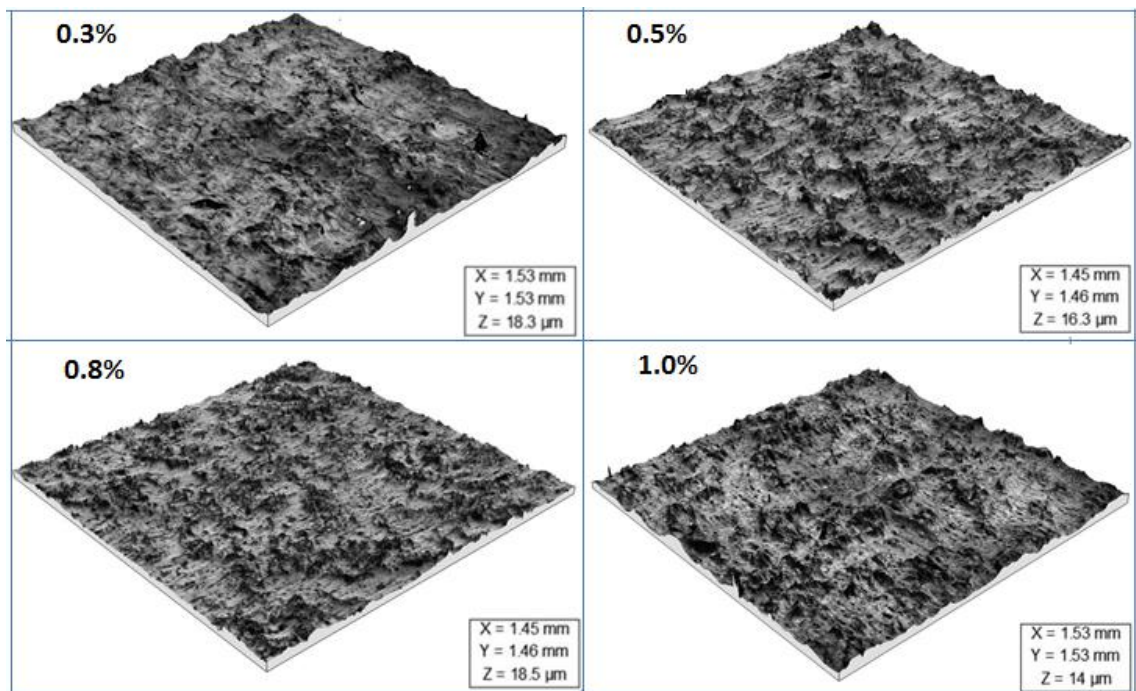


Figure 5.1.9: Sheet metal surface topography evolution as a function of skin pass reduction. - SBT condition (NanoFocus).

Regards the size of the measured areas, there were differences in the results of the α_{clm} and V_{cl} parameters, in the order of up to 10 %, with increasing sample size, as shown in fig. 5.1.10.

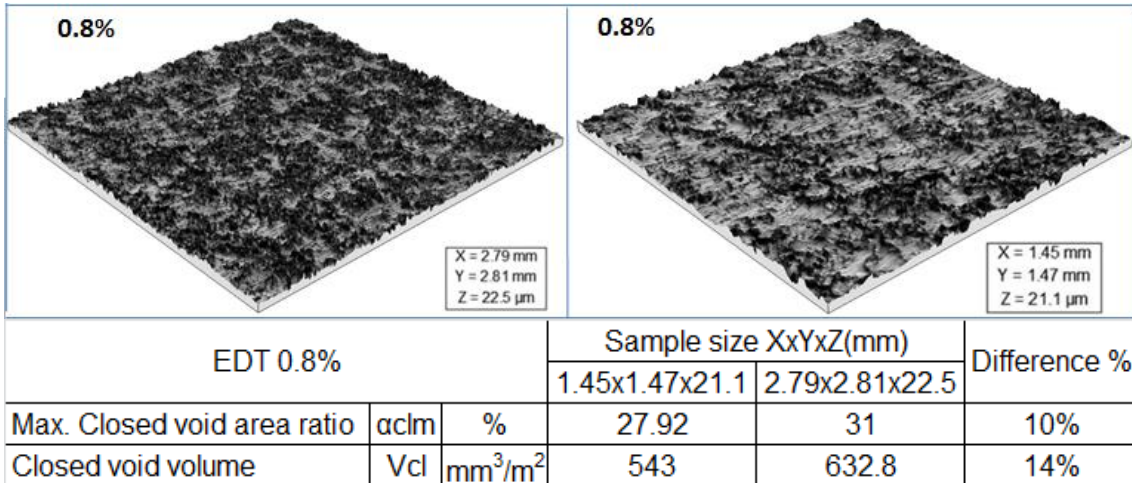
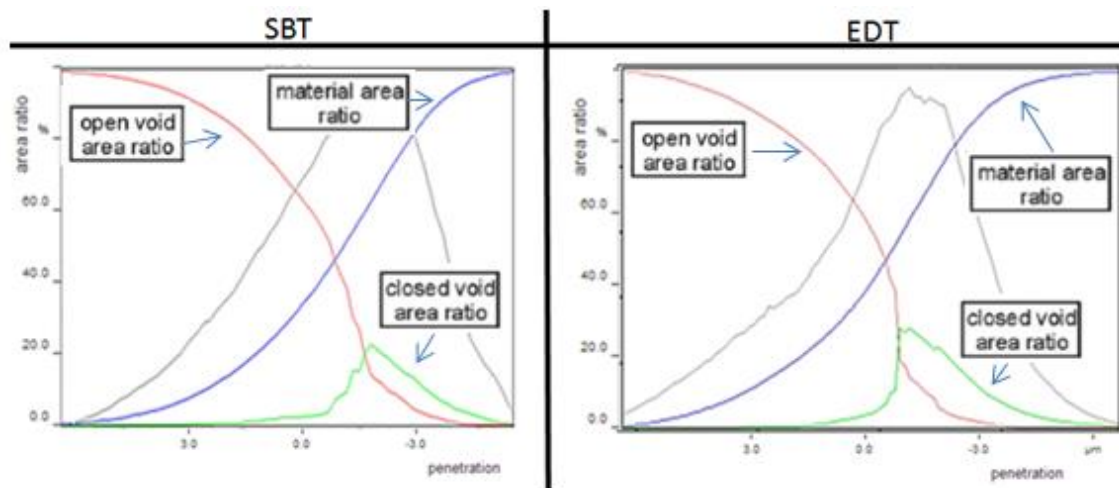


Figure 5.1.10: Effect of sample size on the results of α_{clm} and Vcl parameters. Measurements were done in the same region (of the sample test nr. 11) (NanoFocus).

This gave us an idea of the importance associated with sample size and its influence of the parameter accuracy.

Fig. 5.1.11 shows the bearing area ratio curves (which contains the highest value of α_{clm}), for the SBT condition (Test 1) and for the EDT condition (Test 17). (sample size of approximately 1.5x1.5 mm).



			SBT	EDT
Max. Closed void area ratio	α_{clm}	%	25.9	29.58
Closed void volume	Vcl	mm ³ /m ²	448	567.6

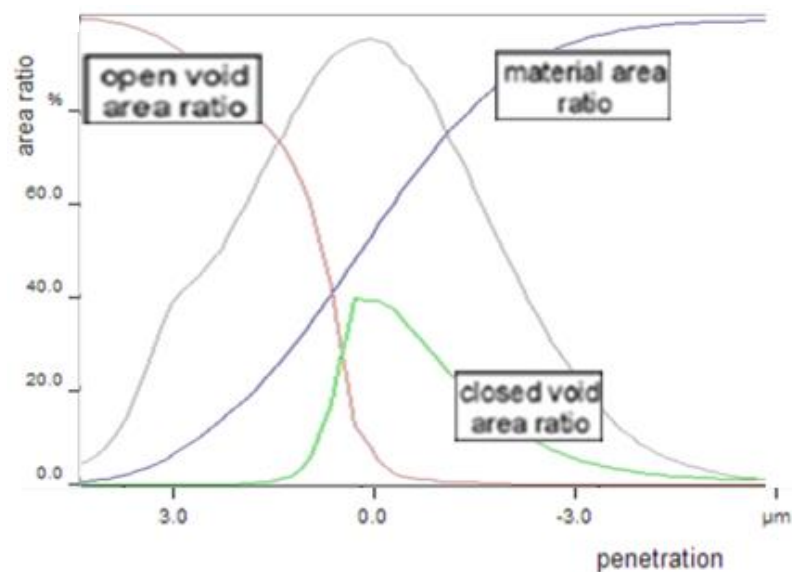
Figure 5.1.11: Comparison between the bearing area ratio curves for SBT and EDT conditions (NanoFocus).

Further details will be given in chapter 6.1.

From this figure it may be observed that the V_{cl} and the α_{clm} parameters are larger for the EDT condition, i.e., there may be a larger volume to retain oil and improve material stampability. The reasons for that will be objective to subsequent discussion (chapter 6.1 and 6.2.2.3)

EDT rolls (test conditions 17 to 22)

Fig.5.1.12 shows the best conditions in terms of V_{cl} and α_{clm} .



			Test Nr. 18
Max. Closed void area ratio	α_{clm}	%	39.74
Closed void volume	V_{cl}	mm^3/m^2	874.8

Figure 5.1.12: Best condition of V_{cl} and α_{clm} . Sample Nr 18. (sample size of approximately 2.8x2.8 mm) (NanoFocus).

5.2 – Tests

5.2.1 – First Run

5.2.1.1 - The first step of the first run

The twenty two (22) test conditions of the steel sheet materials (with 5 samples for each condition), were processed (under industrial conditions), in the paint shop (of GM SCS Brazil), in the process stages named *phosphate* and *E coat*. Following, the 110 samples were evaluated for their *rating* index. The procedure utilized was as shown in fig. 5.2.1.

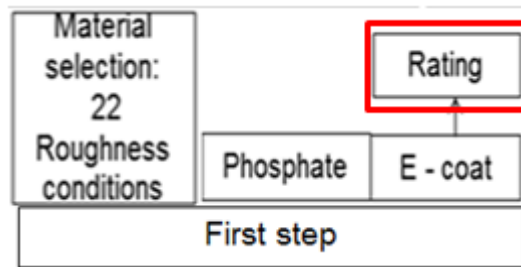


Figure 5.2.1: First run - First step (same as fig. 4.1, left side).

The results of the roughness parameters (3D and 2D) that had shown a correlation factor with the paint appearance (*rating*), at the E coat stage, higher than 0.6, are shown in table 5.2.

Table 5.2: 3D and 2D roughness parameters and corresponding paint appearance (*rating*), at the E coat stage, for the twenty two (22) test conditions.

TEST	Input																	Output	
	3D											2D					Rating		
	Cclm μm	Vmp ml/m^2	Ctop μm	aclm %	Sq μm	Vmc ml/m^2	Vvc ml/m^2	Sha mm^2	Vv mm^3/mm^2	Sa μm	Sp μm	Sr2 %	Sz μm	Sk μm	Ra μm	Pc pk/cm		Rq μm	Rz μm
1	6,30	0,10	5,44	25,90	1,88	2,72	2,68	3,69	5,63	1,54	5,63	95,70	9,08	5,40	1,66	54	2,05	10,65	4,1
2	6,10	0,15	5,38	14,90	1,71	2,23	2,08	0,83	5,11	1,38	5,11	94,40	8,34	4,31	1,45	58	1,81	9,93	4,1
3	5,20	0,13	4,54	22,78	1,48	1,92	1,79	0,64	4,32	1,19	4,32	93,90	7,23	3,72	1,23	63	1,53	8,38	4,7
4	5,20	0,14	4,25	23,64	1,39	1,78	1,65	1,95	4,38	1,12	4,38	94,70	6,92	3,42	1,27	67	1,59	8,97	5,0
5	5,50	0,09	4,55	18,53	1,74	2,42	2,37	3,35	4,69	1,42	4,69	93,30	7,94	4,78	1,63	57	1,99	10,90	3,5
6	6,20	0,10	5,44	20,80	1,95	2,76	2,72	0,94	5,40	1,60	5,40	93,40	9,15	5,48	1,32	58	1,65	8,94	4,0
7	6,40	0,15	5,52	25,02	1,84	2,26	2,17	0,97	5,43	1,45	5,43	91,10	9,69	4,44	1,32	60	1,66	9,38	4,7
8	6,10	0,17	4,97	15,39	1,46	1,73	1,61	2,66	5,08	1,14	5,08	94,00	7,92	3,34	1,20	70	1,52	8,63	4,8
9	6,10	0,18	5,28	14,89	1,88	2,49	2,28	2,49	5,33	1,52	5,33	95,30	8,56	4,76	1,62	57	2,06	10,68	3,5
10	10,70	0,20	9,40	19,27	1,96	2,50	2,31	0,92	6,12	1,57	6,12	95,40	9,77	4,81	1,56	70	1,95	10,24	3,6
11	6,40	0,21	5,61	27,92	1,94	2,36	2,17	0,82	5,59	1,55	5,59	93,60	9,63	4,54	1,46	77	1,76	9,79	4,3
12	5,60	0,19	5,04	26,96	1,73	2,18	1,99	1,71	5,13	1,39	5,13	94,80	8,35	4,18	1,50	84	1,89	10,20	4,7
13	6,30	0,19	5,04	19,81	1,73	2,18	1,97	3,14	5,14	1,40	5,14	95,80	8,11	4,15	1,54	60	1,84	9,39	3,6
14	9,10	0,23	8,39	22,12	1,91	2,30	2,06	0,95	5,53	1,54	5,53	94,20	9,23	4,36	1,50	73	1,91	10,20	4,1
15	6,70	0,18	5,92	29,58	1,85	2,25	2,11	0,81	5,40	1,47	5,40	92,50	9,43	4,36	1,45	77	2,01	10,63	4,4
16	5,90	0,19	4,73	20,58	1,61	1,97	1,78	1,61	4,72	1,29	4,72	94,20	7,82	3,74	1,47	79	1,91	10,09	4,5
17	3,00	0,01	2,57	29,40	1,36	1,75	1,98	0,55	2,68	1,16	2,68	85,50	5,54	3,72	1,27	132	1,50	6,94	6,3
18	3,60	0,05	3,68	39,74	1,49	1,98	1,99	0,42	3,48	1,20	3,48	90,00	7,56	3,97	0,82	118	1,04	6,31	6,0
19	1,50	0,01	1,31	24,85	0,66	0,70	0,77	0,31	1,37	0,53	1,37	82,40	3,40	1,47	0,61	100	0,78	4,23	5,6
20	5,10	0,18	4,64	29,01	1,66	2,03	1,88	0,82	4,63	1,33	4,63	93,40	7,96	3,92	1,12	85	1,37	7,98	4,6
21	3,90	0,03	3,42	26,23	1,75	1,61	1,82	0,60	3,33	1,38	3,33	79,40	8,66	3,43	1,12	101	1,44	8,18	4,7
22	2,00	0,01	1,54	25,05	0,76	1,19	1,20	0,30	1,63	0,64	1,63	94,50	3,29	2,38	1,21	101	1,42	6,39	4,9
Corr fact	-0,69	-0,60	-0,64	0,66	-0,63	-0,66	-0,54	-0,53	-0,70	-0,63	-0,70	-0,58	-0,59	-0,61	-0,73	0,83	-0,76	-0,78	

Fig. 5.2.2 shows (for all tests conditions given in table 5.2), the surface topography (represented by the 2D roughness parameters Pc and Rz), and its relationship with the *rating* index, at the E coat stage. It may be observed that the *rating* increases with increasing Pc and decreasing Rz values.

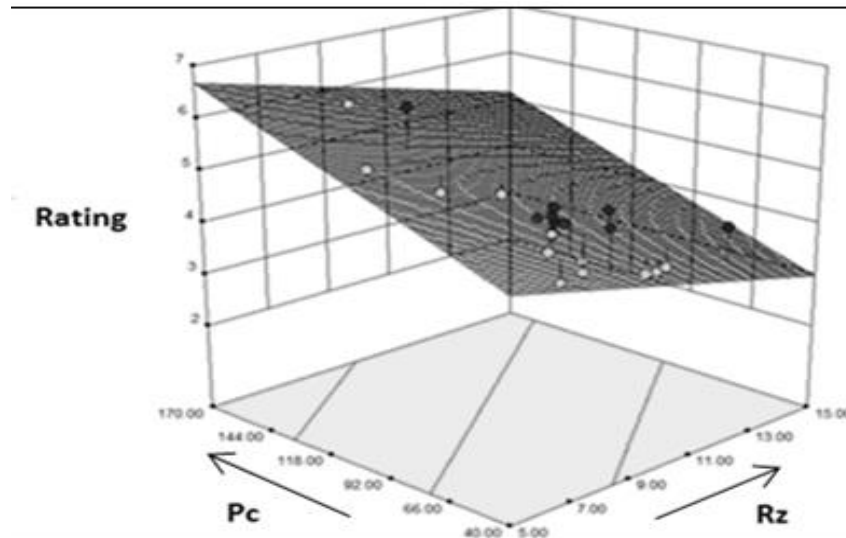


Figure 5.2.2: Effect of sheet metal surface topography (P_c and R_z) on the paint appearance (*rating*), at the E coat stage.

Looking at the effect of skin pass reduction on the *rating* (test 1 to 16) it may be observed, in fig. 5.2.3, an increase in the *rating* with increasing skin pass reduction. However there was no significant difference between the EDT and SBT conditions.

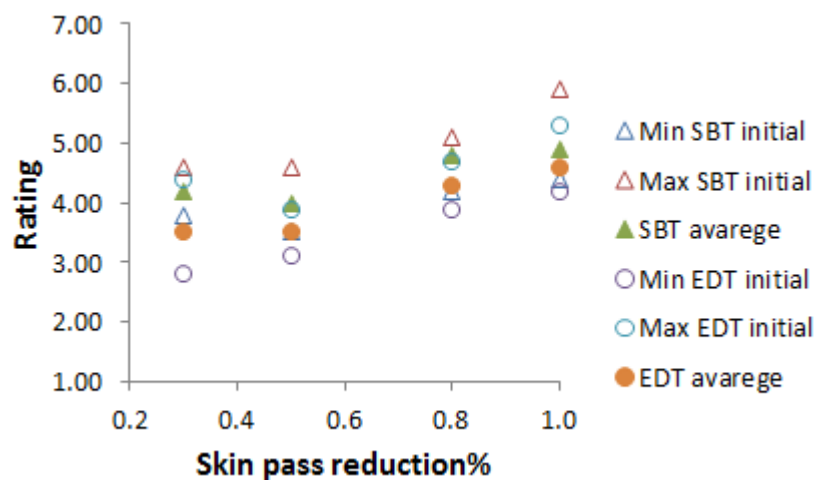


Figure 5.2.3: Effect of skin pass reduction on the *rating* (For tests 1 to 16).

In fig. 5.2.4 it is shown the effect of initial and end of coil for both process (SBT and EDT) on the *rating* at the E coat stage.

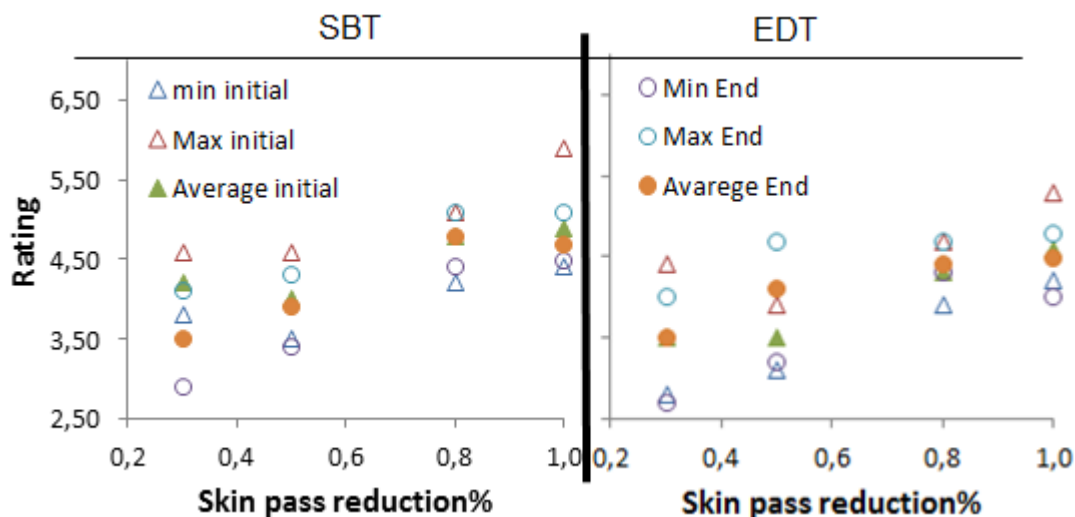


Figure 5.2.4: Effect of initial and end of coil for both texturing methods on the *rating* (for tests 1 to 16).

It can be noted from fig. 5.2.4 the lowest dispersion occurs for EDT with skin pass reduction between 0.8%. This result is aligned with fig. 5.1.7 that reports the 2D roughness dispersion.

It also can be observed from fig. 5.2.4 that rating was not sensitive to texturing method (SBT and EDT, tests 1 to 16), but it was sensitive to surface topography (roughness). So, in fig. 5.2.5 it will be analyzed the effect of surface topography on rating for all tests conditions without considering their processing history.

From table 5.2 all different roughness parameters could be plotted against the *rating* index (paint appearance index). Specifically, for the Rz and Pc roughness parameters we obtain fig 5.2.5. Here we can observe that the rating increases with decreasing Rz parameter (expressed by the minus signal of the correlation factor - see bottom of table 5.2). Conversely, *rating* increases with the increase in the Pc parameter. Actually, these two parameters are those that best represent the group of 2D roughness parameters. The first one is related to the peak and valley density (Pc and α_{clm}), for which the tendency line increases with increasing rating. The second one is related to the peak and valley height (profile height), for which the tendency line decreases with increasing *rating*, as also indicated by the arrows shown on the left side of fig. 5.2.5.

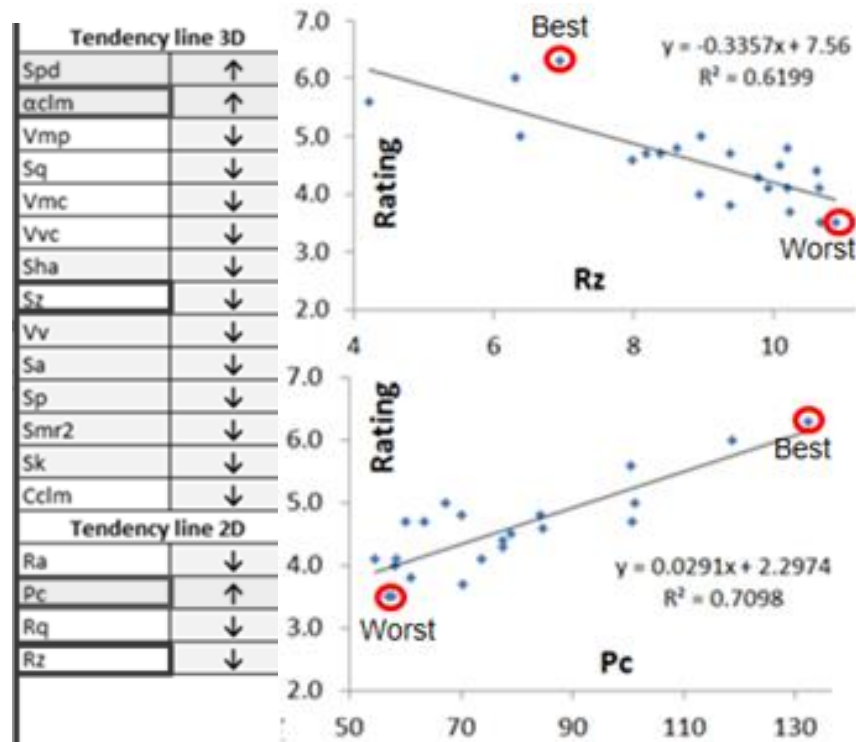


Figure 5.2.5: Left: Tendency line for the 2D roughness parameters listed in table 5.2. Right: Rz versus rating and Pc versus rating for the 22 test conditions, at the E coat stage.

From fig. 5.2.5 (right side): the best and worst conditions have been selected according to their *rating* index and were analyzed in terms of their surface topography, see fig. 5.2.6. The worst and best condition of rating, which are test 9 (worst) and 17 (best) had shown a rating dispersion of 2.8 to 4.4 (worst) and 6.0 to 6.7 (best).

Table 5.2.1: 3D roughness parameters (α_{clm} , v_{cl}) for the best and worst paint appearance (rating) condition of fig. 5.2.5.

			Best	Worst
Max. Closed void area ratio	α_{clm}	%	29.4	14.89
Closed void volume	V_{cl}	mm^3/m^2	530	302.8

It also should be pointed out from table 5.2.1 that the sample 17 which was considered best in the paint appearance criteria (rating), also showed better results in terms of 3D roughness parameters (α_{clm} , V_{cl}) compared with sample 9 (worst in paint appearance). This should confer also a better stampability, according to the stampability criteria mentioned in chapter 3.2.2.

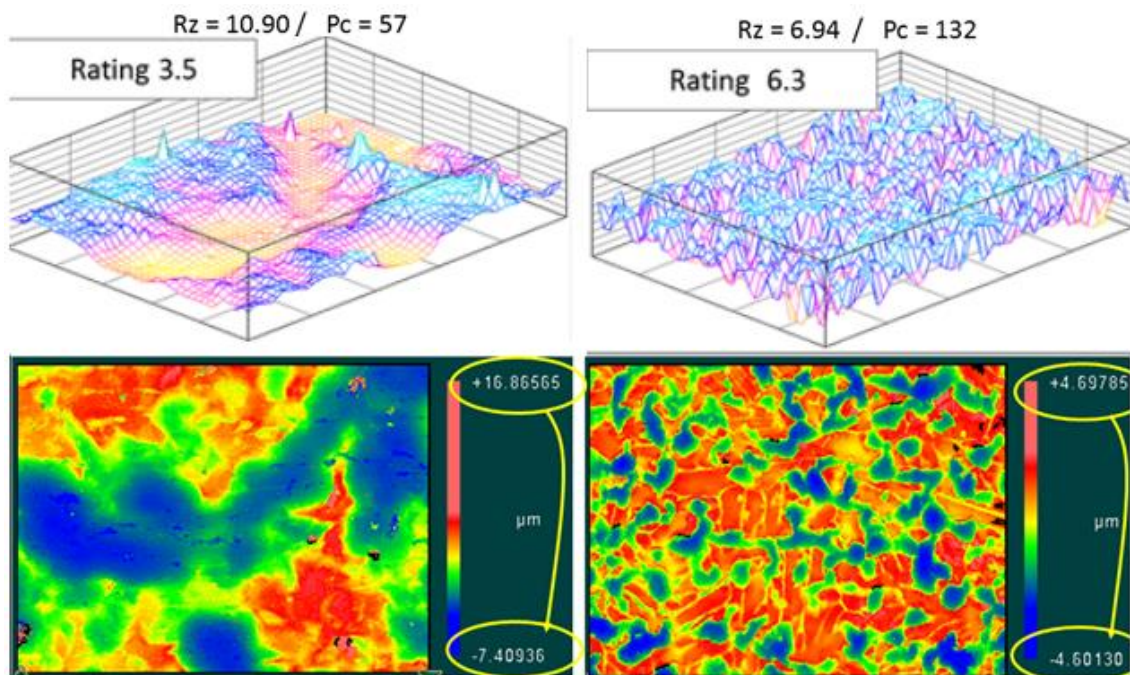


Figure 5.2.6: sheet metal surface topography for the best and the worst rating index/condition (at the E coat stage) and the corresponding 2D roughness parameters - Rz and Pc (Zygo).

The images from fig. 5.2.6, for the worst and the best “rating” condition are associated with the tests 9 and 17, respectively (both are for the EDT condition). As a further observation, the test 5 (SBT condition), has also shown a rating index of 3.5.

Furthermore it should be pointed out that the worst rating test conditions (samples of tests 5 and 9), should be associated with the skin pass reduction of 0.3%. The best rating should be associated with a higher peak and valley density and the lower peak and valley height. Moreover, this sample (best rating condition) was a HDG (hot dip galvanized) steel sheet and it appears from these results that the zinc coating produces a benefic effect on the paint appearance. This may be associated to the degree of transfer during skin pass rolling, which could be higher for the HDG sheets as compared to the bare steel sheet, because the zinc coating is softer than the steel substrate.

Here it must be pointed out that these samples 1 to 16 (that include SBT and EDT samples), have been manufactured at a steel plant that does not have HDG facilities. The samples 17 to 22 (except 18 and 20) were all HDG steel sheet samples manufactured at the steel plant that does have this facility, but does not report the

skin pass rolling reduction. It is well known that for car manufacturing purposes, sheet metals have to be submitted to HDG and subsequently submitted to skin pass rolling. It is due to those industrial conditions that the best and worst rating conditions, at the E coat stage, have been selected.

From these observations, at the E coat stage, we have to notice that the best *rating* (sample condition) was related to :

- the sheet metal surface having a low value of Rz (<7 μm) and a high Pc (>130 peaks/cm) value.

5.2.1.2 - The second step of the first run (Figure 5.2.7)

The best and worst conditions of the *rating* index (measured in the first step), were processed (under the same industrial conditions), until the E coat stage and simultaneously in a laboratory (under the same conditions) for the sequence of processes: primer, base coat and clear coat. These experiments were planned in such a way that, at the end of the painting process, one sample from each process stage (sheet metal, phosphate, E coat, primer, base coat and clear coat) was available. For each sample the roughness profile (2D and 3D), was measured. Also, on the clear coat layer, the following characteristics have been evaluated: *rating*, spectral curve and the DOI= Distinctiveness of Image (see topic 3.4 for details).

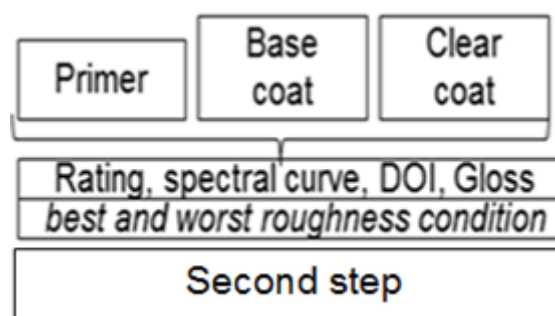


Figure 5.2.7: First run - Second step (same as fig 4.1, right side).

The results of the thickness of the layers are shown in the micrographs of fig. 5.2.8.

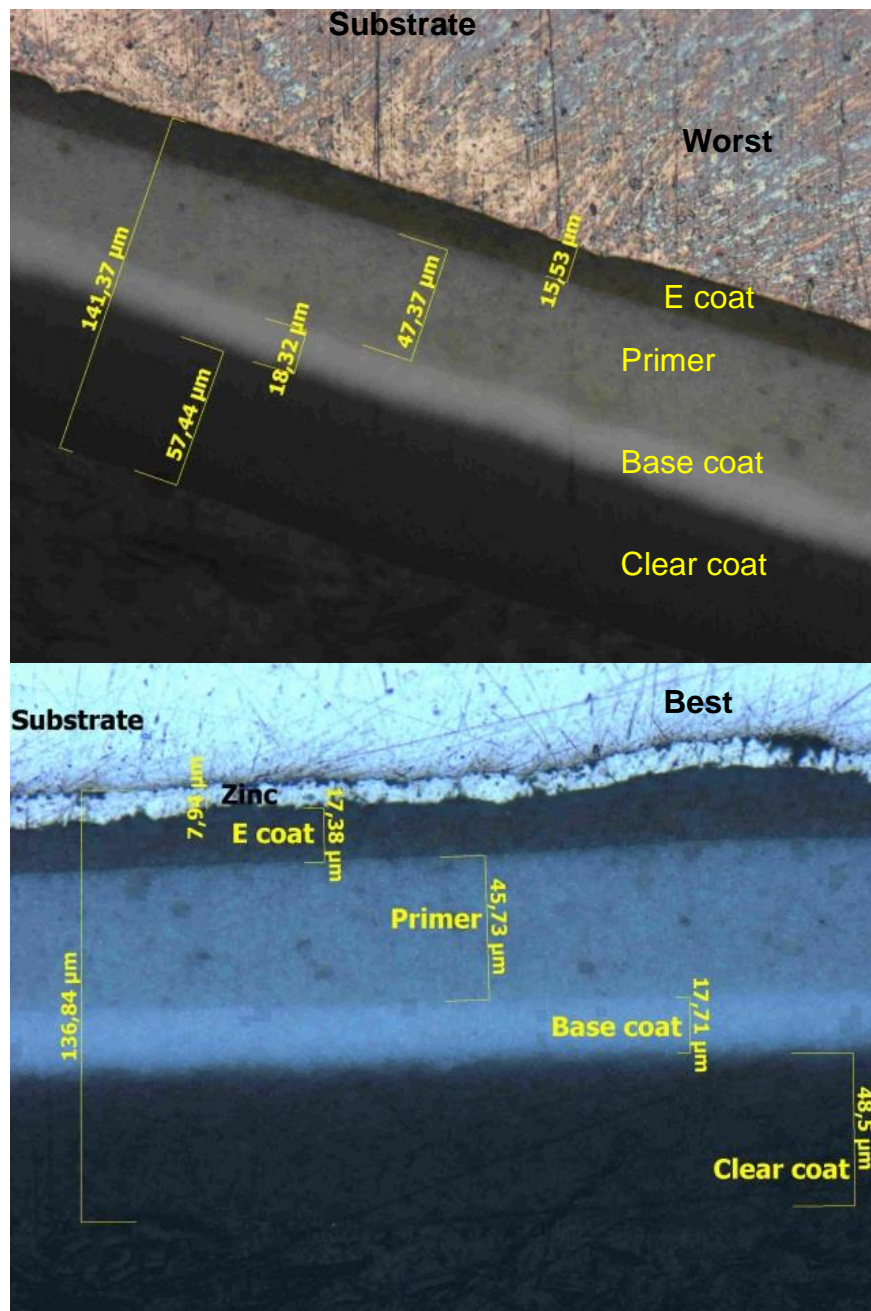


Figure 5.2.8: The layers: From substrate to clear coat of the best and worst paint appearance (rating) condition of fig. 5.2.5.

The results of the 2D roughness profile are shown in fig. 5.2.9.

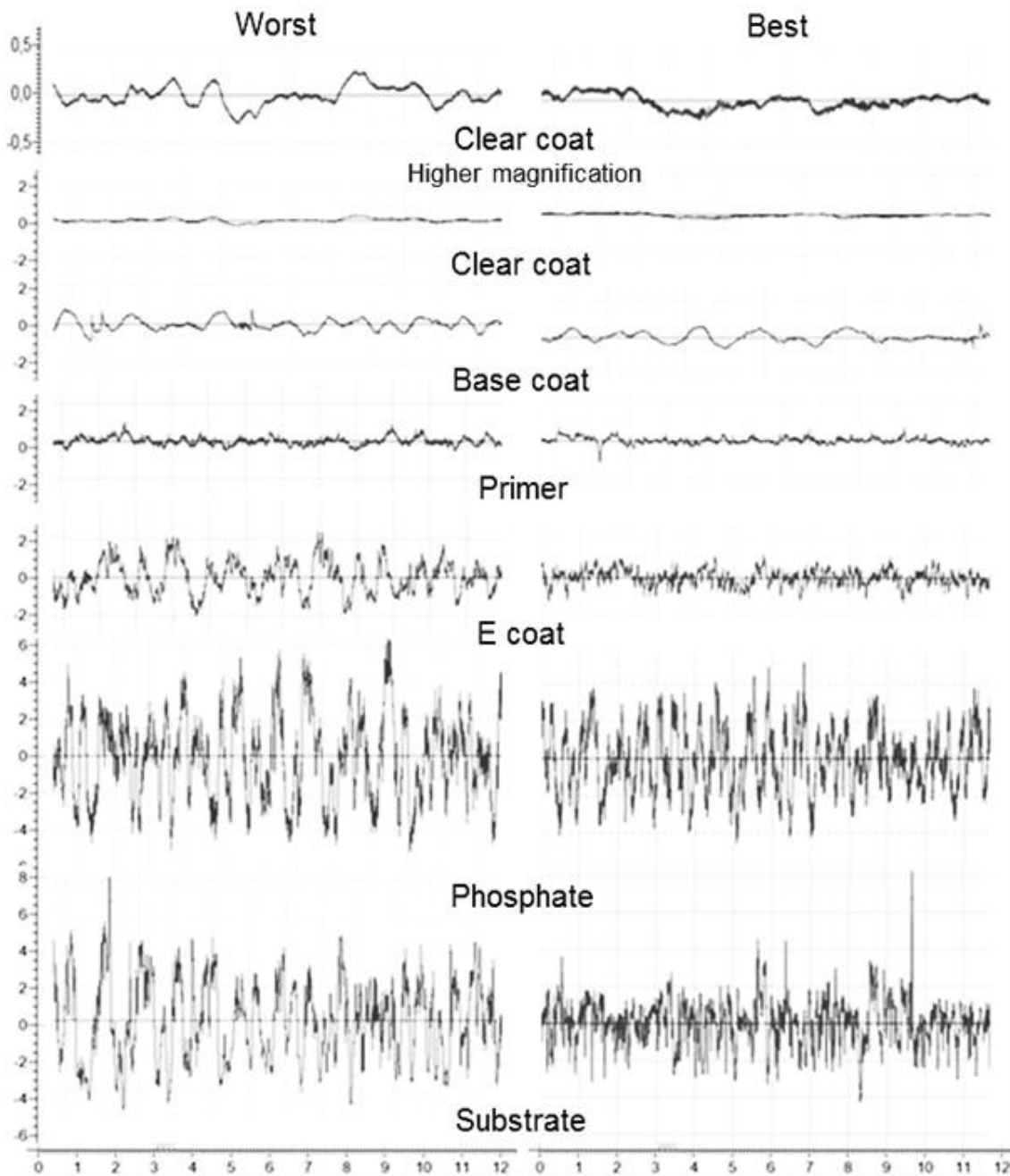


Figure 5.2.9: 2D roughness profile evolution for the best and worst “rating” conditions (measured in the first step) (Taylor Hobson).

The same evolution (in 3D roughness), for the worst and best conditions (tests n. 9 and 17) are shown in the appendix 2 (there, attention should be given to the scale provided on the right hand side of the figures).

It is clearly noticeable (fig. 5.2.9) the effect of the roughness substrate (steel sheet) on the roughness evolution on the others painted layers. The roughness amplitude is transmitted to the subsequent layers, however with a lower intensity. Therefore, peak

density do not seem to lose intensity until the E coat layer. Until the primer stage the roughness amplitude decreases, but on the base coat it increases. This happens because, besides the phosphate layer, the base coat is the thinnest layer (due to its higher cost). The samples were painted with a white color (containing TiO_2 -Titanium dioxide pigment). This pigment has an irregular shape, see fig. 5.2.10, and it seems to be the main responsible for the increase in roughness amplitude, as can be seen in the SEM analysis of the surface topography of the base coat in fig. 5.2.11.

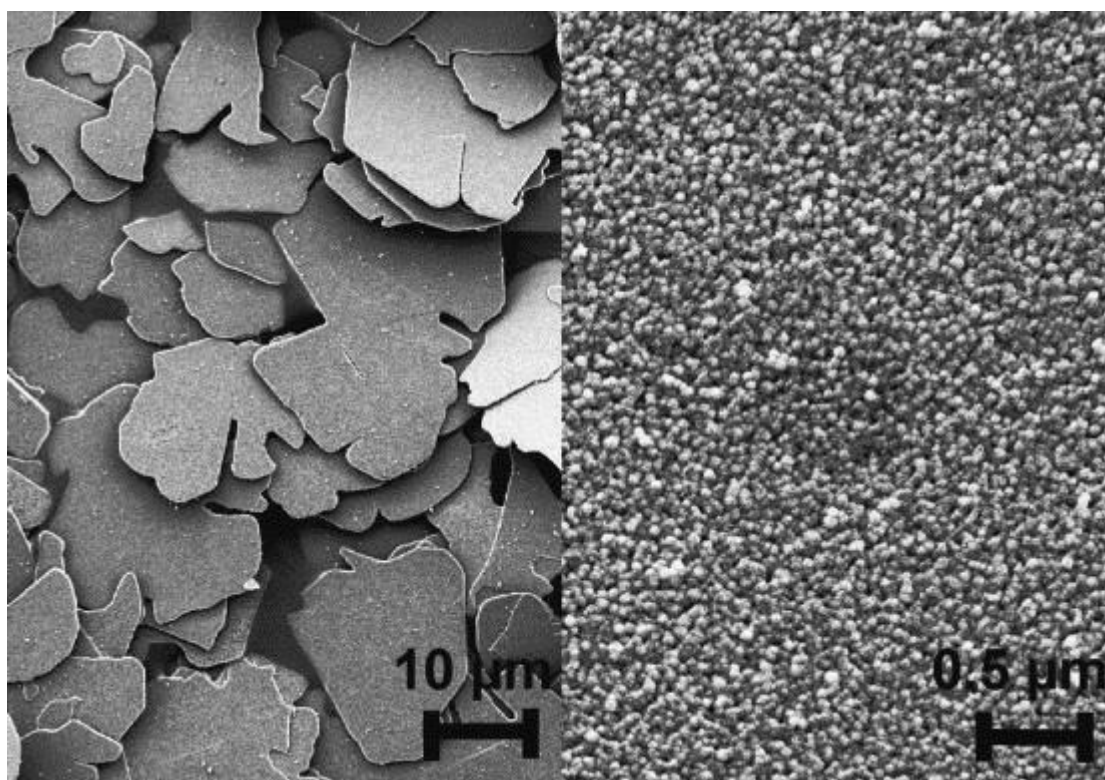


Figure 5.2.10: Scanning electron micrographs of (a) pure alumina flakes and (b) alumina flakes coated with TiO_2 (rutile) as used for pearlescent pigments (MAILE, PFAFF, REYNDERS, 2005).

It should be remembered that a different pigment color will bring the corresponding alterations in the final paint appearance due to the shape and size of pigment which may vary according to color.

Fig. 5.2.12 shows the evolution of the Rz parameter along all painted layers.

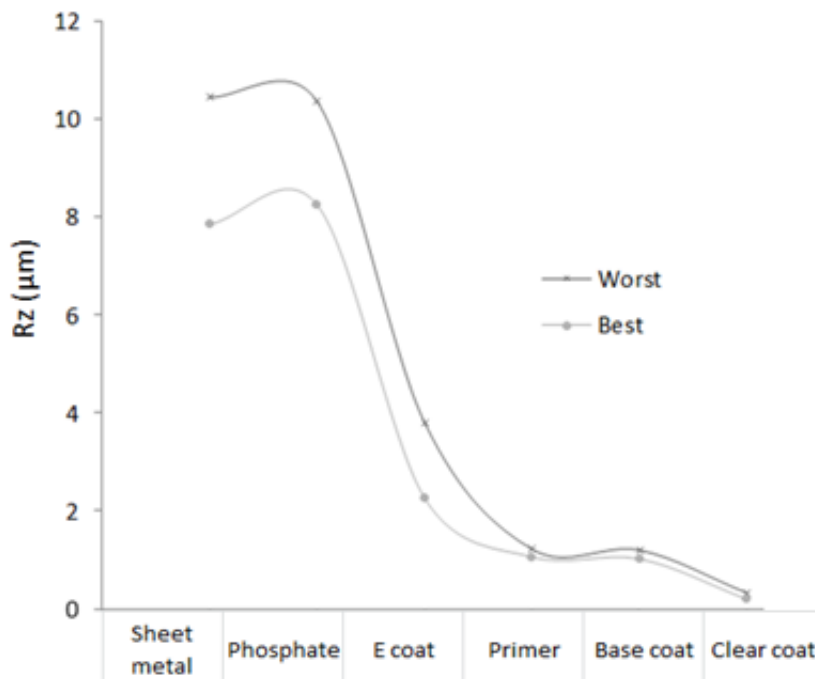


Figure 5.2.12: Rz roughness evolution along all painted layers.(worst and best samples).

From this figure we may observe the substantial drop in the values of the Rz parameter starting from the sheet metal surface towards the clear coat layer. Despite the small difference in the Rz value measured at the clear coat surface, it shows that the Rz value is not appropriate to differentiate the best and the worst painted surface. Some further procedure has to be added to better select the paint surface appearance.

Towards this objective figs. 5.2.13 to 5.2.16 present the results of the paint appearance (for the clear coat stage), of the worst and best rating conditions obtained according to the classification mentioned in fig. 5.2.5 of this chapter.

The first one (fig. 5.2.13), refers to the spectrum analysis (that have been mentioned in figs. 3.4.1 to 3.4.3 of the literature review).

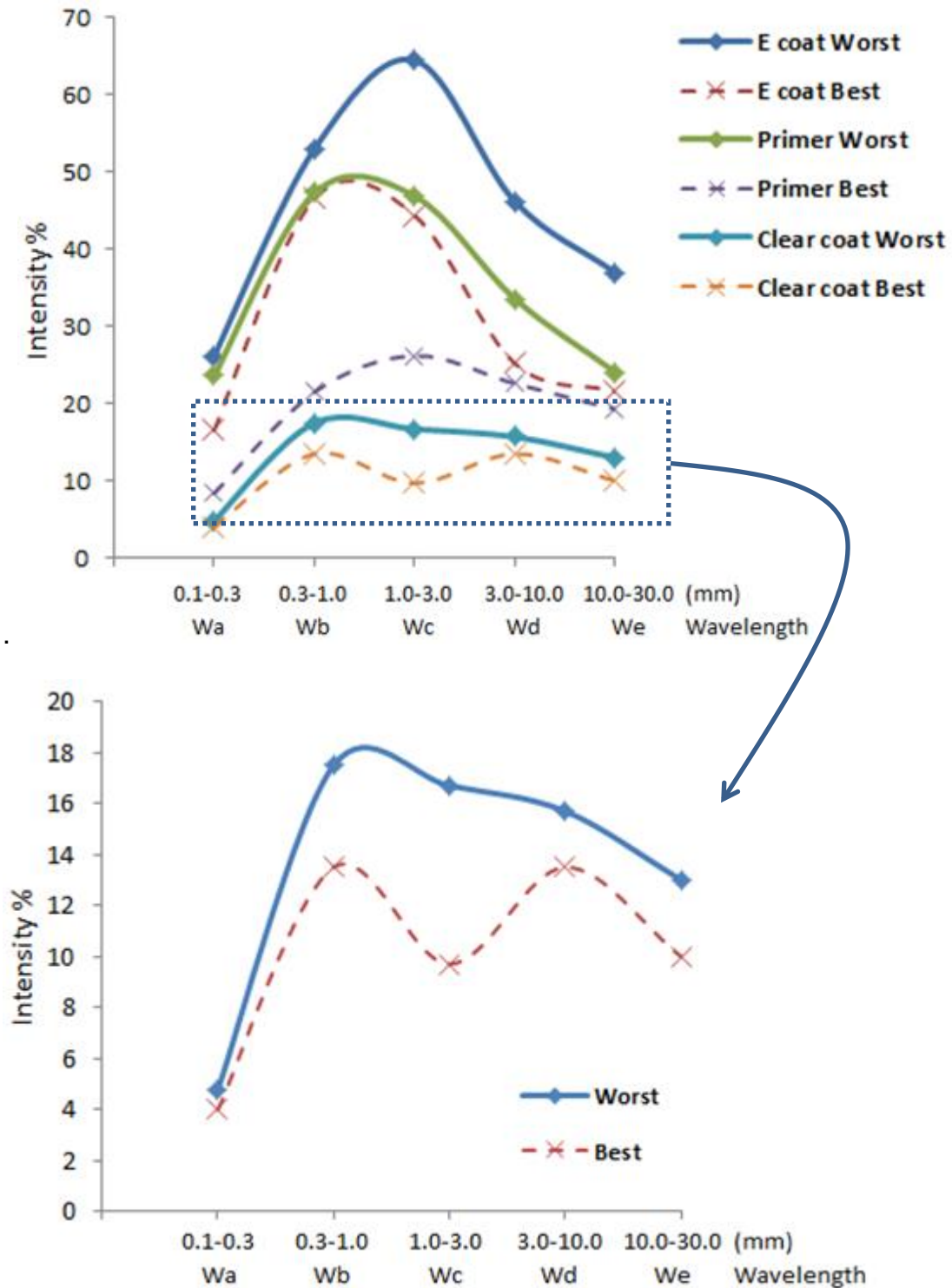


Figure 5.2.13: Spectral curves of the best and worst *rating* index conditions (mentioned in fig. 5.2.5). Top: E coat, primer and clear coat layers. Bottom: clear coat layer with higher magnification. Measurements made with the wave scan dual equipment.

The importance of form and intensity of these spectra will be subject to discussion in chapter 6.4.1

Fig. 5.2.14 shows the gloss evolution from the primer to the clear coat layers. (its analysis has been mentioned in table 3.4.1 of the literature review and its methodology is described in the attachment 2).

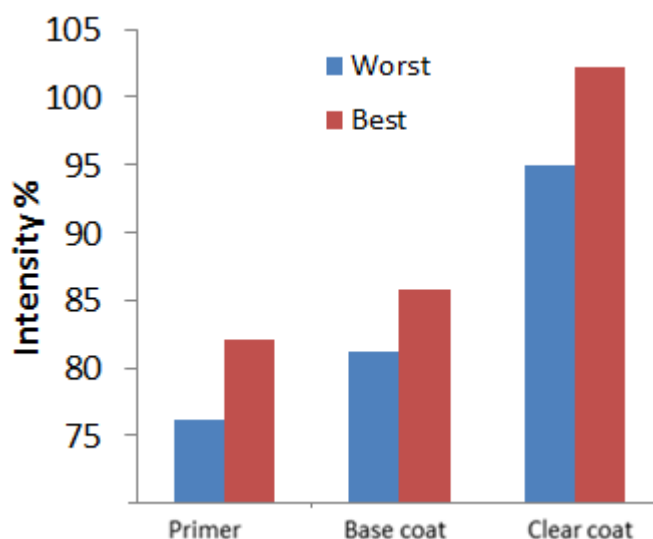


Figure 5.2.14: Gloss evolution of the best and worst rating conditions (mentioned in fig. 5.2.5). Measurements made with the glossmeter equipment.

The gloss intensity increases from the primer towards the clear coat layer, however not linearly.

Fig. 5.2.15 shows the DOI evolution for the E coat, primer and clear coat layers (its analysis had been mentioned in table 3.4.1 of the literature review and the methodology described in the attachment 2).

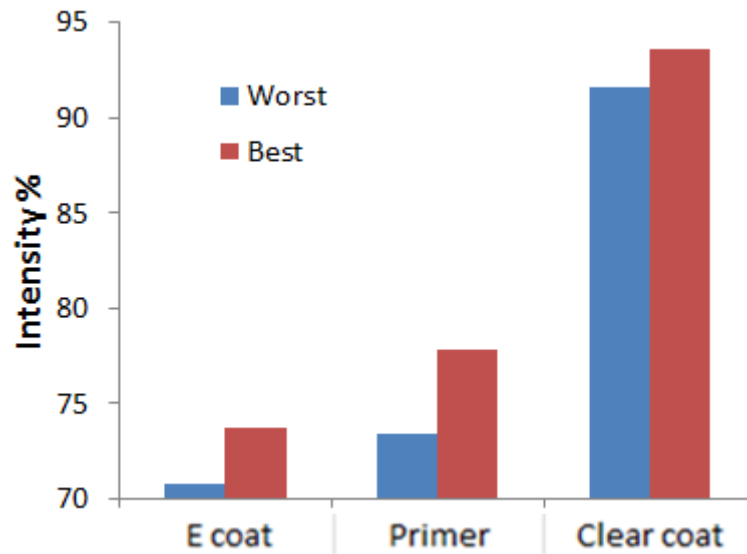


Figure 5.2.15: DOI evolution of the best and worst *rating* index conditions (mentioned in fig. 5.2.5). Measurements made with the wave scan dual equipment.

Again, the DOI intensity increases from the E coat towards the clear coat layer, however not linearly.

Finally, fig. 5.2.16 presents the *rating* index evolution for the E coat, primer and clear coat layers (their analysis has been mentioned in fig. 3.4.2 of the literature review).

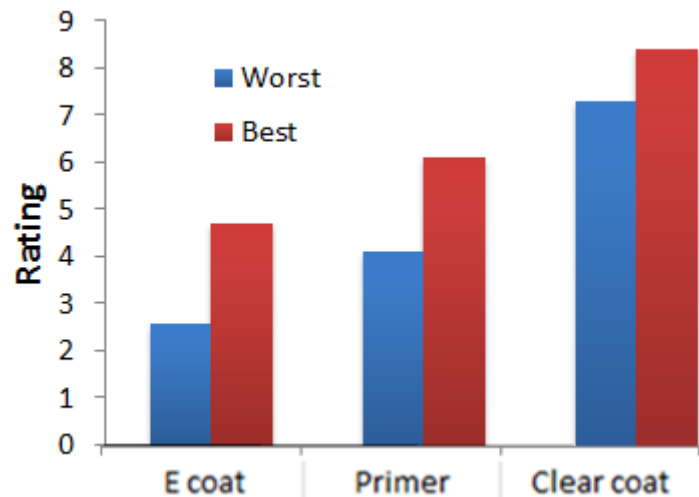


Figure 5.2.16: *Rating* evolution of the best and worst rating conditions (mentioned on fig. 5.2.5). Measurements made with the wave scan dual equipment.

Rating index also increases from the E coat towards the clear coat layer, fairly linearly.

From these observations, at the clear coat stage, we have to notice that the best *rating* (sample condition) was related to :

- The best spectrum curve (in the range of 10 to 14%);
- The highest gloss intensity (at the level of 104%);
- The best DOI intensity (at the level of 95%);
- The highest *rating* (at the level of 8.4).

5.2.2 Second run:

The second run (summarized in fig. 5.2.2.1) was sub divided into 2 steps in order to evaluate the following main topics:

First step: Analyze the influence of the sheet metal surface topography on the stampability of the materials.

Second step: Analyze the roughness change/evolution after stamping, which comprises the deformation modes on the sheet metal (related to the sliding and bending during stamping operation), and its effect on the paint appearance.

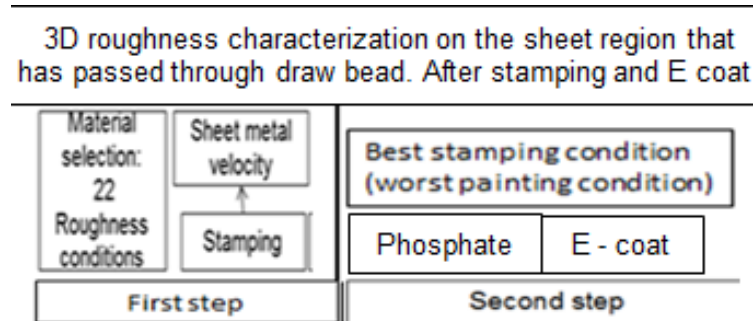


Figure 5.2.2.1: Second run (same as fig. 4.3).

5.2.2.1 The first step of the second run (Figure 5.2.2.2):

The twenty two (22) test conditions (again, five samples for each condition) have been stamped under industrial conditions and a curve of displacement (mm) versus time (s) has been collected for each one of the studied samples.

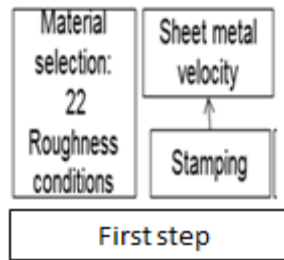


Figure 5.2.2.2: Second run – First step.

The results for the “best” and “worst” conditions and their speeds are shown in fig. 5.2.2.3, related to the displacement x time evolution.

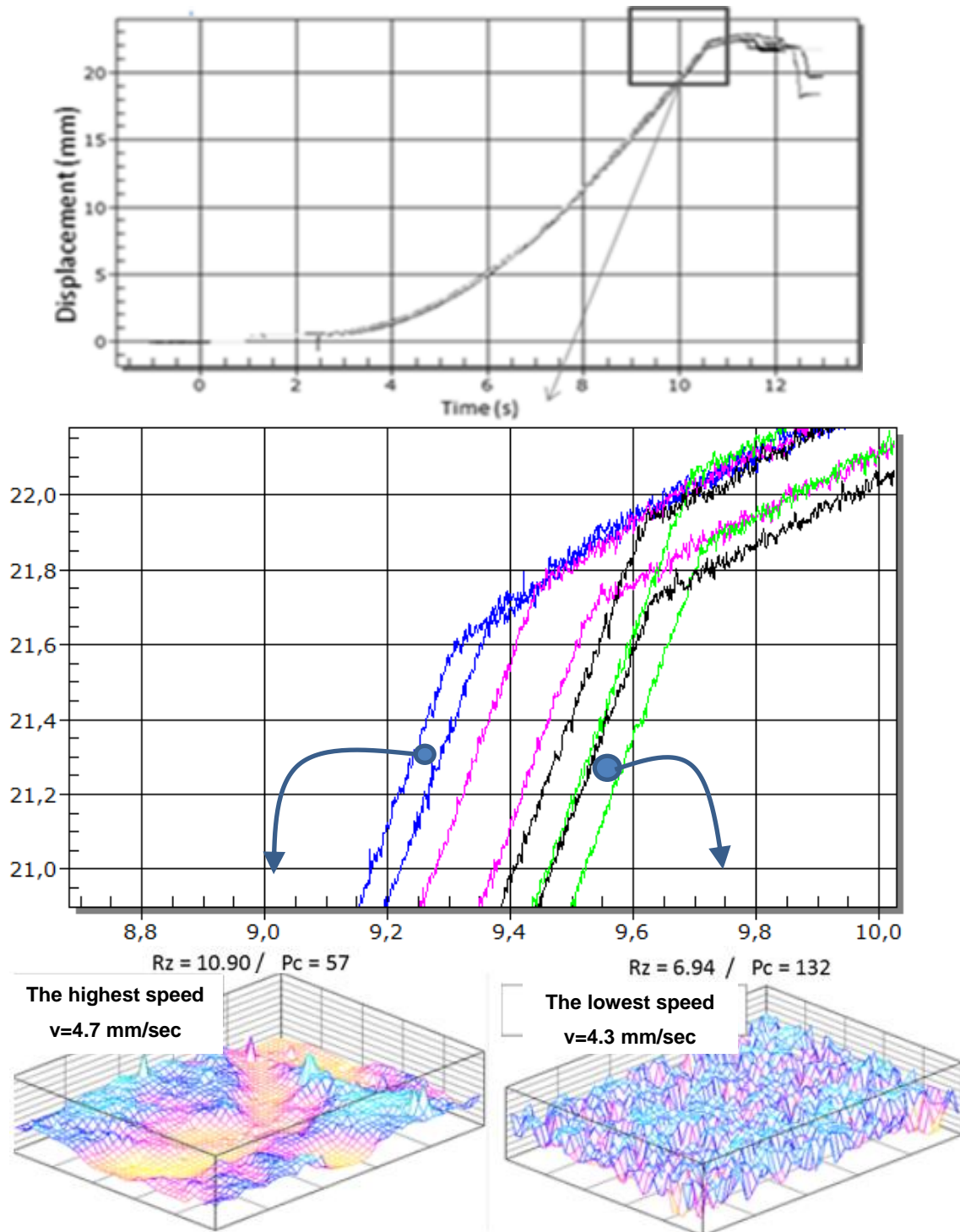


Figure 5.2.2.3: (Top figure) displacement (mm) x time(s) - Sheet metal surface topography of the “best” and “worst” conditions (and the final speed differences - angular coefficient) (HBM).

(Bottom figure)- Detail of the square shown in the top figure and their surface topographies respective to these curves (Zygo).

It may be observed that there is a slight difference in time (delay of about 0.35s), between the “fastest” (4.7 mm/sec) and the “slowest” (4.3 mm/sec) sample and that the correspondence is: “Best” rating is associated with the “slowest” speed and “worst” rating is associated with the “highest” speed. This seems to be contradictory! The reasons for such a difference in behavior in these curves will be objective to subsequent discussion (chapter.6.2.2.3).

5.2.2.2 The second step of the second run (Figure 5.2.2.4)

The roughness (measured in 2D and 3D), was characterized in the region A (that has NOT passed through the draw bead) and B (that has passed through the draw bead), as shown in fig. 5.2.2.5. Subsequently, the sample has been processed (under the same industrial conditions), until the E coat stage and again the roughness (measured in 2D and 3D), was characterized in the same regions A and B.

At this stage the criteria adopted was to select the sample which presented the worst painting condition. This criterion has been associated with the curve which presented the “highest” stamping speed (left curve in fig 5.2.2.3 – displacement=21 mm at time= 9.2 s). Hence, there is a conflict of interests, as already pointed out in the literature. This aspect will be further detailed in the discussion (chapter 6.2.2.3).

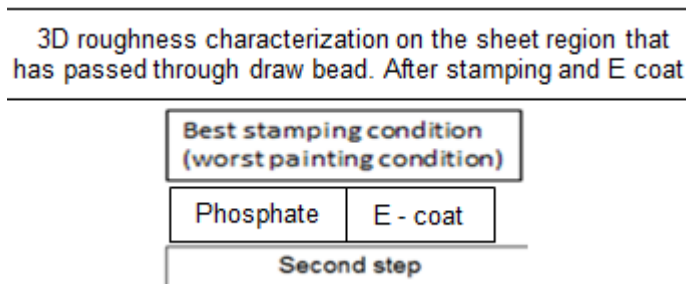


Figure 5.2.2.4: Second run – Second step.



Figure 5.2.2.5: Regions A and B.

Fig. 5.2.2.6 shows the Abbott curves (see details in the attachment 1), overlapped with the stamped sample (test 9) in the region A (without surface roughness flattening) and in the region B (with surface roughness flattening).

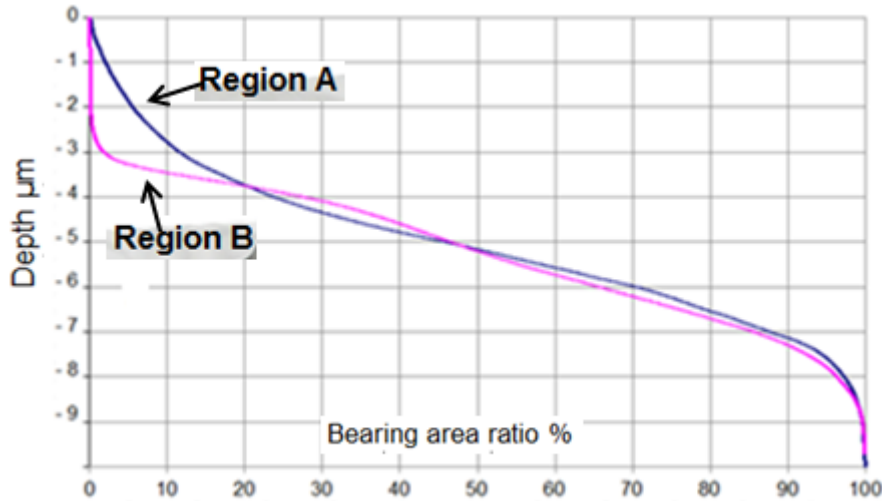


Figure 5.2.2.6: Effect of die contact deformation on sheet metal surface topography.

In this figure we may observe that the major difference between them is in the zone associated with the flattening of peaks.

Indeed, fig. 5.2.2.7 shows the surface topography of region A (see figs. 5.2.2.5 and 5.2.2.6) that may be linked to the surface without roughness flattening, and the values of the 2D roughness- Ra and Rz. Fig. 5.2.2.8, shows the same results for the region B (of fig. 5.2.2.6), that may be linked to the surface with roughness flattening.

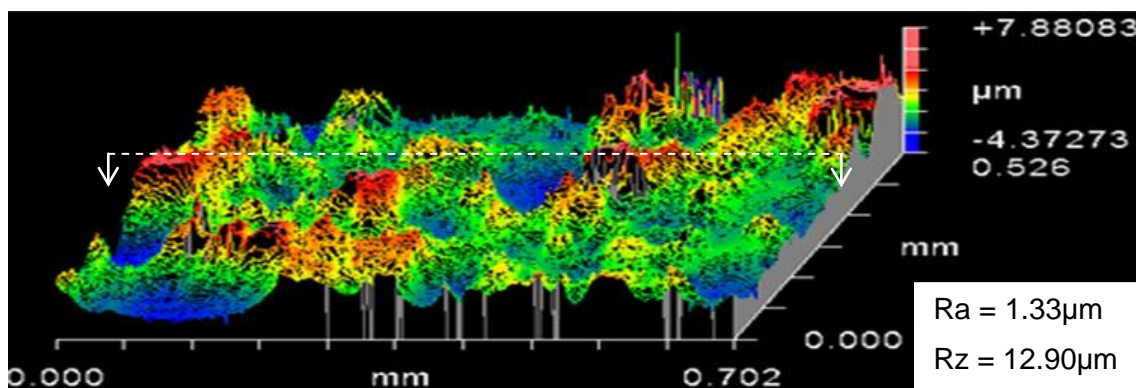


Figure 5.2.2.7: Surface topography for region A of fig. 5.2.2.6. Ra and Rz were measured at the white dashed line. Measurements made with the Zygo New View 7000 equipment.

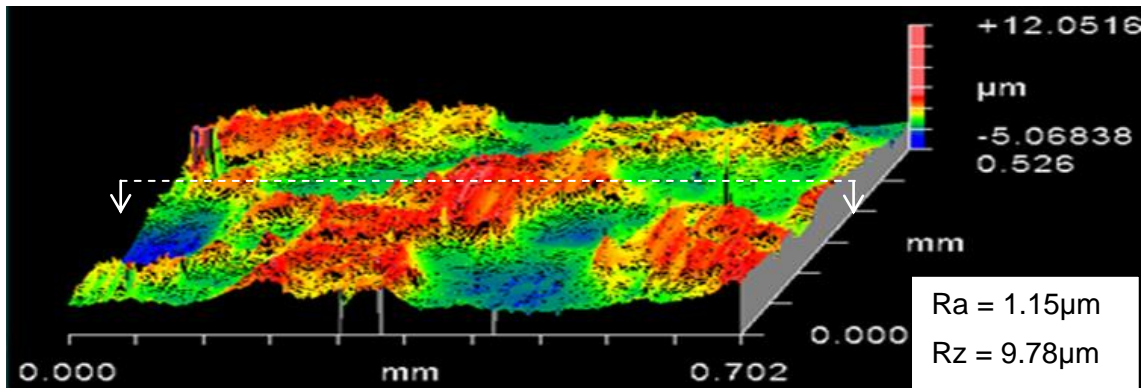


Figure 5.2.2.8: Surface topography for region B of fig. 5.2.2.6 (2D and 3D roughness analysis). Ra and Rz were measured at the white dashed line. Measurements made with the Zygo New View 7000 equipment.

These results will be compared with data from literature in the discussion (chapter 6.2.1)

Following, the samples were further processed (under the same industrial conditions), until the E coat stage and again the roughness (measured in 2D and 3D), was characterized in the same regions A and B.

Fig. 5.2.2.9 shows the 2D roughness evolution (original surface – region A vs. the flattened surface – region B) at the E coat stage.

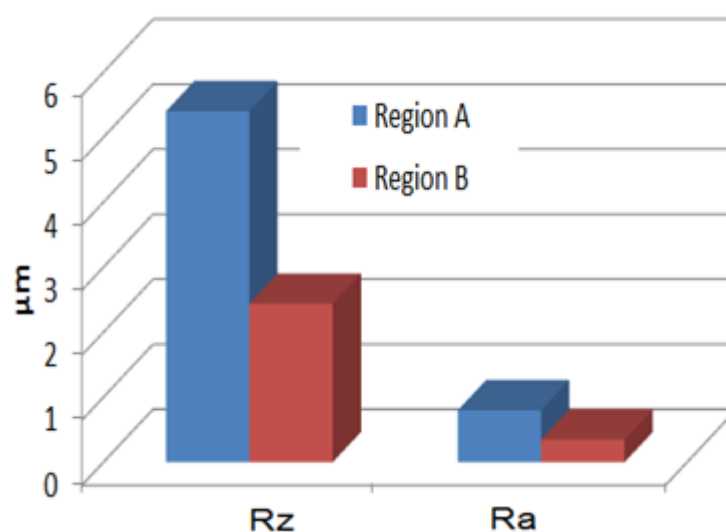


Figure 5.2.2.9: 2D roughness Rz and Ra at the **E coat** stage in the regions A and B of fig. 5.2.2.5 (with and without surface roughness flattening).

From this figure it may be observed that the Rz parameter clearly shows quite a significant difference for the two regions under analysis.

In fig. 5.2.2.10 we have the same analysis of fig. 5.2.2.9, but now using the 3D roughness parameters.

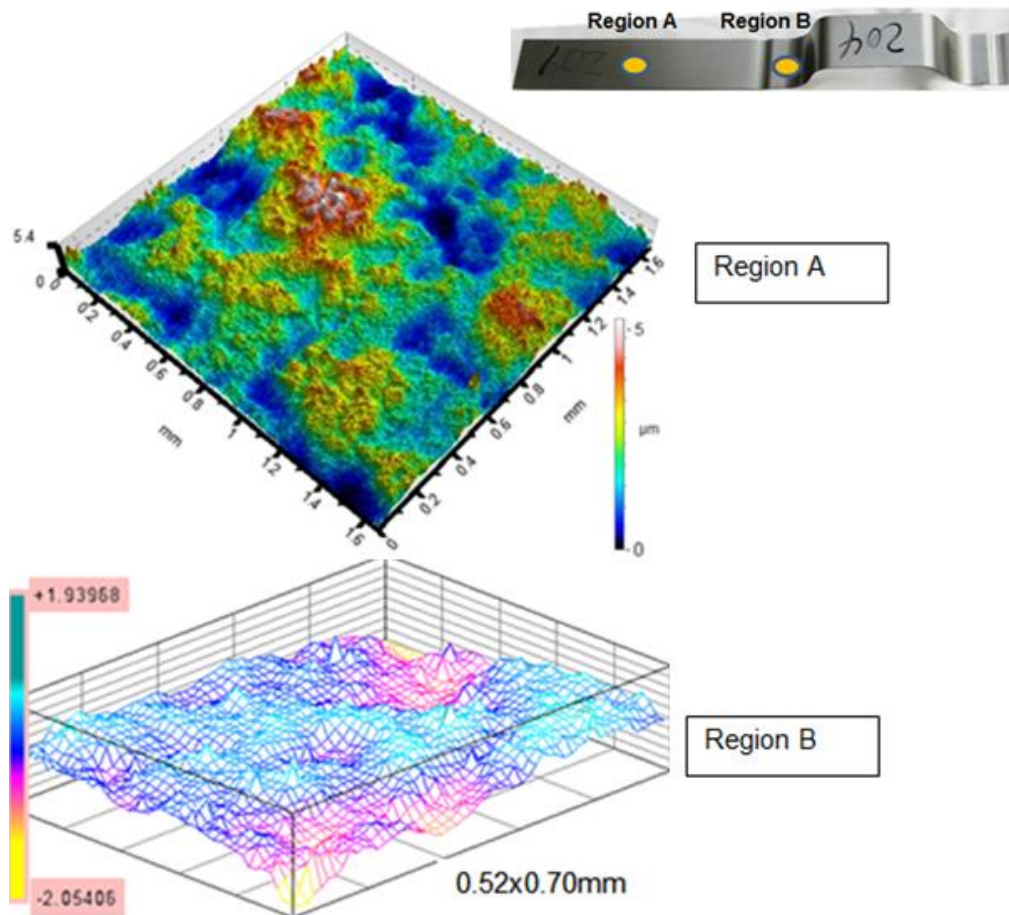


Figure 5.2.2.10: 3D roughness at the **E coat** stage in the regions A (Taylor Hobson) and B (Zygo) of fig. 5.2.2.5.

Clearly it can be seen that deformation, due to die contact, decreases the roughness values, as could be expected and we can conclude that the peak flattening is beneficial for paint appearance.

This item will be, again, detailed further in the discussion (chapter 6.3.1)

As in these stamping experiments it has been observed that the sheet samples presented no thinning. Hence, it became necessary to conduct a further third run, this in order to evaluate the thinning effect on the roughness evolution.

5.2.3 Third run

The third run was sub divided into 2 steps in order to evaluate the following main topics:

First step: Sheet metal roughness evolution under *tensile strain* condition and through the painted layers.

Second step: Roughness evolution under *plain strain* condition.

5.2.3.1 The first step of the third run: Tensile strain condition (fig. 5.2.3.1)

A material DIN EN 10346 DX54D+Z, thickness 0.75mm, was submitted to a tensile rupture test (in the LD rolling direction), and the strain path and the 2D roughness was evaluated in the marked regions. These samples were further taken to be painted in a way that, at the end of the painting process, one sample from each process step was available (sheet metal, phosphate, E coat, primer, base coat and clear coat). For each sample, measurements were made to obtain the 2D roughness profile, along the whole sample length, in order to attain also the associated roughness Rz in the regions close to the positions 1, 2, 3 and 4.

The results are shown in fig. 5.2.3.2.

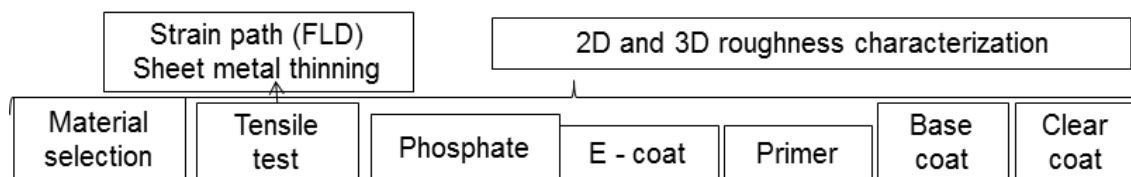
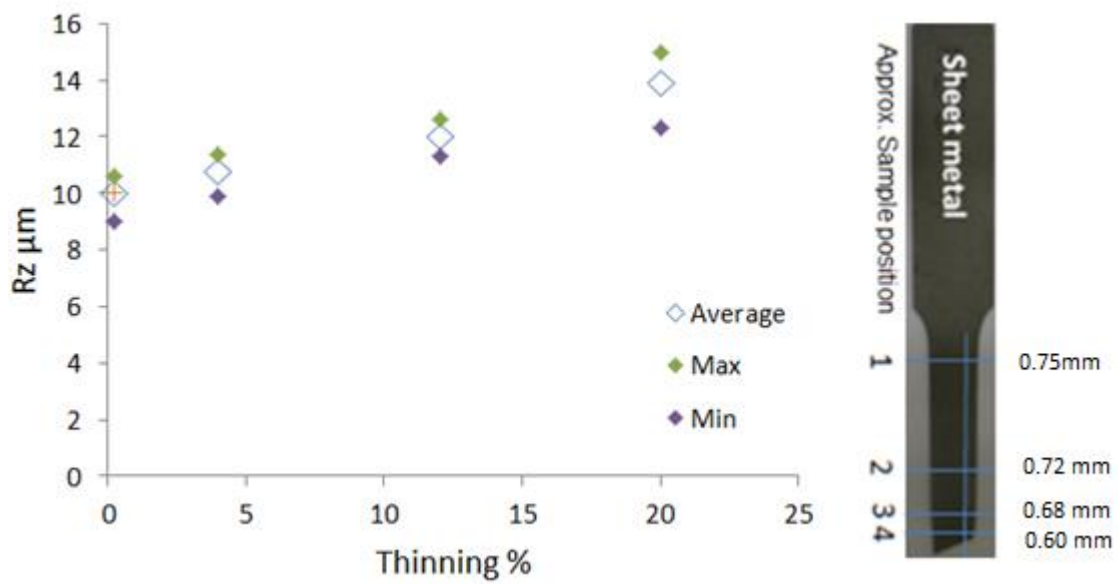


Figure 5.2.3.1: Third run – First step (same as fig. 4.7).

In fig. 5.2.3.3 the 2D (Rz) and 3D (Sz) roughness values of the positions 1 to 4 are compared. It can be noted a gap between them, which increases with sheet thinning.



Figure

5.2.3.2: Roughness evolution R_z versus thinning evolution at the positions (1) one to (4) four (fig. 6.2.8).

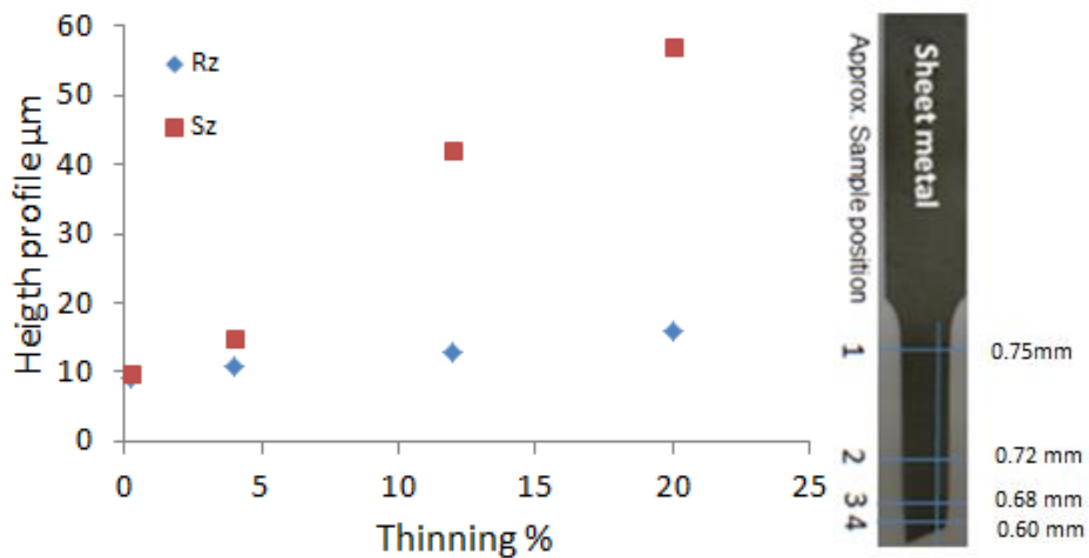


Figure 5.2.3.3: Gap between 2D and 3D roughness measurements (position shown in fig. 5.2.3.2).

In figs. 5.2.3.4 to 5.2.3.6 show the 3D roughness evolution close to fracture. It can be noted that for a small distance variation of approximately 2 mm there was a huge change in the roughness, as for example S_z , which changed from 57.7 to 171 μm .

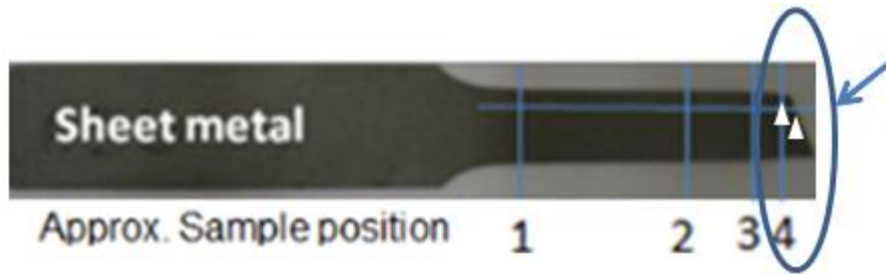


Figure 5.2.3.4: Upper triangle refers to analysis presented in fig. 5.2.3.5 and lower triangle to the analysis presented in fig. 5.2.3.6 (both triangles are about 2mm apart).

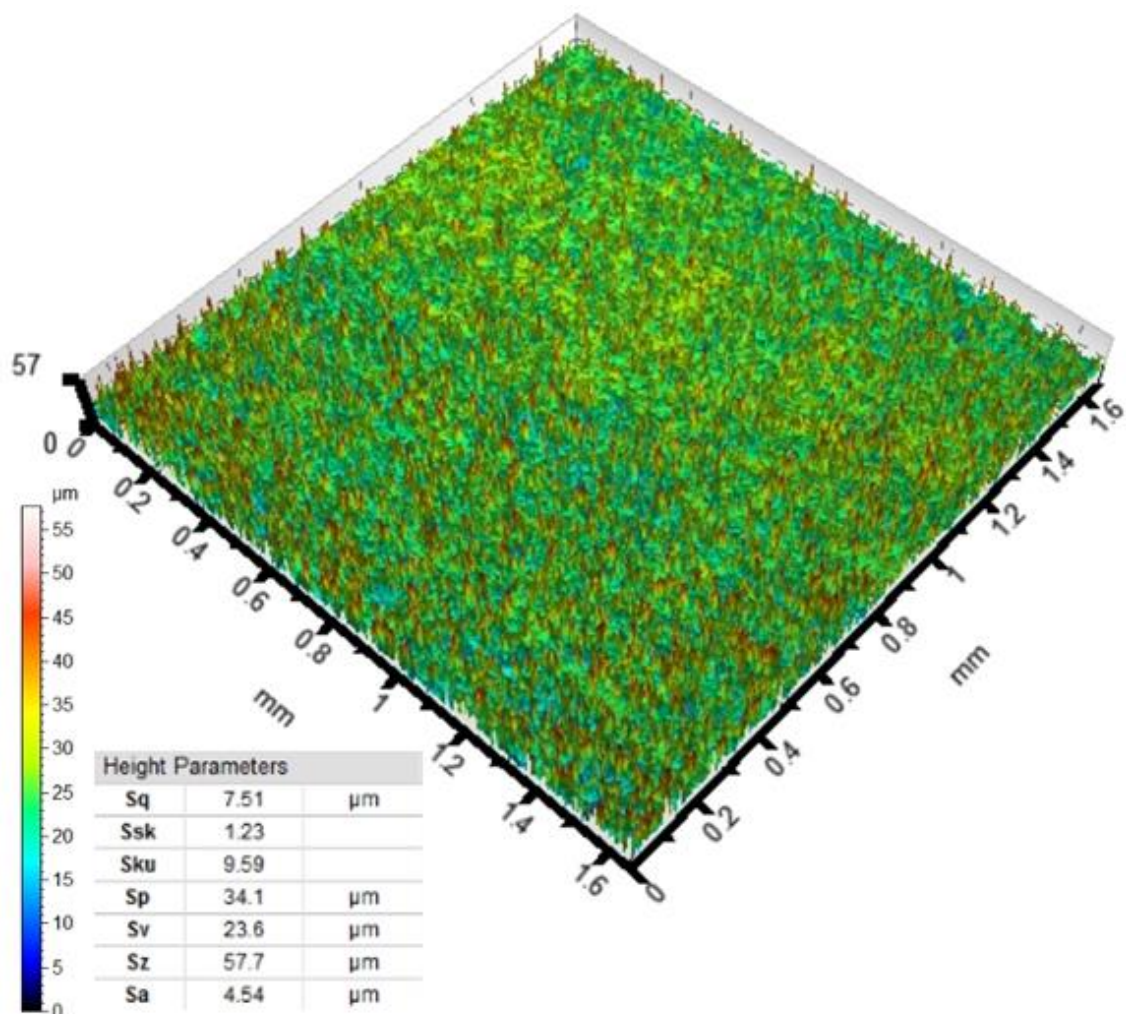


Figure 5.2.3.5: 3D surface topography at the position 4, upper triangle (fig. 5.2.3.4).

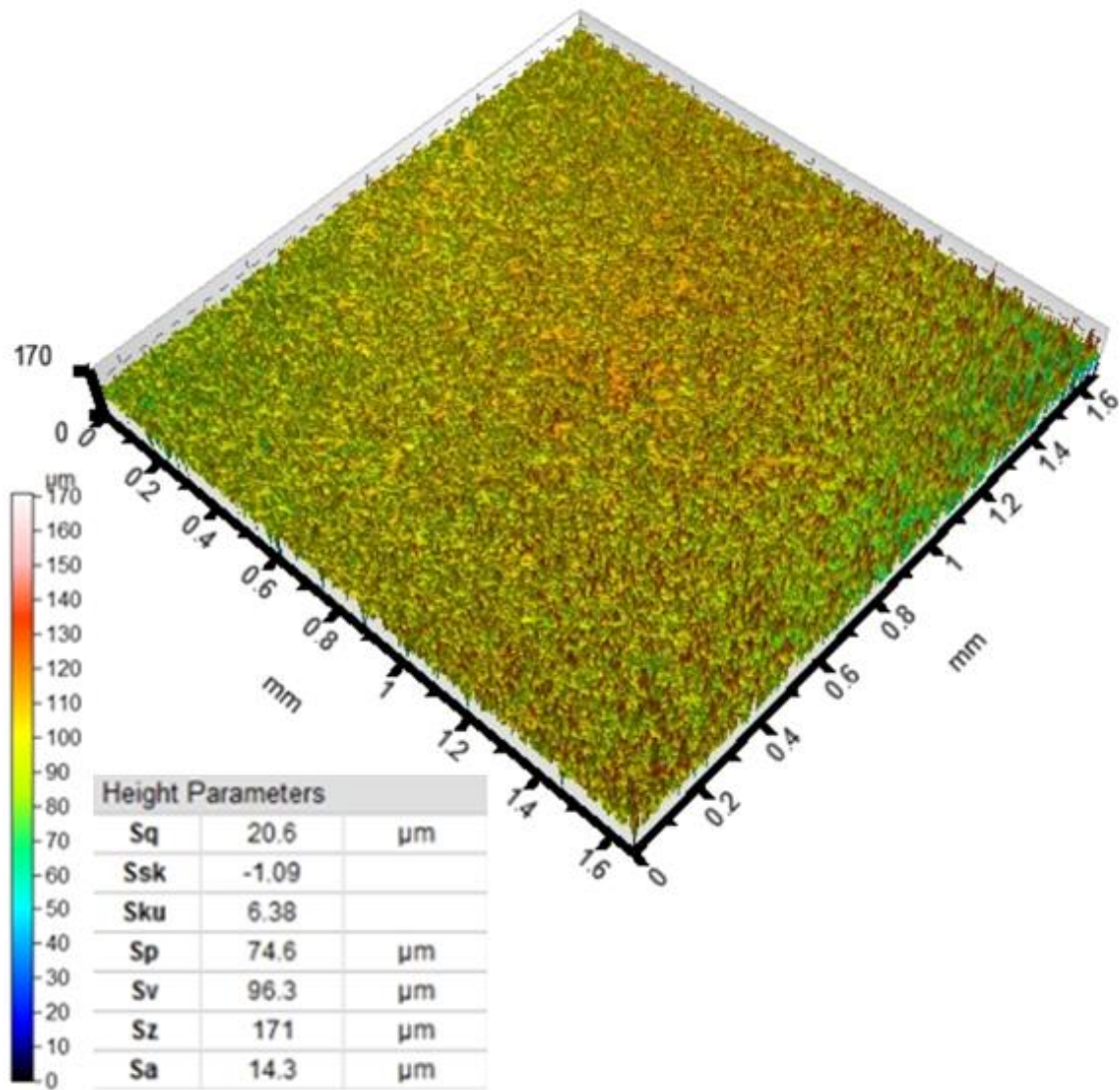


Figure 5.2.3.6: 3D surface topography at the position 4, lower triangle (fig. 5.2.3.4).

These items (figs. 5.2.3.2 to 5.2.3.6) will be detailed further in the discussion (chapter 6.2.2.1).

In fig. 5.2.3.7 it is possible to see the effect of sheet metal roughness evolution under tensile strain condition and its evolution through all the painted layers.

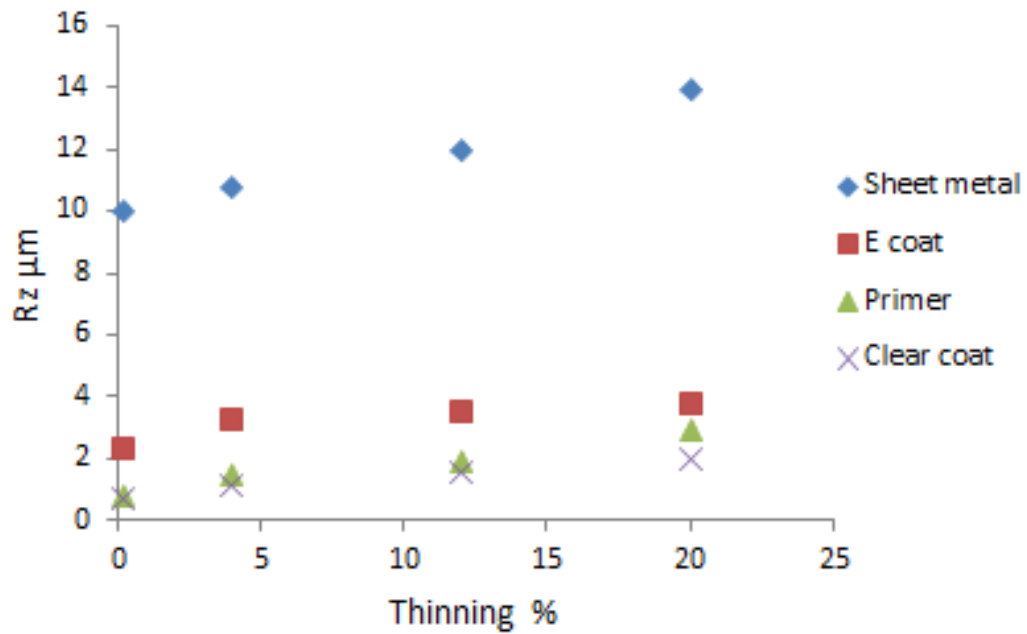


Figure 5.2.3.7: Sheet metal roughness evolution under tensile strain condition and its evolution through all the painted layers.

From this curve we may conclude that, under tensile conditions, as thinning increases, roughness (Rz) also increases with the higher rate for the sheet metal and lower rate for the clear coat layer.

Similar results from literature will be given in the discussion (chapter 6.2.2.1).

5.2.3.2 The second step of the third run: Near plain strain condition

Sample nr. 17 (see table 4.1) was submitted to a tensile rupture test (in the LD rolling direction). The results of the 2D roughness evolution are shown in fig. 5.2.3.8.

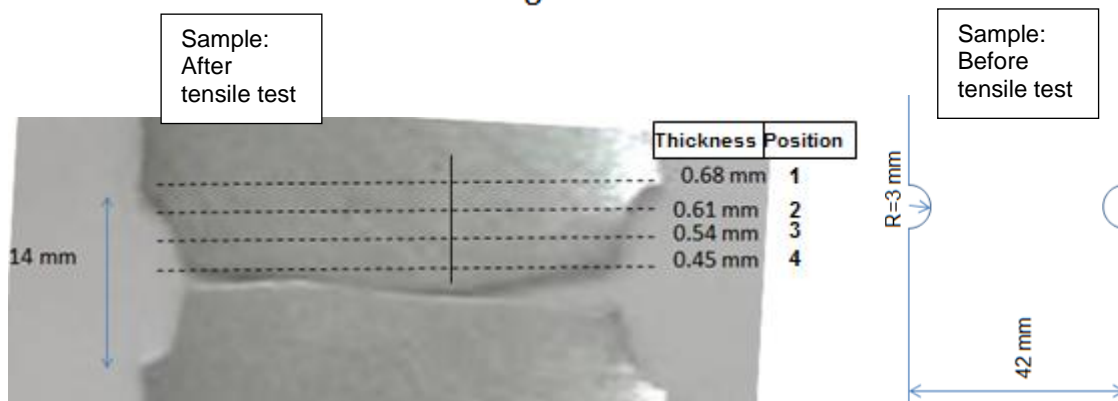
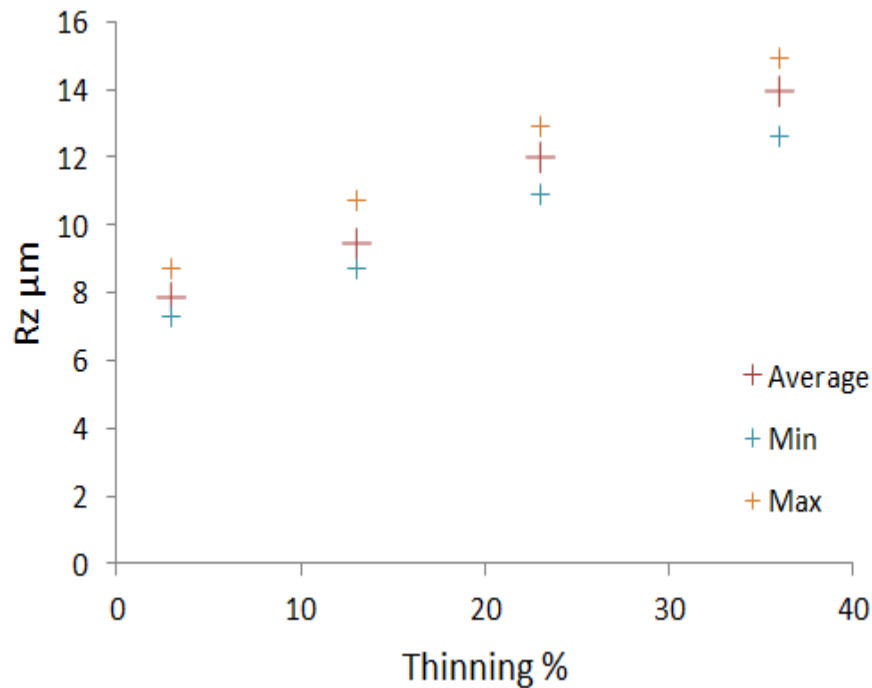


Figure 5.2.3.8: 2D Roughness evolution Rz versus thinning evolution at the positions (1) one and four (4) for the “near” plain strain condition sample.

From this curve we may conclude that, under “near plain strain” conditions, as strain increases (thinning so on), roughness (Rz) also increases.

Fig. 5.2.3.9 shows the strain measurements of the points related to the positions 1 to 4. The FLD was built according to the standards given by the NADDRG (North American Deep Drawing Research Group).

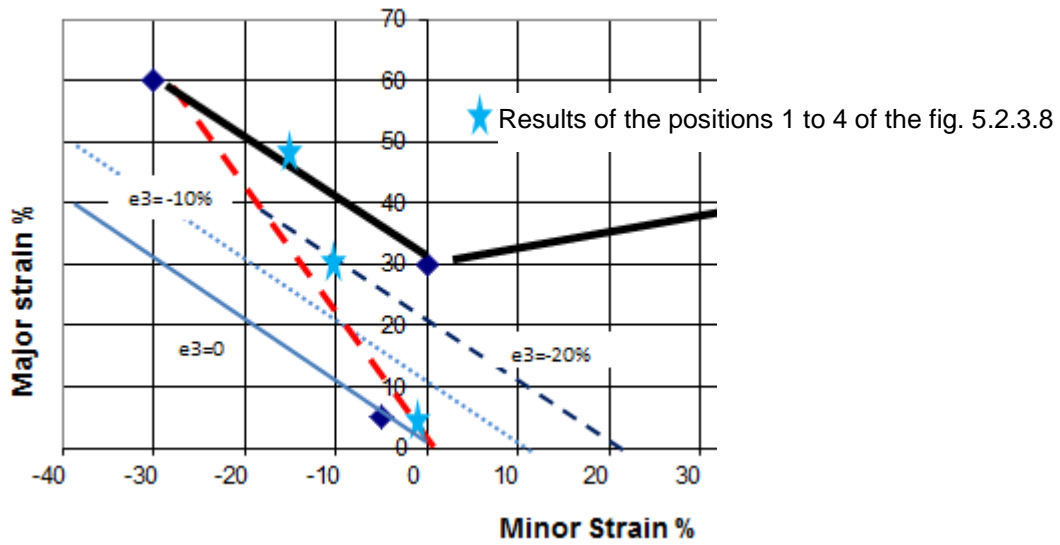
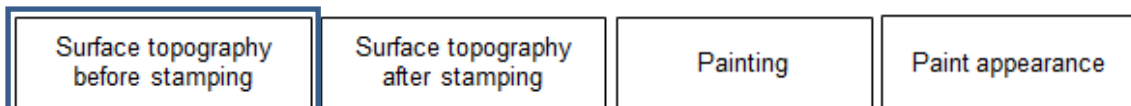


Figure 5.2.3.9: Strain path for the "near" plain strain testing condition.

Similar results from literature will be given in the discussion (chapter 6.2.2.2).

6 DISCUSSION

In the following a discussion will be presented relating the experimental results obtained from the present work with the literature, following the same sequence that has been used and shown in the summary of the literature review (chapter 3), namely:



6.1 Surface topography before stamping

In this topic the effect of the skin-pass reduction and texturing method (EDT and SBT) on surface topography will be analyzed, as well as the roughness standard deviation for the initial and end position in the coil.

Fig. 6.1.1 shows the effect of skin pass reduction and texturing method (EDT and SBT) on surface topography characterized by 2D roughness parameters Ra and Pc.

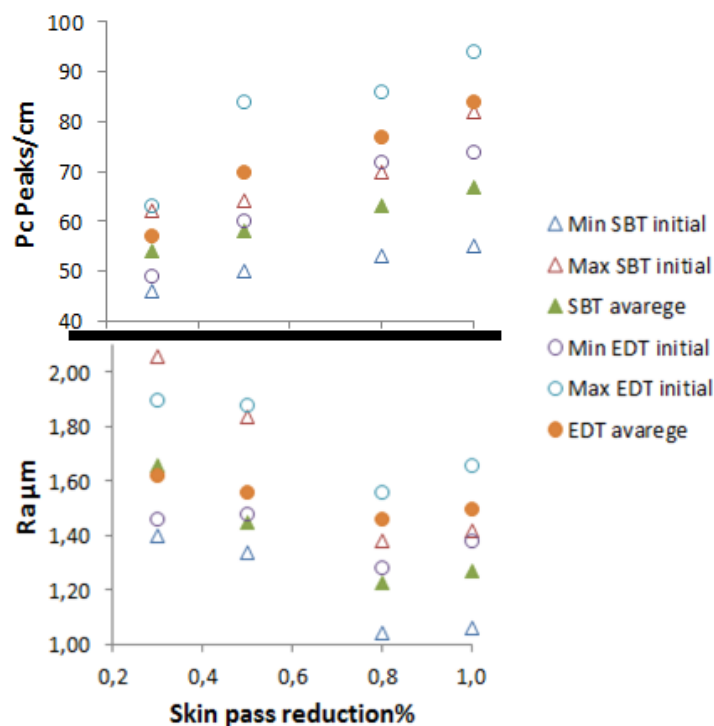


Figure 6.1.1: (same as figure 5.1.6) Comparison between sheet metal surface topography parameters (average Rz and Pc) for the SBT and EDT roll conditions, for different skin-pass reductions (test conditions 1 to 16).

We may observe from fig.6.1.1 that, in general, an increase in skin-pass reduction leads to an increase in the Pc (2D) roughness parameter for both EDT and SBT

processes, however in a more accentuated manner for the EDT process. Also it may be observed the decrease in the Ra roughness parameter for both processes, now in a more accentuated manner for the SBT processes. There seems to be a minimum roughness for a reduction of 0.8%, indicating a possible saturation in the transference level of the roll to the sheet surface. Indeed, Pawelsky (1996) showed in fig 6.1.2 that elongation (which is related to skin pass reduction) is a function of the degree of transference. It can be observed, in a similar way as shown in the present work, that the level of roughness transference from the roll to the sheet surface increases with the elongation, reaching a saturation level. It may be observed that saturation reaches first for the EDT and then for the SBT process.

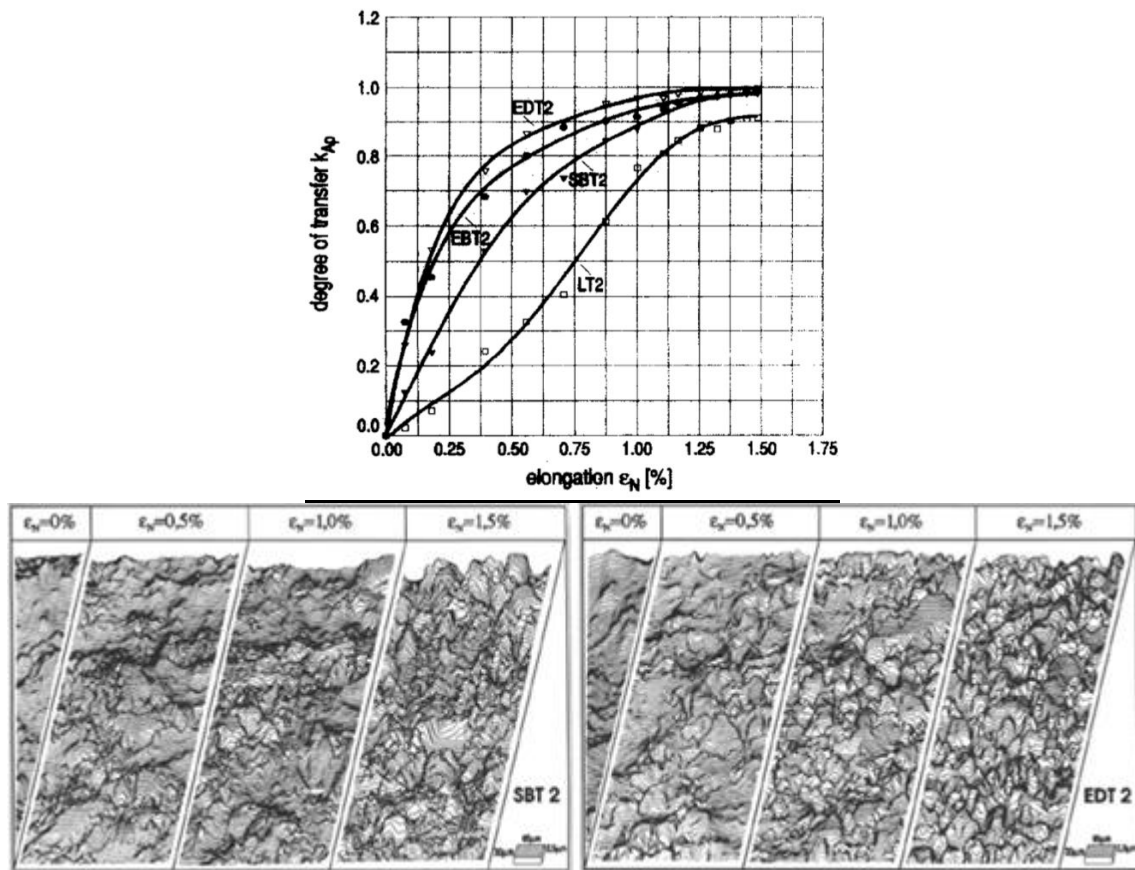


Figure 6.1.2: Degree of transfer as function of elongation for SBT and EDT (PAWELSKY, 1996).

Following, the concept and correlation between elongation and skin pass reduction is given. In fact, the variation in roll speed, that is observed at the entry and exit of the roll mill stand in the skin-pass rolling operation, enables establishing the strip speed variation (or strip elongation) and the consequent thickness variation, i.e. the thickness reduction in the specific rolling pass.

Returning to the results of the present work, the 3D roughness parameters V_{cl} and α_{clm} (fig. 6.1.3), both present the maximum values at 0.8% skin-pass reduction, which might be considered as another indication of the saturation level achieved in the roughness transference. From the point of view of stampability and paintability of the material, this would be the best working condition, because, as pointed out in the literature (PFESTORF et al., 1998; WEIDEL, ENGEL, 2009), these two parameters, namely V_{cl} and α_{clm} , are those mainly responsible for the lubrication (oil film build-up between the tool and the sheet metal) and, consequently, the reduction in friction as well as a reduction in the sheet metal thinning (in the case it happens). As discussed in topic 3.2.8 of the literature review and in the topic 6.2.2 of this chapter, sheet metal thinning leads to an increase in surface roughness which, in turn, leads to a worsening of the paint appearance.

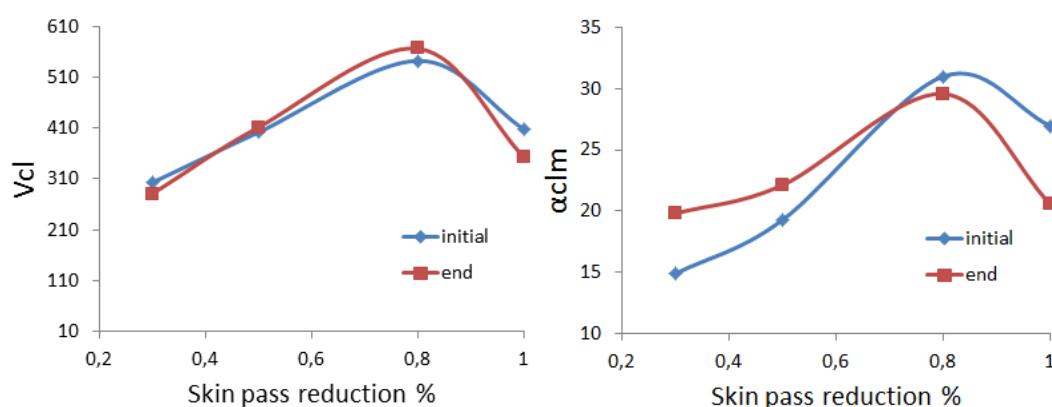


Figure 6.1.3 (same as fig. 5.1.4): 3D Roughness parameter evolution: closed void (V_{cl}) and maximum closed void ratio (α_{clm}) as a function of skin pass reduction %, for the initial and end along the coil length – EDT condition.

In the case of the SBT condition, these parameters did not present any correlation between skin-pass reduction and the roughness parameters V_{cl} and α_{clm} , as shown in fig. 6.1.4, showing significant randomness. They had lower values if compared to EDT, which, from literature (BAY et al., 2010; BFINTEN et al., 1996; WEIDEL, ENGEL, 2009; PFESTORF et al., 1998), means a poorer material stampability and paintability.

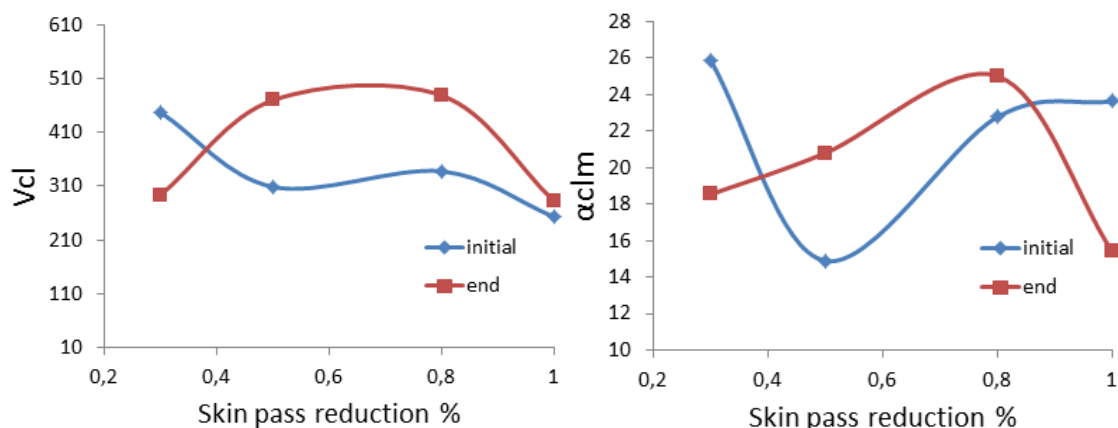


Figure 6.1.4 (same as fig. 5.1.2): 3D Roughness parameter evolution. Closed void (Vcl) and maximum closed void area ratio (α_{clm}) as a function of skin pass reduction % for the initial and end of the coil length (SBT condition).

In fig. 6.1.5 is shown the effect of the texturing method (EDT and SBT), skin-pass reduction and coil position (initial and end) on the roughness standard deviation. It can be clearly seen that for both processes (EDT and SBT) a tendency for a decreasing Ra standard deviation with increasing skin-pass reduction up to 0.8%. It may be also observed a tendency of having a lower value of Ra standard deviation for the end of coil compared to the initial part of coil. Indeed, it has been a common practice, in some car companies, to leave the end part of the coil for the outer panels; those designated to car parts with higher aggregated values.

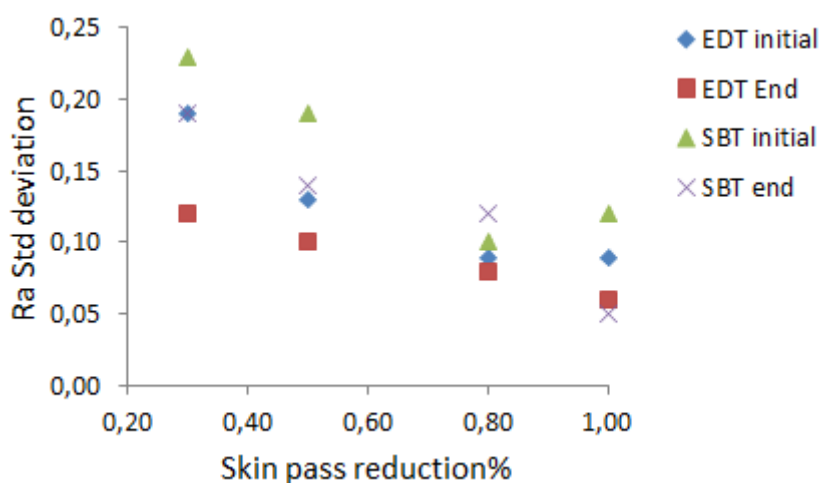


Figure 6.1.5 (same as fig. 5.1.7): Ra standard deviation for the SBT and EDT roll conditions, for different skin pass reductions (Test conditions 1 to 16).

It seems quite natural that we may obtain a more homogeneous roughness (smaller roughness standard deviation), with an increase in the level of transference during the skin-pass reduction. However, the relative difference observed between the initial and end parts of the coil may be associated with the phenomena of breaking-up of the roll higher peaks (see fig 6.1.6). As the peaks (roughness) of the roll tend to create the valleys in the sheet, it seems natural that with the roll wear there is a simultaneous decrease in the volume of the valleys, as shown, for instance, in the V_{cl} of fig 6.1.7 and in the average R_a value of the sheet, given by Pfestorf et al. (1998) and Meyer (2013) (fig. 3.1.9).

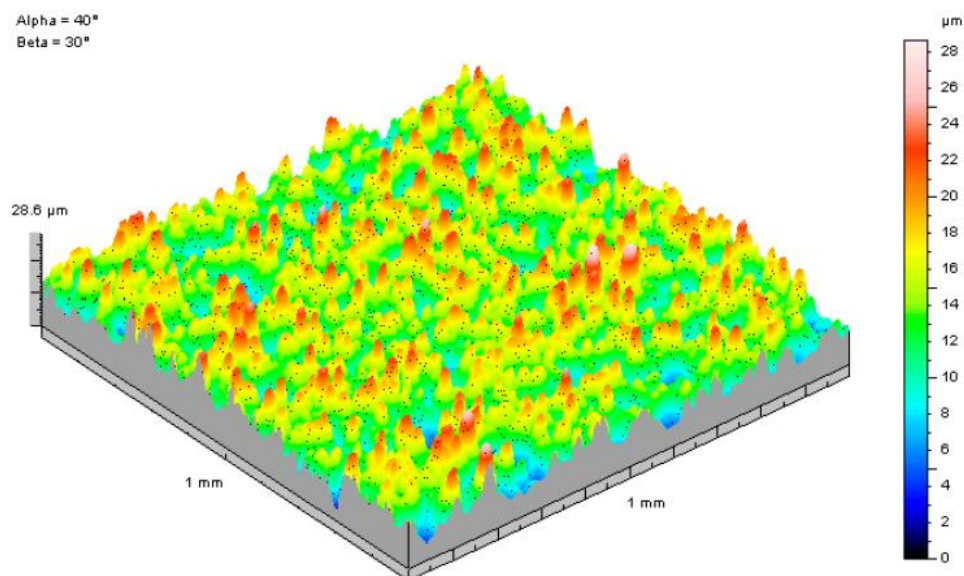


Figure 6.1.6 (same as fig. 3.1.10): An example of a section of a barrel surface of a texturized roll (TSCHERSCHKE, NITSCHKE, 2012).

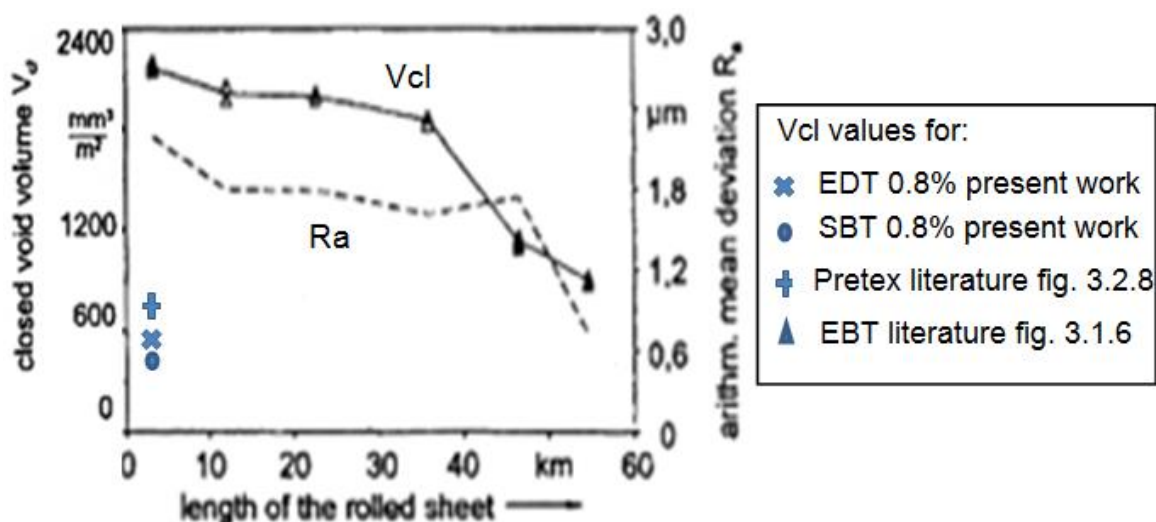


Figure 6.1.7 (same as fig. 3.1.6): Wear of the work roll during skin pass rolling and its effect on surface topography characterized by the 3D parameter V_{cl} and 2D parameter R_a (GEIGER, ENGEL, PFESTORF, 1997).

It is important to observe in fig 6.1.7 how the values of V_{cl} increase as the deterministic level of the structure also increases. For structures considered as being stochastic, the V_{cl} values here presented tend to increase in the following order: SBT, EDT and Pretex. In the case of a deterministic structure, EBT presented a V_{cl} value 300% greater than the stochastic structures. Another interesting point is that despite the negative effect associated with the decrease in the value of V_{cl} (which decreases the stampability, see chapter 3.2.2), due to the roll wear, there is a positive effect which is the decrease in the standard deviation in the R_a value, i.e., it increases the level of homogeneity of the roughness.

In the present work, however, no significant difference for both processes (EDT and SBT) in the average roughness R_a values could be observed, mostly between the initial and end part of the coil, since the corresponding interval is of about 2Km only. However, in the case of the values of R_a -standard deviation, it was possible to observe a slight decrease from the initial to the end of the coil, as shown in fig 6.1.5

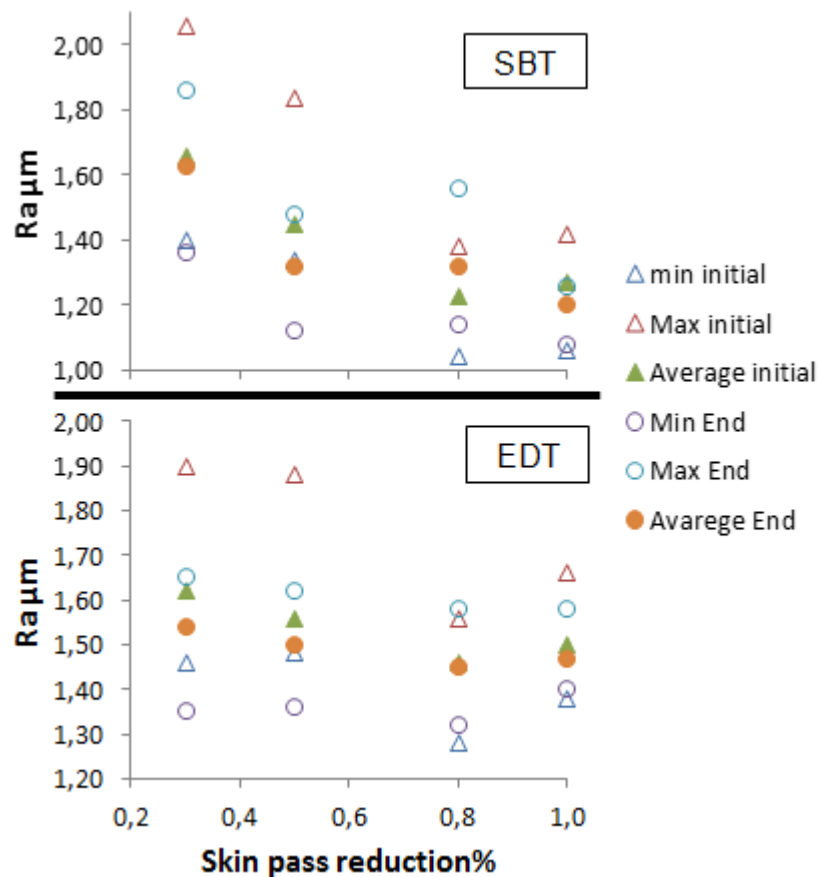


Figure 6.1.8 (same as figs. 5.1.3 and 5.1.6): Comparison between sheet metal 2D roughness parameters Ra for the initial and end positions along the coil length (EDT and SBT conditions), for different skin pass reductions.

In fig 6.1.9 a comparison is made between the results of the present work with those from the literature for the 3 D roughness parameters α_{clm} e V_{cl} (for the present work the values of the end of coil have been adopted for a 0,8% skin-pass reduction)

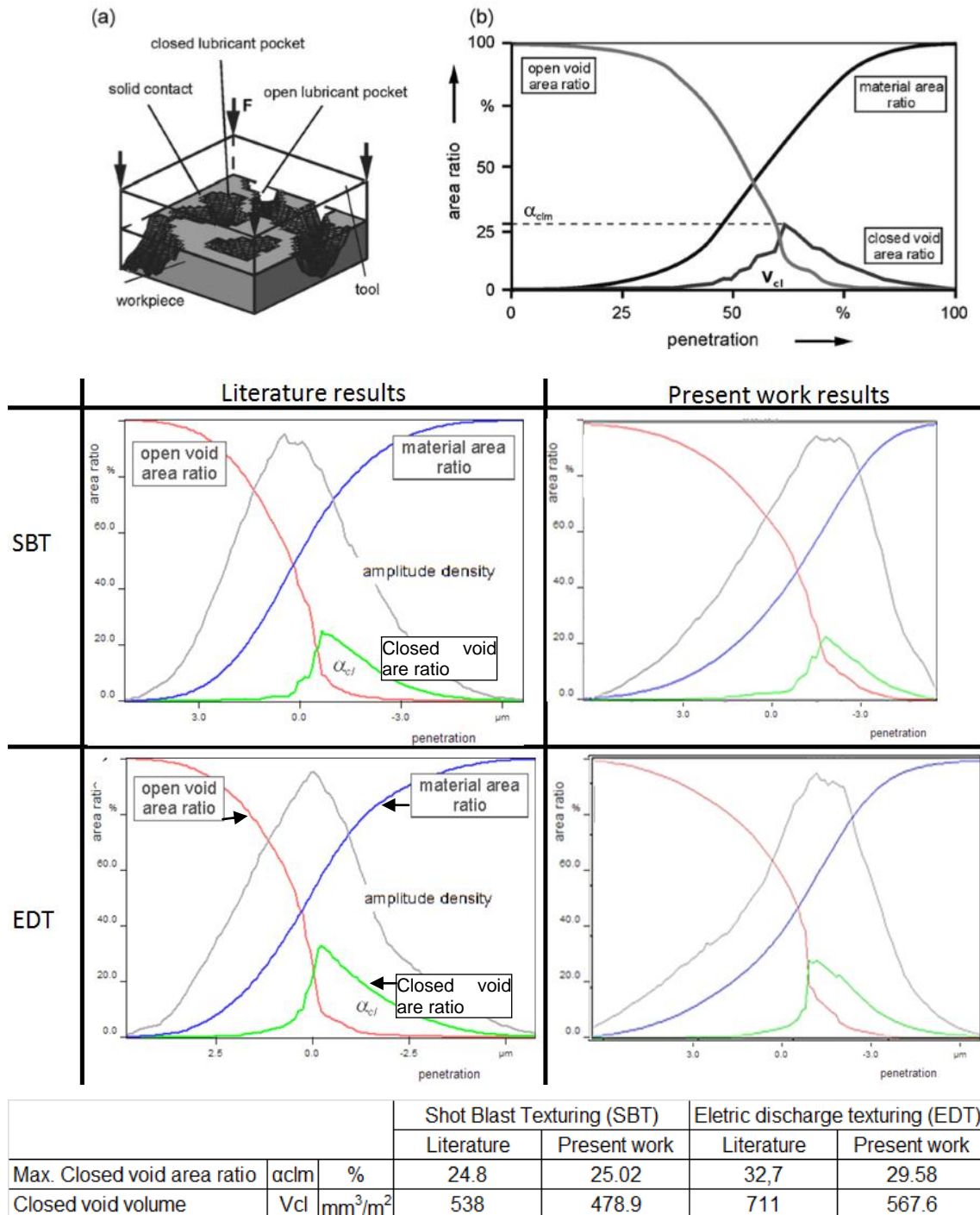


Figure 6.1.9: Comparison between 3D Roughness parameters, namely, closed void (V_{cl}) and maximum closed void ratio (α_{clm}) for EDT and SBT condition with the results in literature (VALENTIN et al., 2005).

From fig 6.1.9 we may observe that the values for the SBT rolls of the present work are quite close to those from the literature (difference smaller than 10%). In the case

of EDT rolls, the α_{clm} values were very close; however for the V_{cl} values the difference was higher than 20%.

A possible explanation for that aspect may be linked to the difference due to the Cr-layer given to the rolls of these samples. In the case of the EDT results here reported, the Cr-layer was the conventional (electrolytic) process, in which the Cr-layer follows the roll surface roughness. In the case of the EDT roll, as presented in the literature, the commercial Pretex method provides an electrolytic Cr-layer that also follows the roll surface roughness; however the deposition occurs through the usage of small particles with a geometry close to semi-spheres, which aim maximizing the values of α_{clm} and V_{cl} (parameters associated with the closed voids) of the sheet surface. These parameters, as mentioned in chapter 3.2.2, are those mainly responsible for the lubrication during stamping. The surface image given in fig 6.1.10 (for the Pretex method), clearly shows the phases: material ratio, open and closed voids.

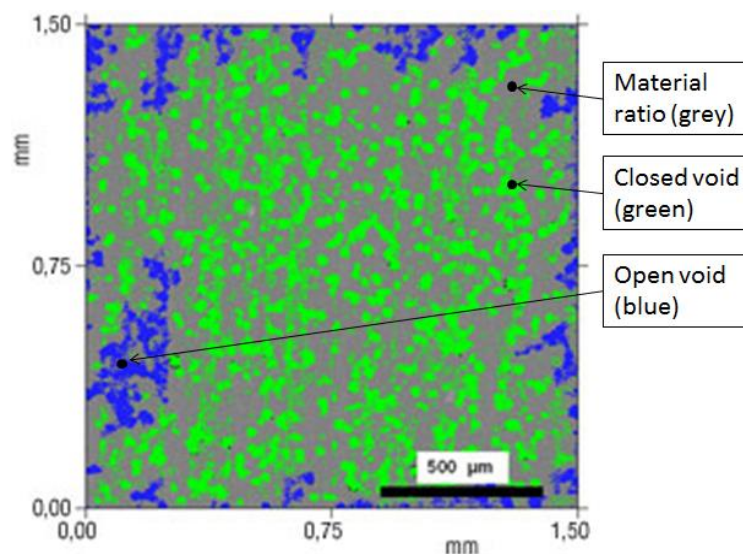
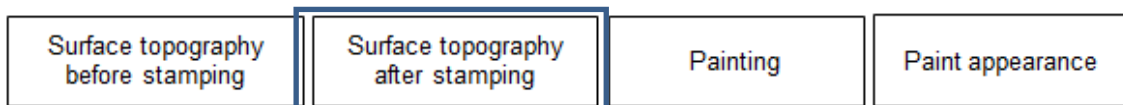


Figure 6.1.10 (same as fig. 3.2.7): Lubricant reservoir (closed void) of EDT (Pretex) structure (GRETHE, 2013).

Conclusions:

6.1.1 The degree of transfer saturation occurs for the EDT process at a level of 0.8% of skin-pass reduction (figs 6.1.1, 6.1.3 and 6.1.8). The SBT process did not show to reach the degree of transfer saturation even at a 1.0% of skin-pass reduction (figs. 6.1.4 and 6.1.8)

- 6.1.2 The EDT process promotes much less randomness for the surface topography along the initial and end of the coil than the SBT process, when analyzed by the 3D parameters V_{cl} and α_{clm} (figs 6.1.3 and 6.1.4).
- 6.1.3 At a 0.8% skin-pass reduction the average (between initial and end of the coil) 3D roughness parameter presents the following results: V_{cl} (mm^3/m^2) for EDT = 520 and SBT = 400. α_{clm} (%) for EDT = 30 and SBT = 23% (figs 6.1.3 and 6.1.4).
- 6.1.4 The R_a standard deviation for both processes (EDT and SBT), decreases with increasing skin-pass reduction up to 0.8% and, in general, it was smaller for the EDT process (fig. 6.1.5).
- 6.1.5 The α_{clm} and V_{cl} results for the SBT process were near to those reported in the literature (α_{clm} = 25.02 vs. 24.8 % and V_{cl} =478.9 vs. 538 mm^3/m^2). However, in the case of the EDT process the difference was a bit larger (α_{clm} = 29.58 vs. 32.7 % and V_{cl} =567 vs. 711 mm^3/m^2) (fig. 6.1.9).



6.2 Surface topography after stamping

This item will be subdivided into three sub items, namely:

- Surface topography evolution due to die contact (surface flattening);
- Surface topography evolution due to sheet metal straining without die contact;
- Inter-relationship between these two conditions with and without die contact.

6.2.1 Surface topography evolution due to die contact (surface flattening)

The surface topographical analysis have been concentrated in the A and B regions (fig 6.2.1). The region A represents the original surface of the blank (before stamping), and region B that has greatest contact with the die (after stamping).



Figure 6.2.1 (same as fig. 5.2.2.5): Regions A and B

In accordance with the FEA (fig 6.2.2) and thickness measurements (micrometer) performed in these regions, no significant thinning has been observed. The maximum thinning measured was 0.02 mm and FEA was 0.03 mm. As region B visually presented intensive contact scratches, this has been chosen for analysis.

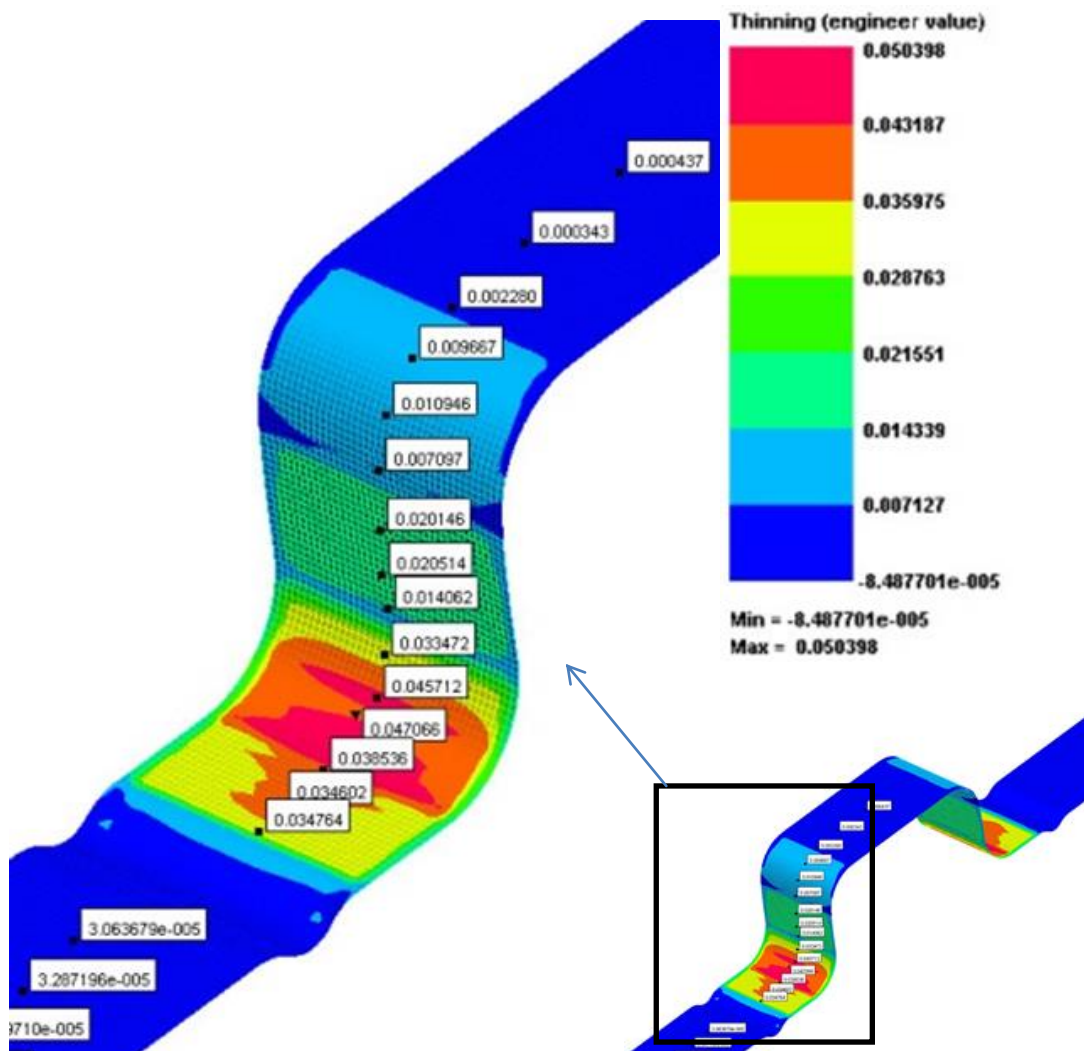


Figure 6.2.2: FEA - “No significant thinning” for the experiment .

The no significant thinning observation of the test piece is important because this fact did not introduce “noise” into the experiment, once the main objective was to verify

(through strip speed measurements during stamping), the effect of the roughness on the sheet stampability.

The direct contact between tool and sheet metal which occurs in the regimes of boundary lubrication (BL) or mixed lubrication (ML) (these regimes will be detailed in the next topic), causes surface flattening, as evidenced by the present work (fig. 6.2.3) and also in the literature (fig. 6.2.4) (JONASSEN et al., 1997).

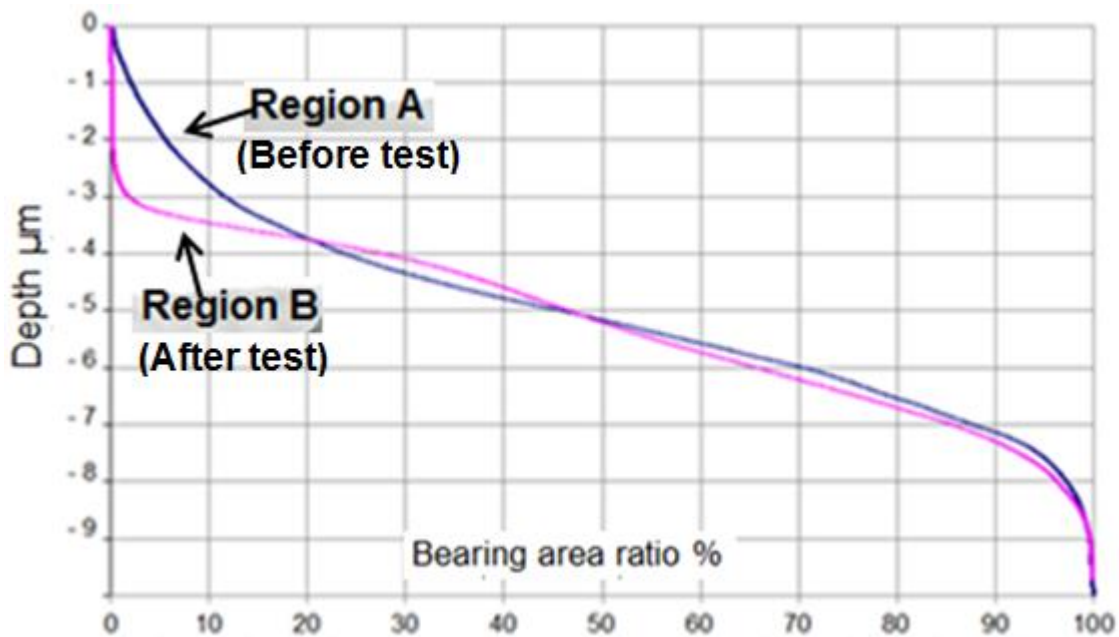


Figure 6.2.3 (same as fig. 5.2.2.6): Effect of the die contact leading to the deformation on the sheet metal surface topography (present work). Sample Nr 12. (EDT condition, 1.0 % skin-pass reduction). (Zygo).

Each curve in this figure (regions A and B), is the read-out of 2000 different points, all related to the analysis performed on an area of 0.702 x 0.526 mm (fig. 6.2.6).

Fig 6.2.4 illustrates the evolution of the surface topography, for the same slipping condition mentioned in fig 6.2.3., as also the same material (Deep Drawing Quality) and texturizing method EDT.

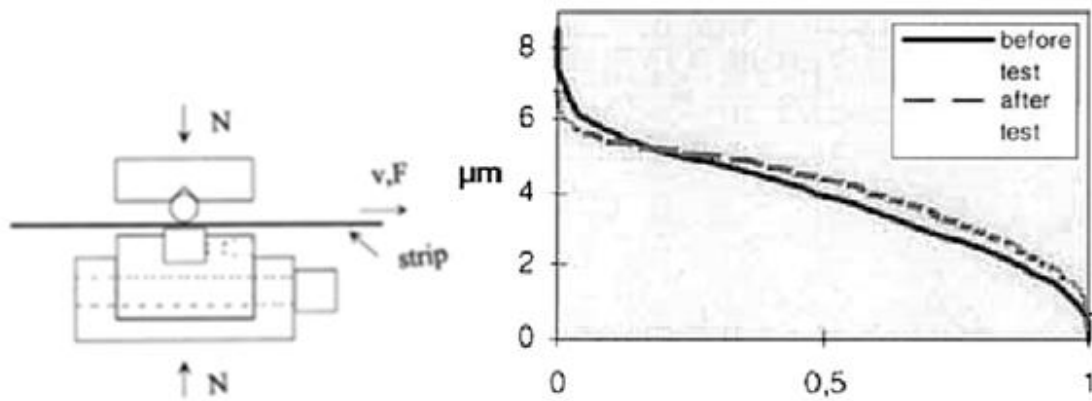


Figure 6.2.4 (same as fig. 3.2.16): Left: Strip drawing test scheme. Right: Typical Abbot-Firestone curve before and after the strip drawing test (JONASSEN et al., 1997).

Fig 6.2.5 presents the superposition of figs 6.2.3 and 6.2.4. Both curves showed the same trend in terms of surface topography, however there is a larger rate in the peak flattening for the present work and a larger growth in core roughness for the work of Jonassen et al. (1997).

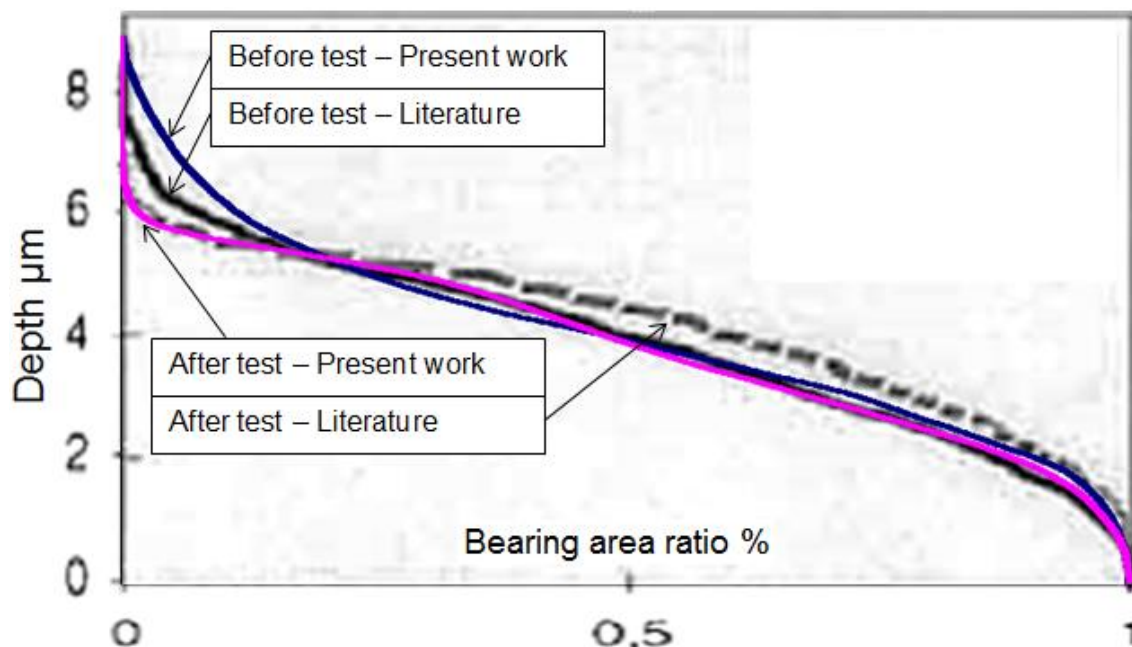


Figure 6.2.5: Comparison between Abbot-Firestone curves before and after the strip drawing test from present work (fig. 6.2.3) and from the literature (fig. 6.2.4).

The peak flattening effect which can be observed more clearly in fig. 6.2.6, shows the 2D roughness cross section profile and its corresponding Abbott-Firestone curve before and after the drawing test.

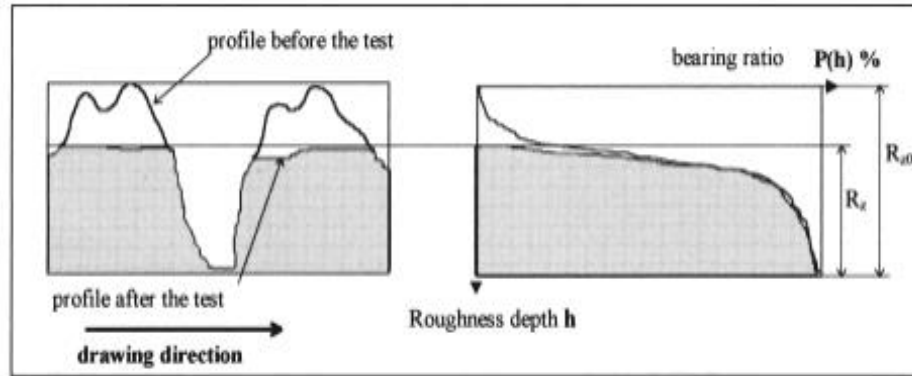


Figure 6.2.6 (same as fig. 3.2.20): Evolution of Abbott curve (right) in relation to the roughness flattening after a strip drawing pass. There is a decrease in the Rz parameter (RAHARIJAONA, ROIZARD, STEBUT, 1999).

Fig. 6.2.7 shows the results of the 3D surface topography corresponding to the conditions: Before stamping (region A) and after the stamping (region B) (see also fig. 6.2.1).

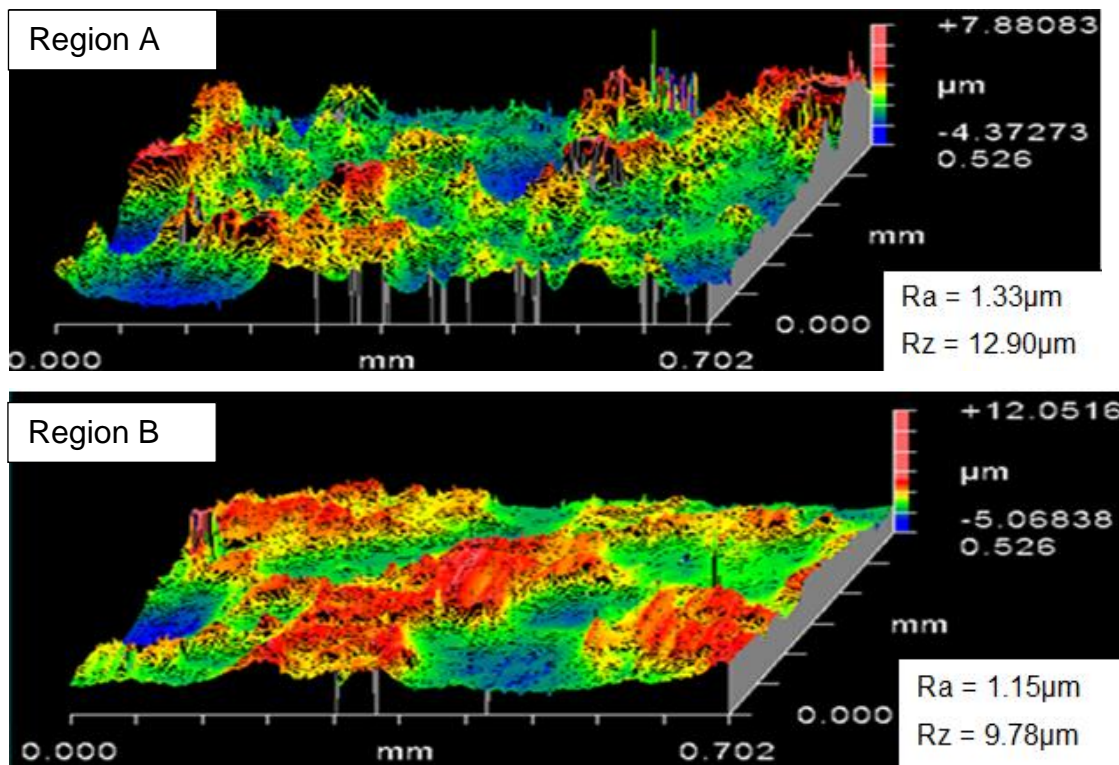


Figure 6.2.7 (same as figs 5.2.2.7 and 5.2.2.8): Surface topography for regions A and B (fig.6.2.1).

Conclusion:

6.2.1.1 Direct die contact of sheet metal surfaces during stamping causes a peak (surface) flattening of the surface topography. The roughness Ra decreased from 1.33 to 1.15 μm and Rz decreased from 12.9 to 9.78 μm in the regions A and B (fig. 6.2.7), respectively.

6.2.2 Surface topography evolution due to sheet metal strain without die contact

In this chapter the roughness evolution for different strain path conditions in a steel sheet metal forming limit diagram (FLD), has been evaluated. Therefore this item was subdivided into two sub-items, namely: Tensile condition and near to “plain strain” condition.

6.2.2.1 Tensile condition

The roughness evolution was analyzed at the positions (1) one to (4) four, as shown in fig. 6.2.8, in the sample described in the topic 4.3.1. The conventional tensile test has been conducted up to rupture.



Figure 6.2.8: Approximately sample position for 2D and 3D roughness measurements.

Fig. 6.2.9 presents the roughness evolution in 2D Rz as a function of the sample thinning. It clearly may be noted the increase in roughness with the increase in the the sheet metal thinning.

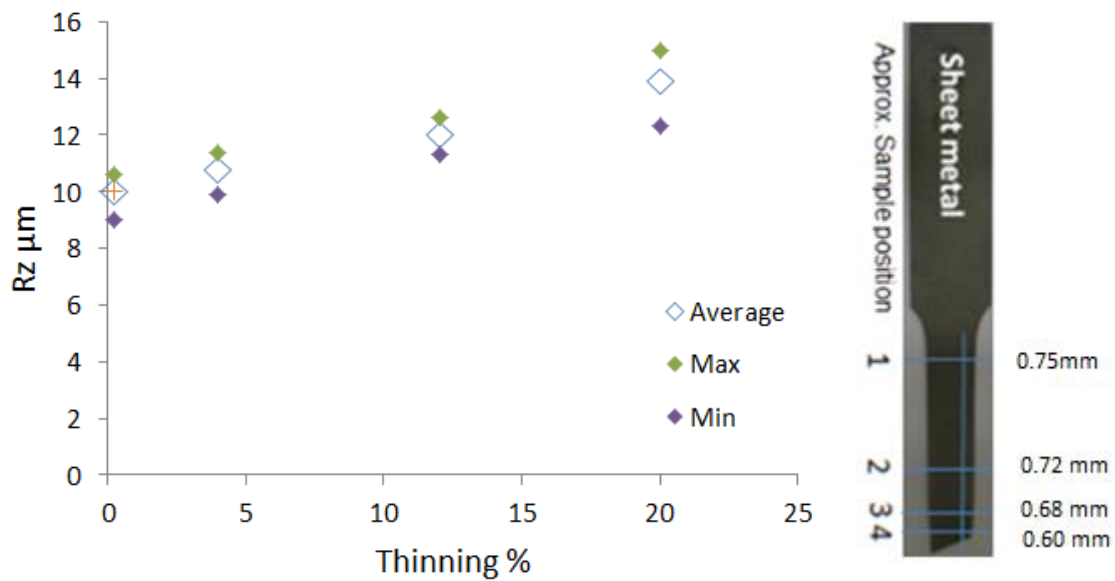


Figure 6.2.9 (sames as fig. 5.2.3.2): Roughness evolution Rz versus thinning evolution at the positions (1) one to (4) four (fig. 6.2.8).

In fig 6.2.10 the 2D roughness values of the present work are compared with the results from the literature (UNFER, BRESSAN, 2012) where it is possible to observe that they follow the same trend in terms of the increase in roughness with increase in strain.

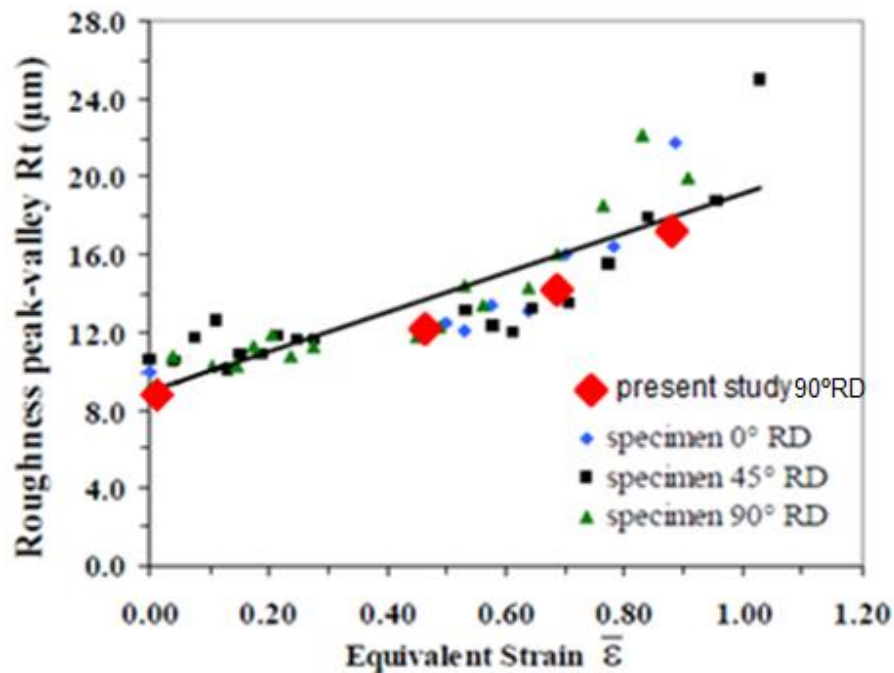


Figure 6.2.10 (same as fig. 3.2.27): Comparison between present work and data from the literature (UNFER, BRESSAN, 2012) on the evolution of roughness (peak - valley Rt) with strain.

In a similar way, in fig 6.2.11, the 3D roughness parameter, Sq , the results of present work are directly compared to the results from the literature (WICHERN et al. 2005) on the FLD- forming limit diagram for a similar steel sheet material as the one used in the present work. Again, there is good consistency of results.

However, in fig 6.2.12 the same analysis is performed, now in terms of the 3D roughness parameter, Sq , against iso- ϵ_{vme} (equivalent Von Mises strains). We may observe that the values of Sq of the present work are about 50% higher when iso-deformation is about 0.6. This may be related to the accuracy of strain measurements performed in that region, taking into account that near to the fracture the deformation intensity and path do change quite abruptly, as will be seen in the following figures 6.2.15 and 6.2.16.

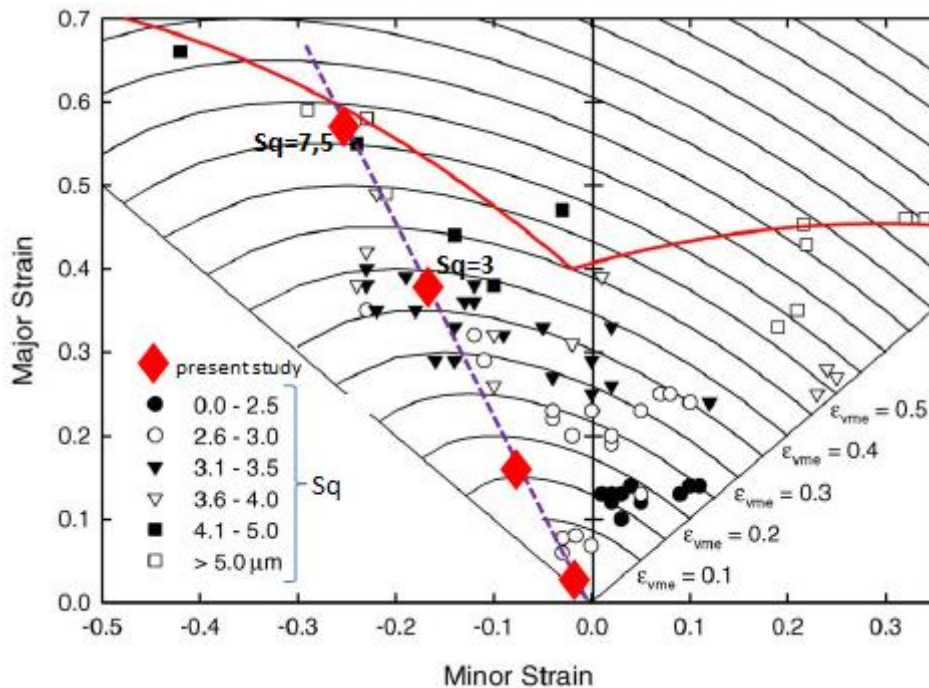


Figure 6.2.11 (same as fig. 3. 3.2.29): Forming limit diagram for the HDG sheet steel with iso- ϵ_{vme} lines and the comparison of the roughness values for different strains. Data are from literature (WICHERN et al. 2005) and from the present work.

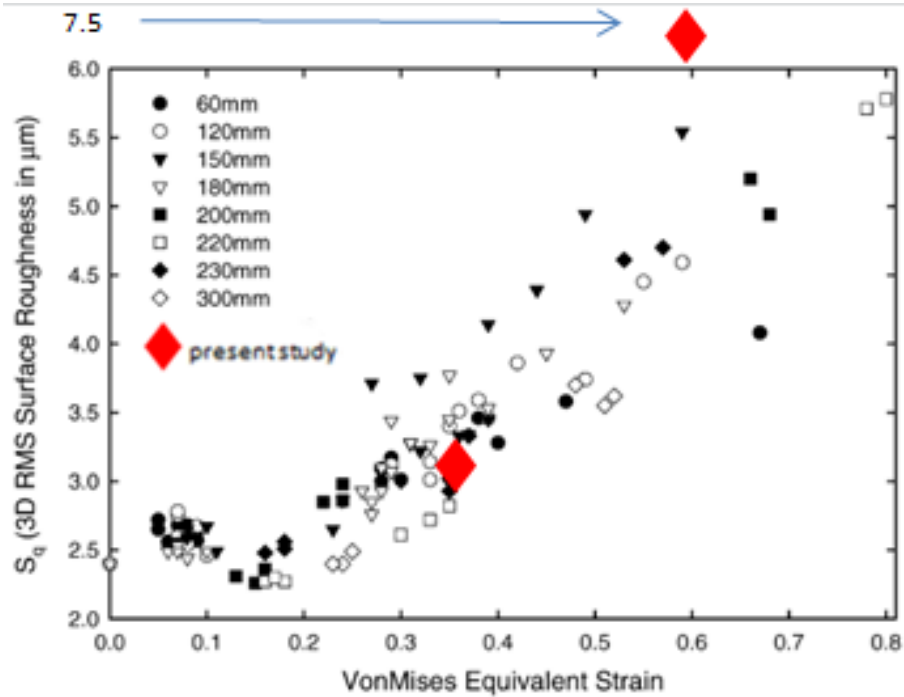


Figure 6.2.12 (same as fig. 3.2.31): Plot of the 3D roughness parameter S_q versus the iso- ϵ_{vme} for the HDG sheet steel and the comparison of the roughness values for different strains. Data are from literature (WICHERN et al. 2005) and from the present work.

Fig. 6.2.13 compares the 3D roughness parameter S_z values of the present work to those from the literature (WICHERN et al. 2004)

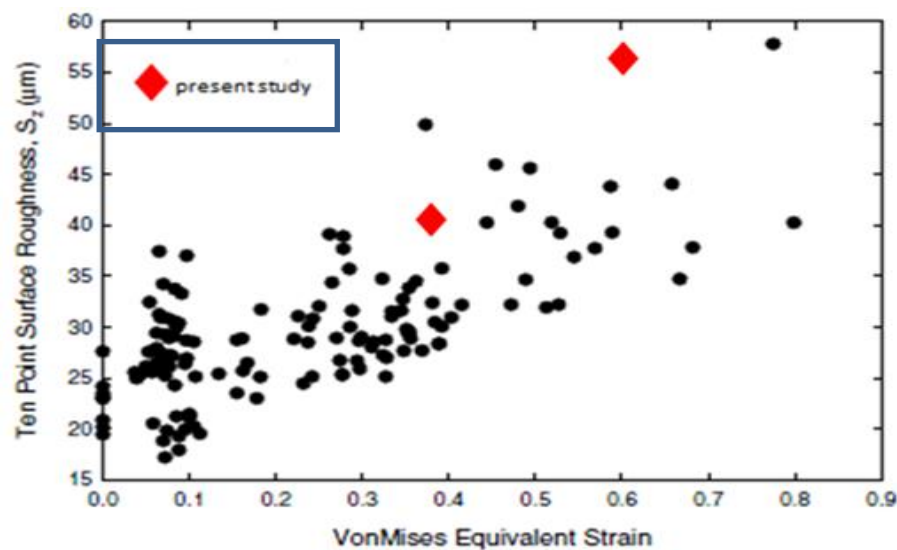


Figure 6.2.13 (same as fig. 3.2.28): Ten-point peak-valley 3D roughness parameter, S_z , as a function of strain (ϵ_{vme}) for a strain imposed by a Marciniack punch test (WICHERN et al., 2004) and the results of the present work (tensile test condition).

Although the strain path is different in the comparison made in fig 6.2.13, it may be observed that the same trend has been observed as in fig 6.2.12, in which there is a better correlation of results for iso-strains lower than 0.5 and not so good ones for values higher than 0.5. This fact may be related again to the accuracy in the strain measurements in the region of the fracture, as will be shown in figs 6.2.15 and 6.2.16.

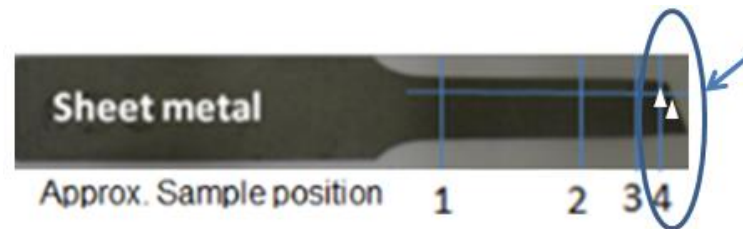


Figure 6.14 (same as fig. 5.2.3.4): Upper triangle refers to analysis presented in fig. 6.2.15 and lower triangle to the analysis presented in fig. 6.2.16.(both triangles are about 2mm apart)

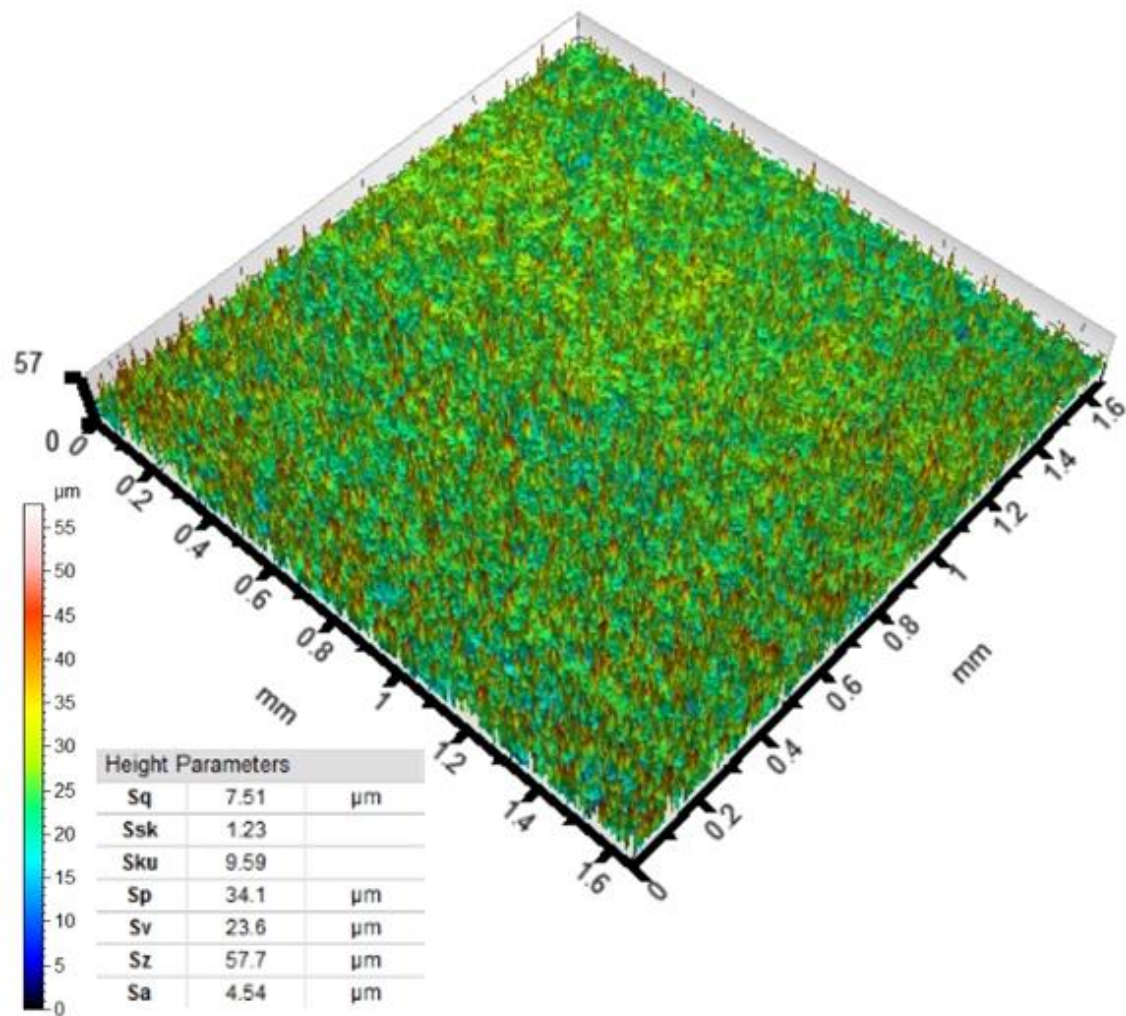


Figure 6.2.15 (same as fig. 5.2.3.5): 3D surface topography at the position 4, upper triangle (fig. 6.2.14) (Taylor Hobson).

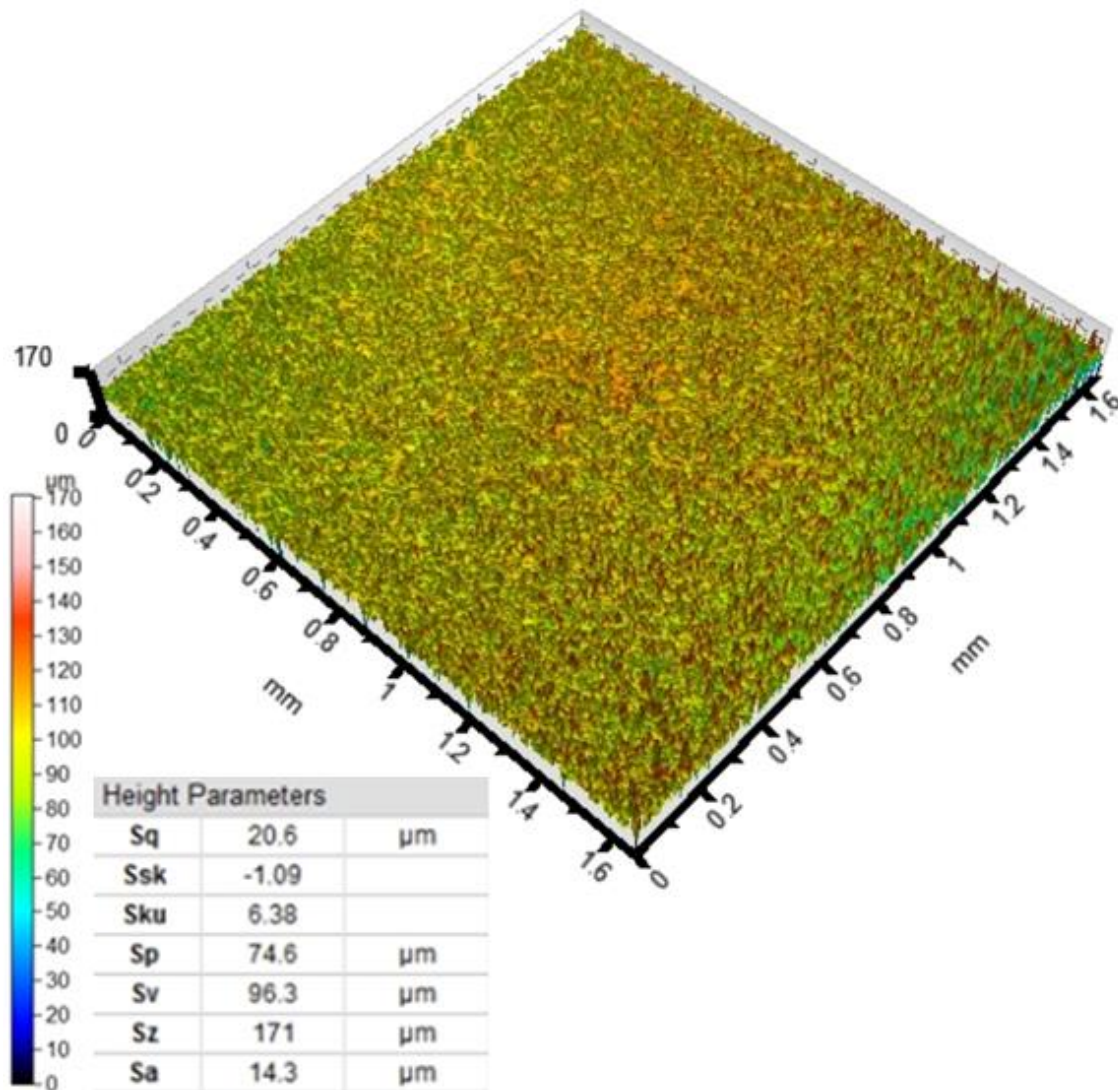


Figure 6.2.16 (same as fig. 5.2.3.6): 3D surface topography at the position 4, lower triangle (fig. 6.2.14) (Taylor Hobson).

From the literature it is well known (GRILHE, 1993; UNFER, BRESSAN, 2012) that as closer we come to fracture (fig 6.2.14) the dislocation density significantly increases and that they tend to move towards the surface, hence increasing the surface roughness.

However, a real increase in roughness has not been detected in the 2D roughness measurements. The gap between 2D and 3D roughness measurements can be seen more clearly in fig 6.2.17.

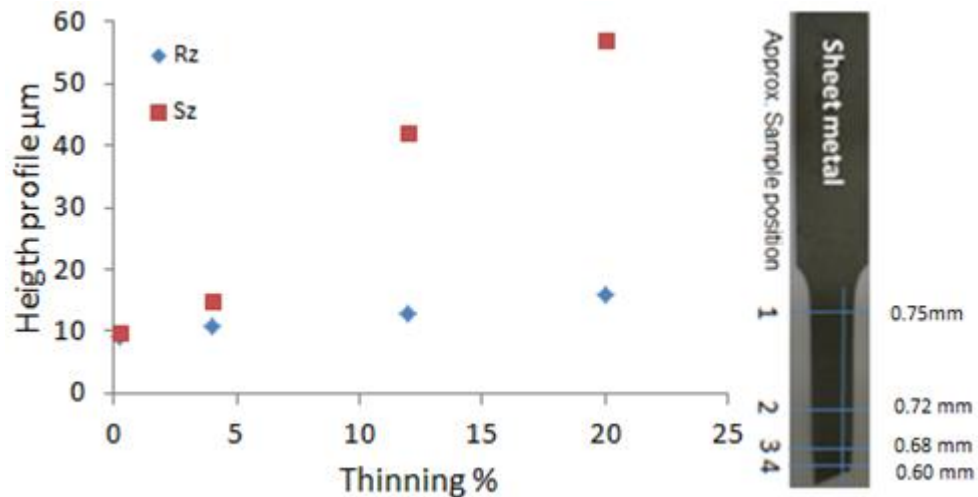


Figure 6.2.17 (same as fig. 5.2.3.3): Gap between 2D and 3D roughness measurements (position shown in fig. 6.2.8)

A possible explanation for this difference can be illustrated with the fig 6.2.18 where Dagnall (1998) showed the effect of the stylus tip radius in reducing the amplitude of the irregularities associated with the surface roughness.

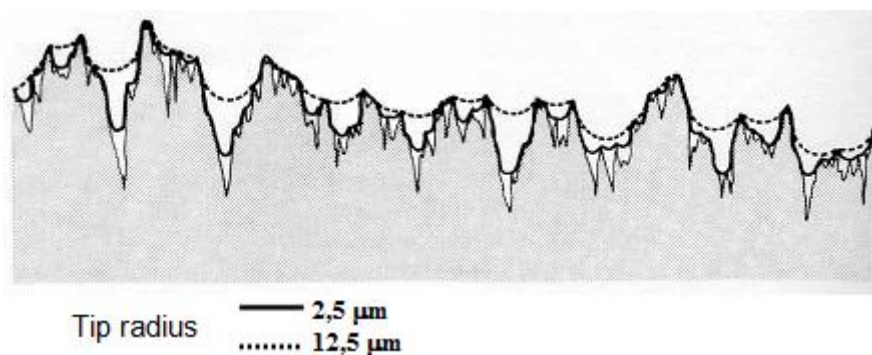


Figure 6.2.18: Effect of the tip radius of the stylus on the reduction of the amplitude of the irregularities of the surface roughness (DAGNALL, 1998).

Fig. 6.2.19 relates the increase in the density of peaks (left side) and the arithmetic mean peak curvature (right side) as a function of sheet metal thinning. This evolution indicates that the distance between peaks decreases, hence contributing to the gap represented in the fig 6.2.17.

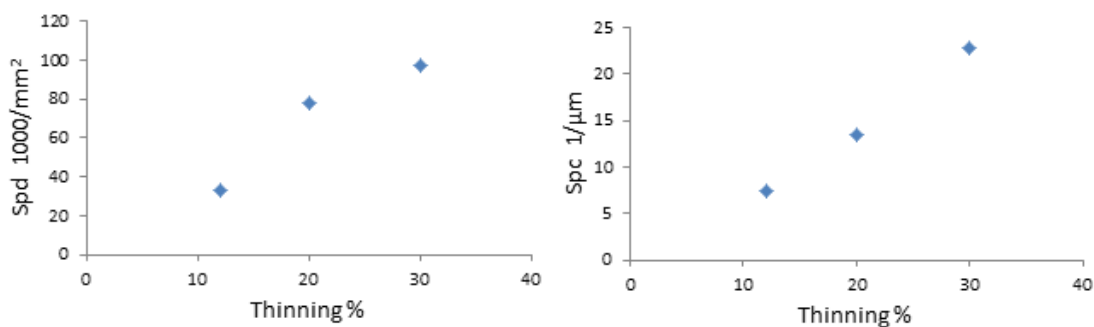


Figure 6.2.19: 3D surface roughness evolution, left: Peak density (Spd) and right: Arithmetic mean peak curvature (Spc), as a function of sheet metal thinning.

Conclusions:

6.2.2.1 Roughness evolution increases with the increase in sheet thinning. At 4% of thinning, Rz was 8.7 μm and at 20%, Rz was 13.2 μm (fig. 6.2.9).

6.2.2.2 There was a gap between 2D and 3D roughness measurements for values of thinning higher than 4%, and the gap increases more than 4 times for thinning higher than 12% (fig 6.2.17).

6.2.2.2 Near to “Plain strain” condition

The roughness evolution has been analyzed at the positions (1) one to (4) four, as shown in fig. 6.2.21, for the material of test nr. 17 (best paint appearance condition), given in table 4.1 and that have been led to rupture in a tensile test.

Fig. 6.2.20 shows the FEA analysis for this particular test that has been used only as a secondary/supplementary analysis in the present work (and should be used for future work).

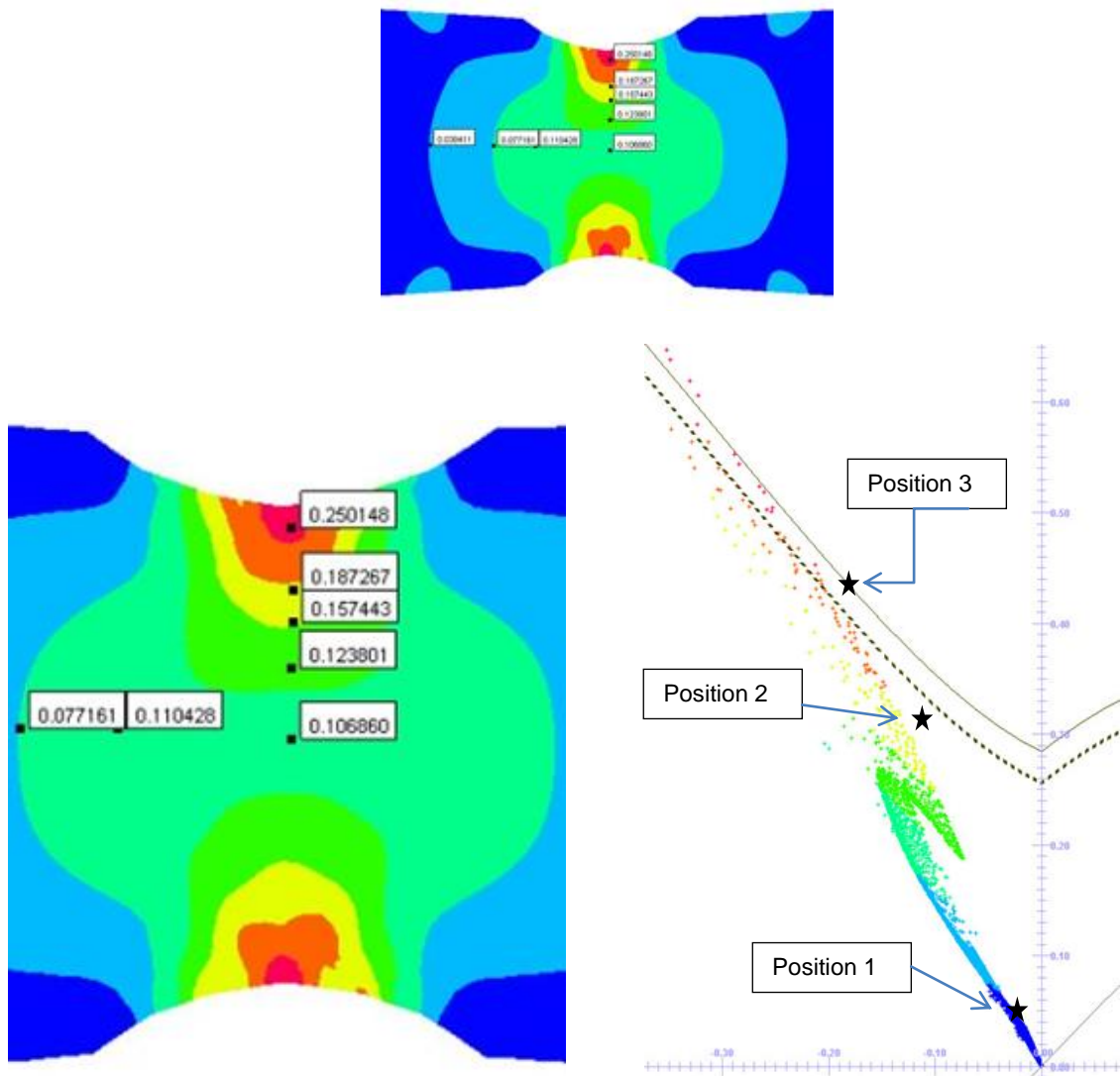


Figure 6.2.20: (Commercial) *Pamstamp* analysis: “Near” to plain strain condition (for strain of about $\epsilon=0.15$) - FEA analysis- left: true strain distribution. Right: strain path for the near to plain strain sample on the FLD. The star points are the ones measured on the sample.

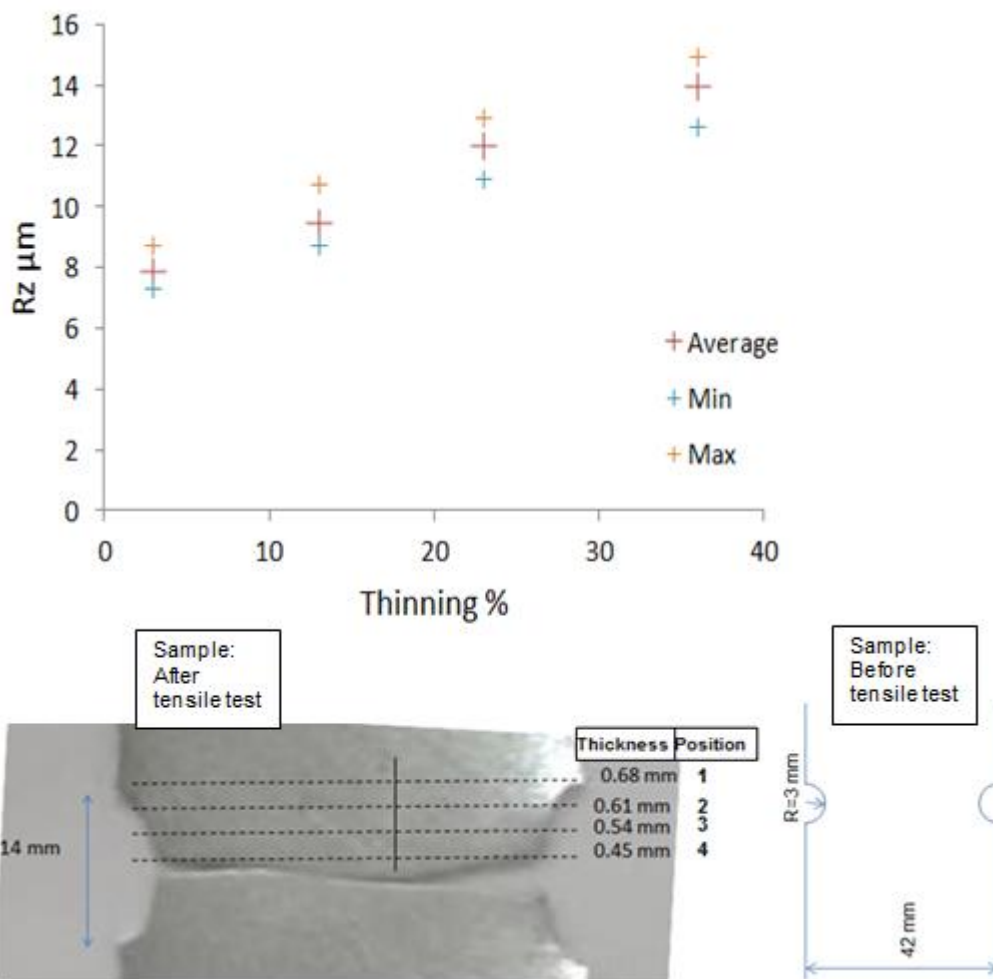


Figure 6.2.21 (sames as fig. 5.2.3.8): Roughness evolution R_z versus thinning evolution at the positions (1) one and four (4).

As a future work the 3D roughness evolution should be analyzed at the same points to obtain the corresponding S_q values and those incorporated into fig 6.2.11 (as well as the 3D roughness evolution in the painted layer).

Fig 6.2.22 compares the evolution of the 2D R_z roughness evolution obtained for both mentioned tests (the tensile test and the near-to-plain strain tensile test), both as a function of sheet metal thinning.

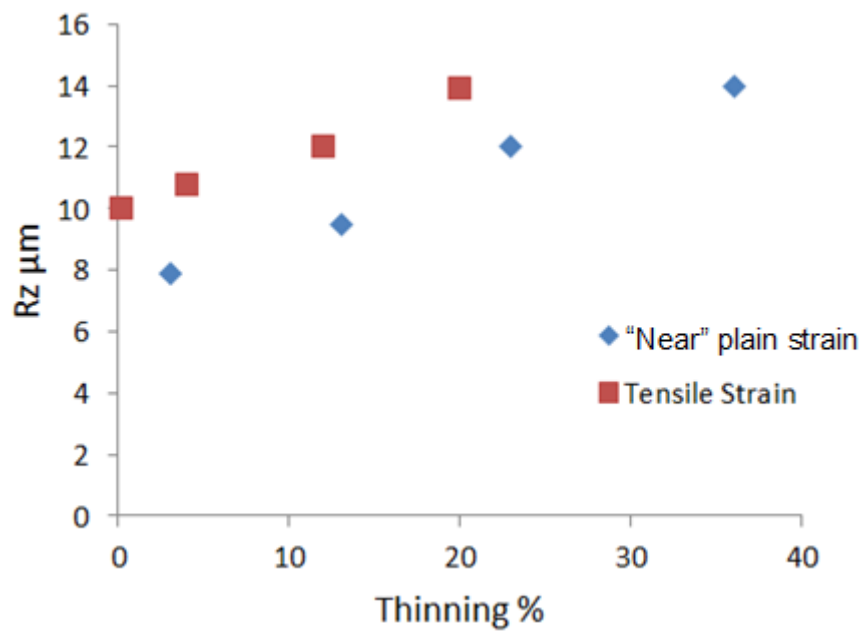


Figure 6.2.22: Roughness evolution R_z as a function of sheet thinning (for the tensile and the near-to-plain strain conditions).

In a similar way fig 6.2.23 presents the results for these two test conditions (two different strain path), compared in a FLD curve.

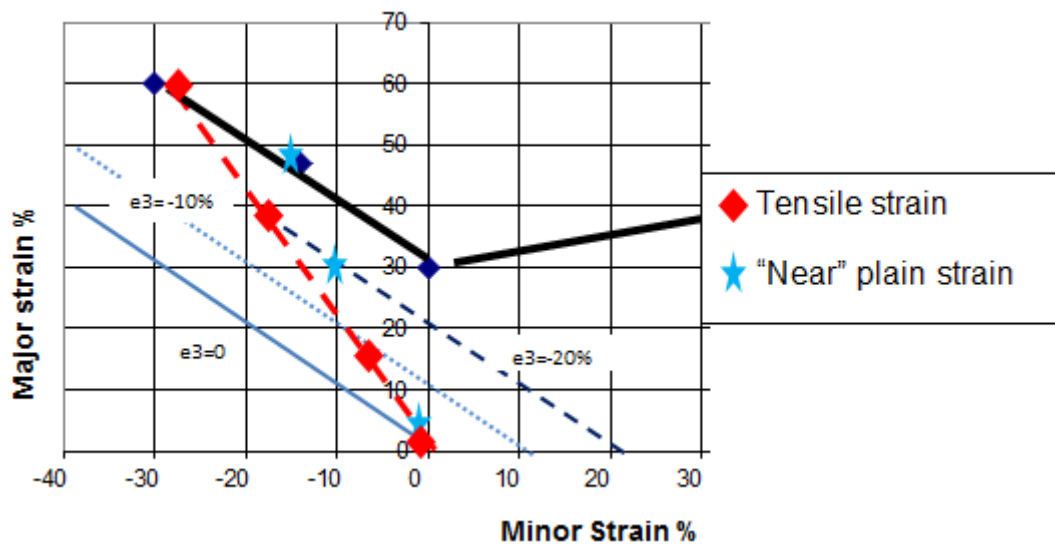


Figure 6.2.23: Different strain paths for the tensile and the "near" plain strain testing conditions.

The basic implication of these observations is that, although a material and a forming process might be safe according to the forming limit diagram (FLD) criteria, the

surface of the sheet maybe be roughened to the point where the surface quality (appearance) becomes problematic (WICHERN et al., 2005).

Conclusions

6.2.2.3 - The degree of roughening for the tensile and the near to plain strain conditions showed a similar trend of increasing roughness with sheet thinning (fig. 6.2.22);

6.2.2.4 – For the sheet metal there is a FLD, however it must also be taken into consideration that there is a further (and more restrictive) limit in terms of strains, associated with the surface quality (appearance). This could be named tentatively as a “PALD- Paint Appearance Limit Diagram”, being more restrictive than the FLD.

6.2.2.3 Inter-relationship between the two testing two conditions, with and without die contact

From the paint appearance point-of-view we have shown that the tendency, for sheet materials with stochastic structures (EDT and SBT) have shown that decreasing values of Ra and Rz there is an increase in the paint appearance (figs 5.1.6, 5.2.3, 5.2.5). This reduction of Ra and Rz values can be obtained in two ways. The first one may be related to the skin-pass reduction (fig 5.1.6) and the second one during the actual stamping operation, due to the contact of the tooling with the sheet strip, as pointed out in the topic 6.2.1. However, this second alternative, which apparently could increase the paint appearance, is directly related to the second variable, leading to the worsening in appearance, named as sheet metal straining *without die contact*. Indeed, as roughness decreases due to the increase in contact pressure between the die and the sheet, the friction coefficient will be also altered. If the latter is getting larger, this may lead to a decrease in the sheet speed, increase in strip strain and stress in other regions of the strip (in which there is no tooling contact). These strains (see topic 6.2.2) will conduce to a surface roughness increase, hence compromising the paint appearance.

Compression (being one of the main variables that influence friction) is, furthermore, closely associated with surface topography, contact pressure, speed and lubrication and these are of fundamental importance to understand the lubrication regime as being boundary lubrication (BL), mixed lubrication (ML) or hydrodynamic lubrication (HL).

As a reference, therefore, the Stribeck curve has been employed in order to evaluate the lubrication regime observed in the present work, as shown in fig 6.2.26. To build this curve, the entry data have been: oil dynamic viscosity, $\nu=1.3\text{Pas}$ (GM oil specification - average), strip speed $v= 0.0045\text{ m/s}$ (fig. 5.2.2.4), contact pressure $p=150\text{ MPa}$ (figs.6.2.24 and 6.2.25) and sheet roughness $R_a =1.0\text{ }\mu\text{m}$ (table 5.2).

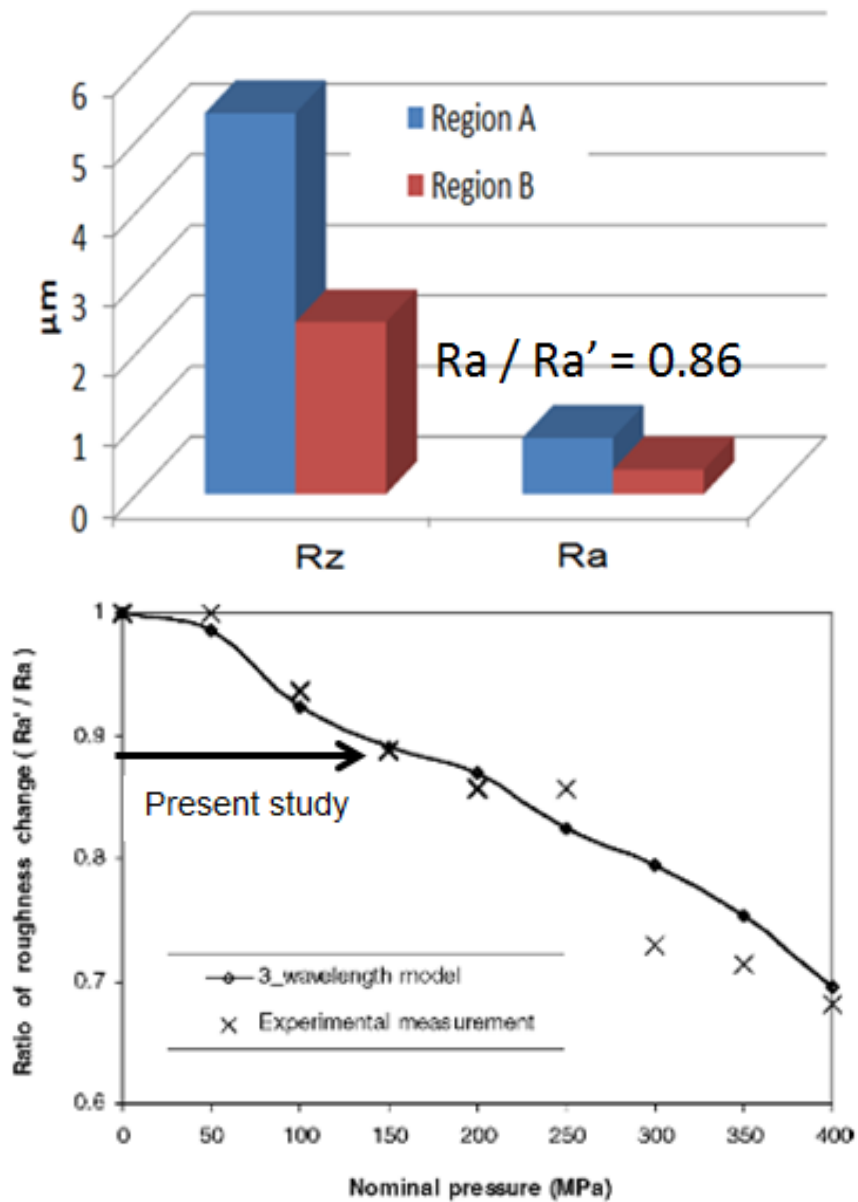


Figure 6.2.24: Contact pressure at region B (see fig 6.2.25) is about 150MPa, according to the model suggested by Ma et al. (2002).

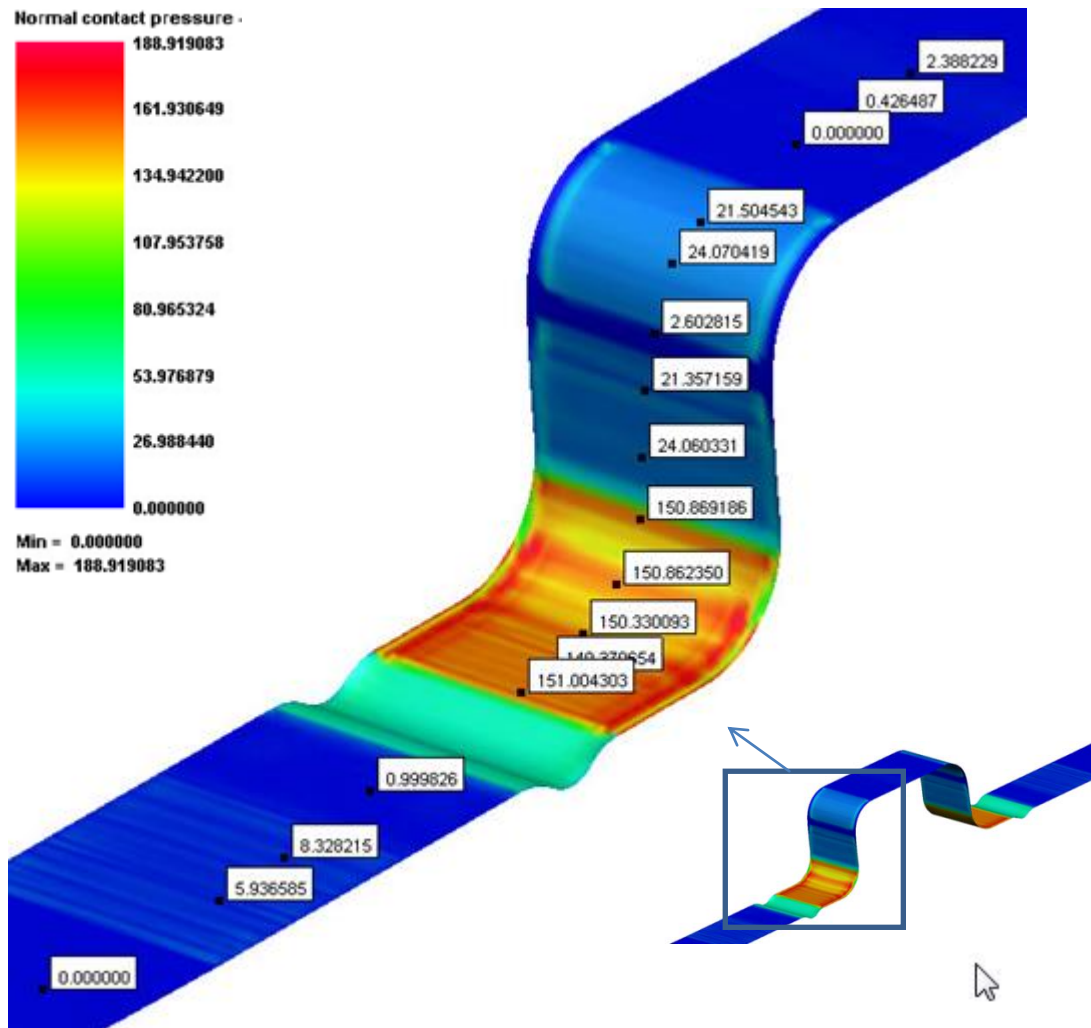


Figure 6.2.25: (Commercial) *Pamstamp* analysis: Contact pressure in region B is about 150MPa.

Fig. 6.2.25 shows the FEA and results for the contact pressure. Although this FEA has been used only as secondary analysis for the present work (this analysis will be used for future work), it showed very good agreement with the contact pressure estimate given from fig. 6.2.24.

Fig. 6.2.26 shows the Stribeck curve and an estimative of the lubrication regime for the present work, as mentioned previously.

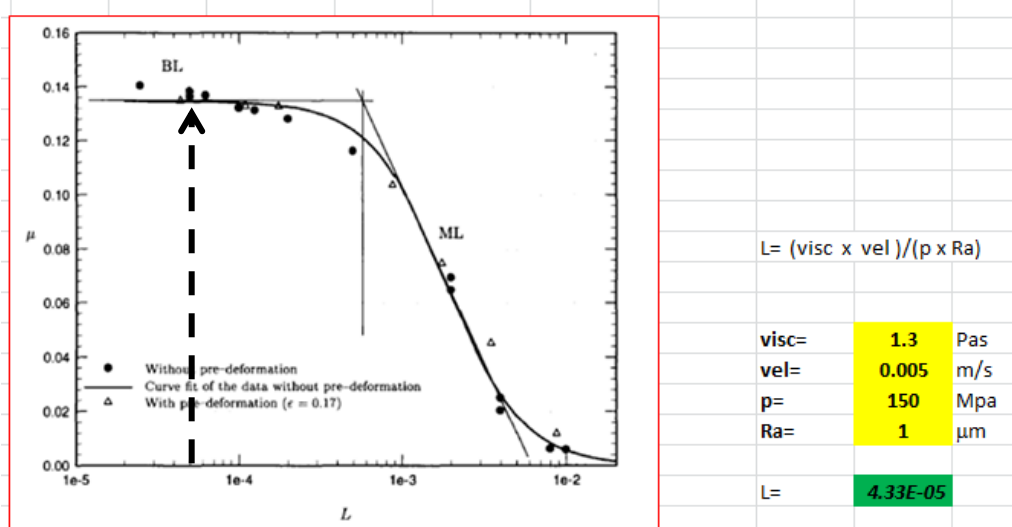


Figure 6.2.26 (same as fig. 3.2.2): Generalized Stribeck curve (LUBBING, HAAR, SCHIPPER, 1996).

From this figure it can be concluded that the stamping experiments of the present work have been carried out in the boundary lubrication regime (BL).

Therefore, under the experimental conditions of this work (BL regime), the surface topography did not present significant influence on the results. The α_{clm} and V_{cl} parameters, whose main functions is related to continuous or semi-continuous oil film formation (that happens in the ML and HL regimes), did not happen in the present case. Under industrial conditions the speeds are much greater (as compared to those used in the present research, by one to two orders of magnitude) and tend to lead to the ML regime (LUBBING, HAAR, SCHIPPER, 1996). Accordingly, the strip speeds tend to be more sensitive to changes in surface topography.

In the present work a low sensitivity to changes in strip speed as a function of surface topography has been noticed (fig 6.2.27). However, in samples presenting higher values of α_{clm} and v_{cl} presented smaller speeds. Conversely, samples with lower values of α_{clm} and v_{cl} (but larger values of Ra and Rz), presented the highest speeds. The opposite is what would be expected, in the case if it would be under the ML lubrication regime.

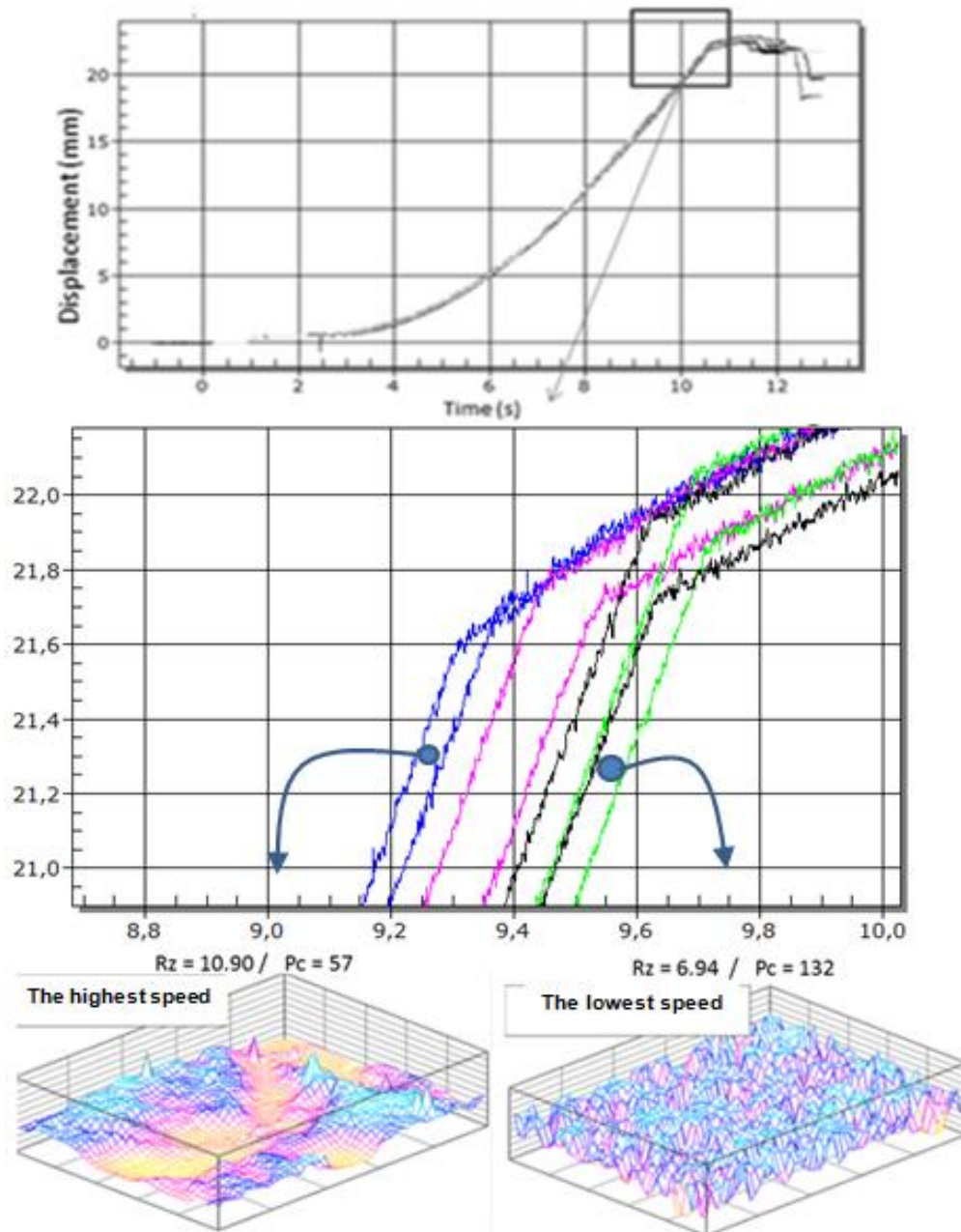


Figure 6.2.27 (same as fig. 5.2.2.3):

(Top figure) displacement (mm) x time(s) - Sheet metal surface topography of the “best” and “worst” conditions (and the final speed differences - angular coefficient)

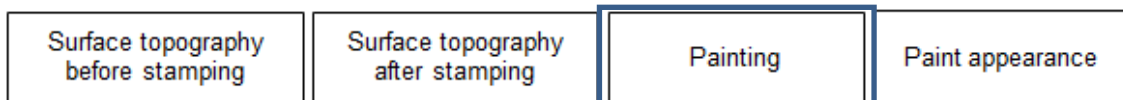
(Bottom figure)- Detail of the square shown in the top figure and their surface topographies respective to these curves.

Pawelsky (1996) offered a possible explanation for the better performance of the sheets having higher roughness. He pointed out that lubricant storage and take-up of surface abrasion products is achieved by means of a relatively high roughness (in terms of the Ra and Rz parameters).

Conclusion:

6.2.2.5 - Despite the increase of the 3D surface parameters V_{cl} and a_{clm} that can be linked to a better stampability for the mixed lubrication condition, the present work shows that for boundary lubrication conditions, there is an increase in the friction coefficient (fig.6.2.27) that could lead to sheet metal thinning and to Von Mises equivalent strains (ϵ_{vm}) of levels higher than those given by the Forming Limit Diagram (FLD).

6.2.2.6 - However the differences in roughness from test 1 to 22 caused a difference in the speed of the sheet metal but they were not enough to cause significant differences in the material thinning.



6.3 Painting

This chapter will be subdivided into two topics, namely:

6.3.1 - *Painted before stamping*: It analyzes the roughness evolution on the painted layers of the material before stamping, according to topic 4.1 first run – second step (best and worst rating condition).

6.3.2 - *Painted after stamping*: This topic will be subdivided into two sub-topics:

6.3.2.1 – Deformed with die contact: It analyzes the 2D and 3D roughness evolution up to the E coat painted layer of the material after stamping, according to topic 4.2.2 second run – second step (deformed due to die contact).

6.3.2.2 – Deformed without die contact: It analyzes the 2D roughness evolution on the painted layers of the material after stamping, according to topic 4.3.1 third run – first step (deformed without die contact);

6.3.1 Painted before stamping

In the following, in fig. 6.3.1 shows the photos related to the best and worst rating conditions (chapter 5.2.1.2) for each stage of the painting process. Fig 6.3.2 shows the cross section for both conditions at the clear coat stage and the layer thickness comparison with data from the literature. Fig 6.3.3 shows the 2D roughness profile evolution for each sample of fig. 6.3.1 and in figs. 6.3.4 to 6.3.7 the same analysis for 3D roughness evolution.

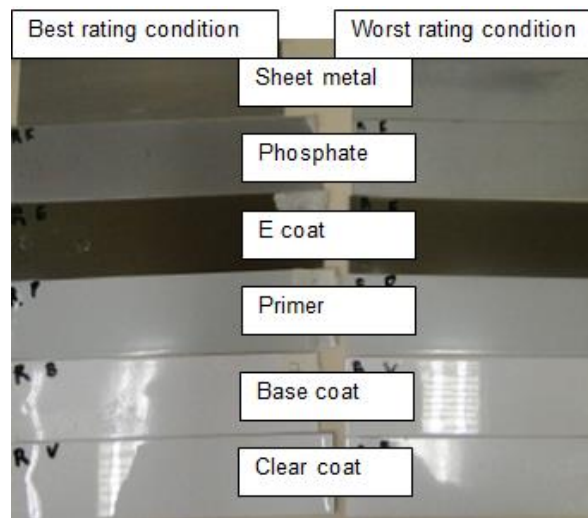


Figure 6.3.1: Samples from best and worst “rating” condition that has been taken for each paint stage.

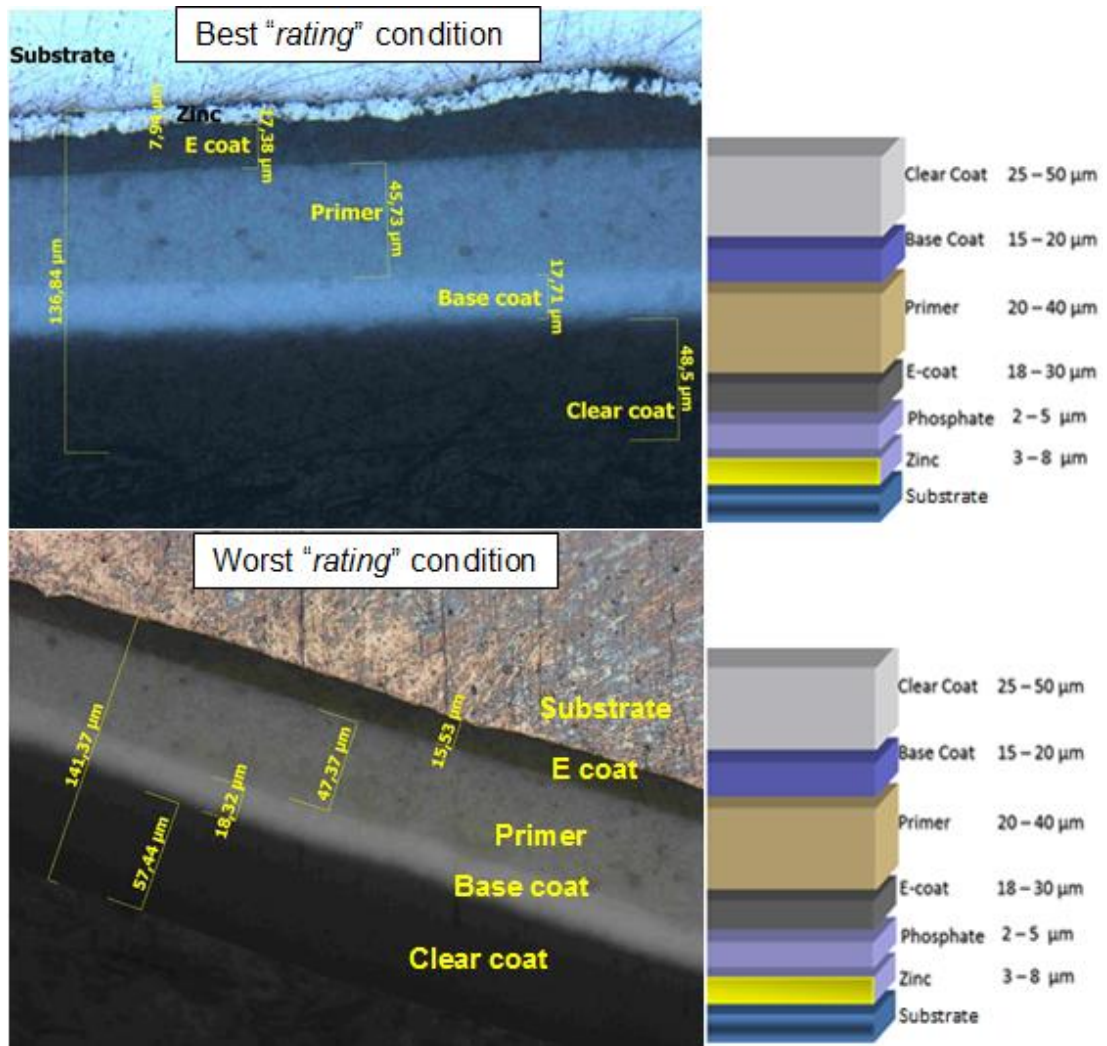


Figure 6.3.2: Cross section for both conditions at the clear coat stage and the layers thickness comparison with the literature (LEX, 2010).

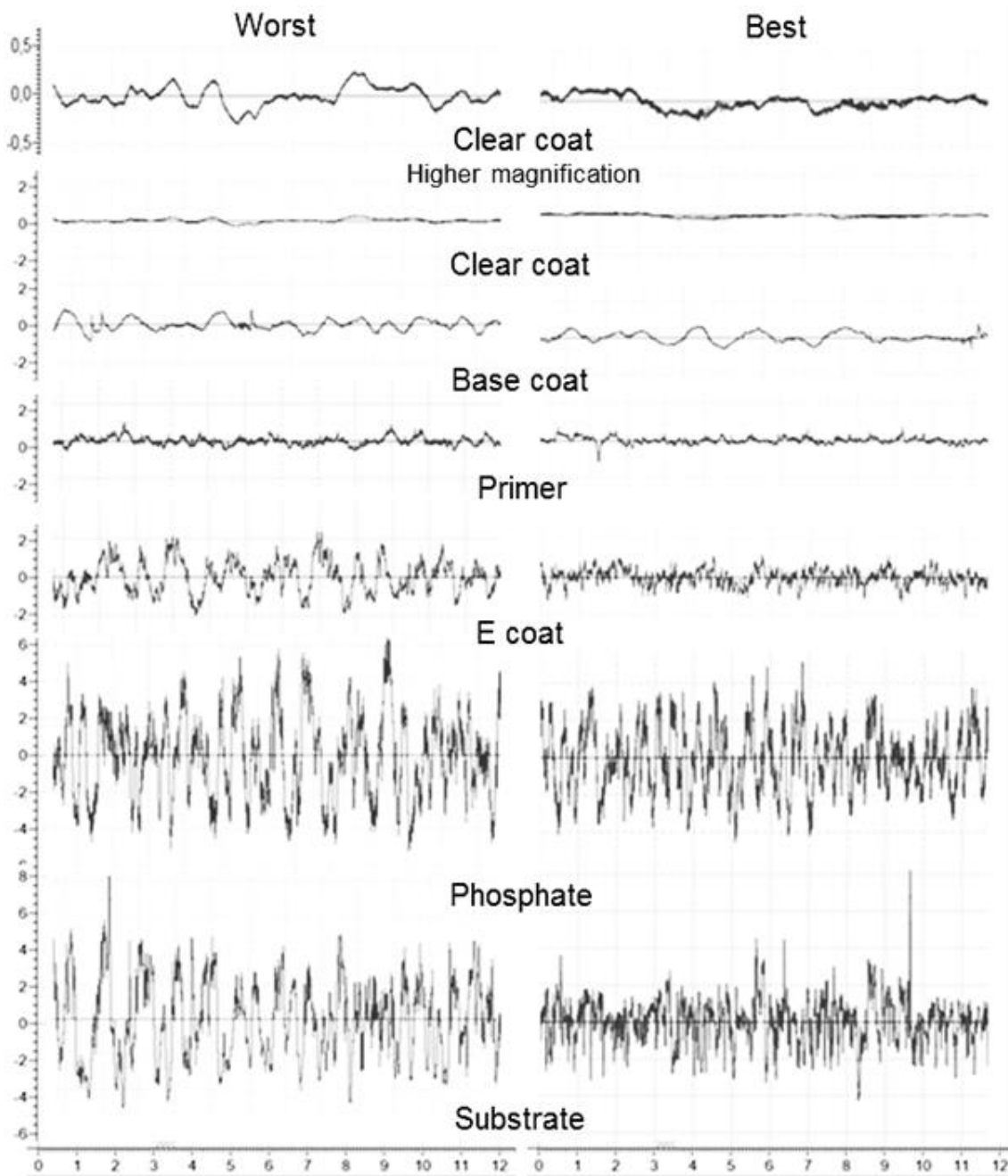
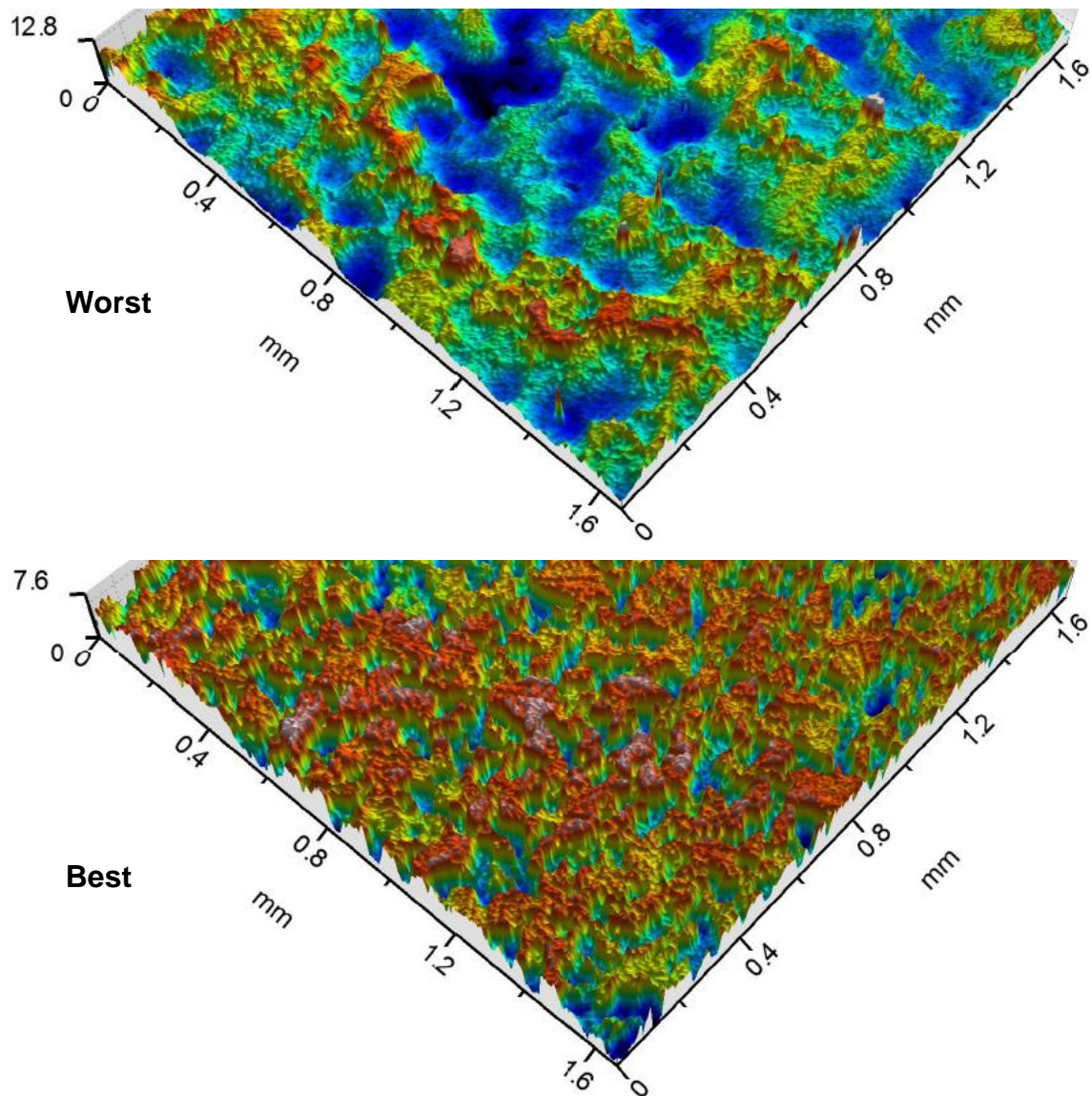


Figure 6.3.3 (same as fig. 5.2.9): 2D Roughness profile evolution for the best and worst conditions of rating (measured in the first step).

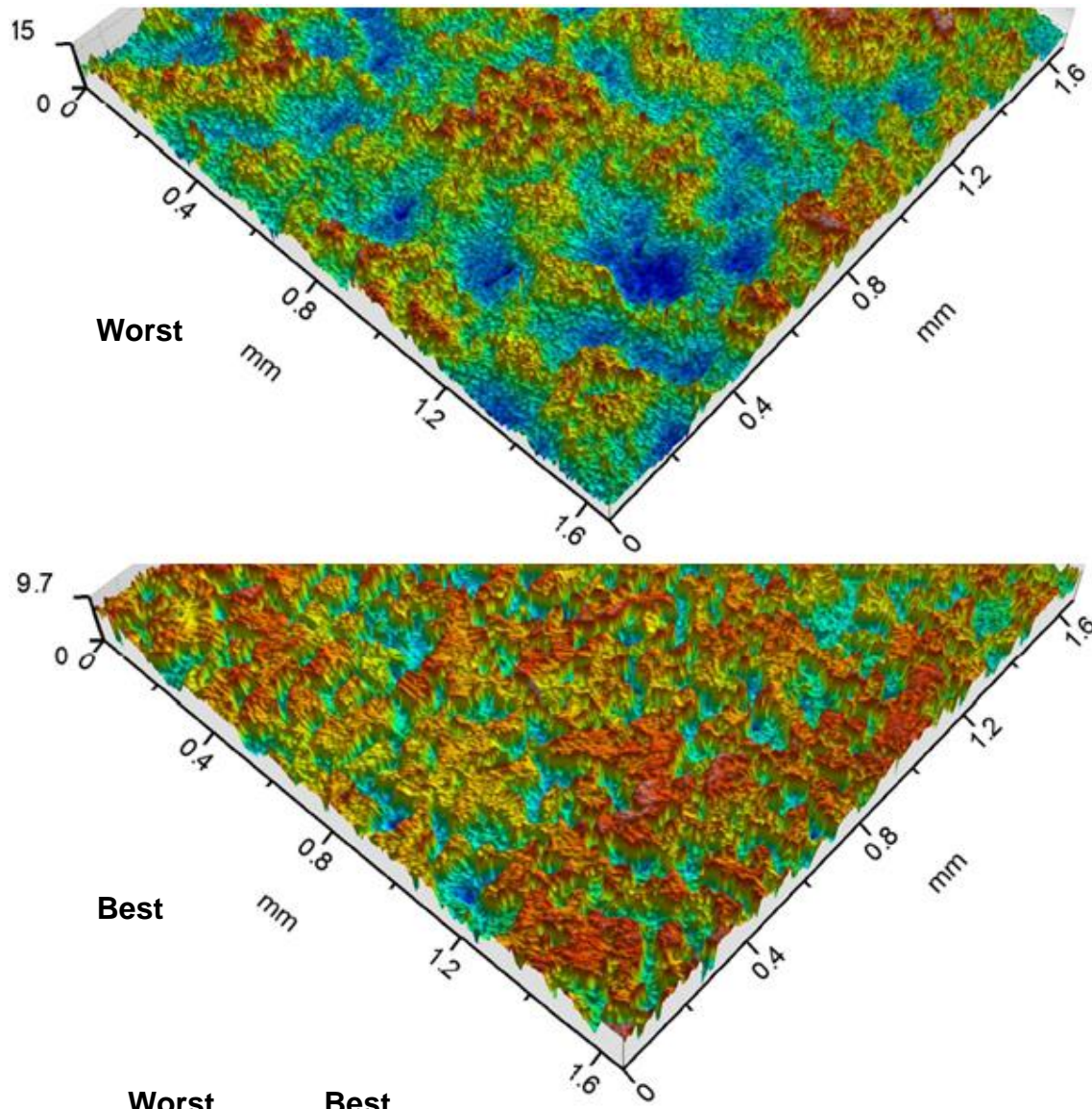
Substrate (sheet metal)



Worst		Best				
Sq	2.26	Sq	1.60	μm		<i>Root mean square height</i>
Ssk	0.319	Ssk	-0.406			<i>Skewness</i>
Sku	2.54	Sku	2.13			<i>Kurtosis</i>
Sp	7.90	Sp	3.39	μm		<i>Maximum peak height</i>
Sv	5.06	Sv	4.25	μm		<i>Maximum pit height</i>
Sz	13.0	Sz	7.64	μm		<i>Maximum height</i>
Sa	1.86	Sa	1.37	μm		<i>Arithmetic mean height</i>
Feature Parameters		Feature Parameter				
Spc	851	Spc	482	$1/\text{mm}$	<i>pruning = 5%</i>	<i>Arithmetic mean peak curvature</i>
Spd	1096	Spd	3228	$1/\text{mm}^2$	<i>pruning = 5%</i>	<i>Density of peaks</i>

Figure 6.3.4: Sheet metal 3D Roughness for the best and worst conditions of rating (measured in the first step) (Taylor Hobson).

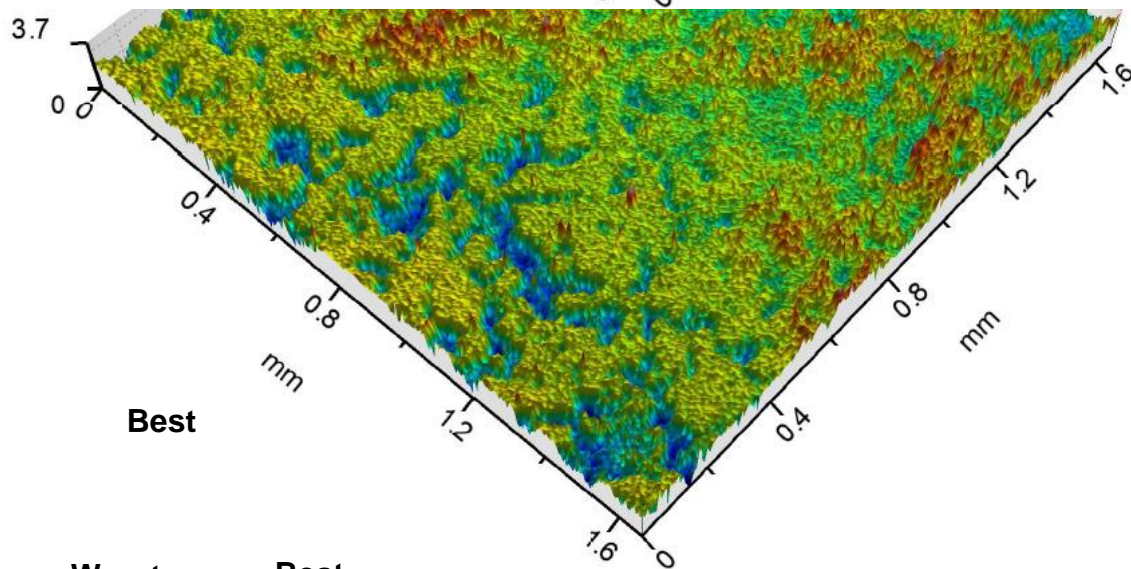
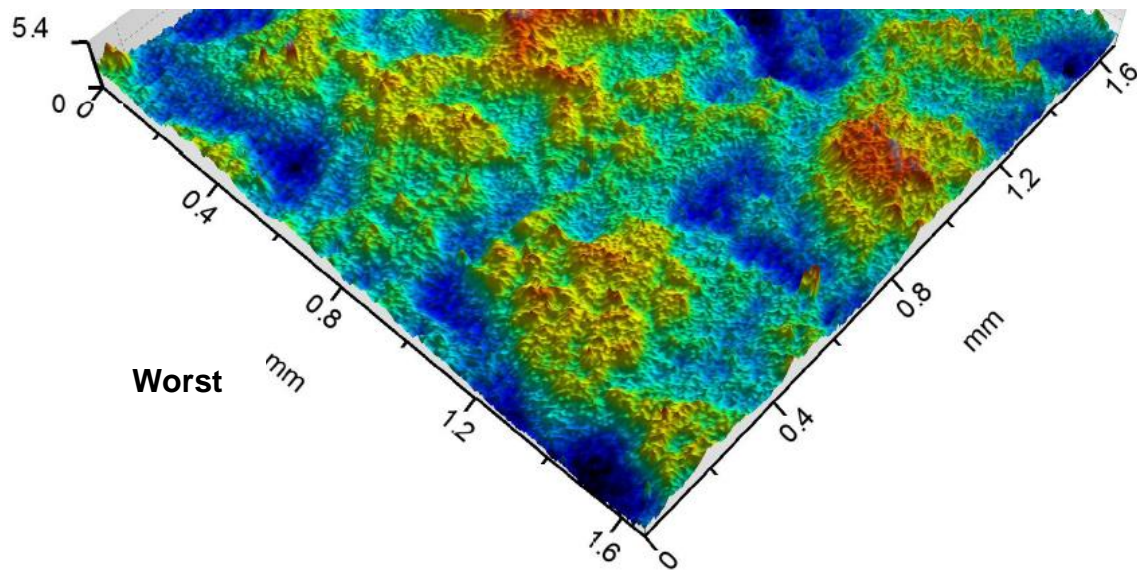
Phosphate



Worst		Best			
Sq	2.44	Sq	1.69	μm	Root mean square height
Ssk	0.382	Ssk	-0.423		Skewness
Sku	2.78	Sku	2.14		Kurtosis
Sp	8.40	Sp	4.26	μm	Maximum peak height
Sv	6.65	Sv	5.48	μm	Maximum pit height
Sz	15.0	Sz	9.74	μm	Maximum height
Sa	1.99	Sa	1.46	μm	Arithmetic mean height
Feature Parameters		Feature Parameters			
Spc	1291	Spc	610	1/mm	pruning = 5% Arithmetic mean peak curvature
Spd	4291	Spd	1869	1/mm ²	pruning = 5% Density of peaks

Figure 6.3.5: Phosphate 3D Roughness for the best and worst conditions of rating (measured in the first step).

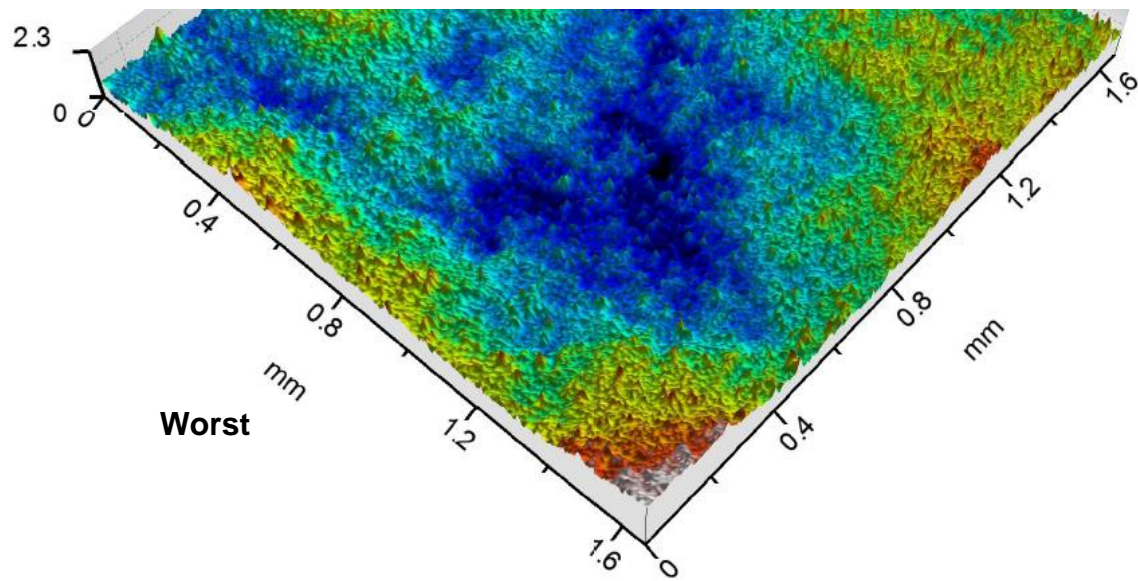
E coat



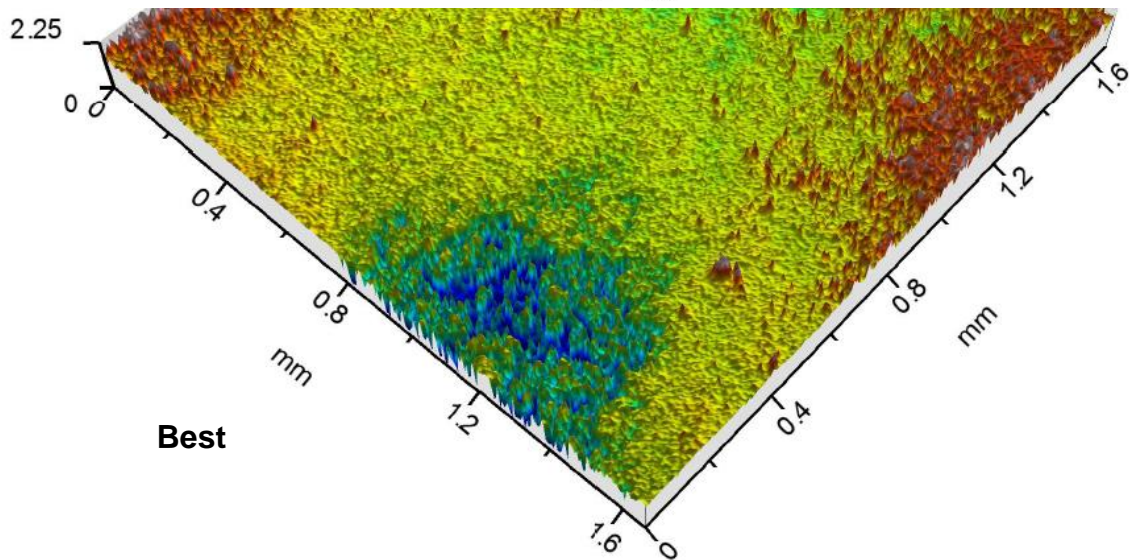
Worst		Best			
Sq	1.00	Sq	0.469	µm	Root mean square height
Ssk	0.482	Ssk	-0.363		Skewness
Sku	3.00	Sku	4.01		Kurtosis
Sp	3.37	Sp	1.95	µm	Maximum peak height
Sv	2.07	Sv	1.75	µm	Maximum pit height
Sz	5.44	Sz	3.70	µm	Maximum height
Sa	0.804	Sa	0.359	µm	Arithmetic mean height
Feature Parameters		Feature Parameters			
Spc	210	Spc	279	1/mm	pruning = 5% Arithmetic mean peak curvature
Spd	1579	Spd	4925	1/mm ²	pruning = 5% Density of peaks

Figure 6.3.6: E coat 3D Roughness for the best and worst conditions of rating (measured in the first step).

Base coat



Worst



Best

Worst Best

Sq	0.382	Sq	0.307	μm	Root mean square height
Ssk	0.423	Ssk	-0.543		Skewness
Sku	2.92	Sku	5.71		Kurtosis
Sp	1.53	Sp	1.06	μm	Maximum peak height
Sv	0.817	Sv	1.20	μm	Maximum pit height
Sz	2.35	Sz	2.25	μm	Maximum height
Sa	0.318	Sa	0.210	μm	Arithmetic mean height
Feature Parameter		Feature Parameter			
Spc	64.9	Spc	126	1/mm	pruning = 5% Arithmetic mean peak curvature
Spd	2121	Spd	3258	1/mm ²	pruning = 5% Density of peaks

Figure 6.3.7: Base coat 3D Roughness for the best and worst conditions of rating (measured in the first step).

It should be pointed out that the zinc coating maybe taken as being partially responsible for obtaining the “best surface”, however there is no sufficient information on the process of these steel sheets (related to the cold rolling reduction). On the other hand, these two conditions (as shown in fig. 6.3.3) should be compared carefully, since the degree of transference of the skin pass roll roughness onto the bare sheet metal is different to the transfer obtained onto the zinc layer, as pointed out previously in chapter 3.1.2. Nevertheless, at the saturation level (see fig. 3.1.4), the goal is that surface roughness should be similar for both conditions (uncoated and zinc coated sheet metal). Indeed, it should be remembered that paint appearance, measured at the clear coat layer, has to be improved irrespective of the sheet metal being zinc coated or not.

In figs. 6.3.8 (present work) and 6.3.9 (literature) it can be observed the decrease in the 2D roughness parameter, R_z , as the painted layer evolves. However, the differences at the clear coat stage are not so significant as those at the sheet metal stage.

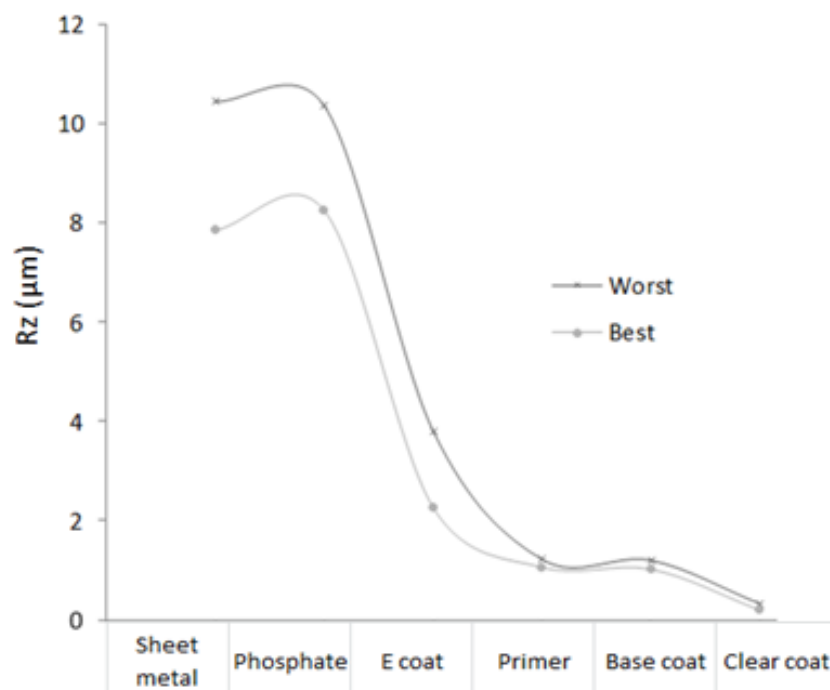


Figure 6.3.8 (same as fig. 5.2.12): R_z roughness evolution along all painted layers (worst and best samples).

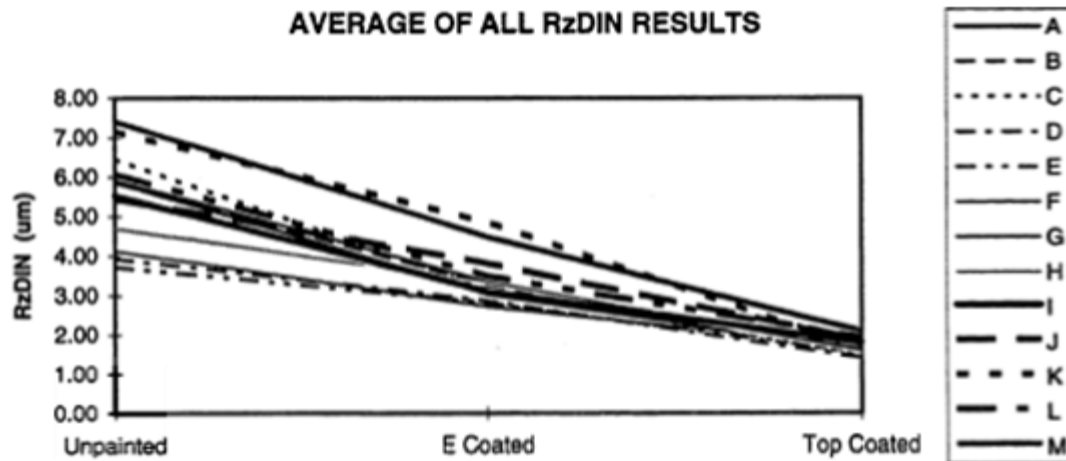


Figure 6.3.9 (same as fig. 3.4.8): Rz roughness evolution along all painted layers for 13 different steel sheets (BURGIN, 1996).

Conclusion:

6.3.1.1 – Under lab-conditions the primer layer was approximately 8 μm thicker for both conditions (best and worst) than the used under industrial condition and the clear coat layer (for the worst condition only) was also approximately 8 μm thicker than the used under industrial condition (fig. 6.3.2).

6.3.1.2 – Sheet metal roughness is transferred to all painted layers with a decreasing intensity (fig. 6.3.3).

6.3.1.3 – The 2D roughness parameter Rz is not an appropriate parameter to evaluate the surface topography at the clear coat stage, mainly for samples which have large differences in Rz values at the sheet metal stage (figs. 6.3.8 and 6.3.9).

6.3.2 – Painted after stamping

6.3.2.1 – Deformed with die contact

Fig. 6.3.10 shows the 3D surface topography for region A and B at the E coat stage.

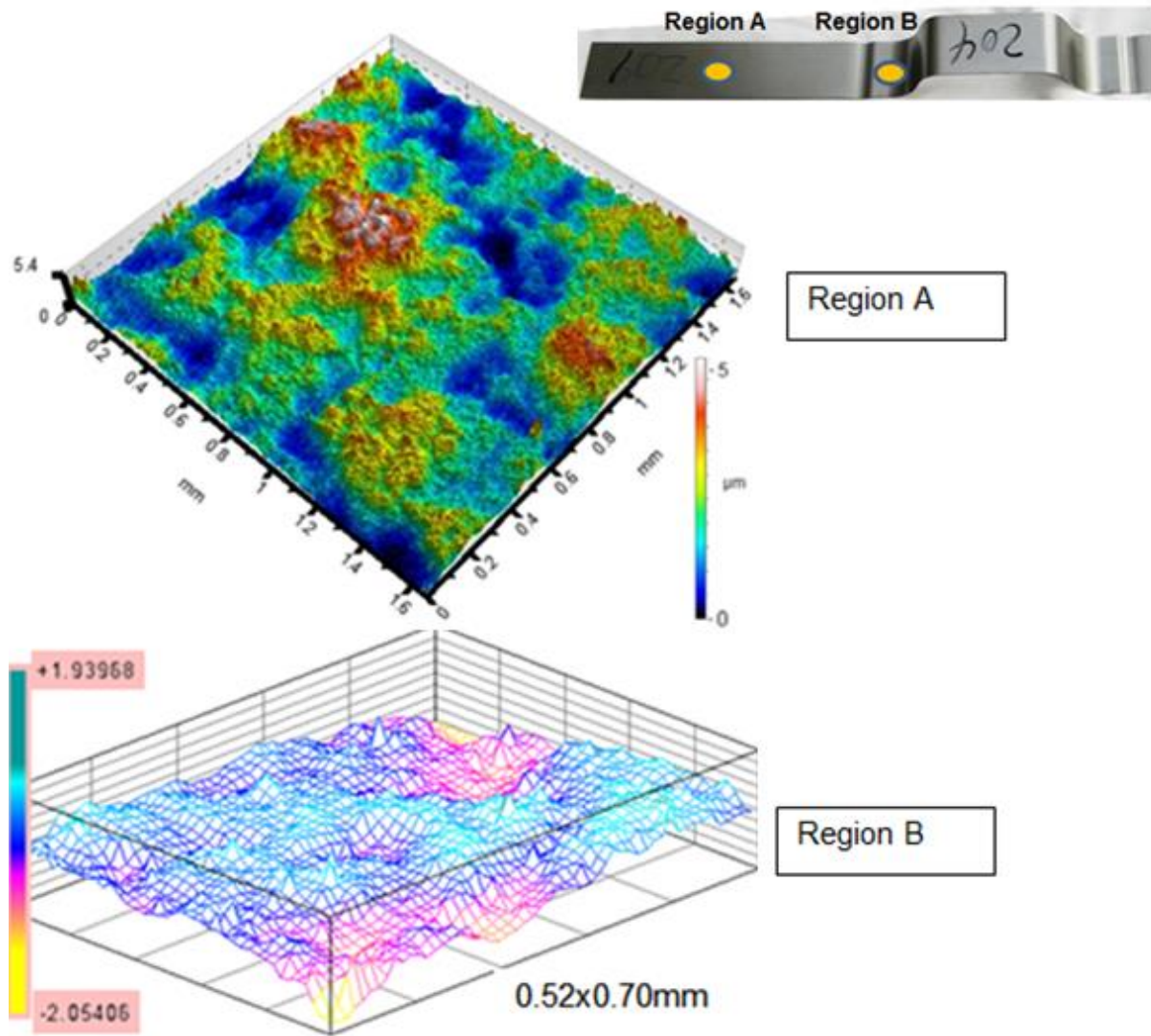


Figure 6.3.10 (same as fig. 5. 2.2.10): 3D roughness at the E coat stage in the regions A (without deformation) and B (with die contact deformation).

Fig. 6.3.11 shows the comparison between 2D roughness parameter Ra and Rz for region A and B at the E coat stage.

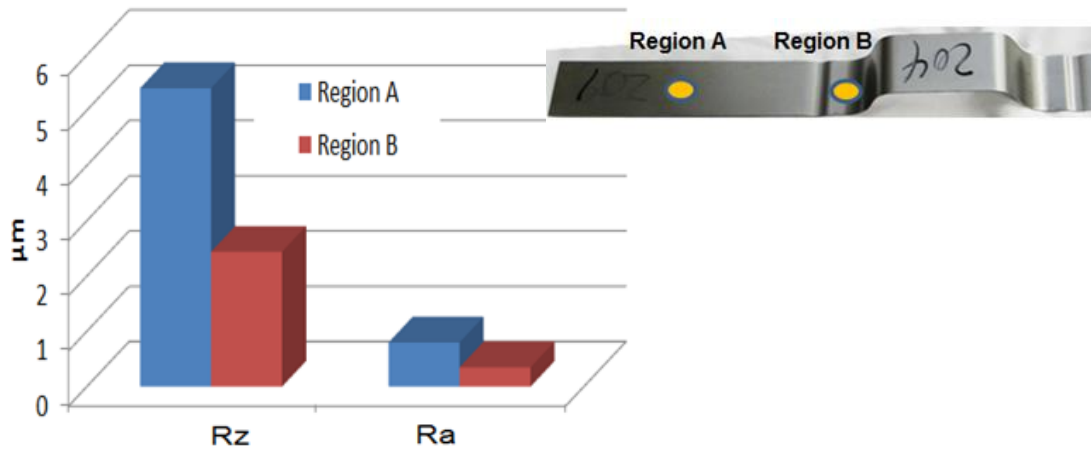


Figure 6.3.11 (same as fig. 5.2.2.9): 2D roughness at the **E coat stage** in the regions A (without deformation) and B (with die contact deformation).

Conclusion

6.3.2.1 The die contact deformation causes a decrease in sheet metal roughness. This difference in roughness between region B and region A are notice with a lower intensity at the E coat stage (figs. 6.3.11 and 6.3.12).

6.3.2.2 – Deformed without die contact

Fig. 6.3.12 shows the sheet metal roughness evolution under tensile strain condition and its evolution through all the painted layers.

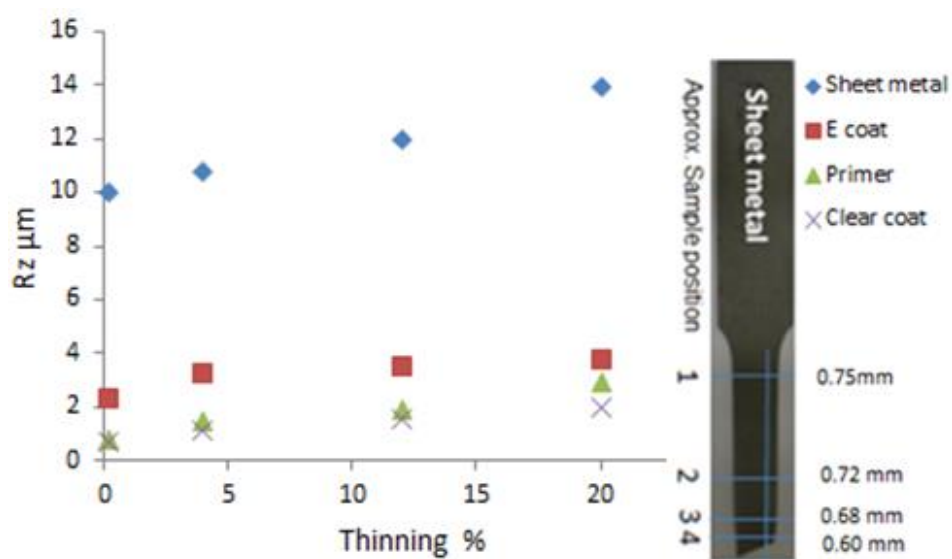
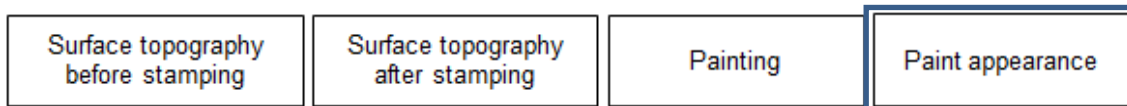


Figure 6.3.12 (same as fig. 5.2.3.7): Sheet metal roughness evolution under tensile strain condition and its evolution through all the painted layers.

Conclusion

6.3.2.2 The deformation without die contact causes an increase in sheet metal roughness proportional to the thinning rate. These differences in roughness between these two conditions (with and without thinning) are notice with a lower intensity through all the painted layers (fig. 6.3.13).



6.4 Paint appearance

This chapter will be subdivided into two topics, namely:

6.4.1 - Painted before stamping: It will evaluate the paint appearance on the painted layers of the material without stamping, according to topic 4.1 first run – second step (best and worst rating condition).

6.4.2 - Painted after stamping: This topic will be subdivided into two sub- topics:

6.4.2.1 – Deformed with die contact: Paint appearance at the E coat layer of the material after stamping, according to topic 4.2.2 second run – second step (deformed due to die contact).

6.4.2.2 – Deformed without die contact: Paint appearance on the painted layers of the material after stamping, according to topic 4.3.1 third run- first step (deformed without die contact);

6.4.1 Painted before (without) stamping:

The present work has been divided into two steps in order to evaluate the effect of initial strip (blank) surface roughness on the paint appearance. In the first step (item 6.4.1.1), which could be called the “coarse filter”, in which have been analyzed (at the E coat stage), twenty two (22) different roughness conditions (first run –first step- fig 4.1), using the rating index of the surface appearance of the paint (see details in chapter 3.4). The second step (item 6.4.1.2), which could be called the “fine filter”, in which the worst and best conditions of the ”coarse filter” are analyzed until the clear coat stage, using a more accurate paint appearance scale named (in the literature), as being the “spectral curve”.

6.4.1.1 Paint appearance (rating) at the E coat stage

Figs 6.4.1 and 6.4.2 present the comparison between data from present work and from the literature with reference to the 2D roughness parameters of Pc and Ra, as a function of paint appearance.

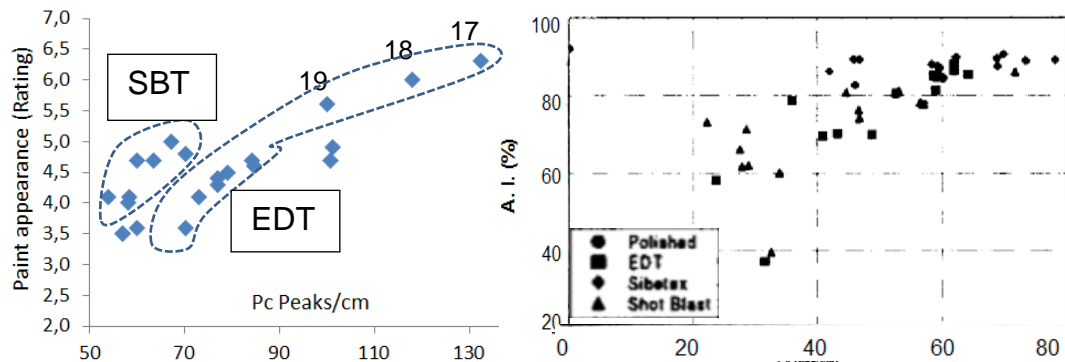


Figure 6.4.1: Left: Paint appearance (rating) as a function of the 2D roughness parameter, Pc (present work). Right: Literature (SCHEERS et al., 1998).

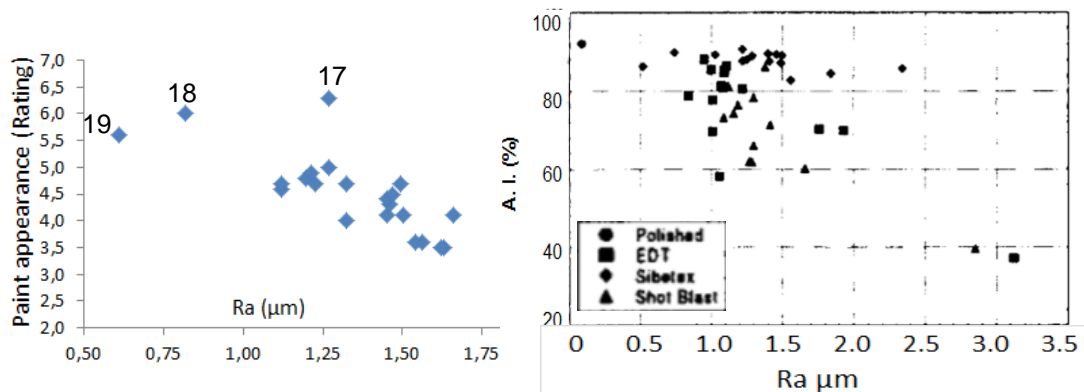


Figure 6.4.2: Left: Paint appearance (rating) as a function of the 2D roughness parameter, Ra (present work). Right: Literature (SCHEERS et al., 1998).

From both figures above mentioned, comparing data from present work and from literature, despite they have been compared at different stages of the paint process, they present similar trends, in which there is an increase in the paint appearance with an increase in the 2D roughness parameter Pc (strong trend) and with the decrease in the 2D roughness parameter Ra (weak trend)

Conclusions

6.4.1.1 Sheet metal surface roughness should have a 2D roughness parameter $P_c > 100$ peaks/cm (the higher the better) and a 2D roughness parameter $0.8 < Ra < 1.3 \mu\text{m}$, despite the quite large dispersion in the Ra values.

Figs 6.4.3 and 6.4.4 analyze the influence of the skin-pass reduction on the paint surface appearance, with reference to the test 1 to 16 (table 4.1).

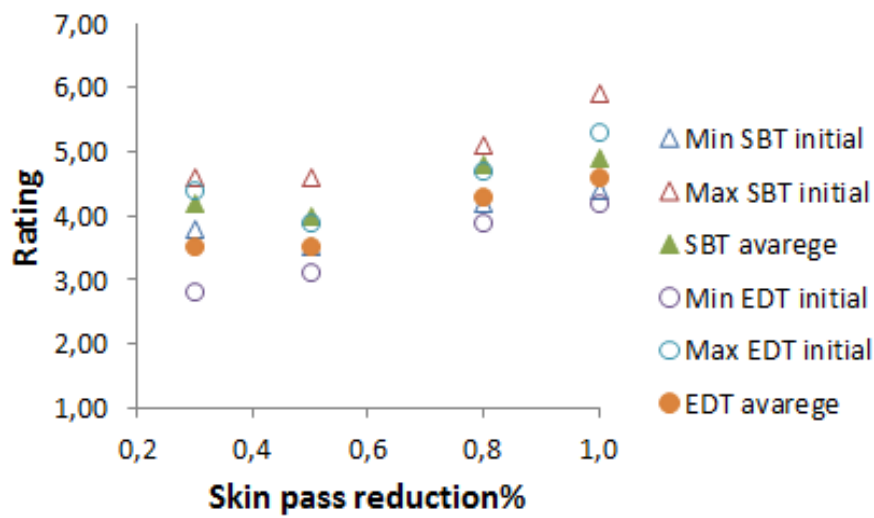


Figure 6.4.3 (same as fig. 5.2.3): Effect of skin-pass reduction (of the sheet) on the paint appearance (rating index) - Effect of the texturing condition.

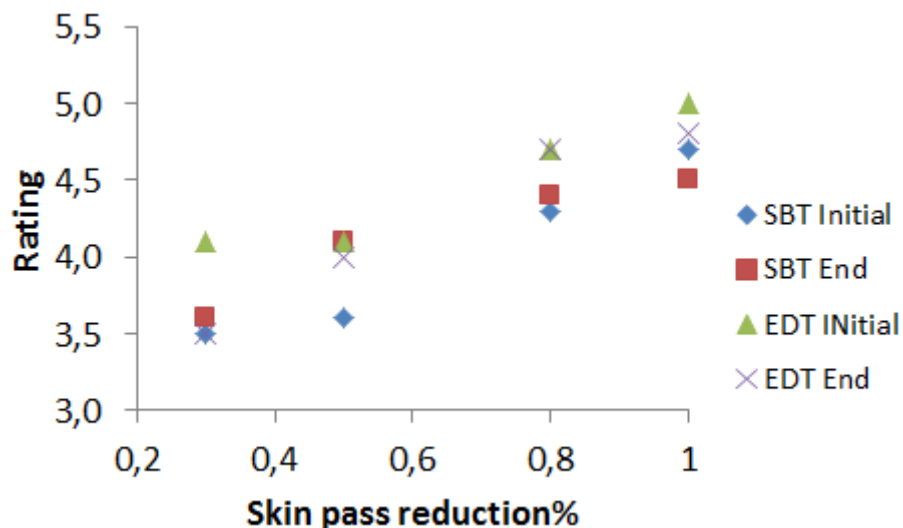


Figure 6.4.4 (same as fig. 5.2.4): Effect of skin-pass reduction (of the sheet) on the paint appearance (rating index) - Effect of the sample position on the coil (for both SBT and EDT texturizing).

Conclusions

6.4.1.2 - For both texturizing conditions (SBT and EDT), the skin-pass reduction should be higher than 0.8% (to attain better paint surface appearance).

6.4.1.3 - There was no significant difference in the paint appearance (rating at the E coat stage), between the initial or end part of the coil.

6.4.1.2 Paint appearance up to clear coat stage

The following analysis refer of the first run – second step –fig. 4.1, “best” and “worst” rating condition, for which the sheet metal surface topographies are shown in fig. 6.4.5.

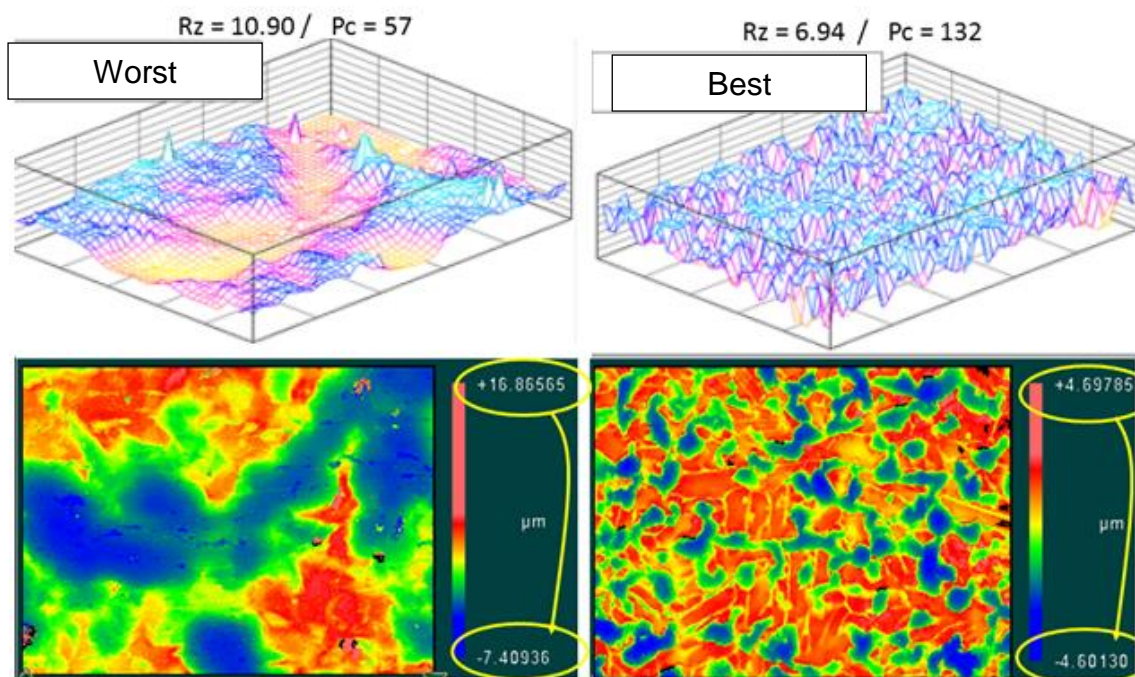


Figure 6.4.5 (same as fig. 5.2.6): Worst and best rating surface – sheet surface topographies.

Fig 6.4.6 illustrates the paint appearance (rating) evolution in the E-coat, primer and clear coat layers. It is important to observe that the difference in rating tends to decrease with the evolution in the paint layers. However, this difference is significant

in the clear coat layer and can lead to further “classifications” (sometimes given under industrial conditions), such as “premium” and non-premium”

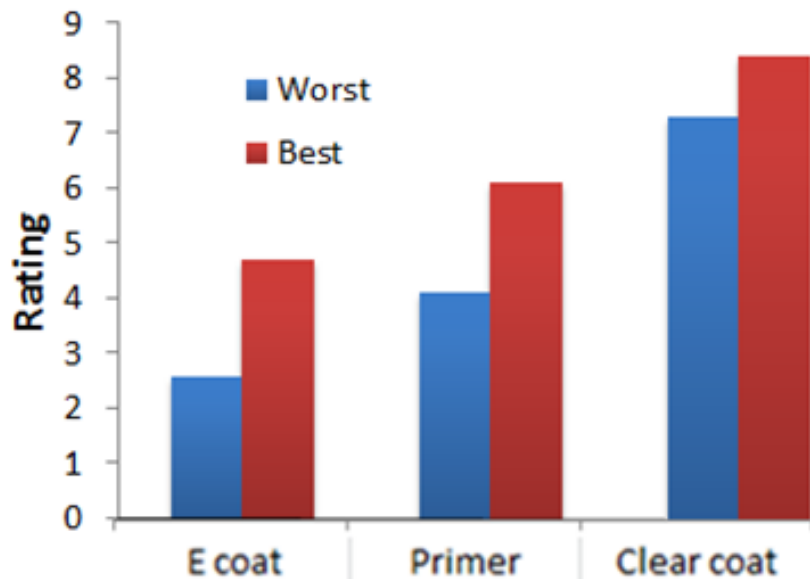


Figure 6.4.6: Rating evolution at the different paint layers (“worst” x “best”).

Up to this point, the paint appearance has been performed on the rating scale which, according to the already shown fig 6.4.7 and eq 1., takes into consideration only two wave lengths (namely the SW-short wave and the LW-long wave), however with a larger bias towards the LW. It should be remembered that in chapter 3.4 of the literature review a more detailed explanation has been given.

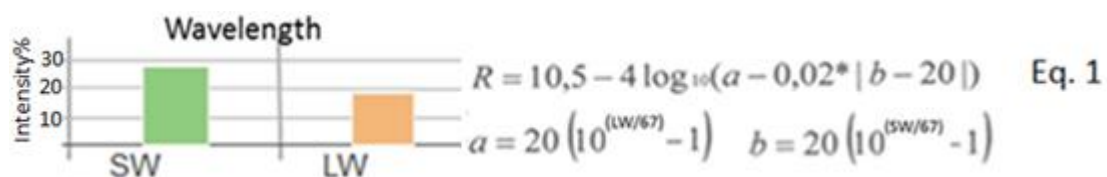


Figure 6.4.7 (same as fig. 3.4.2): “traditional” rating equation, taking into account the LW (mostly) and SW intensities.

The major advantage of this more “traditional” method is the fact that numerical results may be obtained, better than a comparative simplistic analysis. Therefore this method has been used in the present work as the “coarse filter”, mainly in the initial stages of investigation.

Conclusions:

6.4.1.4- The primer and clear coat layers decrease the difference in paint appearance “best / worst”, in terms of rating (see fig 6.4.6)

6.4.1.5- The rating scale advantage is that it is a numerical scale (easy to work with under industrial conditions), however it presents a major disadvantage because it has little information, mainly related to ranges in wave length (long wave).

In the following the results related to the scale of the spectral curve will be presented. This scale has been utilized in the present work as a “fine filter” for the analysis of the paint appearance, since it represents all the wave lengths visible to the human eye.

Spectral curves (fine filter)

The spectral curves take into consideration five (5) wave length (major details were given in chapter 3.4).

Fig 6.4.8 presents the paint appearance evolution in the paint layers from the E-coat, primer to the clear coat for the “best “ and “worst” rating conditions , given in fig 6.4.6.

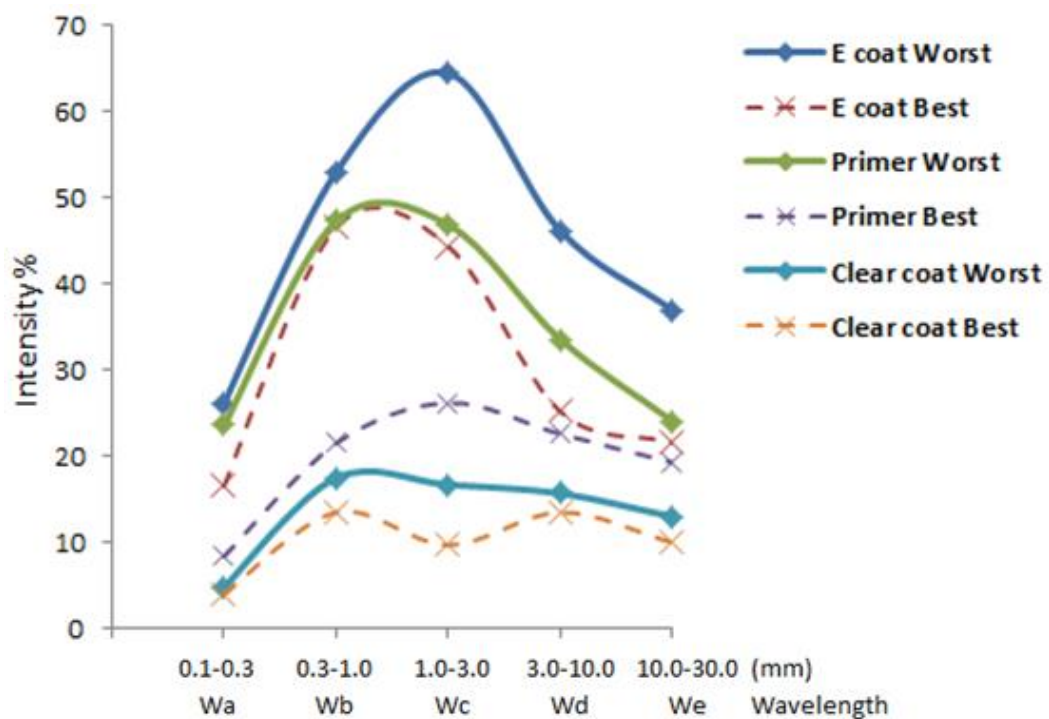


Figure 6.4.8 (same as fig. 5.2.13): Spectral curves for the “best” and “worst” conditions at the different paint layers.

It should be observed that long wavelengths are normally associated with a residual strength that originated from the skin- pass rolling operation or even during the stamping operation due to the particular format of the stamping. Conversely, short wavelengths are mostly associated with surface roughness. Fig. 6.4.9 (taken from fig. 6.4.8) clearly shows that the best clear coat (layer) is obtained with the lowest intensity, evenly distributed between short and long wavelength in the spectral curve.

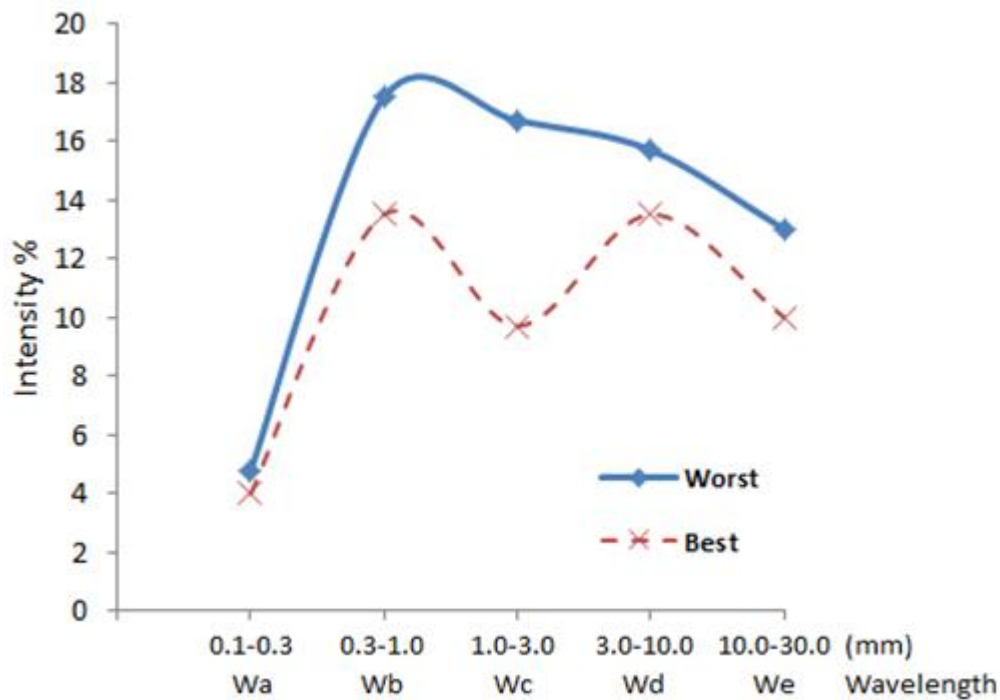


Figure 6.4.9 (same as fig. 5.1.13): Spectral curves for the “best” and “worst” surface appearances, measured at the clear coat layer.

As a comparison, fig. 6.4.10 shows a similar analysis, extracted from the literature (LEX, 2010), for rough and smooth steel sheets

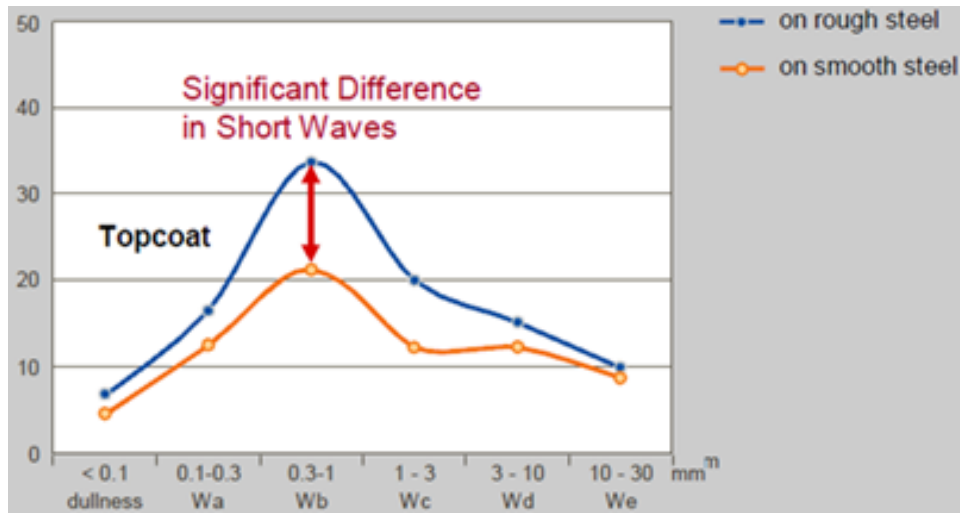


Figure 6.4.10 (same as fig. 3.4.7): Comparing Spectral curves according to sheet surface finish (LEX, 2010).

The results shown in fig 6.4.9 and 6.4.10 were similar, where the effect of sheet roughness has been more pronounced for the short wavelengths Wb and Wc and less pronounced for the long wavelengths Wd and We.

From the industrial point-of-view it is important to mention that the possibility to improve paint quality, through the optimization of sheet roughness can also be used for studies related to cost reductions.

Fig 6.4.11 (LEX, 2010) shows that decreasing the thickness of the clear coat layer, there is also a decrease in the paint appearance (due to the increase of the long waves). Hence, starting from an “optimized” roughness it is possible to obtain the same paint appearance with thinner paint layers. However, it should be mentioned that the analysis related to the reduction in the thickness of the paint layer should not only take into consideration the appearance criteria, knowing that these layers do have other functions, as shown in table 3.2.1 of chapter 3.3.

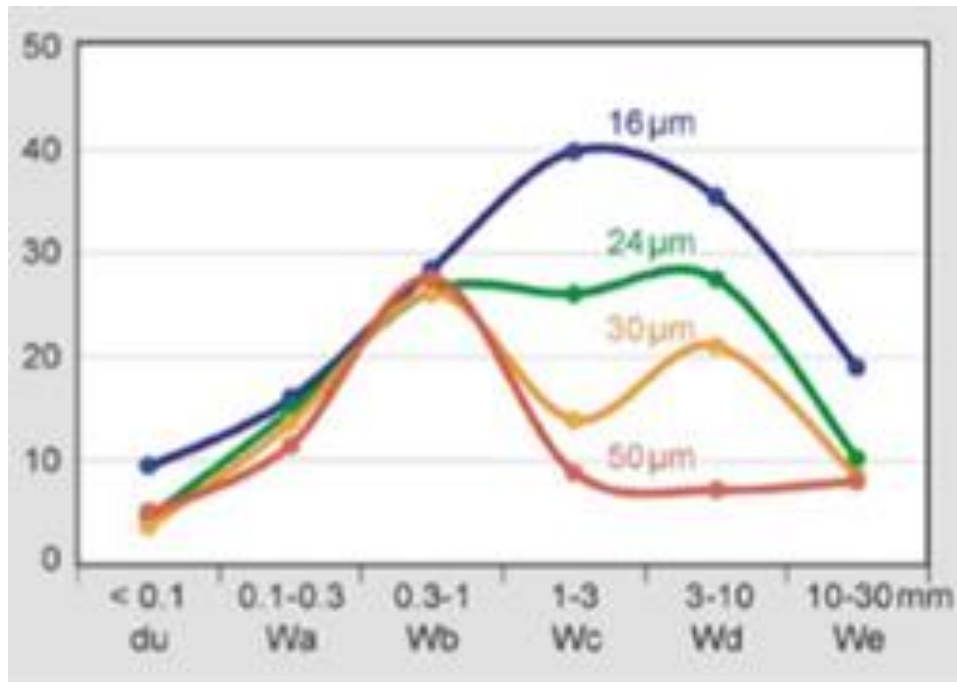


Figure 6.4.11: Spectral curves for different paint layers (LEX, 2010).

In order to put into perspective the importance of this subject we should mention that, in very rough numbers, a 5% economy in the paint layer can be obtained (taking an average value of 7 liters paint per car with a cost of the paint ranging between U\$ 5.00 up to U\$ 30.00 per liter, depending on the type of layer). It follows that for 600 thousand cars there would be an economy of about U\$ 3 million. As extra benefits would follow a productivity increase, minimizing the final product cost (main industrial goal) and decrease on the impact on the environment (also called “foot print”).

Despite the increase in thickness of the clear coat layer as being a means to enhance paint appearance, there are other means that may be used, as shown in fig 6.4.12.

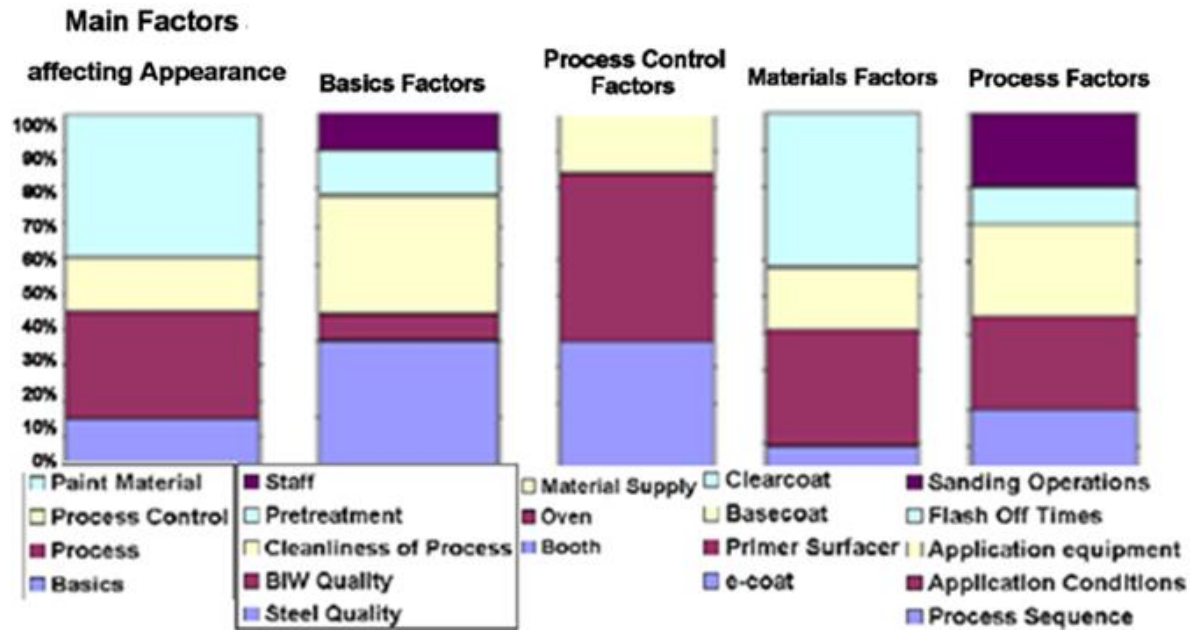


Figure 6.4.12 (same as fig. 3.3.4): Result of a design of experiment (DOE) relating the main factors affecting paint appearance (KLENT, MINKO, 2008).

Furthermore, this figure shows that for one determined painting condition, the steel quality represented approximately only 6% of the total paint appearance.

However, according to fig. 6.4.6, the gain in paint appearance, as shown in the present work, related to the clear coat layer is about 15%.

Conclusions:

6.4.1.6 The primer and clear coat layers diminished the difference in paint appearance (more accentuated for SW (Wb and Wc) and less for LW (Wd and We), taking the best and worst rating conditions (fig 6.4.8).

6.4.1.7 For optimizations related to paint appearance the spectral curve is recommended since it represents all wavelengths associated with the surface topography while the rating only presents an average value of the Wc, Wd and We values.

Another important factor related to surface appearance is the gloss. Fig 6.4.13 shows the evolution in paint appearance (gloss) on the E coat, primer and clear coat layers for the best and worst rating conditions of the figs 6.4.6 and 6.4.8.

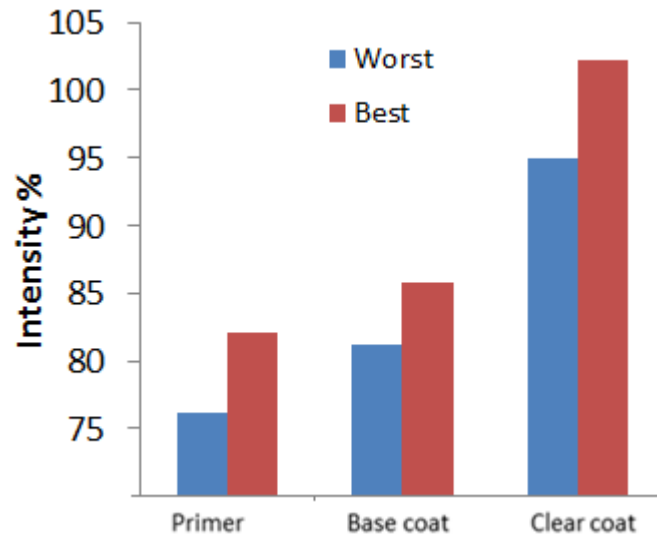


Figure 6.4.13 (same as fig.5.2.14): Gloss evolution for the best and worst rating conditions

Conclusion

6.4.1.8 Sheet roughness also influences the gloss. The difference between the samples rated as best and worst conditions at the clear coat layer was of 8% in intensity, which for industrial conditions is significant.

6.4.2 - Painted after stamping:

With the wave scan equipment it was not possible to measure the paint appearance in the two following conditions: deformed with die contact and deformed without die contact. This was due to the fact that the minimum measuring length is of 100 mm (further details related to the measuring method are given in the attachment 2).

Nevertheless, the modifications in roughness, due to the stamping operation, as shown in the topic 6.3.2, are transferred to the paint layers and possibly will affect the paint appearance. Despite the roughness parameters used in topic 6.3 related to the characterization of the painted surface are not the best ones to analyze the paint appearance, it was the method available at the moment.

It should be pointed out that the present research is in line with the USCAR (www.uscar.org) project named "Steel Surface Measurement for Paint Performance Prediction" which is trying tentatively to obtain a relationship between steel sheet

surface roughness and paint appearance, taking into account the sheet metal strains observed during stamping and the evolution of surface roughness on the E coat stage and other layers up to the clear coat stage.

6.5 Suggestion for future work

As a suggestion for future works related to the characterization on the paint appearance where there are size limitations, the micro wave scan should be utilized (further details are given in the attachment 2).

More specifically, some studies using the micro wave scan are listed in the following:

The roughness peak flattening (topic 6.3.2.1) seems that does not have a direct effect in the degradation of the surface appearance in terms of short waves since it leads to the reduction in roughness. However, as shown in topic 3.2.1, the larger the peak deformation, the larger will be the friction and the possibility of introducing waviness into the sheet (study of the effect of the LW in these regions). On the other hand, the increase in friction can cause also strip thinning which, in turn, will cause an increase in roughness, as seen in topic 6.2.2 (study on the effect of SW in the regions of thinning).

The correlation of strip roughness (as its evolution during stamping, its relation to the strain path along the FLD), with the paint appearance, allows the creation of the PALD (Paint Appearance Limit Diagrams), with similarities to the FLD, yet more restrictive. The limits of the PALDs could be obtained through the usage of the micro wave scans. A sketch of a PALD is shown in fig 6.4.14

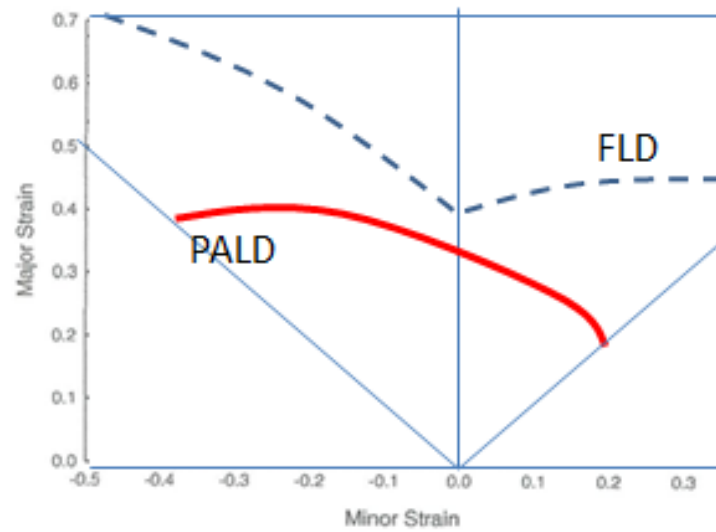


Figure 6.4.14 – Sketch of a PALD

It should be pointed out that in this PALD further variables can be and should be added. In a similar way a PALD-Stress (PASLD) could also be obtained.

Another study possibility would be the correlation between the 3D roughness parameters on the clear coat layer with the wave lengths of the spectral curve.

7 CONCLUSIONS

7.1 Skin pass reduction

In terms of material stampability the following trends have been observed:

7.1.1 SBT and EDT with a skin pass reduction of 0.3% has shown similar performance, which means, the highest material speed for the present research condition of $v=5\text{mm/s}$. For industrial stamping speeds, conditions may differ (future study).

In terms of material paint appearance the trend observed was:

7.1.2 SBT and EDT have shown similar performance and the best results were achieved with a skin pass reduction higher than 0.8%

In terms of degree of transfer during skin pass rolling the trend observed was:

7.1.3 The degree of transfer characterized by 3D (V_{cl} and α_{clm}) and 2D (R_a) reached the saturation level at 0.8% for EDT.

7.2 Paint appearance of the material without stamping

Comparison of samples (“worst and best” ratings at the E coat stage) the following results have been observed at the clear coat stage:

7.2.1 Sheet metal surface topography (2D and 3D) is transmitted all over the painted layers with decreasing intensity.

7.2.2 Sheet metal surface topography could improve 15% in terms of Rating.

7.2.3 Sheet metal surface topography could improve 8% in terms of Gloss.

7.2.4 Sheet metal surface topography could improve 2% in terms of DOI.

7.2.5 Sheet metal surface topography in terms of spectral curve can decrease intensity of wavelengths within a good balancing between short and long waves.

7.3 Paint appearance of the material with stamping

Surface topography after stamping evolves in the following ways:

7.3.1 Strain with die contact

7.3.1.1 It causes peak (surface) flattening of the surface topography, which in turn, improves paint appearance. (Beware of sheet waviness and/or sheet metal thinning, which in turn, decreases paint appearance).

7.3.2 Strain without die contact

7.3.2.1 It causes the sheet metal thinning which increases roughness, which in turn, decreases paint appearance. There was a gap between the 2D and 3D roughness measurements in the thinning area. At 4% thinning, Rz was 10.2 μm and Sz was 13.5 μm . At 20% thinning, Rz was 13.2 μm and Sz was 57.7 μm .

7.4 Sheet metal surface topography and Paint appearance

7.4.1 The sheet metal surface topography before painting should have a 2D roughness parameter $P_c > 100$ peaks/cm (the higher the better) and a 2D roughness parameter $0.8 < R_a < 1.3$ μm . Correlation factor for 3D roughness parameters related to rating was lower than for 2D roughness parameters.

7.5 - SUMMARY OF CONCLUSIONS

Table 7.5.1: The best sheet metal surface topography (for the present research condition) for stampability and paint appearance and some of the main process variables that influences it.

Chapter 7.1 / 7.4		Before stamping					
Process	Main aim	Skin pass reduction	Main figures	Surface topography	Main figures	Page	Slide
Stamping	↓Coefficient of friction	0.3%	6.1.3, 6.1.5, 6.1.8	Pc < 60 pks /cm Ra > 1.5 μm	5.1.12, 6.1.9	108/138/140/143/144	9/25/34
Painting	↑Paint appearance	>0.8%	6.4.3, 6.4.4	0.8 < Ra < 1.3 μm and Pc > 100 peaks/cm	6.4.1, 6.4.2	182-184	24/25/29
Chapter 7.2/7.3/7.4		After stamping					
Process	Main aim	Surface topography		Main figures		Page	Slide
Stamping	↓Thinning*	0.8 < Ra < 1.3 μm and Pc > 100 peaks/cm		6.2.17, 6.2.20, 6.3.13		152/160/180	39
Painting	↑Paint appearance	0.8 < Ra < 1.3 μm and Pc > 100 peaks/cm		6.4.1, 6.4.2, 6.4.5, 6.4.9		182/184/187	42

Chapter 3.2 / 7.2	*Main Variables affecting thinning		Figures / topics	Page
↓Thinning	Material Property	↑ r	topic 3.2.8	67/68/70
	Material coating	Chemical	3.2.15	54/70
	Material Roughness	αcm and Vcl ↑	3.2.6	45 - 49
	Tool coating	Cr	topic 3.2.8	53
	Tool roughness	Rz ↓	topic 3.2.8	
	Tool design	Ratios, Beads, etc	topic 3.2.8	67/69-71
	Lubricant	Type	3.2.9	50-52
		Thickness	3.2.9	
		Homogeneity	3.2.11, 3.2.12	
	Press	Variable bead	topic 3.2.8	71
		Alignment	topic 3.2.8	
		Variable punch	topic 3.2.8	
		Variable blank holder force	topic 3.2.8	
	Part design	Ratios, shapes, etc	topic 3.2.8	
	Process	Temperature	3.2.13	52-53
Strain path		3.2.29	67/69/70	

REFERENCES

ALTAN, T. **Evaluating dry film lubricants for automotive applications Part II, The ironing test.** June 13, 2006. Available in:

<http://www.thefabricator.com/article/toolanddie/evaluating-dry-film-lubricants-for-automotive-applications-part-ii>. Accessed in Sep., 10, 2013.

ALTAN, T. **Evaluating dry film lubricants for automotive applications Part III, Testing through deep drawing.** November 8, 2005. Available in:

<http://www.thefabricator.com/article/toolanddie/evaluating-dry-film-lubricants-for-automotive-applications-part-iii>. Accessed in Sep., 10, 2013.

ARRIEUX, R., BEDRIN, C., BOIVIN, M. **Determination of an intrinsic forming limit stress diagram for isotropic metal sheets.** Proceedings of the 12th Biennial Congress of the IDDRG, pp. 61–71, 1982.

ASPINWALL, D.K.; WISE, M.L.H.; STOUT, K.J.; GOH, T.H.A.. **Electrical Discharge Texturing.** International Journal of Machine Tools & Manufacture, v. 32, p. 183-192, 1992.

BANABIC, D.; BUNGE, H. J.; PÖHLANDT, K.; TEKKAYA, A.E. **Formability of metallic materials. Plastic anisotropy, Formability testing, Forming limits.** p. 176 – 203, 2000.

BAY, N.; OLSSON, D.D.; ANDREASEN, J. L. **Lubricant test methods for sheet metal forming.** Tribology International, v. 41, p. 844-853, 2008.

BAY, N.; AZUSHIMA, A.; GROCHE, P.; ISHIBASHI, I.; MERKLEIN, M.; MORISHITA, M.; NAKAMURA, T.; SCHMID, S.; YOSHIDA, M. **Environmentally benign tribo-systems for metal forming** - CIRP Annals – Manufacturing Technology, v. 59, p.760–780, 2010.

BFINTEN, L; STEINHOFF, K.; RASP, W.; KOPP, I.L.; PAWELSKI, O. **Development of a FEM-model for the simulation of the transfer of surface structure in cold-rolling processes.** Journal of Materials Processing Technology, v. 60, p. 369-376, 1996.

BLOCK, K.F.; BERGOLD, W. B.; ENDERLE, W. **Oil layer measurement in rolling and stamping plants – online**. 48th Rolling Seminar - Processes, Rolled and Coated Products, ABM, Santos – SP – Brazil. 2011.

BURGIN, D. **The Paintability of Various Metallic Coated Sheet Steels Through Australian Automotive Paint Facilities**. International Congress & Exposition Detroit, Michigan, Feb 26-29, p. 27–42, 1996.

CHOI, Y. - M.; CHUNG, J.-H.; SPEER, J.G.; MATLOCK, D.K. **Topography assessment of coated steel sheet surface imperfections in relation to appearance after painting**. SAE 2003-01-2766, p. 237-242, 2003.

DE MARK, M. V. **The Course: Coatings System**. Missouri S&T Coatings Institute. 2013.

DEMARE, C.; SCHEERS, J.; MESEURE, K. ; VERMEULEN, M. **Sibetex steel sheet textures: an effective way to improve quality and reduce cost in car manufacturing**. International Body Engineering Conference (IBEC97), Proceedings. p. 157-164, 1997.

DOEGE, E.; ELEND, L.-E. **Design and application of pliable blank holder systems for the optimization of process conditions in sheet metal forming**. Journal of Materials Processing Technology, v. 111, p. 182-187, 2001.

DUBAR, L; HUBERT, C.; CHRISTIANSEN, P.; BAY, N; DUBOIS, A. **Analysis of fluid lubrication mechanisms in metal forming at mesoscopic scale -CIRP Annals – Manufacturing Technology**, v. 61, p. 271–274, 2012.

DUCHÊNE, L.; GODINAS, A.; CESCOTTO, S.; HABRAKEN, A.M. **Texture evolution during deep-drawing processes**. Journal of Materials Processing Technology, v. 125–126, p. 110–118, 2002.

FERREIRA FILHO, A. ; PLAUT, R. L.; BOMFIM, M. F.; LIMA; N. B. **Efeito da textura cristalográfica na anisotropia plástica planar em aços para estampagem profunda**. 42th Rolling Seminar - Processes, Rolled and Coated Products, ABM, São Paulo – SP – Brazil, October, 25 to 28, 2005.

FLECTHER, D. **Sensing a change**. Metalforming magazine, tooling technology, p. 44-47, edition may 2003.

GAZIOLA, E. **Private communication** on May 2013.

GEIGER, M.; ENGEL, U.; PFESTORF, M.. **New developments for the qualification of technical surfaces in forming processes**. Annals of CIRP, v. 46, n.1, p. 171–174, 1997.

GERHARDT, L. J. **Paint Perceptual Quality: Measuring What the Customer Values**. 6th BYK-Gardner User Meeting Dearborn, MI on April 12 – 13, 2011.

GRETHE, U. **Pretex**. Available in: http://www.salzgitter-flachstahl.de/en/Produkte/kaltfein_oberflaechenveredelte_produkte/pretex/. Accessed in Sep., 10, 2013.

GRILHE, J. **Study of roughness formation induced by homogeneous stress at the free surfaces of solids**. Acta Materialia, v. 41, n. 3, p. 909-913, 1993.

HOGENDOORN, P. **Finding the “Pulse” of Your Process – A New Way to Monitor Manufacturing Quality**. SAE 2009-01-1189.

HU, Z.; NIEHOFF, H.; VOLLERTSEN, F. **Determination of the Friction Coefficient in Deep Drawing**. 1 st Colloquium Process scaling, Bremen, p. 1-8, 2003.

HUTCHINSON, B.; RYDE, L.; BATE, P. **Transformation textures in steels**. Materials Science Forum, v. 495-497, p. 1141-1150, 2005.

JONASSON, M.; PULKKINEN, T.; GUNNARSSON, L.; E. SCHEDIN. **Comparative study of shot blasted and electrical-discharge-textured rolls with regard to frictional behavior of the rolled steel sheet surfaces**. - Wear, v. 207, p. 34–40, 1997.

JONASSON, M.; WIHLBORG, A.; GUNNARSSON, L. **Analysis of surface topography changes in steel sheet strips during bending under tension friction test**. International Journal of Machine Tools & Manufacture, v. 38, n. 5-6, p. 459-67, 1998.

KAWABE, H.; MATSUOKA, S.; SHIMIZU, T.; FURUKIMI, O.; SAKATA, K.; ITO, Y. **Effect of increase in r-value on press formability for cold-rolled steel sheet**. JSAE Review, v. 23, p. 139–141, 2002.

KIM, H. **Evaluating dry film lubricants for automotive applications Part I, A general review**. June 13, 2006. Available in:

<http://www.thefabricator.com/article/toolanddie/evaluating-dry-film-lubricants-for-automotive-applications-part-i>. Accessed in Sep., 10, 2013.

KLEEMOLA, H.J., PELKKIKANGAS, M.T. **Effect of pre deformation and strain path on the forming limits of steel, copper and brass**. Sheet Metal Industries, v. 63, p. 559–591, 1977.

KLEMT, M.; MINKO, P. **Top appearance – Improvements based on chemistry, Physics and process technology**. 8th Byk – Gardner User Meeting. 03 June 2008.

KLIMCZAK, T.; JONASSON, M. **Analysis of real contact area and change of surface texture on deep drawn steel sheets**. Wear, v. 179, p. 129-135, 1994.

LEX, K. **New Structure Space with Balance Chart Analysis**. 9th BYK-Gardner User Meeting. Bad Tölz, Germany – November 16 - 17, 2010.

LUBBING, H.; HAAR, R.; SCHIPPER, D.J. **The Influence of Plastic Bulk Deformation on Surface Roughness and Frictional Behavior during Deep Drawing Processes**. p. 705-711. 1996. Available in:

<http://doc.utwente.nl/73246/1/Lubbinge96influence.pdf>. On line: Accessed in Apr 2013

MA, B.; TIEU, A.K.; LU, C.; JIANG, Z. **A finite-element simulation of asperity flattening in metal forming**. Journal of Materials Processing Technology, v. 130–131, p. 450–455, 2002.

MAILE, F.J.; PFAFF, G.; REYNDERS, P. **Effect pigments—past, present and future**. Progress in Organic Coatings, v. 54, p. 150–163, 2005.

MENDES, I. **Private communication** on Jun 2013.

MERKLEIN, M.; GEIGER, M.; KAUPPER, M. **Tribology and influence of tool coatings on frictional conditions within forming of advanced high strength steels**. Proceedings of the 7th international conference. The coatings in Manufacturing Engineering, p. 39-46. Greece, 2008.

MEYER, R. **Private communication** on Jul 2013.

MILLER, W.S.; ZHUANG, L.; BOTTEMA, J.; WITTEBROOD, A.J.; SMET, P.; HASZLER, A.; VIEREGGE, A. **Recent development in aluminum alloys for the automotive industry**. Materials Science and Engineering, v. A 280, p. 37–49, 2000.

MULLER, E. **Aramis and the detection of flow behavior for sheet metal material in high speed tensile test**. p. 1-3, 2009. On line: <http://www.gom.com/metrology-systems/digital-image-correlation.html>. accessed in Sep 2013.

NISHIMURA, K. **Cold rolled steel sheets with ultra-high Lankford value and excellent press formability**. Kawasaki Steel Technical Report, n. 42, p.8–11, 2000.

OLIVEIRA, A. F. **Private communication** on Jun 2013. Usiminas Cubatão Brazil.

PAWELSKI, O.; RASP, W.; ZWLCK, W.; NETTELBECK, H.-J.; STEINHOFF, K. **The influence of different work - roll texturing systems on the development of surface structure in the temper rolling process of steel sheet used in the automotive industry**. Journal of Materials Processing Technology, v. 45, p. 215-222, 1994.

PAYEN, G.R.; FELDER, E.; REPOUX, M.; MATAIGNE, J.M. **Influence of contact pressure and boundary films on frictional behavior and on the roughness changes of galvanized sheets**. Wear, v. 276-277, p. 48 – 52, 2012.

PFESTORF, M.; ENGEL, U.; GEIGER, M. **3DSurface Parameters and their Application on Deterministic Textured Metal Sheets** International Journal of Machine Tools & Manufacture, v. 38, p. 607-614, 1998.

RAHARIJAONA, F.; ROIZARD, X.; STEBUT, VON J. **Usage of 3D roughness parameters adapted to the experimental simulation of sheet-tool contact during a drawing operation.** Tribology International, v. 32, p. 59–67, 1999.

RODRIGUES, J. G. **Otimização do processo de pintura automotiva através da metodologia operação evolutiva (EVOP).** 2011, 55 p. Monograph - Escola Politécnica, Universidade de São Paulo, São Paulo, 2011.

SCHEERS, J.; VERMEULEN, M. ; DE MARE,C. ; MESEURE, K. **Assessment of steel surface roughness and waviness in relation with paint appearance.** International Journal of Machine Tools & Manufacture. v. 38, n. 5-6, p. 647–656, 1998.

SEKERES, T.; FERNANDES, C.; SANTOS, J.C.; NUNES, E.; PLAUT, R.L. **FEM modeling and press signature evaluation of a typical car stamping.** Materials Science Forum, v. 704-705, p. 717-727, 2011. doi: 10.4028/www.scientific.net/MSF.704-705.717.

SIMÃO, J.; ASPINWAAL, D. K. **Hard chromium plating of EDT mill work rolls.** Journal of Materials Processing Technology, v. 92-93, p. 281-287, 1999.

SOBIS, T.; ENGEL, U.; GEIGER, M. **A theoretical study of wear simulation in metal forming processes.** Journal of Materials Processing Technology, v. 34, p. 233–240, 1992.

STAEVES, J. **Beurteilung der Topografie von Blechen im Hinblick auf die Reibung bei der Umformung.** 1998. Vortrag zur Dissertation. Technische Universität Darmstadt. Institut für Produktionstechnik und Umformmaschinen. Tag der mündlichen Prüfung: 09.09.1998.

STOUGHTON, T. B. **The Influence of the Material Model on the Stress-Based Forming Limit Criterion.** SAE 2002 World Congress Detroit, Michigan, March 4-7, 2002. SAE Nr. 2002-01-0157.

STOUGHTON, T. B., ZHU, X. **Review of theoretical models of the strain-based FLD and their relevance to the stress-based FLD.** International Journal of Plasticity, v. 20, p. 1463–1486, 2004.

STOUGHTON, 2013. **Nonlinear Strain Path Effects on FLD**, NADDRG (2013).

STOVER, J.C. **Optical Scattering, Measurement and Analysis**, SPIE Press (1995). Available in: http://en.wikipedia.org/wiki/Visual_appearance. Accessed in Sep.,10, 2013.

TERPÁK, J.; DORCÁK, L. ; REVAJ, J. **Quality control of the electro-discharge texturing**. METALURGIJA, v. 49, n. 1, p. 19-22, 2010.

TRUNG, T. N. **New Structure Space with Balance Chart Analysis and Introduction of the “B”-parameter in PSA**. 6th BYK-Gardner User Meeting Dearborn, MI on April 12 – 13, 2011.

TSCHERSCHE, S.; NITSCHKE, M. **Roll texturing by electronic discharge texturing machines “EDT“ and superfinishing unit1**. Technical contribution to the 49th Rolling Seminar – Processes, Rolled and Coated Products, October, 22-25th, 2012.

UNFER, R. K; BRESSAN, J.D.; **Evolution of Roughness on Straining of Interstitial Free – IF Steel Sheet**. Key Engineering Materials, v. 504-506, p. 83-88, 2012. doi:10.4028/www.scientific.net/KEM.504-506.83.

UTHAISANGSUK, V.; PRAHL, U.; BLECK, W. **Stress based failure criterion for formability characterization of metastable steels**. Computational Materials Science 39, p. 43–48, 2007.

VALENTIN, J.; WEBER, M. A.; BRODMANN, R.; SHARP, A. **3D-Characterisation of Sheet Metal and Roller Surfaces by Means of Confocal Microscopy**. Advanced Materials Research, v. 6-8, p. 543-550, 2005.

VERMEULEN, M.; SCHEERS, J. **Micro-hydrodynamic effects in EBT textured steel sheet**. International Journal of Machine Tools & Manufacture, v. 41, p. 1941–1951, 2001.

WARD, D. **Dry Film Lubrication**. Quality Metal Finishing Haward. Available in: <http://www.haward.com/dryfilmlubrication/>. Accessed in Sep., 10, 2013.

WARRENDER, T.E.; ASPINWALL, D. K.; DEWES, R.C.; SIMAO, J.M.T.; SCAMANS, G.. **Electrical discharge texturing of rolls for the manufacture of aluminum strip: effects of processing parameters on roll surface topography and strip formability.** Proceedings of the Rolls 2003 Conference. Birmingham, UK. On line: <http://publicat.bham.ac.uk/19624/> accessed in Jun 2013.

WEIDEL, S.; ENGEL, U. **Characterization of the flattening behavior of modeled asperities.** Wear, v. 266, p. 596–599, 2009.

WICHERN, C. M.; VAN TYNE, C. J.; BELANGE, P. J. **Analysis of Surface Morphology Change Due to Forming of Zinc-Coated Sheet Steels for Automotive Panel Applications.** SAE 2000 World Congress Detroit, Michigan March 6-9. SAE nr. 2000-01-0310 . p. 1-11, 2000.

WICHERN, C. M.; COOMAN, B.C.; VAN TYNE, C. J. **Surface roughness changes on a hot-dipped galvanized sheet steel during deformation at low strain levels.** Acta Materialia, v. 52, p. 1211–1222, 2004.

WICHERN, C. M.; COOMAN, B.C.; VAN TYNE, C. J. **Surface roughness of a hot-dipped galvanized sheet steel as a function of deformation mode.** Journal of Materials Processing Technology, v. 160, p. 278–288, 2005.

APPENDIX 1: STAGES OF THE PAINTING PROCESS

The following explanations have been extracted from the following address: DE MARK, M. V. **The Course: Coatings System**. Missouri S&T Coatings Institute, 2013 and private communication with Isaac Mendes and Edmilson Gaziola, 2013.

A.1: PHOSPHATE

The first layer to be applied at the paint shop is the phosphate, as shown in fig. A.1.1. The main functions of the phosphate layer are:

- Improve E coat adherence;
- Minimize filiform corrosion;
- Improve corrosion resistance at the edges.

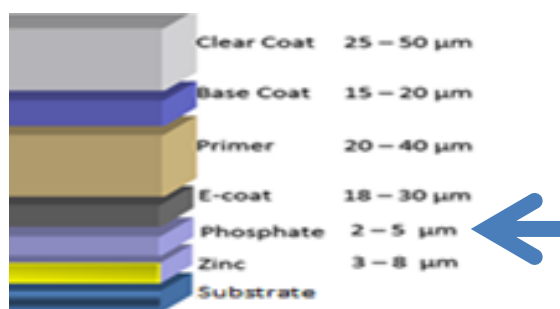
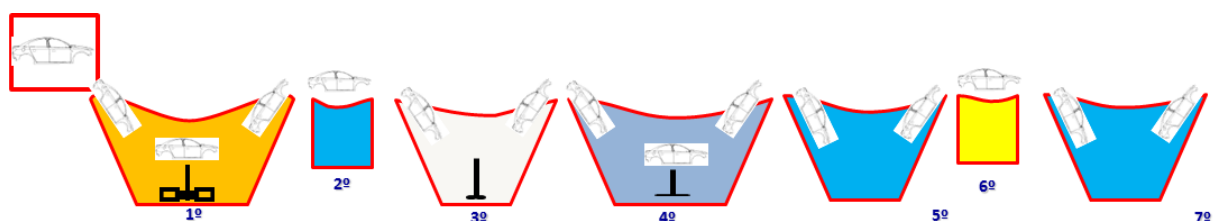


Figure A1.1.1: The first layer.

The summary of the process step are shown in fig. A1.1.2



STAGES	FUNCTION	APPLICATION METHOD	COMMENTS
1º	DEGREASING 2	IMMERSION	Chemical cleaning – oil removal
2º	WASHING	SPRAY	Mechanical and chemical cleaning -
3º	REFINER	IMMERSION	Titanium powder (controls final grain size)
4º	PHOSPHATING	IMMERSION	Chemical reactions above. Note there is a gradient of PH.
5º	WASHING	IMMERSION	Chemical cleaning
6º	PASSIVATION	SPRAY	
7º	WASHING	IMMERSION	

Figure A1.1.2: Phosphate Process step.

The main process chemical reactions are shown in fig. A1.1.3

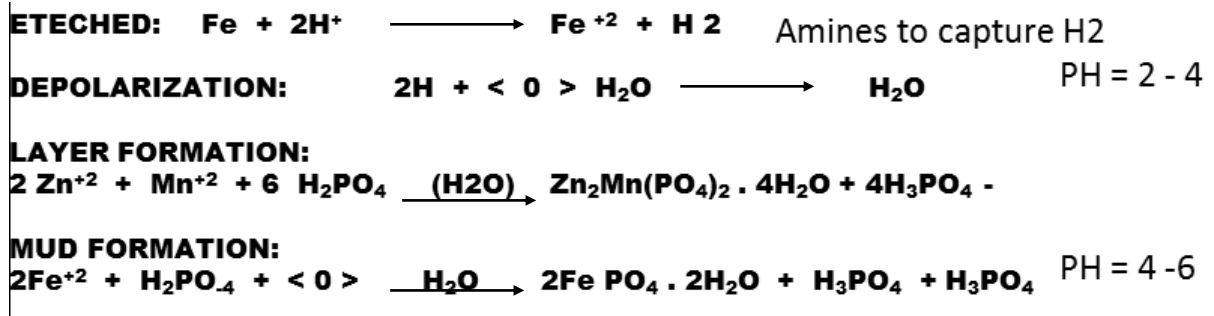


Figure A1.1.3: Phosphate main process chemical reactions.

Fig. A1.1.4 shows the surface topography of the phosphate layer deposited on hot dip galvanized steel.

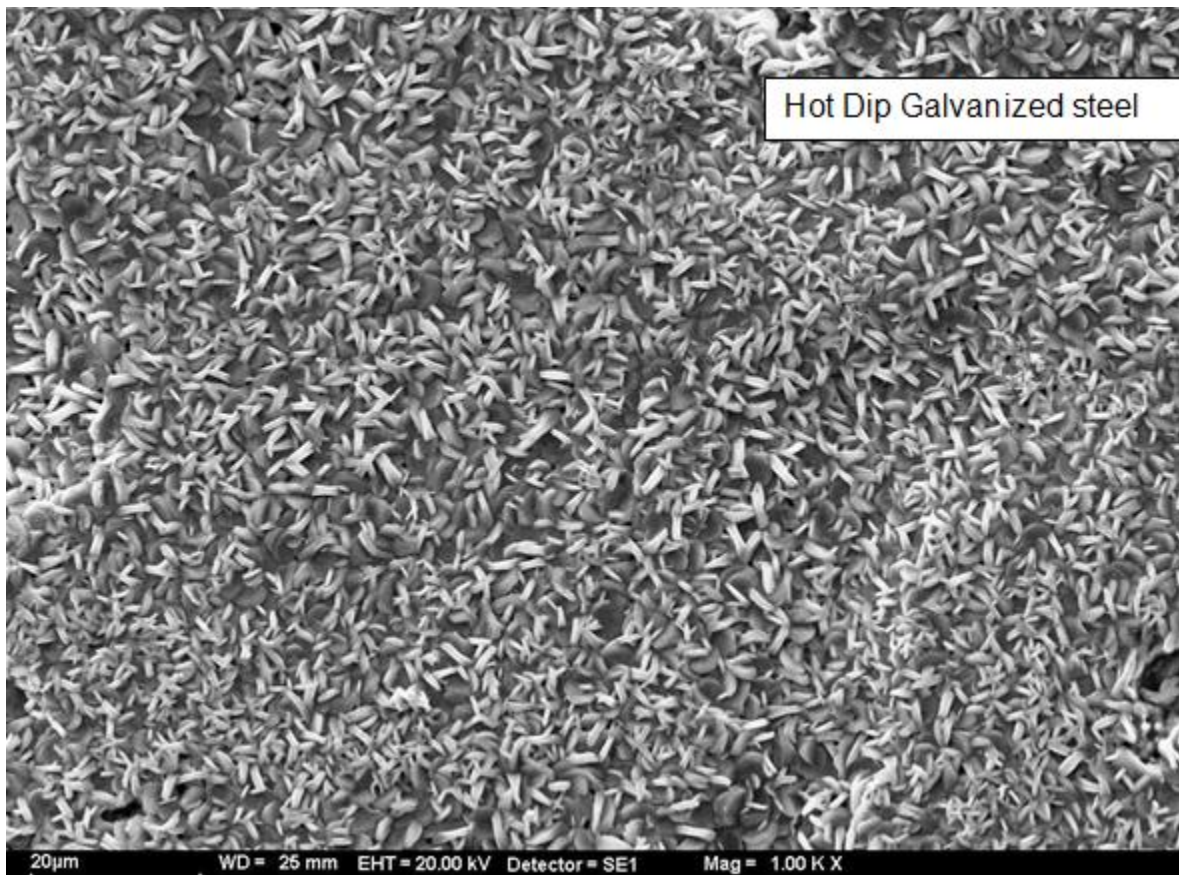


Figure A1.1.4: Phosphate layer. SEM analysis. Zeiss EVO MA 10.

A1.2: E COAT

The second layer to be applied at the paint shop is the E coat, as shown in fig. A1.2.1. The main functions of the E coat layer are:

- Improve Primer adherence;

- Very low vapor permeability;
- Improve corrosion resistance.

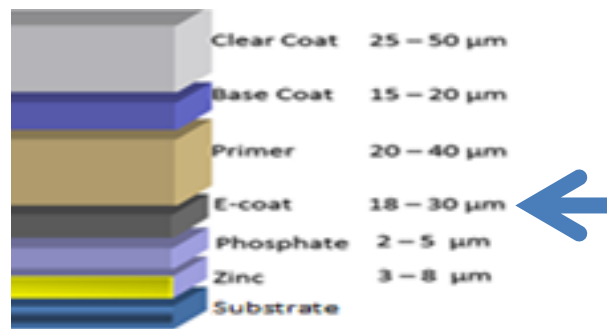
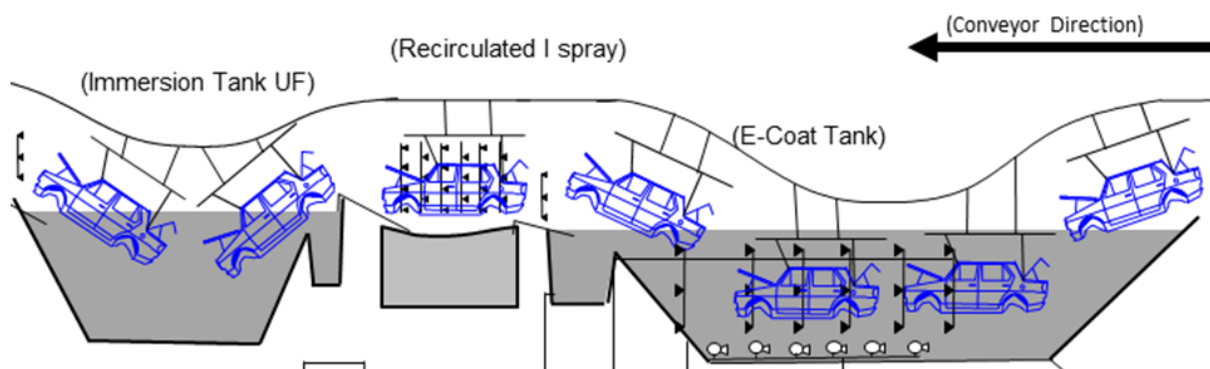


Figure A1.2.1: The second layer.

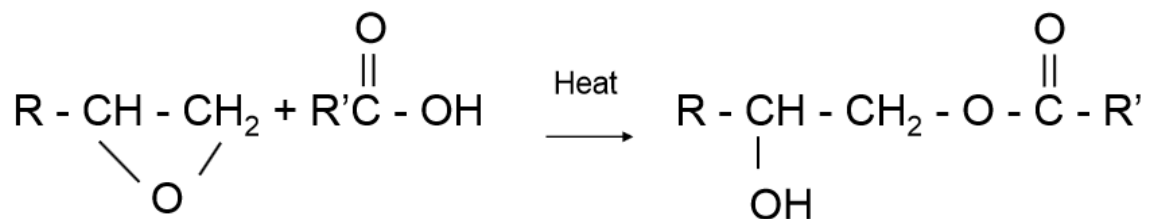
The summary of the process step are shown in fig. A1.2.2



STAGES	FUNCTION	APPLICATION
E-COAT	ELECTRODEPOSITION	IMMERSION
RECIRCULATED I	WASHING	SPRAY
IMMERSIOR TANK	WASHING	IMMERSION

Figure A1.2.2: E coat Process step.

The E coat is acrylic resins with epoxy groups reacted with polyester resins with an acid group.



Adhesion is dependent on the substrate surface tension and the functional groups on the resin. This interaction determines the strength of adhesion. Ionic Bonds 100-300 kcal/mole • Covalent 30-110 kcal/mole • Hydrogen 1-10 kcal/mole

The surface tension or surface energy is the force, measures in dynes/cm, on the surface of a liquid which opposes the expansion of the surface area. Every object has surface energy. As in most physical laws of nature, given a choice, a dynamic system will preferentially go into the lowest energy state. If the coating has a higher surface tension than the substance that is to be coated, dewetting, orange peel or cratering may occur. If the coating has a lower surface tension than the substrate, the coating will flow continuously over the substrate. In high solids coatings, there can be a minor adjustment made to the surface tension of the coating by varying solvents blends. Major changes are very difficult because the resin system plays the major role in the surface energy of the coating.

A1.3: PRIMER

The third layer to be applied at the paint shop is the Primer, as shown in fig. A1.3.1. The main functions of the Primer layer are:

- Improve base coat adherence;
- Color;
- Improve paint appearance;
- Improve stone impact resistance.

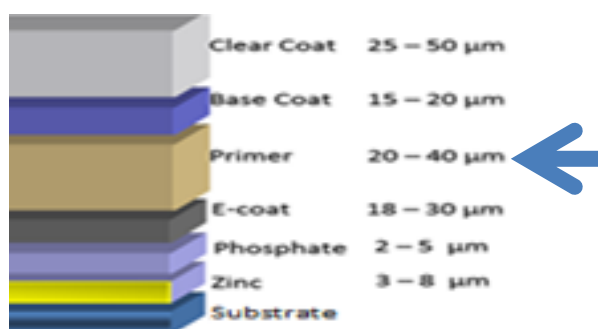


Figure A1.3.1: The third layer.

The summary of the process is shown in fig. A1.3.2

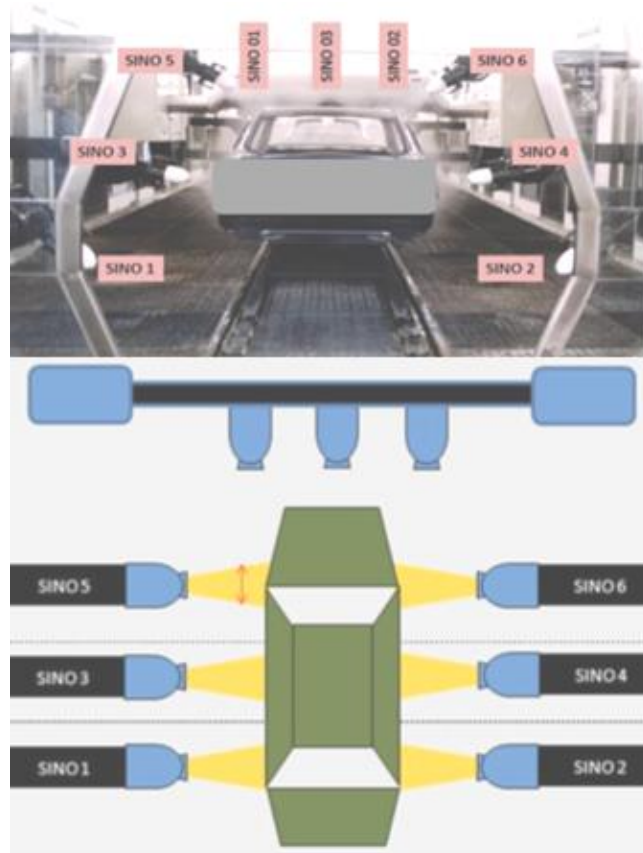


Figure A1.3.2: Conventional spray deposition (RODRIGUES, 2008)

The primer main material consists of a Polyester Resin which represent approximately 25 – 30% of the compost. The other part is the solvent (65-70%). It also may contain some additives for a specific function (color, impact resistance, paint appearance, etc).

A1.4: BASE COAT

The fourth layer to be applied at the paint shop is the Base coat, as shown in fig. A1.4.1. The main function of the base coat layer is:

- Color;

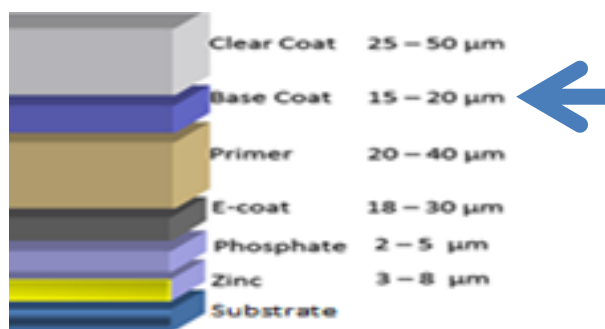


Figure A1.4.1: The fourth layer.

The spray method is used for this application, as in the case of primer.

The basecoat components are described in fig. A1.4.2.

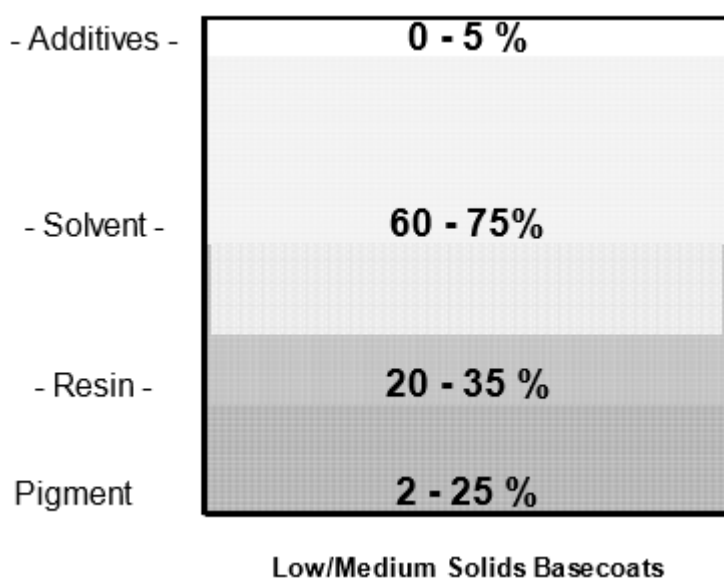


Figure A1.4.2: Typical components of the base coat paint.

In the following there is a general explanation of each of the components function:

ADDITIVES

Viscosity Control Agents (Solvents Paints) – Small amounts of clays or rod-like polymers used in alkyd and oil type paints to increase viscosity. • Other Additives – Various additives are available for both solvent and water systems that contribute various properties such as non-sagging, mar resistance, antifreeze, wet edge, etc.

Film former – in solution or emulsion form. Imparts characteristics of toughness, durability, dry time, etc. (Resins: Melamine, Urethanes and Epoxy)

SOLVENTS

Used to dissolve the vehicles and make them into a usable liquid form. Choice of solvents with varying evaporation rates can change the drying characteristics of the paint. Choice of solvents with varying solvent strength can change the viscosity of the paint. (M.S., V.M. & P., Toluene, Xylene, MIBK, MEK, Cellosolve, etc.) These liquids which evaporate from the film during drying are also called VOC or volatile organic compounds.

Solvents are essential formulation ingredients for many coatings. For most applications, solvents are intended to evaporate. The primary function of solvents in paint is to dissolve the resins or polymers (i.e., film formers or solventborne) to produce a useable liquid that is able to be applied to the vehicle. They are also able to lower the viscosity of the coating. The solvents then evaporates during the drying process helping to level the wet paint. Some of the other key functions of solvents are evaporation rate, resistivity, solvency, odor, surface tension, and toxicity.

RESINS (BINDER)

The important component of paint is the binder. A binder is the resinous part of paint (liquid or solid in the case of powder paint) that holds all the paint's constituents into a continuous system: it is the main film former.

The resinous material in binders is made up of polymers. A polymer is a chain linkage composed of many repeating individual chemical structures called monomers. The properties of the final paint film are determined based on the monomers chosen for the paint – whether the film is thermoplastic (no crosslinking i.e. lacquers) or thermoset (crosslinking i.e. enamels).

Crosslinking is the process where the functional groups on the polymer chains combine to form a 3 dimensional matrix.

PIGMENT

- Powdery materials that impart hiding and color to the paint. (TiO₂, Chrome Yellow, Lampblack, etc.)

Also powdery materials, but do not impart hide or color – they are used to control gloss and primarily to reduce cost. (Clays, talcs, calcium carbonates.) These

materials increase volume of low cost and if properly chosen can enhance the performance of a coating.

In the following, in greater detail, there are some of the components that can be used in the base coat.

UV Absorber: Protects Paint from UV Rays of Sun

PCA: Pattern Control Additive Produces Proper Flake Orientation during Spraying and Prevents Sagging during Initial Bake

Melamine: Cross-linker - Binds Resins Together to Form Film

Acrylic Resin: Hardness and Durability

Polyester Resin: Flexibility

Anti-Settling Agent: Prevents pigment from Settling

Aluminum Pigment: Imparts Metallic Appearance

Mica Pigment: Imparts Metallic Appearance and Color

Alcohol: Stability Protection

Acid Catalyst: Aids in Cure

A1.5: CLEAR COAT

The fifth layer to be applied at the paint shop is the Base coat, as shown in fig.

A1.5.1. The main function of the base coat layer is:

- Physical protection (higher hardness and tough);
- Chemical protection (higher density);
- Paint appearance;
- UV protection.

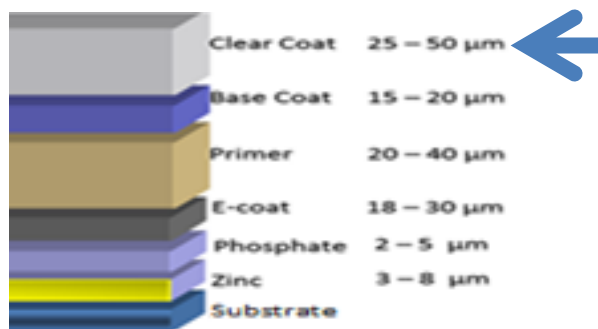


Figure A1.5.1: The fifth layer.

The spray method is used for this application, as in the case of primer and base coat.

The clear coat components are similar to base coat components, except of the pigment.

The main resin is the Acrylic Melamine. These coatings are based on acrylic polyols (Ac) and amino crosslinker (MF, melamine resins) which, are baked at 130C–150C for 12–20 minutes. Condensation reaction between alkoxyatedmelamine resin with the hydroxyl group of the polyol forms an ether cross-link polymer. This polymer bonding easily hydrolyze below pH 6, leading clear coat polymer degradation at surface. In hostile environment, this polymer desintegrate from the surface, which lowers the gloss giving permanent visible damage. Acrylic melamine systems are made by making acrylic polymers with hydroxyl (-OH) and acid (-COOH) groups on the backbone.

The Acrylic polymer is cross-linked with melamines. These used today for many basecoat and clearcoat systems. These system are prone to environmental damage.

Some advantages of this chemistry are high solids, hardness and appearance. The major disadvantages are long term durability and etch resistance.

In the following, in greater detail, some of the components that can be used in the clear coat.

UV Absorber: Protects Paint from UV Rays of Sun

PCA: Flow Control Additive

Melamine: Cross-linker - Binds Resins Together

Acrylic Resin: Hard, Durable

Polyester Resin: Flexible

Surface Agent: Added to Clearcoat to Promote Flow, Alleviate Differences in Surface Tension

Alcohol: Stability Protection

Acid Catalyst: Aids in Cure

The fig. A1.5.2 shows the main advantages and disadvantages of the Acrylic/Melamine Systems.

.

Advantages	Disadvantages
Established technology	Poor acid etch resistance
Low cost	(the higher the melamine level, the poorer the etch)
One package system	Prone to cracking when
Potential for high solids	monomeric melamines are
Fair durability	used
Good appearance	

Figure A1.5.2: Main advantages and disadvantages of the Acrylic/Melamine Systems

In the following is presented two relevant aspects in the painting process variables that influence paint appearance.

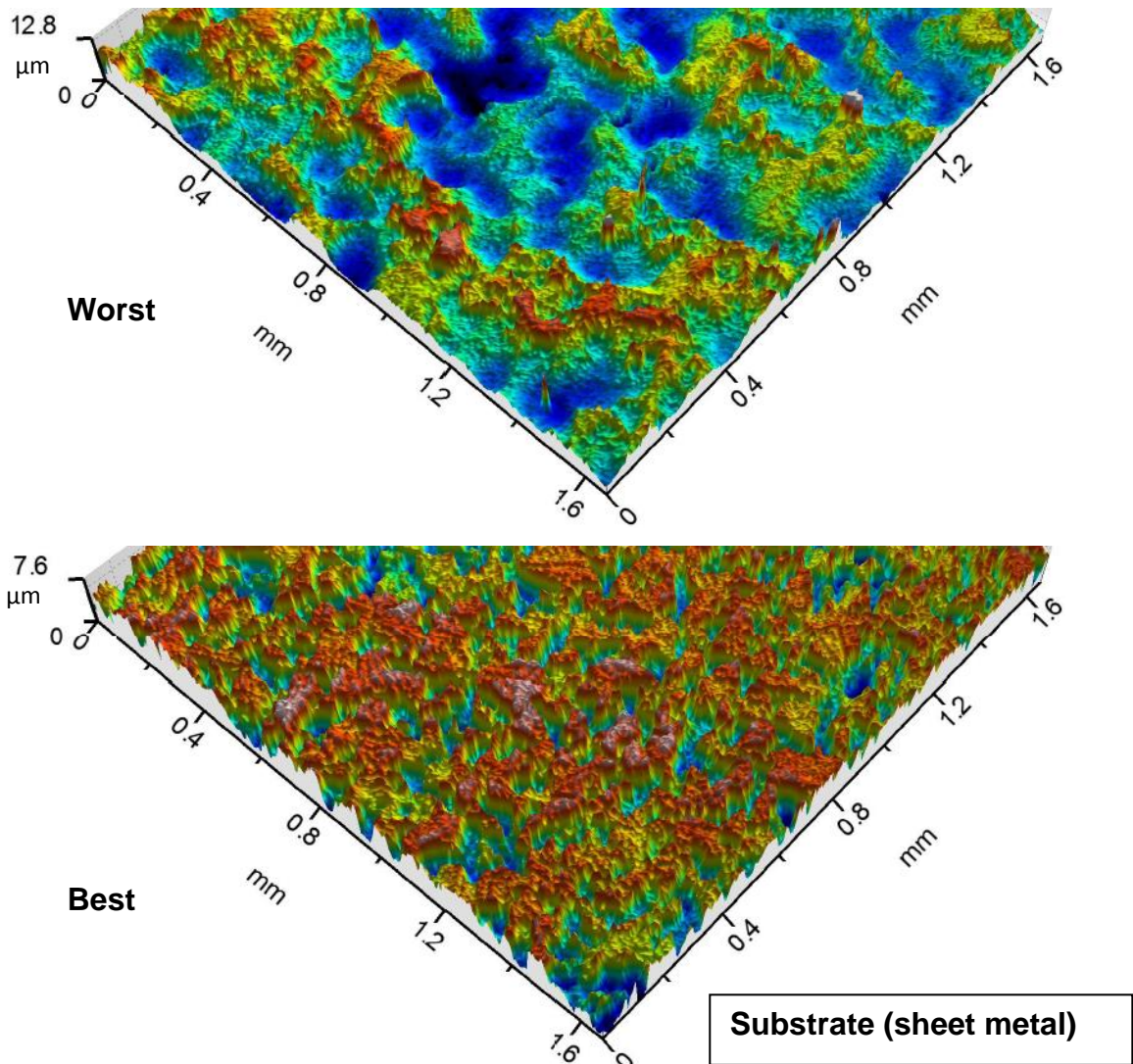
Surface effects –The properties of surface like surface tension and surface roughness and surface structure affect the behavior of paint on the substrate. For a coating to form a film on the substrate, it must first wet the substrate. This wetting depends on the interaction (affinity) of the coating with surface of the substrate. One of the main conditions for the paint to wet the surface is a low surface tension at the interface with air. The contact angle is small and so the paint spreads out on the substrate and does not form droplets, giving good leveling and flow. Substrate with a rough surface is wetted more readily than one with a smooth surface. Adhesion is closely related to wetting. For optimum adhesion, the physical bonds formed during wetting should be rendered permanent during film formation. The adhesion is more strong for a rough surface than a smooth surface. The paint layer should be able to

cover the surface structure of the substrate and produce a smooth film with a structure of its own

The various types of pretreatments given to the metal surface to improve its corrosion resistance also affects wetting and adhesion of the paint to it. The phosphating which is done on the metal surface improves adhesion of surface to the E coat to be coated on it. For inter-coat adhesion, the degree of cross-linking of the first coat plays an important role in the adhesion of further coats. If the cross-linking density is high, then adhesion of further coats is poor. The inter-coat adhesion can be improved by using special pigments. Usually, they are very finely dispersed pigments or those with a platelet like structure. These pigments influence rheology, leveling and generate special surface structures that can improve adhesion of further coats of paint

Temperature – During the evaporation of solvents from a solvent-borne coating the surface temperature at the air/substrate interface should not fall below the dew point, otherwise water vapor will condense on the uncured film. Low temperature will also retard the curing process, allowing more time for dirt to stick on the wet paint. If the surface temperature is high then the paint wont flow and level properly.

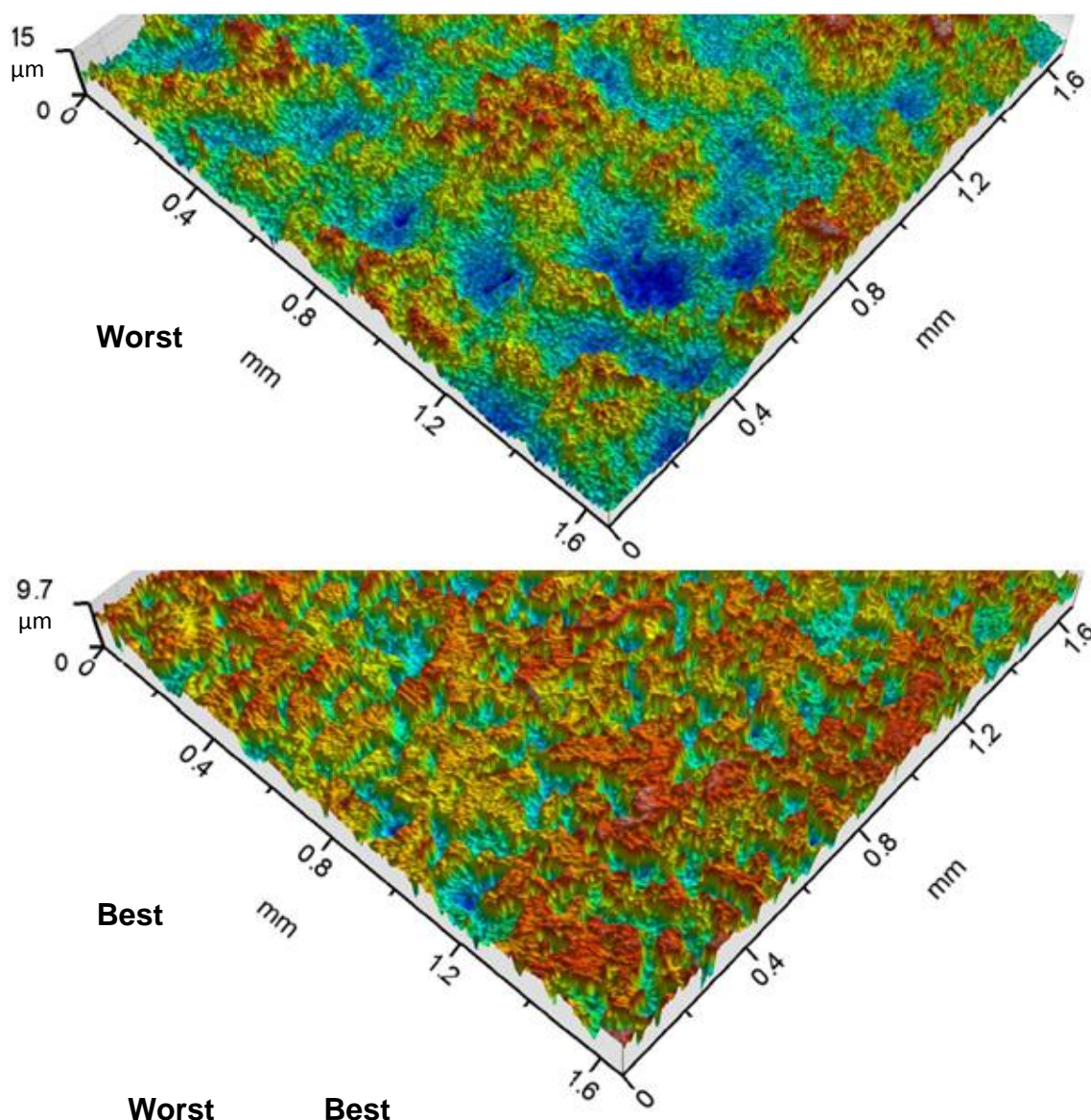
APPENDIX 2: 3D ROUGHNESS RESULTS



	Worst		Best			
Sq	2.26	Sq	1.60	μm		Root mean square height
Ssk	0.319	Ssk	-0.406			Skewness
Sku	2.54	Sku	2.13			Kurtosis
Sp	7.90	Sp	3.39	μm		Maximum peak height
Sv	5.06	Sv	4.25	μm		Maximum pit height
Sz	13.0	Sz	7.64	μm		Maximum height
Sa	1.86	Sa	1.37	μm		Arithmetic mean height
Feature Parameters		Feature Parameters				
Spc	851	Spc	482	$1/\text{mm}$	pruning = 5%	Arithmetic mean peak curvature
Spd	1096	Spd	3228	$1/\text{mm}^2$	pruning = 5%	Density of peaks

Figure A2.1: Sheet metal 3D Roughness for the best and worst conditions of rating (measured in the first step) (Taylor Hobson).

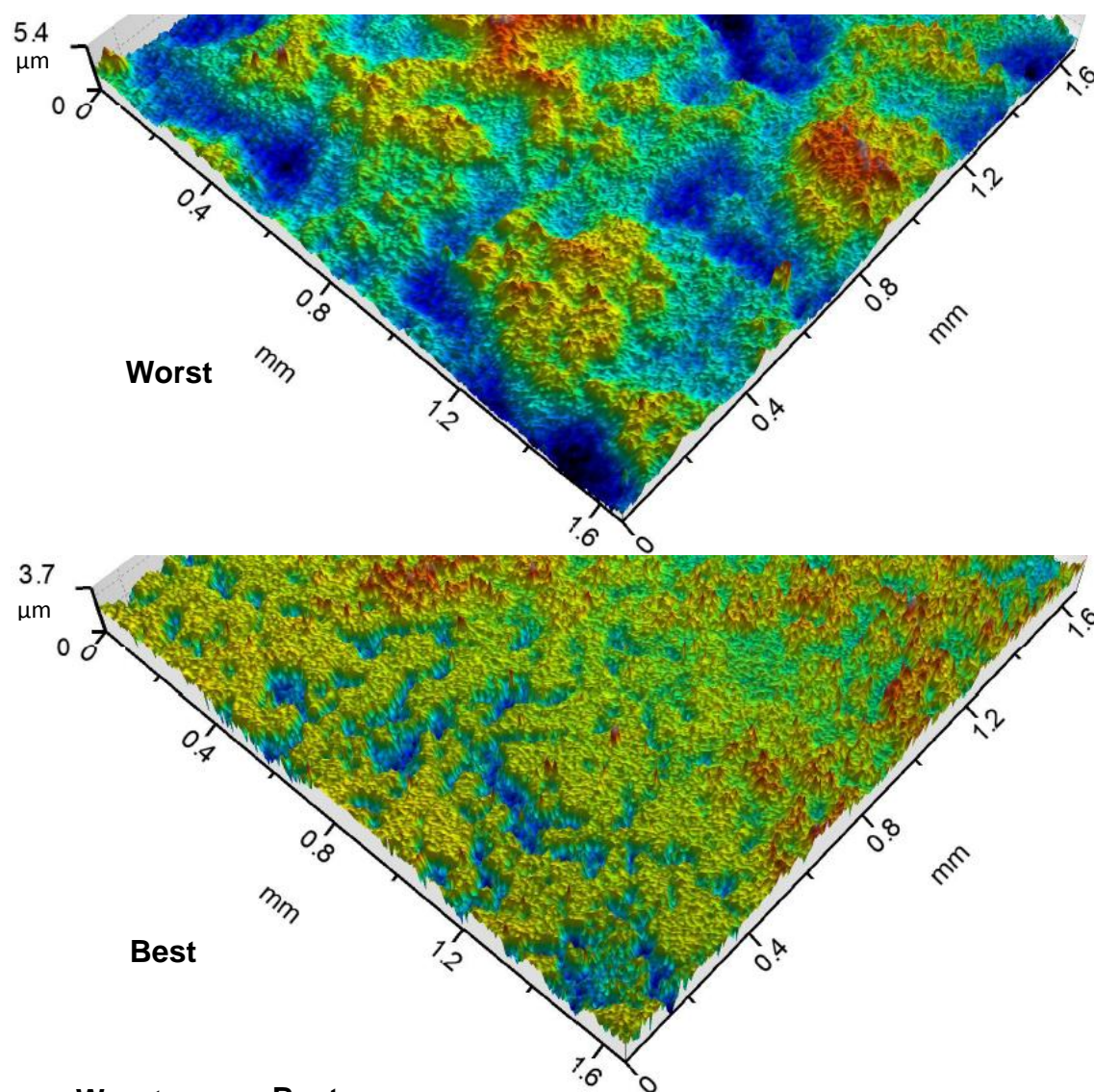
Phosphate



Worst		Best			
Sq	2.44	Sq	1.69	μm	Root mean square height
Ssk	0.382	Ssk	-0.423		Skewness
Sku	2.78	Sku	2.14		Kurtosis
Sp	8.40	Sp	4.26	μm	Maximum peak height
Sv	6.65	Sv	5.48	μm	Maximum pit height
Sz	15.0	Sz	9.74	μm	Maximum height
Sa	1.99	Sa	1.46	μm	Arithmetic mean height
Feature Parameters:		Feature Paramete			
Spc	1291	Spc	610	1/mm	pruning = 5% Arithmetic mean peak curvature
Spd	4291	Spd	1869	1/mm ²	pruning = 5% Density of peaks

Figure A2.2: Phosphate 3D Roughness for the best and worst conditions of rating (measured in the first step).

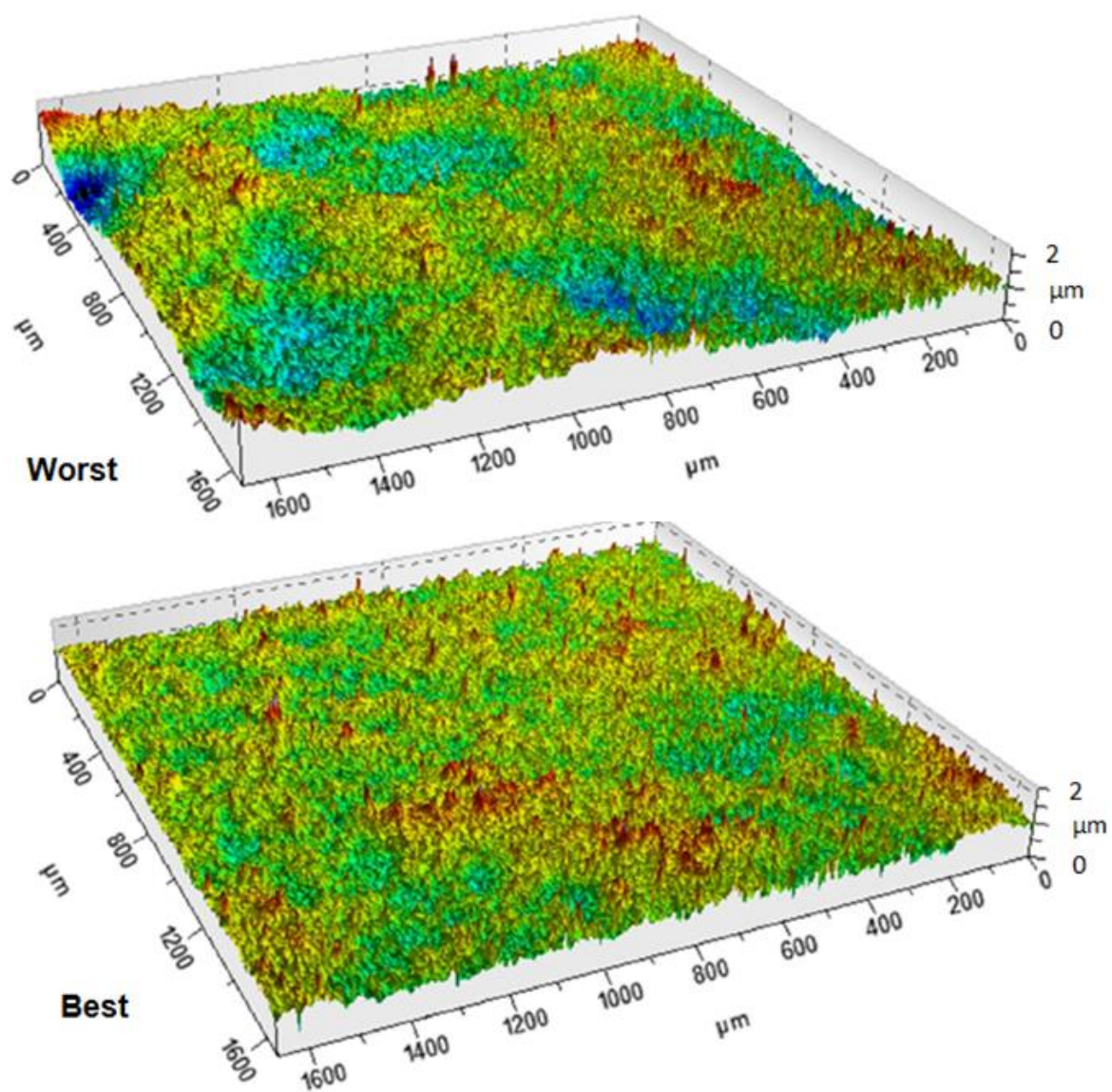
E coat



Worst		Best			
Sq	1.00	Sq	0.469	μm	Root mean square height
Ssk	0.482	Ssk	-0.363		Skewness
Sku	3.00	Sku	4.01		Kurtosis
Sp	3.37	Sp	1.95	μm	Maximum peak height
Sv	2.07	Sv	1.75	μm	Maximum pit height
Sz	5.44	Sz	3.70	μm	Maximum height
Sa	0.804	Sa	0.359	μm	Arithmetic mean height
Feature Parameters		Feature Parameters			
Spc	210	Spc	279	1/mm	pruning = 5% Arithmetic mean peak curvature
Spd	1579	Spd	4925	1/mm ²	pruning = 5% Density of peaks

Figure A2.3: E coat 3D Roughness for the best and worst conditions of rating (measured in the first step).

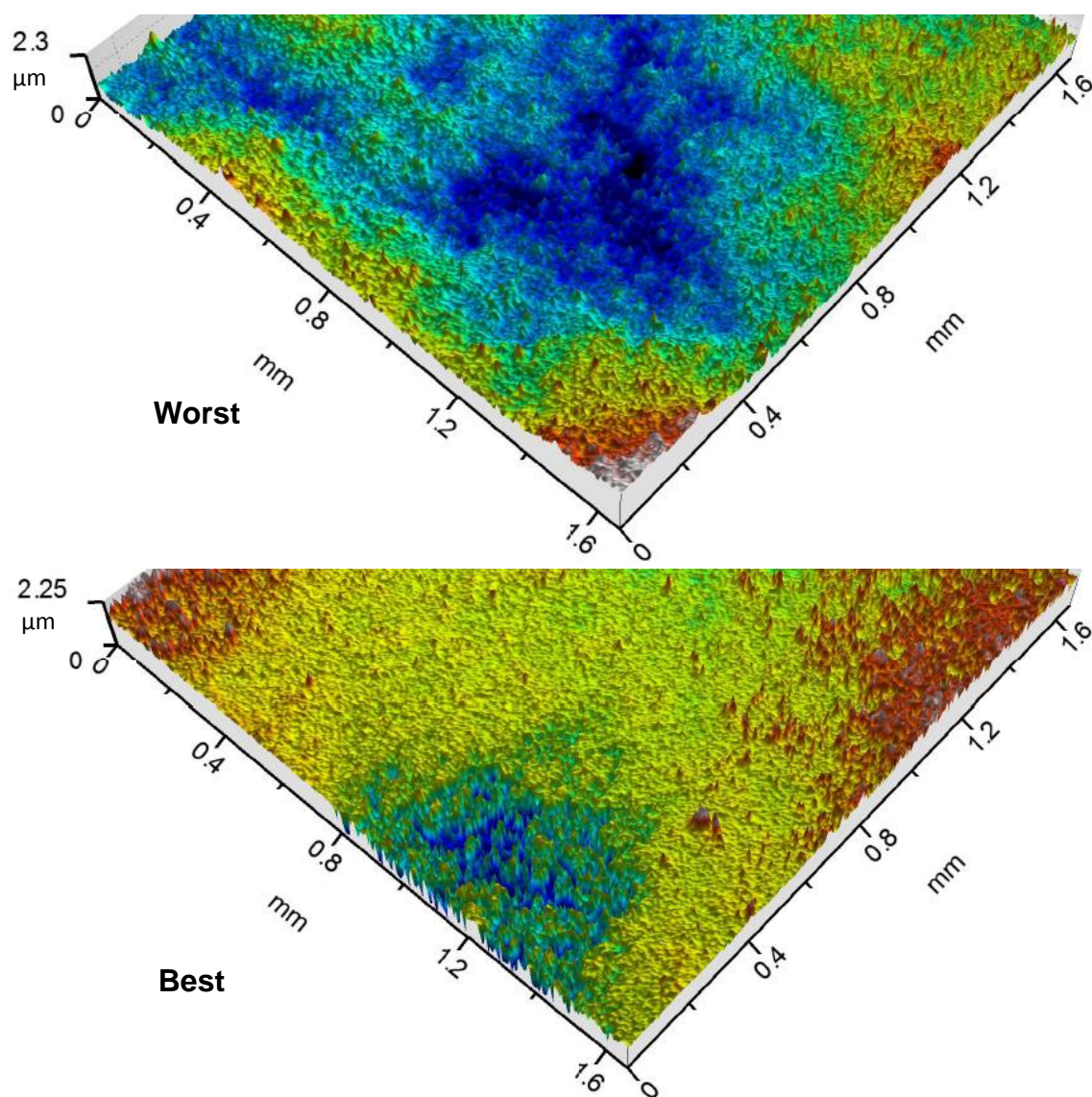
Primer



Worst		Best			
Sq	0.2302	Sq	0.1617	μm	Root mean square height
Ssk	-0.2112	Ssk	0.4663		Skewness
Sku	4.731	Sku	4.741		Kurtosis
Sp	2.244	Sp	1.730	μm	Maximum peak height
Sv	1.966	Sv	2.470	μm	Maximum pit height
Sz	4.210	Sz	4.200	μm	Maximum height
Sa	0.1781	Sa	0.1248	μm	Arithmetic mean height
Spd	0.001506	Spd	0.001342	$1/\mu\text{m}^2$	pruning = 5% Arithmetic mean peak curvature
Spc	0.1892	Spc	0.1913	$1/\mu\text{m}$	pruning = 5% Density of peaks

Figure A2.4: Primer 3D Roughness for the best and worst conditions of rating (measured in the first step).

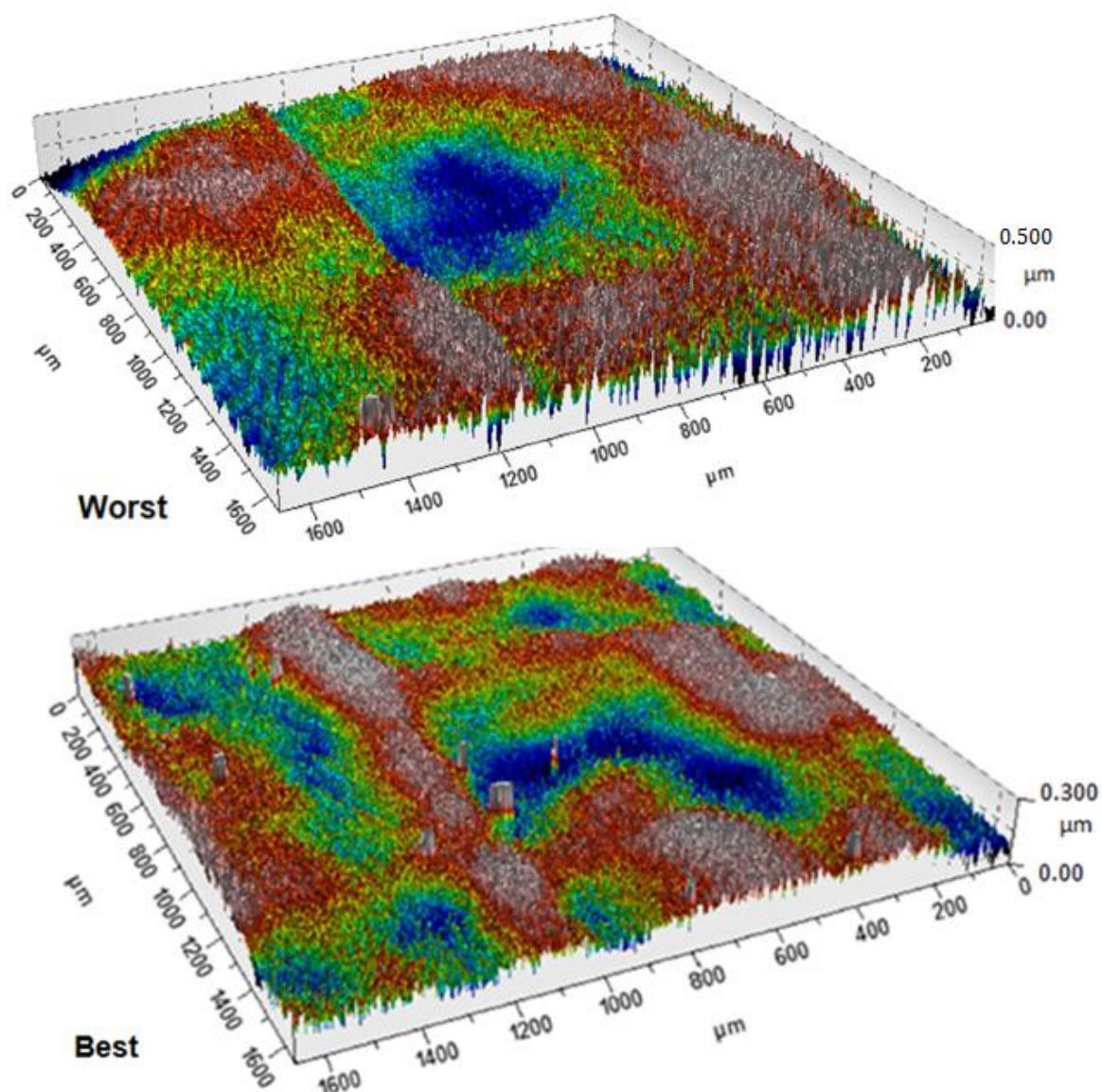
Base coat



Worst		Best			
Sq	0.382	Sq	0.307	μm	Root mean square height
Ssk	0.423	Ssk	-0.543		Skewness
Sku	2.92	Sku	5.71		Kurtosis
Sp	1.53	Sp	1.06	μm	Maximum peak height
Sv	0.817	Sv	1.20	μm	Maximum pit height
Sz	2.35	Sz	2.25	μm	Maximum height
Sa	0.318	Sa	0.210	μm	Arithmetic mean height
Feature Paramete		Feature Paramete			
Spc	64.9	Spc	126	1/mm	pruning = 5% Arithmetic mean peak curvature
Spd	2121	Spd	3258	1/mm ²	pruning = 5% Density of peaks

Figure A2.5: Base coat 3D Roughness for the best and worst conditions of rating (measured in the first step).

Clear coat



Worst		Best			
Sq	0.1088	Sq	0.0589	μm	Root mean square height
Ssk	0.3818	Ssk	11.70		Skewness
Sku	11.58	Sku	382.5		Kurtosis
Sp	2.602	Sp	3.102	μm	Maximum peak height
Sv	1.361	Sv	0.8950	μm	Maximum pit height
Sz	3.963	Sz	3.997	μm	Maximum height
Sa	0.08231	Sa	0.03696	μm	Arithmetic mean height
Spd	0.001333	Spd	1.316e-005	1/μm ²	pruning = 5% Arithmetic mean peak curvature
Spc	0.1843	Spc	0.2856	1/μm	pruning = 5% Density of peaks

Figure A2.6: Clear coat 3D Roughness for the best and worst conditions of rating (measured in the first step).

ATTACHMENT 1: THE SURFACE TEXTURE

In the following, table A1.1 shows the summary of the 2D and 3D roughness parameters which will be explained in detail in the next pages of this attachment.

Table AT1.1: INDEX

	Symbol	Parameter Name	unity	Standard (Term and definitions)	Standard (Measurement procedure)
2D	Pc	Peak Density	Peaks / cm	ANSI/ASME B46.1-2002 "Surface Texture (Surface Roughness, Waviness and Lay)," American Society of Mechanical Engineers, 2002.	SEP 1940
	Ra	Average Roughness	μm	ISO 4287:1997 "Geometrical Product Specifications (GPS) - Surface texture: Profile method - Terms, definitions and surface texture parameters"	
	Rq	Root Mean Square Roughness	μm		
	Rz	Average Maximum Height of the Surface	μm		
3D	Sa	Average Roughness	μm		ISO 25178-2:2009 "Geometrical product specifications (GPS) – Surface texture: Areal Part 2 Terms, definitions and surface texture parameters.
	Sq	Root Mean Square Roughness	μm		
	Sp	Maximum Peak Height	μm		
	Spc	Arithmetic mean peak curvature	$1 / \mu\text{m}$		
	Spd	Density of peaks	$1000 / \text{mm}^2$		
	Sz	Maximum Height of Surface	μm		
	Sk	Core Roughness Depth	μm		
	Smr2	Peak Valley Portion	%		
	Sha	Mean hill area	mm^2		
	Vv	Void Volume	$\text{mm}^3 / \text{mm}^2$		
	Vw	Dale Void Volume	ml / m^2		
	Vvc	Core Void Volume	ml / m^2		
	Vmp	Peak Material Volume	ml / m^2		
	Vmc	Core Material Volume	ml / m^2		
aclm	Maximum closed void area ratio	%	M. Geiger, U. Engel, M. Pfestorf - New developments for the qualification of technical surfaces in forming processes-Annals of the CIRP vol.46/1/1997, pp.171-174, 1997.		
Vcl	Closed void volume	mm^3 / m^2			
Cclm	Distance from highest peak to aclm	μm			

The explanations below have been extracted from the following literature:

1 - http://www.michmet.com/Texture_parameters.htm. Accessed on 09/23/13.

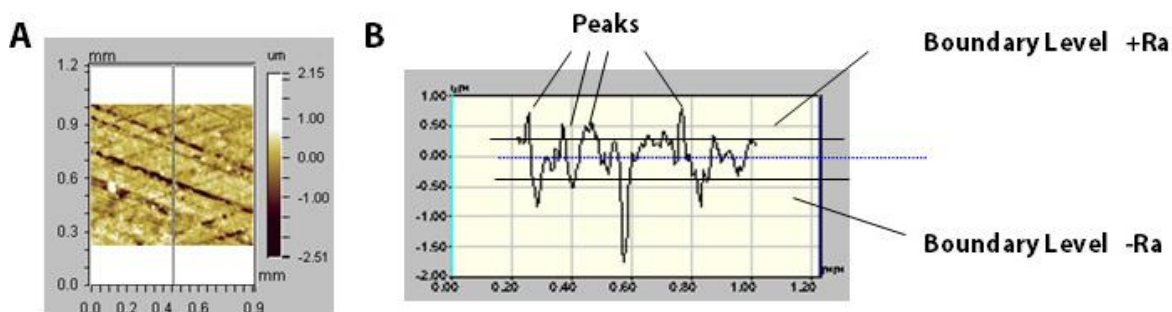
2 - STAEVES, J. **Beurteilung der Topografie von Blechen im Hinblick auf die Reibung bei der Umformung.** 1998. Vortrag zur Dissertation. Technische Universität Darmstadt. Institut für Produktionstechnik und Umformmaschinen. Tag der mündlichen Prüfung: 09.09.1998

3 - GEIGER, M.; ENGEL, U.; PFESTORF, M.. **New developments for the qualification of technical surfaces in forming processes.** Annals of CIRP, v. 46, n.1, p. 171–174, 1997

4 - ISO 25178-2; SEP 1940; ANSI/ASME B46.1; ISO 4287.

2D parameters

Pc is the peak density along profile, and determines the number of peaks per unit length. A peak for the Pc calculations is defined as when the profile intersects consecutively a lower and upper boundary level set at a height above and depth below the mean line, equal to **Ra** for the profile being analyzed.



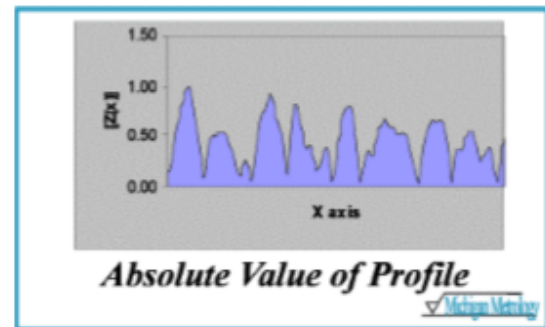
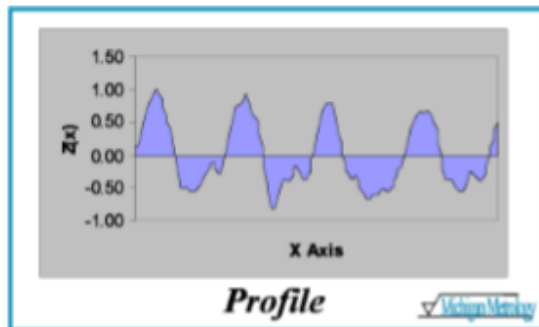
The contour plot (A) shows a line through the center over which the profile (B) is selected to determine Pc..

Application

Pc is useful parameter for assessing the peak density (e.g. peaks/mm) along a given direction. Applications involved in coating a surface, or when fluid leakage/retention is of issue may make use of the Pc parameters to optimize the surface texture design. Sometimes the combination of parameters such as Rz with Pc will yield additional information about the spacing and depth of dominant surface features that may affect the function of a component. This parameter is often used where control of surface coating adhesion is required. When used by the sheet steel industry it is a good parameter for controlling characteristics related to bending, forming, painting and rolling.

Ra, the roughness average, is the arithmetic average of the absolute values of the surface height deviations measured from the best fitting plane, cylinder or sphere. Ra is described by:

$$R_a = \int_a \int_b |f(x, y)| dx dy$$



Note: Profiles are shown above for simplicity. When evaluating the 3D parameters the various surface functions are understood to apply to the complete 3D dataset.

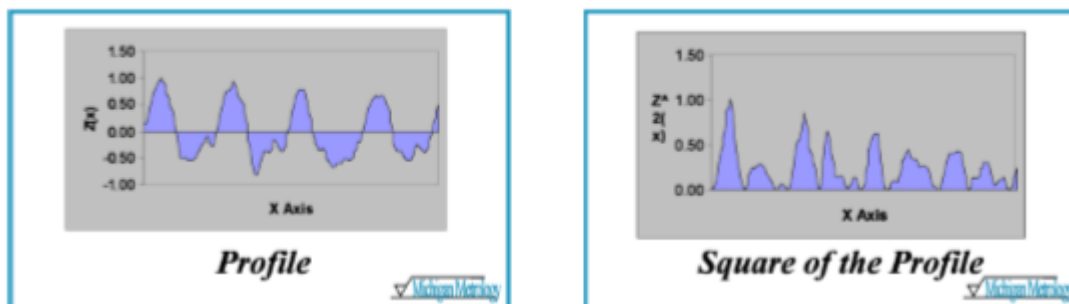
Application

Historically, R_a was one of the first parameters used to quantify surface texture. Most surface texture specifications include R_a either as a primary measurement or as a reference. Unfortunately, R_a may be misleading in that many surfaces with grossly different features (e.g., milled vs. honed) may have the same R_a , but function quite differently.

R_a only quantifies the “absolute” magnitude of the surface heights and is insensitive to the spatial distribution of the surface heights. R_a is also insensitive to the “polarity” of the surface texture in that a deep valley or a high peak will result in the same R_a value. Despite its shortcomings, once a process for forming a surface has been established, R_a may be used as a good monitor as to whether something may have changed during subsequent production of the surface.

R_q , the root mean square (rms) roughness is the rms (standard deviation) or “first moment” of the height distribution, as described by:

$$Rq = \sqrt{\int_a^b \int_c^d (z(x,y))^2 dx dy}$$

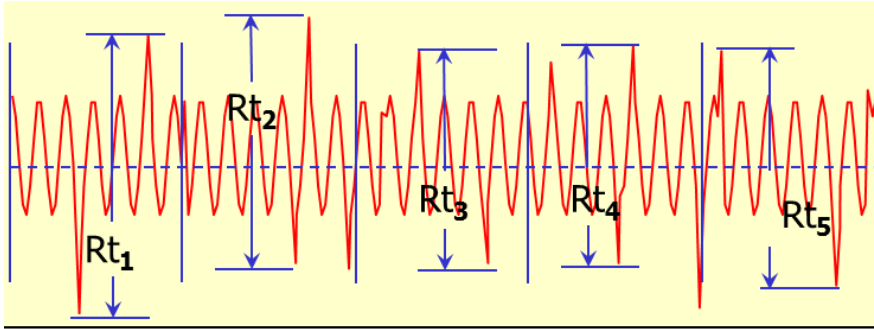


Note: Profiles are shown above for simplicity. When evaluating the 3D parameters the various surface functions are understood to apply to the complete 3D dataset.

Application

Rq, or the rms of the surface distribution, is very similar to Ra and will usually correlate with Ra. Since the surface heights are “squared” prior to being integrated/averaged, peaks and valleys of equal height/depth are indistinguishable. As for Ra, a series of high peaks or a series of deep valleys of equal magnitude will produce the same Rq value. The Rq value is also insensitive to the spatial distribution of the surface heights, in that two very high peaks will contribute the same to Rq whether the peaks are close to each other or separated over the measurement field. The Rq parameter is typically used in the optics industry for specifying surface finish, since various optical theories relating the light scattering characteristics of a surface to Rq have been developed.

Rz (ISO) is the Maximum Height of Profile. Mathematically, the highest Peak to Valley within a Sampling Length - usually analysed as a mean over a minimum of 5 Sampling Lengths.



Also known in the past as $Rz(din)$, Rz , Ry and Rtm .

Application:

This parameter has similar uses to the Rt parameter but is a little more stable as it has averaging involved when assessed over a number of Sampling Lengths. Rz is an alternative to Rt as a controlling parameter.

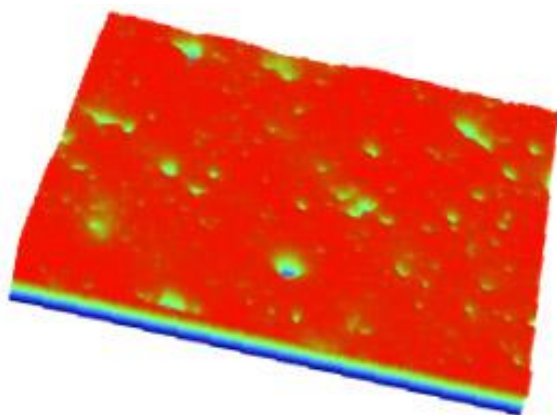
Limitations: This is the most commonly used height parameter and gives a fairly stable reading but can be influenced by dirt in the positive direction and deep scratches in the negative direction. $Rz = R_p + R_v$ (ISO 4287 - 1997 terminology) over 1 Sampling Length.

3D parameters

Sa and **Sq** are the Average Roughness and Root Mean Square Roughness are evaluated over the complete 3D surface respectively. Mathematically, Sa and Sq are evaluated as follows:

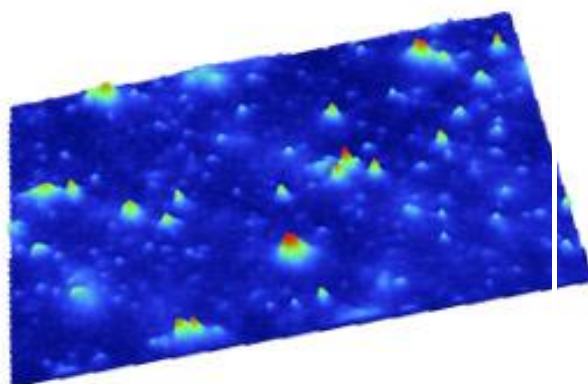
$$S_a = \iint_a |Z(x, y)| dx dy$$

$$S_q = \sqrt{\iint_a (Z(x, y))^2 dx dy}$$



Plateau-like surface

Sa = 16.03 nm Sq= 25.4 nm



Surface with Peaks

Sa = 16.03 nm Sq= 25.4 nm

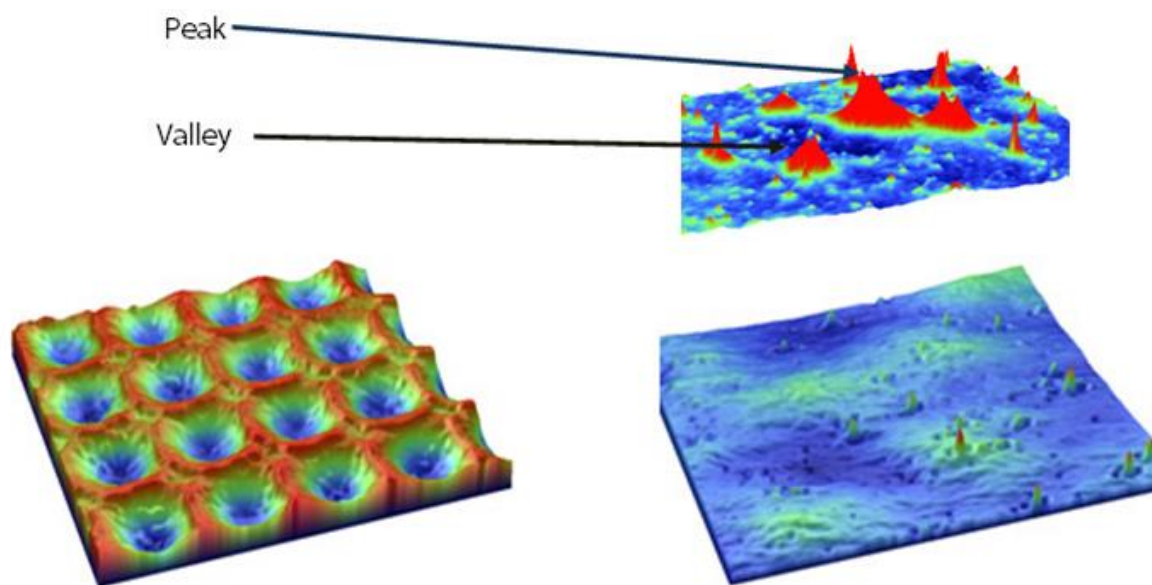
Application

The Sa and Sq parameters represent an overall measure of the texture comprising the surface. Sa and Sq are insensitive in differentiating peaks, valleys and the spacing of the various texture features. Thus Sa or Sq may be misleading in that many surfaces with grossly different spatial and height symmetry features (e.g., milled vs. honed) may have the same Sa or Sq, but function quite differently. The figure above demonstrates two very different surfaces with identical Sa and Sq values, indicating the insensitivity of the Sa and Sq parameters. Nonetheless, once a surface type has been established, the Sa and Sq parameters may be used to indicate significant deviations in the texture characteristics. Sq is typically used to specify optical surfaces and Sa is used for machined surfaces.

Sp (Max Peak Height), Sv (Max Valley Depth) and Sz (Max Height of Surface)

Sp, **Sv**, and **Sz** are parameters evaluated from the absolute highest and lowest points found on the surface. Sp, the Maximum Peak Height, is the height of the highest point, Sv, the Maximum Valley Depth, is the depth of the lowest point (expressed as a negative number) and Sz the Maximum Height of the Surface, is found from $Sz = Sp - Sv$.

Note: earlier standards referred to Rz as an average of the 10 highest to 10 Lowest Points and other variations. The ISO community agreed for the newer standard, ISO 25178-2 to establish Sz as strictly the peak to valley height over an areal measurement.



A surface used in the printing industry characterized by deep valley structures with Sv being $\sim -15\mu\text{m}$

A polymer surface prepared with asperities as measured by Sp being $\sim 0.90\ \mu\text{m}$

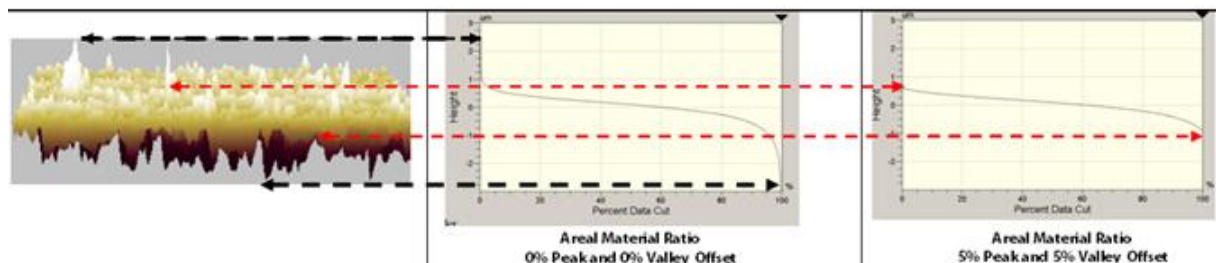
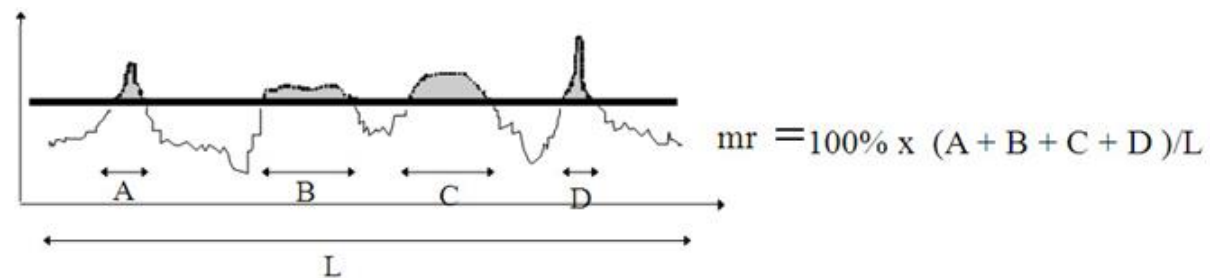
Application

Since Sp, Sv, and Sz are found from single points, they tend to result in unrepeatable measurements. Thus when using these three parameters, one must properly set spatial filtering bandwidths to eliminate erroneous peaks/valleys and average multiple measurements at random locations along the sample, to obtain a statistically significant result. Typical applications for Sz may include sealing surfaces and coating applications. Sp may find application when considering surfaces that will be used in a sliding contact application. Sv may find application when valley depths relating to fluid retention may be of concern such as for lubrication and coating systems.

mr (Material Ratio)

The Material Ratio, mr , is the ratio of the intersecting area of a plane (i.e. parallel to the mean plane) passing through the surface at a given height to the cross sectional area of the evaluation region. The Areal Material Ratio Curve (Bearing Area Curve or **Abbot Firestone Curve**) is established by evaluating mr at various levels from the highest peak to the lowest valley.

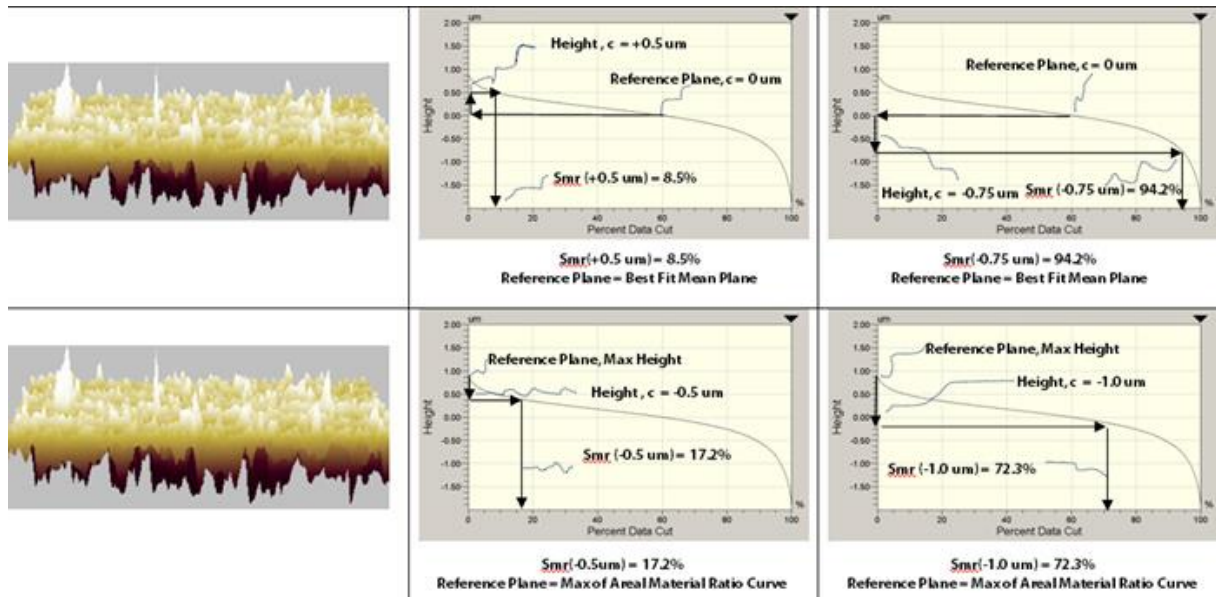
Prior to establishing the Areal Material Ratio Curve, a certain percentage of the peak points (i.e., the peak Offset) and valley points (i.e., the Valley Offset) are eliminated to minimize the effects of outliers. Typically the *Peak Offset* and *Valley Offset* are set to 1%, unless otherwise specified. mr is also referred to as “Percent Data Cut.”



Areal Material Ratio Curve and evaluation of mr . Note that the profiles is shown above for simplicity. When evaluating the 3D (Areal) parameters the analysis applies to the complete 3D dataset.

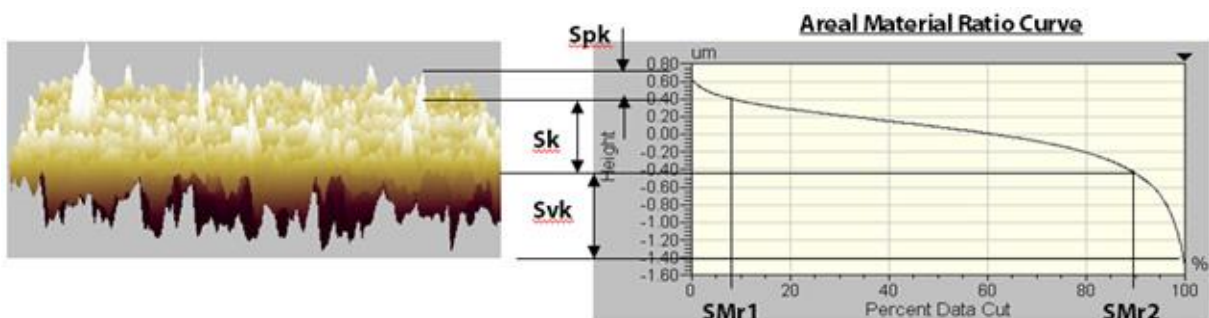
$Smr(c)$ (Areal Material Ratio)

The Areal Material Ratio, $Smr(c)$ is the ratio (expressed as a percentage) of the cross sectional area of the surface at a height (c) relative to the evaluation cross sectional area. The height (c) may be measured from the best fitting least squares mean plane or as a depth down from the maximum point of the Areal Material Ratio Curve.



Spk (Reduced Peak Height), **Sk (Core Roughness Depth)**, Svk (Reduced Valley Depth), SMr1 (Peak Material Portion), **SMr2 (Peak Valley Portion)**

The parameters Spk, Sk, Svk, SMr1, and SMr2 are all derived from the Areal Material Ratio curve based on the ISO 13565-2:1996 standard. The Reduced Peak Height, Spk, is a measure of the peak height above the core roughness. The Core Roughness Depth, Sk, is a measure of the “core” roughness (peak-to-valley) of the surface with the predominant peaks and valleys removed. The Reduced Valley Depth, Svk, is a measure of the valley depth below the core roughness. SMr1, the Peak Material Portion, indicates the percentage of material that comprises the peak structures associated with Spk. The Valley Material Portion, SMr2, relates to the percentage (i.e., $100\% - \text{SMr2}$) of the measurement area that comprises the deeper valley structures associated with Svk.



Application

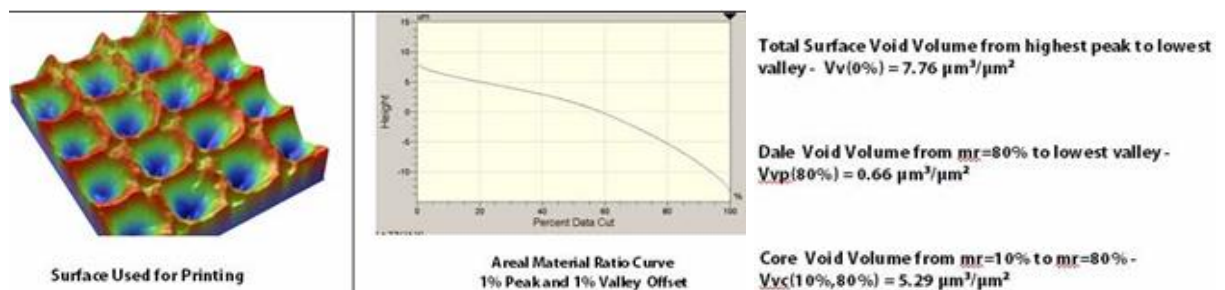
A large Spk implies a surface composed of high peaks providing small initial contact area and thus high areas of contact stress (force/area) when the surface is contacted. Thus Spk may represent the nominal height of the material that may be removed during a running-in operation. Consistent with Spk, SMr1 represents the percentage of the surface that may be removed during running-in. Sk represents the core roughness of the surface over which a load may be distributed after the surface has been run-in. Svk is a measure of the valley depths below the core roughness and may be related to lubricant retention and debris entrapment. Sk is a measure of the nominal roughness (peak to valley) and may be used to replace parameters such as Sz when anomalous peaks or valleys may adversely affect the measurement.

Vv(mr) (Void Volume), Vvv(p) (Dale Void Volume), Vvc(p,q) (Core Void Volume)

Vv(mr), the Void Volume, is the volume of space bounded by the surface texture from a plane at a height corresponding to a chosen “mr” value to the lowest valley. “mr” may be set to any value from 0% to 100%.

Vvv(p), the Dale Void Volume, is the volume of space bounded by the surface texture from a plane at a height corresponding to a material ratio (mr) level, “p” to the lowest valley. The default value for “p” is 80% but may be changed as needed.

Vvc(p,q), The Core Void Volume, is the volume of space bounded by the texture at heights corresponding to the material ratio values of “p” and “q”. The default value for “p” is 10% and the default value for “q” is 80%.



Example of Void, Dale Void, and Core Void volumes. Note: The units for the Vv(mr), Vv(p) and Vvc(p,q) are $\mu\text{m}^3/\mu\text{m}^2$ - the void volume normalized by the cross sectional area of the measurement area. The peak offsets and valley offsets are applied prior to analysis.

Application

Vv(mr), Vvv(p) and Vvc(p,q) all indicate a measure of the void volume provided by the surface between various heights as established by the chosen material ratio(s) values. Thus these three void volume parameters indicate how much fluid would fill the surface (normalized to the measurement area) between the chosen material ratio values. For example, a $Vv(25\%) = 0.5 \mu\text{m}^3/\mu\text{m}^2$ in (note how the units $\mu\text{m}^3/\mu\text{m}^2$ reduce to μm) that a 0.5 μm thick film over the measurement area would provide the same volume of fluid as needed to fill the measured surface from a height corresponding to $mr=25\%$ to the lowest valley.

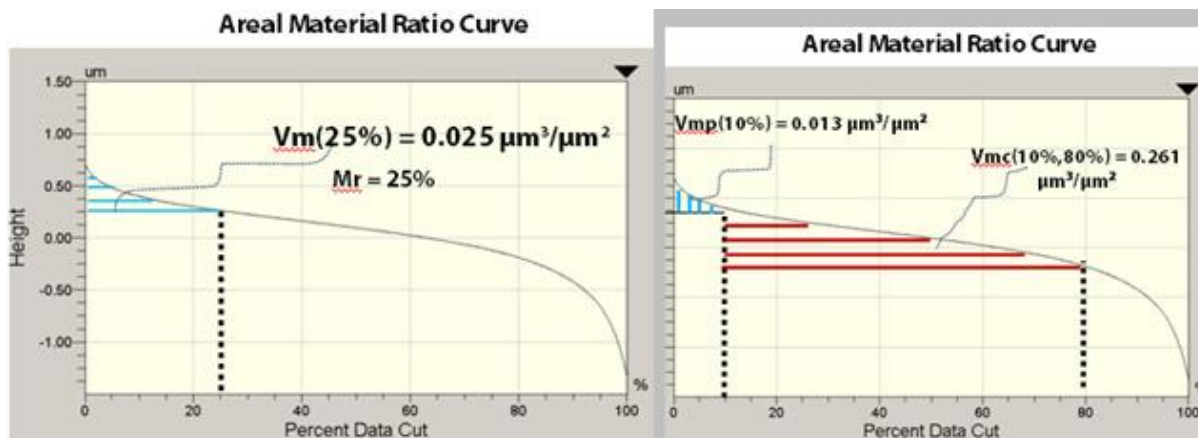
The void volume parameters are useful when considering fluid flow, coating applications and debris entrapment. A new surface may be specified by $Vv(0\%)$ which would indicate the total initial void volume provided by the texture. The Core Void Volume, Vvc , may be useful to establish how much core space is available once a surface has been run-in resulting in decreased peak heights. The Dale Void Volume, $Vvv(p)$ may be useful in indicating the potential remaining volume after significant wear of a surface has resulted.

Vm(mr) (Material Volume) , Vmp(p) (Peak Material Volume), Vmc(p,q) (Core Material Volume)

Vm(mr), the Material Volume, is the volume of material comprising the surface from the height corresponding to mr to the highest peak of the surface. “ mr ” may be set to any value from 0% to 100%.

Vmp(p), the Peak Material Volume, is the volume of material comprising the surface from the height corresponding to a material ratio level, “ p ”, to the highest peak. The default value for “ p ” is 10% but may be changed as needed.

Vmc(p,q), the Core Material Volume, is the volume of material comprising the texture between heights corresponding to the material ratio values of “ p ” and “ q ”. The default value for “ p ” is 10% and the default value for “ q ” is 80% but may be changed as needed.



Note: The units for the $V_v(mr)$, $V_v(p)$ and $V_v(c,p,q)$ are $\mu\text{m}^3/\mu\text{m}^2$ - the void volume normalized by the cross sectional area of the measurement area. The peak offsets and valley offsets are applied prior to analysis.

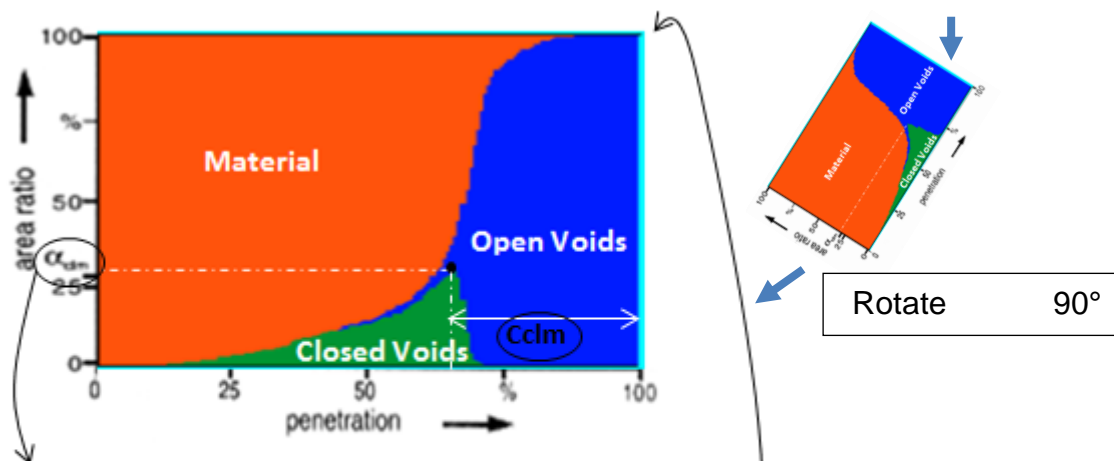
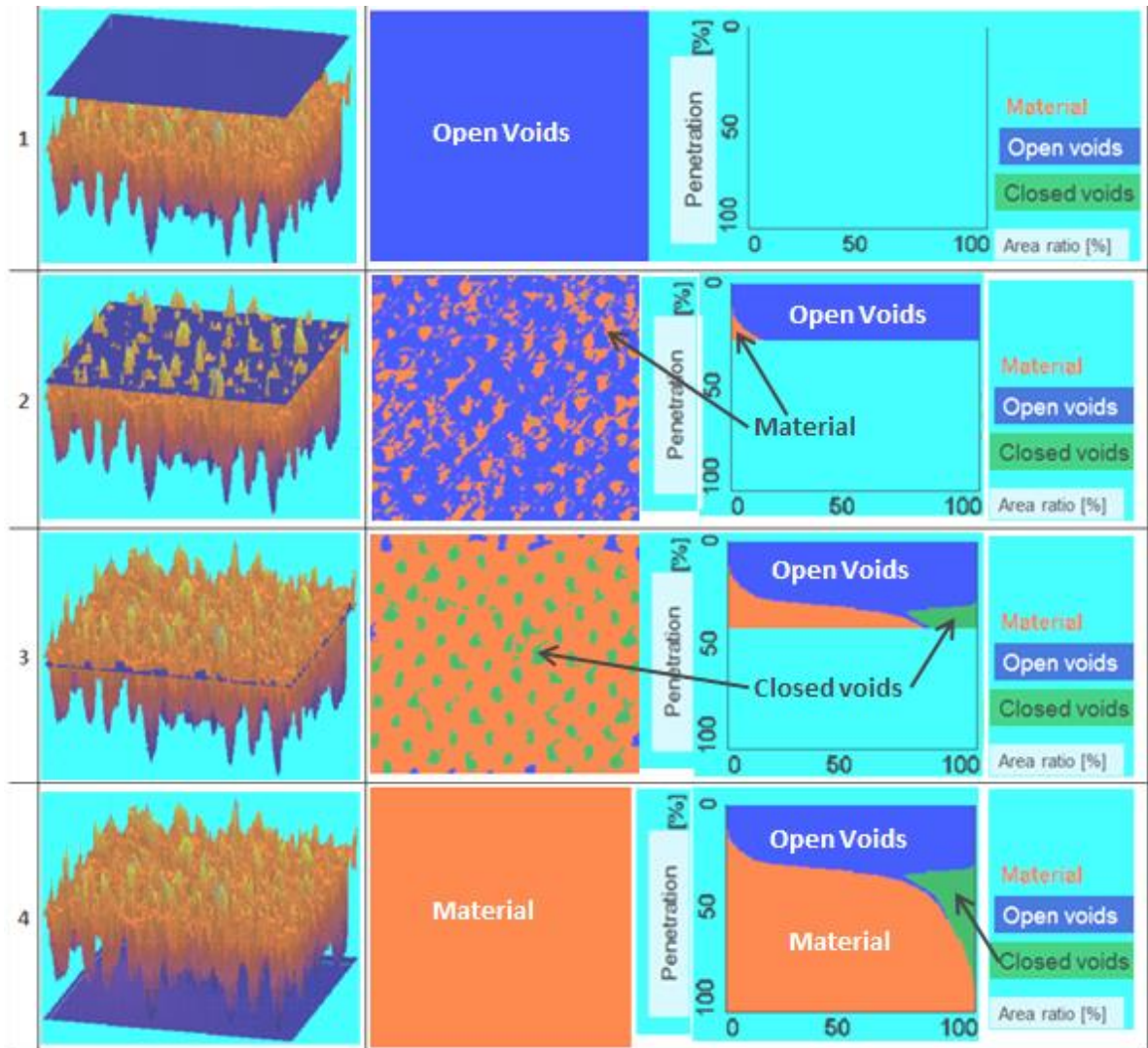
Application

$V_m(mr)$, **$V_m(p)$** and **$V_m(c,p,q)$** all indicate a measure of the material forming the surface at the various heights down from the highest peak of surface or between various heights as defined for $V_m(c,p,q)$.

For example, a $V_m(10\%) = 0.35 \mu\text{m}^3/\mu\text{m}^2$ would indicate (note how the units $\mu\text{m}^3/\mu\text{m}^2$ reduce to μm) that a layer $0.35 \mu\text{m}$ thick of material over the measured cross section would account for all the material from the highest peak to the 10% point on the bearing area curve.

The various Material Volume parameters are useful to understand how much material may be worn away for a given depth of the bearing curve (i.e. $V_m(p)$) and how much material is available for load support once the top levels of a surfaces are worn away (i.e. $V_m(c,p,q)$). For sealing applications, $V_m(p)$ may provide insight into the amount of material available for seal engagement whereas **$V_v(c,p,q)$** (see above) may then provide information about the resulting void volume for fluid entrapment or leakage.

α_{clm} is maximum closed void area ratio (%) and **C_{clm}** is the distance of the highest peak or the Peak Offset to α_{clm} (μm). **V_{cl}** is the closed void volume (mm^3 / m^2) (represented by the green area).



α_{cfm} : Maximum closed void area ratio
 C_{cfm} : Distance (μm) from highest peak to α_{cfm}
 V_{cl} : Closed void volume

Application

Typical examples for these 3D- characteristics are lubricant pockets in the sheet metal surface. It is essential to understand and control the lubrication phenomena on forming processes in order to reduce friction and improve the resulting surface quality.

Spd, Peak density. It is the number of peaks per area. ISO 25178

Application

It is very used to control de quality of steel sheets regarding paint appearance.

Spc, It is the arithmetic mean peak curvature. ISO 25178

Application

Peak curvature, plasticity and elasticity: More accurate calculation of peak curvature has implications in the study of plasticity and elasticity. When a peak with small curvature is in contact with another surface it is likely to be eroded or plastically deformed, whereas a peak with large curvature will provide an elastic contact with a greater surface area.

ATTACHMENT 2: LIST OF EQUIPMENTS

A2.1: RUGOSIMETER 2D.....	240
A2.1.1: RUGOSIMETER 2D: Form Talysurf Intra.....	240
A2.1.2: RUGOSIMETER 2D: Surtronic 3+	241
A2.2: RUGOSIMETER 3D.....	242
A2.2.1: RUGOSIMETER 3D: μ surf basic	242
A2.2.2: RUGOSIMETER 3D: Talysurf CCI	243
A2.2.3: RUGOSIMETER 3D: New View 7300	244
A2.2.4: RUGOSIMETER 2D (without contact) SRM 100: Online.	245
A2.3: WAVE SCAN	246
A2.4: MICRO-WAVE SCAN	247
A2.5: GLOSSMETER	248
A2.6: QUANTUMX MX460	249
A2.7: LVDT.....	250

AT2.1.1: RUGOSIMETER 2D: Form Talysurf Intra

Used for simultaneous measurement of dimension, form and surface roughness.



Horizontal Performance		Environment notes
Traverse length - X Min / Max	0.1mm to 50mm (0.004in to 1.97in)	Storage temperature 5°C to 40°C (41°F to 104°F)
Traverse / measuring speeds	10mm/s (0.39in/s) max - 1mm/s (0.039in/s)	Storage humidity 10% to 80% Relative, non condensing
Data sampling interval in X	0.5µm (20µin)	Operating temperature 15°C to 30°C (59°F to 86°F)
Straightness error (Pt) ¹	0.4µm over 50mm (16µin over 1.96in) 0.2µm over any 20mm (8µin over any 0.78in)	Temperature gradient < 2°C (< 3.6°F) per hour
Vertical Performance		Operating humidity 45% to 75% Relative, non condensing
Nominal measuring range (Z) ²	1mm (0.04in)	Maximum RMS floor vibration 2.5µm/s (100µin/s) at < 50Hz 5.0µm/s (200µin/s) at > 50Hz
Resolution (Z) ²	16nm @ 1mm range (0.63µin @ 0.04in) 3nm @ 0.2mm range (0.12µin @ 0.008in)	Electrical supply 110 / 220 / 240V - 50 / 60 Hz
Range to resolution ratio	65,536 : 1	Power consumption 10VA traverse unit / 18VA processor
Stylus arm length, tip size, force	60mm arm, 2µm radius conisphere diamond stylus, 1mN force	Safety EN 61010 - 1 : 2001
System Performance ²		EMC EN 61000 - 6 - 4 : 2001 EN 61000 - 6 - 1 : 2001
Spherical calibration artifact	12.5mm (0.49in) nominal radius	Note: Taylor Hobson pursues a policy of continual improvement due to technical develop- ments. We therefore reserve the right to deviate from catalog specifications.
Calibration uncertainty - Pt ³	< 0.25µm (10µin)	
Radius measurement uncertainty ⁴	0.1 - 12.5mm (0.004 - 0.5in) = 2% to 0.04% of nominal 12.5 - 25mm (0.5 - 1in) = 0.04% of nominal 25 - 1000mm (1 - 39.4in) = 0.04% to 0.2% of nominal	
Angle measurement uncertainty ⁵	within 1% of measured angle (+ / - 35° maximum range)	
Parameter height uncertainty	within 2% + 6nm (0.24µin) (peak parameters only)	
Dimensions L x D x H	Traverse unit - 343 x 116 x 160mm (13.5 x 4.6 x 6.3in) Control module - 285 x 200 x 80mm (11.2 x .9 x 3.2in)	
Weight	Traverse unit - 4.9Kg (10.8lbs) Control module - 1.9Kg (4.2lbs)	
Analysis		
Primary parameters	Pa, Pc, Pda, Pdc*, Pdq, PHSC*, Pku, Pln, Plo, Plq, Pmr(c)* , Pmr* Pp, Ppc*, Pq, PS, Psk, Psm, Pt, Pv, Pvo*, Pz, Pz(JIS)	Analysis and parameter notes: Pass / Fail tolerances All parameters can be assigned nominal, minimum and maximum values.
Roughness parameters	R3y, R3z, Ra, Rc, Rda, Rdc*, Rdq, RHSC*, Rku, Rln, Rlo, Rlq Rmr(c)* , Rmr*, Rp, Rp1max , Rpc*, Rq, RS, Rsk, RSm, Rt, Rv Rvo*, Rv1max , Rz, Rz(DIN), Rz(JIS), Rz1max	* Qualifiers All parameters marked with an asterisk are suitable for user assigned single or multiple qualifiers. For example, material ratio (mr) may be assessed at one or more slice levels within a single measurement.
Waviness parameters	Wa, Wc, Wda, Wdc*, Wdq, WHSC*, Wku, Wln, Wlo, Wlq, Wmr(c)* Wmr*, Wp, Wpc*, Wq, WS, Wsk, Wsm, Wt, Wv, Wvo*, Wz	Ultra software parameters Parameters highlighted in bold are available only with PC / Ultra based systems.
Rk Parameters	A1, A2, Mr1, Mr2, Rk, Rpk, Rvk	ISO standards Where applicable, parameters conform to and are named as per ISO standards, 4287-1997, 13565-1-2 and 12085.
R + W Parameters	AR, AW, Pt, R, Rke , Rpke , Rvke , Rx, Sar, Saw, Sr, Sw, W, Wte, Wx	
Dimension parameters	Slope, Datum slope, Delta slope, Intercept X / Intercept Z	
Filters / bandwidths	Gaussian, ISO 2CR, 2CR PC / 30:1, 100:1, 300:1	
Cut-offs	0.08, 0.25, 0.8, 2.5 and 8mm (0.003, 0.010, 0.03, 0.1 and 0.3in)	

Further details available on:

http://www.taylorhobson.com.br/pdf/105_espec.pdf. Accessed on 09/22/13.

AT2.1.2: RUGOSIMETER 2D: Surtronic 3+

Used for simple roughness parameters.



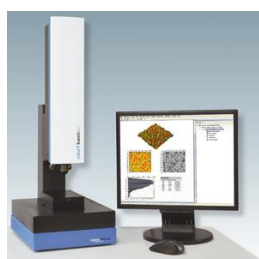
Pick-up	
Gauge range	300 μ m (0.012in)
Resolution	0.01 μ m (0.04 μ in)
Accuracy	2% of reading + LSD μ m
Pick up type	Inductive
Gauge force	150-300mg
Diamond stylus	Tip radius 5 μ m (200 μ in) unless otherwise specified
Instrument	
Cut off value	0.25, 0.8, 2.5, 8mm (0.01, 0.03, 0.1, 0.3in)
Filter	2CR or gaussian (selectable)
Traverse length	0.25-25mm (0.01-0.98in)
Traverse speed	1mm/sec (0.04in/sec)
Display units	μ m / μ in
Data output	RS232
Power	9V battery or mains (optional)

Further details available on:

http://www.taylorhobson.com.br/pdf/5_espec.pdf. Accessed on 09/22/13.

AT2.2.1: RUGOSIMETER 3D: μ surf basic

Surface topography is quantified using the internationally 3D roughness parameters



Hardware				
Image acquisition module	Fast digital camera with progressive scan technology, up to 55 fps, 512x512 Pixel, 10 bit, firewire			
Light Source	High efficiency LED ($\lambda = 505 \text{ nm}$), MTBF: 50,000 h			
x,y-axis module MN 50	Precision positioning module, x,y-table, 50x50 mm ²			
z-axis module MN 35	Precision scanning module, range: 35 mm			
z-axis module NV 250	Fast precision scanning module (piezo), range: 250 μm , resolution: < 10 nm			
Peripherals & controller	PC/ notebook/tablet pc, Windows XP professional, 4 GB RAM, firewire, DVD-RW incl. NeroExpress, ethernet, 3D navigator, integrated into space-saving rollable and transportable container			
Mounting hardware	Special feet for use on roll surfaces, for roll diameters > 200 mm			
Software				
μsoft control	NanoFocus measurement and analysis software, measurement control, setting of measurement parameters, analysis of 2D and 3D parameters in accordance with DIN EN ISO. Illustration: profiles, 2D view, 3D reconstruction, reflection image, confocal curve			
Stitching module	μ soft control plugin for extending the measurement field			
μsoft analysis (optional)	Software to analyse 3D measurement data, layout function, templates for series measurement and analysis			
Optic modules				
	1600 S	800 L, S, XS	320 L, S, XS	160 S
Magnification	10x	20x	50x	100x
Measuring field (μm)	1,600x1,600	800x800	320x320	160x160
Numerical aperture	0.3	0.4/0.45/0.6	0.5/0.8/0.95	0.9
Working distance (mm)	11.0	12.1/3.1/0.9	10.6/1.0/0.3	1.0
Resolution in z-direction (nm)	20	6/5/4	4/2/2	2
Resolution in x,y-direction (μm)	3.1	1.6	0.7	0.31
Allgemein				
File size/ file format	Size: single measurement approx. 0.8 MB format: NMS, OMS, ACII, SDF, TIF, BMP, X3P			
Typical measuring time	5-10 seconds, depending on the amount of confocal images			
Sample properties	Reflectivity: 1-100%, coated, non coated, reflective, diffuse			
Vibration	Isolation unnecessary for most measurements			
Power supply	90-265 V, Frequency 50-60 Hz, input < 50 W, optional: lead gel battery powered			
Cable length	Measurement device: 6 m, power cable 10 m (with internal cable reel)			
Weight/dimensions	Measurement device: 5.5 kg, 390x110x155 mm (lwxhx) rollable container: 25 kg, 460x360x700 mm (lwxhx)			
Miscellaneous	Protection class: IP 52			



Further details available on:

<http://www.nanofocus.com/products/usurf/usurf-basic/>. Accessed on 09/22/13.

Further details about this technology available on:

http://www.nanofocus.com/fileadmin/user_upload/Download-Dokumente/Broschueren_Flyer_E/NanoFocus_Technologybrochure_E_100412_web.pdf

AT2.2.2: RUGOSIMETER 3D: Talysurf CCI

Surface topography is quantified using the internationally 3D roughness parameters.



Talysurf CCI Lite System Specifications	
Measurement technique	Coherence Correlation Interferometry
Vertical range [Z]	2.2 mm as standard (>10 mm with Z-stitching)
Vertical resolution [max]	0.01 nm [0.1 Å]
Noise floor [Z]	<0.08 nm [0.8 Å]
Repeatability of surface RMS [Z]	<0.02 nm [0.2 Å]
Max. Measurement area [X, Y]	6.6 mm (>75 mm with X, Y stitching)
Number of measurement points	1024 x 1024 standard
Optical resolution [X, Y]	0.4 - 0.6 μm (surface dependent)
Step height repeatability	<0.1%
Surface reflectivity	0.3% - 100%
Measurement time	5-40 seconds (typical)

Further details available on:

http://www.taylorhobson.com.br/pdf/147_espec.pdf. Accessed on 09/22/13.

AT2.2.3: RUGOSIMETER 3D: NewView 7300

NewView™ 7300 Specifications

SYSTEM

Measurement Technique	Non-contact, three-dimensional, scanning white light interferometry
Scanner	Closed-loop piezo-based, with highly linear capacitive sensors
Objectives	1X, 2.5X, 5X, 10X, 20X, 50X, 100X; objectives available in Standard/Long/Super-Long Working Distance/Glass-Compensated versions; see page 2 for availability and specifications
Objective Mounting Options	<ul style="list-style-type: none"> • Single objective dovetail • Manual 6-position turret • Motorized 6-position turret
Field Zoom Lenses	High-quality discrete zoom lenses; 0.5X, 0.75X, 1.0X, 1.5X, 2.0X
Image Zoom	Motorized 3-position system zoom
Field of View	From 0.03 to 14 mm; larger area imaged with field stitching; objective and zoom dependent
Illuminator	Unique single white-light LED design with superior life, uniform imaging and high efficiency
Controls	Filter Tray, Aperture Stop, and Field Stop (Focus-aid)
Measurement Array	Selectable, includes standard-640x480, 320x240, 160x120; optional- 992 x 992 (1K)
Part Viewing	Secondary LCD monitor
Focus	Motorized manual and auto focus
Z-Drive (Focus) Stage	DC brushless microstepper motor with ballscrew drive, 4 in. range, and 0.1 μ m resolution.
Part Stage Options	<ul style="list-style-type: none"> • Manual Tip/Tilt/X/Y with $\pm 6^\circ$ tip/tilt, ± 2 in. x/y • Motorized Tip/Tilt/X/Y with $\pm 4^\circ$ tip/tilt, ± 3 in. x/y • Motorized Tip/Tilt/X-Theta (or Y-Theta) with $\pm 4^\circ$ tip/tilt, ± 3 in. linear travel
Computer	High-performance Dell PC with LCD monitor
Software	ZYGO MetroPro software running under Microsoft Windows XP

PHYSICAL

Dimensions (H x W x D)	Overall System: 62 x 52 x 35 in. (157 x 132 x 89 cm) NewView: 32 x 23 x 16 in. (81 x 58 x 41 cm) Vibration Isolation Table: 30 x 24 x 24 in. (76 x 61 x 61 cm) Workstation Table: 33.5 x 52 x 35 in. (85 x 132 x 89 cm)
Weight	System: \approx 950 lb (430 kg) NewView: \approx 200 lb (90 kg)



PERFORMANCE

Vertical Scan Range	150 μ m (5906 μ m); Extended scan range to 20 mm (0.79 in.)
Vertical Res.	< 0.1 nm (0.004 μ m)
Lateral Res.	0.36 to 9.5 μ m; objective dependent
Data Scan Rate	≤ 135 μ m/sec, user-selectable; camera and scan mode dependent
Maximum Data Points	307,200; 984,064 (optional); camera dependent
RMS Repeatability	< 0.01 nm (0.0004 μ m) RMS σ
Step Height	Accuracy $\leq 0.75\%$ Repeatability $\leq 0.1\%$ @ 1 σ

TEST PART CHARACTERISTICS

Material	Various surfaces: opaque, transparent, coated, uncoated, specular, and nonspecular
Maximum Size (H x W x D)	3.5 x 8 x 8 in. (89 x 203 x 203 mm); larger sample sizes possible
Reflectivity	1-100%

ENVIRONMENTAL REQUIREMENTS

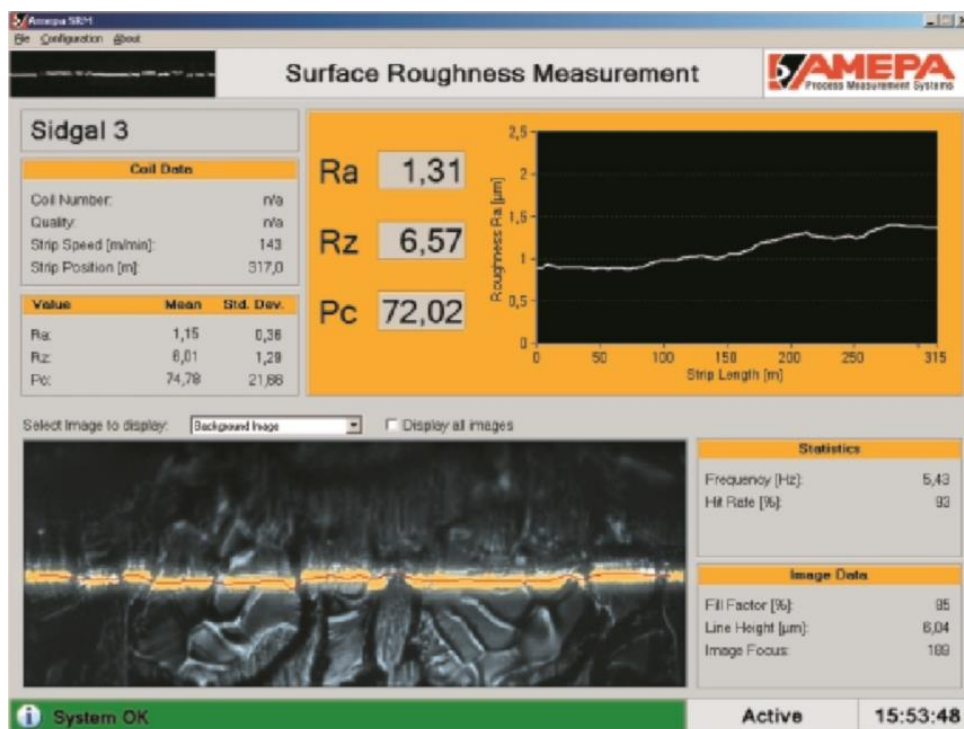
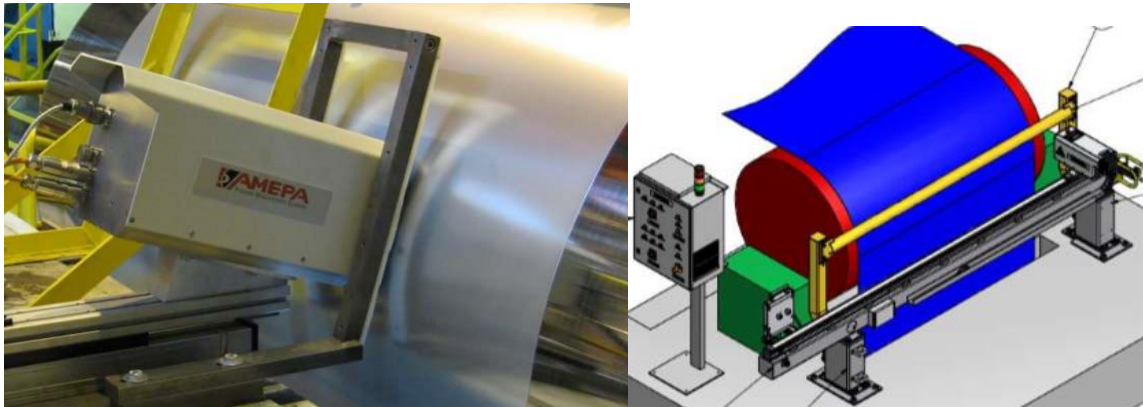
Temperature	15 to 30°C (59 to 86°F)
Rate of Temp. Change	<1.0°C per 15 min
Humidity	5 to 95% relative, noncondensing
Vibration Isolation	Required for vibration frequencies in the range of 1 Hz to 120 Hz

UTILITY REQUIREMENTS

Input Voltage	100 to 240 VAC, 50/60 Hz
Compressed Air	60 to 80 psi (4.1 to 5.5 bar); dry and filtered source; 1/4 in. input

Further details available on: <http://www.zygo.com/?/met/profilers/newview7000/>.
Accessed on 09/22/13.

AT2.2.4: RUGOSIMETER 2D (without contact) SRM 100: Online.



TECHNICAL DATA:

- Measurement range (Ra) 0.3 - 5 μm
- Measurement range R_{Pc} up to 120, threshold changeable
- Resolution (Ra) 0.1 μm
- Measurement frequency up to 20 Hz
- Maximum Strip speed 0 m/min up to 1600 m/min
- Strip thickness 0 – 6 mm
- No calibration necessary
- Working distance 28 mm
- Field of view min. 1,2x0,4 mm
- Automatic optics adjustment according to strip thickness
- Motor controlled positioning and alignment of the sensor
- Sensor dimension approx. 200 x 240 x 450 (mm)

Further details available on Amepa products catalogue.

AT2.3: WAVE SCAN

Used for rating, DOI and spectral curves.

Distinctness of image, DOI, is a quantification of the deviation of the direction of light propagation from the regular direction by scattering during transmission or reflection.



Technical Data			
Measurement Range:	DOI, du	0 to 100	
	LW, SW	0 to 100	
	Wa - We	0 to 100	
Structure Spectrum:	du	< 0.1 mm	
	Wa	0.1 to 0.3 mm	
	Wb	0.3 to 1.0 mm	
	Wc	1.0 to 3.0 mm	
	Wd	3.0 to 10.0 mm	
	We	10.0 to 30.0 mm	
Repeatability*:	du < 40:	4% or > 0.4	
	du > 40:	6% or > 0.6	
Reproducibility*:	du < 40:	6% or > 0.6	
	du > 40:	8% or > 0.8	
Object Curvature:	radius	> 500 mm	
Min. Sample Size:	35 mm x 150 mm		
Scan Length:	5 / 10 / 20 cm		
Resolution:	375 points / cm		
Memory:	1500 readings		
Interface:	USB 1.1		
Light Source:	Laser diode, LED and IR-SLED		
Laser Energy:	< 1mW (Laser class 2)		
Dimensions (LxHxW):	150 x 110 x 55 mm		
	5.9 x 4.3 x 2.2 in.		
Weight:	650 g (1.5 lbs)		
Power Supply:	Rechargeable battery pack or 3 Mignon AA Batteries (alkaline or rechargeable) approx. 1000 readings		
Temperature Range:	Operation:	+10°C to 40°C	+50°F to 104°F
	Storage:	0°C to 60°C	+32°F to 140°
Relative Humidity:	Up to 85% at 35°C (95°F) non-condensing		

* Standard deviation

http://www.gardco.com/pages/gloss/wavescan_dual.cfm. Accessed on 09/22/13.

AT2.4: MICRO-WAVE SCAN



Minimum sample size: 25 mm x 40 mm

Technical Data		
Measurement Range:	DOI, du LW, SW Wa - Wd	0 to 100 0 to 100 0 to 100
Structure Spectrum:	du Wa Wb Wc Wd	< 0.1 mm 0.1 to 0.3 mm 0.3 to 1.0 mm 1.0 to 3.0 mm 3.0 to 10.0 mm
Scan length & Measurement Scales:	Scan length 20cm 10cm 5cm 0cm	Measurement Scales du, Wa...Wd, L, S, DOI du, Wa...Wd, L, S, DOI du, Wa...Wd, L, S, DOI du, Wa, Wb, DOI
Repeatability*:	8% or > 0.8	
Reproducibility*:	12% or > 1.2	
Object Curvature:	radius > 300 mm	
Minimum Sample Size:	25 mm x 40 mm	
Measurement Area:	4 mm x scan length	
Scan Length:	5 / 10 / 20 cm	
Resolution:	375 points / cm	
Memory:	2000 readings	
Interface:	serial RS 232	
Light Source:	Laser diode, LED	
Laser Energy:	< 1mW (Laser class 2)	
Dimensions (H x W x L):	4.7 x 1.6 x 2.7 inches (120 x 40 x 70 mm)	
Weight:	0.6 lbs. (250 g)	
Power Supply:	rechargeable battery pack or 2 AA Batteries (alkaline or rechargeable) approx. 1000 readings	
Temperature Range operation:	+50°F to 104°F +10°C to 40°C	
Storage:	+32°F to 140°F 0°C to 60°C	
Relative Humidity:	up to 85% at 95°F (35°C)	
* Standard deviation		

http://www.gardco.com/pages/gloss/microwave_scan.cfm

AT2.5: GLOSSMETER

Used for Gloss

Gloss is a term used to define an optical property of a surface to reflect light in a specular direction. The factors that affect gloss are the refractive index of the material, the angle of incident light and the surface topography.



Description	Geometry	Application	Measuring Area	Dimensions	Weight
Micro-Gloss II 20°	20°	high gloss	10 x 10 mm (0.4 x 0.4 in)	2.9"H x 6.1"L x 1.9"W (73mm x 155mm x 48mm)	0.9 lbs (0.4 kg)
Micro-Gloss II 60°	60°	semi gloss	9 x 15 mm (0.35 x 0.6in)		
Micro-Gloss II 85°	85°	low gloss	5 x 38 mm (0.2 x 1.5 in)		
Micro-TRI-Gloss II	20°, 60°, 85°	universal	see single angle		

All Units:		
Range:	Repeatability:	Reproducibility:
0 - 99.9 GU	0.2 GU	0.5 GU
100 - 2000 GU	0.2%	0.5%

<http://www.gardco.com/pages/gloss/microgloss.cfm>. Accessed on 09/22/13.

AT2.6: QUANTUMX MX460

Used to collect data from sheet metal displacement versus time during stamping.



General specifications		
Inputs	Number	4, electrically isolated from each other
Transducer technologies		Torque transducers, frequencies in general, counters, rotary encoders, incremental encoders, pulse encoders, shaft encoders (digital, sinusoidal, with/without index)
Data rate	Hz	0.1 ... 96000 per channel, adjustable individually
Bandwidth		
Time domain	kHz	approx. 10
Frequency/Spectrum analysis	kHz	38
Transducer identification (TEDS, IEEE 1451.4)		
max. TEDS module distance	m	100
Transducer connection		D-SUB-15HD
Supply voltage range (DC)	V	10 ... 30, nominal (rated) voltage 24 V
Supply voltage interruption		max. for 5 ms at 24 V
Power consumption		
without adjustable transducer excitation	W	< 6
with adjustable transducer excitation	W	< 9
Transducer excitation (active transducers)		
Adjustable voltage (DC)	V	5 ... 24; adjustable channel by channel
Maximum output power	W	0.7 per channel / 2 in total
Ethernet (data link)		10Base-T / 100Base-TX
Protocol/addressing	-	TCP/IP (direct IP address or DHCP)
Plug connection	-	8P8C-modular plug (RJ-45) with twisted pair cable (CAT-5)
Max. cable length to module	m	100
FireWire (module synchronization, data link, optional voltage supply)		IEEE 1394b
Baud rate	MBaud	400 (approx. 50 MBytes/s)
Max. current from module to module	A	1.5
Max. cable length between nodes	m	5
Max. number of modules connected in series (daisy chain)	-	12 (= 11 hops)
Max. number of modules in a FireWire system (incl. hubs ¹⁾ , backplane)	-	24
Max. hops in a chain ²⁾	-	14
Synchronization options		FireWire (automatically, recommended)
EtherCAT		via CX27
NTP		via Ethernet
IRIG-B (B000 bis B007; B120 bis B127)		via MX440A- or MX840A input channel
Nominal (rated) temperature range	°C [°F]	-20 ... +60 [-4 ... +140]
Operating temperature range	°C [°F]	-20 ... +65 [-4 ... +149]
Storage temperature range	°C [°F]	-40 ... +75 [-40 ... +167]
Relative humidity	%	5 ... 95 (non-condensing)
Protection class		III
Degree of protection		IP20 per EN60529
EMC requirements		EN61326
Mechanical tests³⁾		
Vibration (30 min)	m/s ²	50
Shock (6 ms)	m/s ²	350
Dimensions, horizontal (H x W x D)	mm	52.5 x 200 x 122 (with case protection) 44 x 174 x 119 (without case protection)
Weight, approx.	g	850

http://www.hbm.com/en/menu/products/measurement-electronics-software/compact-universal-data-acquisition-system/quantumx-mx460/?geoip_cn=2. Accessed on 09/22/13.

AT2.7: LVDT WA / 50mm

Used to measure the sheet metal displacement during stamping



Type		WA2	WA10	WA20	WA50	WA100	WA200	WA300	WA500
Nominal displacement	mm	0...2	0...10	0...20	0...50	0...100	0...200	0...300	0...500
Nominal sensitivity Nominal output signal at nominal displacement with output unloaded	mV/V	80							
Characteristic tolerance Deviation of sensitivity from nominal sensitivity	%	± 1							
Zero point tolerance with core in zero position	mV/V	± 1		± 8					
Linearity deviation Greatest deviation between start and end point (including hysteresis by reference to nominal sensitivity)	%	≤ ± 0.2 to ≤ ± 0.1							
Nominal temperature range	°C [°F]	-20...+80							
Operating temperature range Standard	°C [°F]	-25...+80 [-13...+176]							
Variant for high temperature	°C [°F]	-25...+150 [-13...+302]							
Variant for low temperature	°C [°F]	-40...+125 [-40...+257]							
Effect of temperature on zero signal in nominal temp. range per 10 K, by refer. to nominal sensitivity	%	< ± 0.1							
Effect of temperature on output signal in nominal temp. range per 10 K, by refer. to actual value	%	< ± 0.1							
Input resistance	Ω	100 ± 10 %		350 ± 10 %					
Output resistance	Ω	570 ± 10 %		680 ± 10 %					
Nominal excitation voltage	V _{rms}	2.5							
Operating range of the excitation voltage	V _{rms}	0.5...10							
Carrier frequency, Nominal range	kHz	4.8 ± 1 %							
Operating range	kHz	4.8 ± 8 %							
Weight of transducer body	g	54	56	57	68	104	147	190	276
of plunger	g	4	6	7	9	13	20	28	42
Impact resistance , test severity level to DIN IEC 68, Part 2-27; IEC 68-2-27-1987 Number of impacts (per direction)	-	1000							
Impact acceleration	m/s ²	650							
Impact duration	ms	3							
Impact form	-	Half sine wave							
Vibration resistance , test severity level to DIN IEC 68, Part 2-6, IEC 68-2-6-1982 Frequency range	Hz	5 to 65							
Vibration acceleration	m/s ²	150							
Stress duration (per direction)	h	0.5							
Max. permissible plunger acceleration	m/s ²	2500							
	m/s ²	Probe version						Unfixed plunger version	
Service life, typically		10 million stress cycles						-	
Spring constant	N/mm	0.116				0.063		-	
Spring force in zero position (for 1mm initial stroke) approx.	N	2.4				2		-	
Spring force in final position (nom. displ.) approx.	N	2.7	3.6	4.7	8.2	8.3	-		
Max. permissible probe tip acceleration	m/s ²	170		140	95	45	-		
Probe tip cut-off frequency for 1 mm stroke approx.	Hz	60		55	45	30	-		
Probe tip cut-off frequency at nominal displacement	Hz	18		10	5	3	-		
Degree of protection acc. to EN 60 529 for transducer duct and core channel	-	IP67 (depending on connection piece)							
Max. permissible pressure (increasing load)	bar	350							
Overload limit (to VDI/VDE 2600, Sheet 4)	bar	450							
Destructive range (to VDI/VDE 2600, Sheet 4)	bar	> 500							

<http://www.hbm.com/fileadmin/mediapool/hbmdoc/technical/b0553.pdf>. Accessed on 09/22/13.